RADIO ASTRONOMY

Journal of the Society of Amateur Radio Astronomers
July-August 2021

Dennis Farr
SARA President

Dr. Richard A. Russel
Editor

Whitham D. Reeve
Contributing Editor

Radio Astronomy is published bimonthly as the official journal of the Society of Amateur Radio Astronomers. Duplication of uncopyrighted material for educational purposes is permitted but credit shall be given to SARA and to the specific author. Copyrighted materials may not be copied without written permission from the copyright owner.

Radio Astronomy is available for download only by SARA members from the SARA web site and may not be posted anywhere else.

It is the mission of the Society of Amateur Radio Astronomers (SARA) to: Facilitate the flow of information pertinent to the field of Radio Astronomy among our members; Promote members to mentor newcomers to our hobby and share the excitement of radio astronomy with other interested persons and organizations; Promote individual and multi station observing programs; Encourage programs that enhance the technical abilities of our members to monitor cosmic radio signals, as well as to share and analyze such signals; Encourage educational programs within SARA and educational outreach initiatives. Founded in 1981, the Society of Amateur Radio Astronomers, Inc. is a membership supported, non-profit [501(c) (3)], educational and scientific corporation.

Contents

Radio Waves

President's Page

Another annual milestone for SARA, the eastern conference was a great success! Thanks to Richard Russel and a dedicated group of volunteers the ZOOM conference went off without a hitch. Thanks to all who made the best of a bad situation, the pandemic.

The email list continues to be active and provide answers to a wide range of questions on RA. That along with the monthly Drakes Lounge ZOOM meetings provides information for experienced and new people to the hobby.

Once again, we are extremely happy with the success of the Scope In A Box program. People who get it are showing their interest in learning RA by building their own equipment, just like the days when people built their own Dobsonian mounts and Newtonian reflectors.

IBT and SuperSID round out the offerings of kits on the SARA store found on the website. Together these kits provide a solid basic understanding of the concepts of RA and building blocks for further observation and study.

SARA has educational and promotional programs and presentations. Please contact any group that you may meet with and ask if they would like SARA to provide a meeting speaker or presentation. There are a lot of members that would be glad to assist. And I assure you they are always looking for programs and speakers.

So continue to promote SARA and promote the study of RA.

Keep your antennas pointed up!

Dennis

Editor's Notes

We are always looking for basic radio astronomy articles, radio astronomy tutorials, theoretical articles, application and construction articles, news pertinent to radio astronomy, profiles and interviews with amateur and professional radio astronomers, book reviews, puzzles (including word challenges, riddles, and crossword puzzles), anecdotes, expository on "bad astronomy," articles on radio astronomy observations, suggestions for reprint of articles from past journals, book reviews and other publications, and announcements of radio astronomy star parties, meetings, and outreach activities.

New Journal Feature – Observation Reports

We are now accepting 1-2 page observation reports. These reports should include the astronomical objects RA/DEC plus UTC of the observation. Also include the telescope configuration, process used to observe the object and results. Picture of the setup and plots of the observation are a plus to the report.

If you would like to write an article for Radio Astronomy, please follow **the newly updated Author's Guide** on the SARA web site:
http://www.radio-astronomy.org/publicat/RA-JSARA_Author's_Guide.pdf.

Let us know if you have questions; we are glad to assist authors with their articles and papers and will not hesitate to work with you. You may contact your editors any time via email here: edit@radio-astronomy.org.

The editor(s) will acknowledge that they have received your submission within two days. If they do not reply, assume they did not receive it and please try again.

Please consider submitting your radio astronomy observations for publication: any object, any wavelength. Strip charts, spectrograms, magnetograms, meteor scatter records, space radar records, photographs; examples of radio frequency interference (RFI) are also welcome.
Guidelines for submitting observations may be found here: http://www.radio-astronomy.org/publicat/RA-JSARA_Observation_Submission_Guide.pdf

Issue	Articles	Review	Distribution
2021			
Sep-Oct	October 12	October 23	October 31
Nov-Dec	December 12	December 22	December 31
2022			
Jan-Feb	February 12	February 21	February 28
Mar-Apr	April 12	April 25	April 30
May-Jun	Jun 12	Jun 20	Jun 28
Jul-Aug	Aug 12	Aug 22	Aug 31

SARA NOTES

SARA Student & Teacher Grant Program

All, SARA has a grant program that is, sad to say very underutilized. We will provide kits or money to students and teachers including college students to help them with a radio telescope project. SARA can supply any of the following kits:

- SuperSID
- Scope in a Box
- IBT (Itty Bitty Telescope)
- Radio Jove kit
- Inspire
- Sky Scan

We can also provide up to five hundred dollars ($500.00 USD) for an approved radio telescope project.

We have on occasion provided more money based on the merits of the project and the SARA Grant Committee approval.

More information on the grant program can be found at the URL below.
SARA Student and Teacher Project Grants | Society of Amateur Radio Astronomers (radio-astronomy.org)

All that is required is the SARA grant request form be filled out and sent in. If it needs more work for approval, we will work with the student to help ensure their success.

Please pass the word that SARA will fund any legitimate radio telescope project anywhere in the world.

If you have a question, contact me at crowleytj at hotmail dot com.

Tom Crowley
SARA Grant Program Administrator

Drake's Lounge

Join the SARA community as we discuss the latest astronomy and radio astronomy news. The lounge also provides a forum to share and get advice on your radio astronomy projects from very experienced amateur radio astronomers.

Drake's Lounge is every month on the 3rd Sunday at 2 pm Eastern time. ZOOM email notifications will be sent to all members.

See you there!

News: (Jul-Aug 2021)

Hey, Mac, if I read about one more FRB, I'm gonna ...: Universe Today ~ *CHIME Detected Over 500 Fast Radio Burst in its First Year, Providing new Clues to What's Causing Them*: https://www.universetoday.com/151490/chime-detected-over-500-fast-radio-burst-in-its-first-year-providing-new-clues-to-whats-causing-them/

Interesting weblinks:

Public NRAO website:	https://public.nrao.edu/
Ask an Astronomer:	https://public.nrao.edu/ask/
VLA Explorer:	https://public.nrao.edu/explore/vla-explorer/
NRAO Mission Control:	https://public.nrao.edu/explore/mission-control/
VLA Webcam:	https://public.nrao.edu/vla-webcam/
NAC Program:	https://science.nrao.edu/opportunities/student-programs/nac
NASA's Radio Jove Project:	https://radiojove.gsfc.nasa.gov

SETI Institute ~ FRB Discovered by SETI Institute's Allen Telescope Array: https://www.seti.org/frb-discovered-seti-institutes-allen-telescope-array

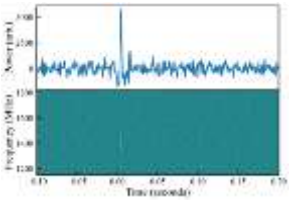

Cornell University ~ *The First CHIME/FRB Fast Radio Burst Catalog*: https://arxiv.org/abs/2106.04352

Square Kilometer Array (SKA) Organization (soon to be SKA Observatory) ~ *Green light given for construction of world's largest radio telescope arrays*: https://www.skatelescope.org/news/green-light-for-ska-construction/

SKA May-June 2021 Bulletin ~ https://ska-france.oca.eu/images/SKA-France-Media/Bulletins/Bulletin52.pdf

Interstellar Probe Study 2019 Report Now Available ~ *This 329-page report covers a lot of ground, from the background and history of this and similar concepts to the development of science goals and the mission architecture. Includes approaches used for making magnetic and radio wave measurements:* http://interstellarprobe.jhuapl.edu/uploadedDocs/papers/588-ISP-Study-2019-Report_PR.pdf

Solar-Terrestrial Centre of Excellence STCE ~ *Space Weather Acronyms*: https://www.stce.be/educational/acronym#T

Practical Engineering ~ *What Really Happened at the Arecibo Telescope?* (YouTube video): https://www.youtube.com/watch?v=3oBCtTv6yOw

History of Geo- and Space Sciences (HGSS) ~ *The Geophysical Observatory in Sodankylä, Finland – past and present*: https://hgss.copernicus.org/articles/12/115/2021/

EDN ~ Big Ear receives 'Wow! Signal,' August 15, 1977: https://www.edn.com/big-ear-receives-wow-signal-august-15-1977/

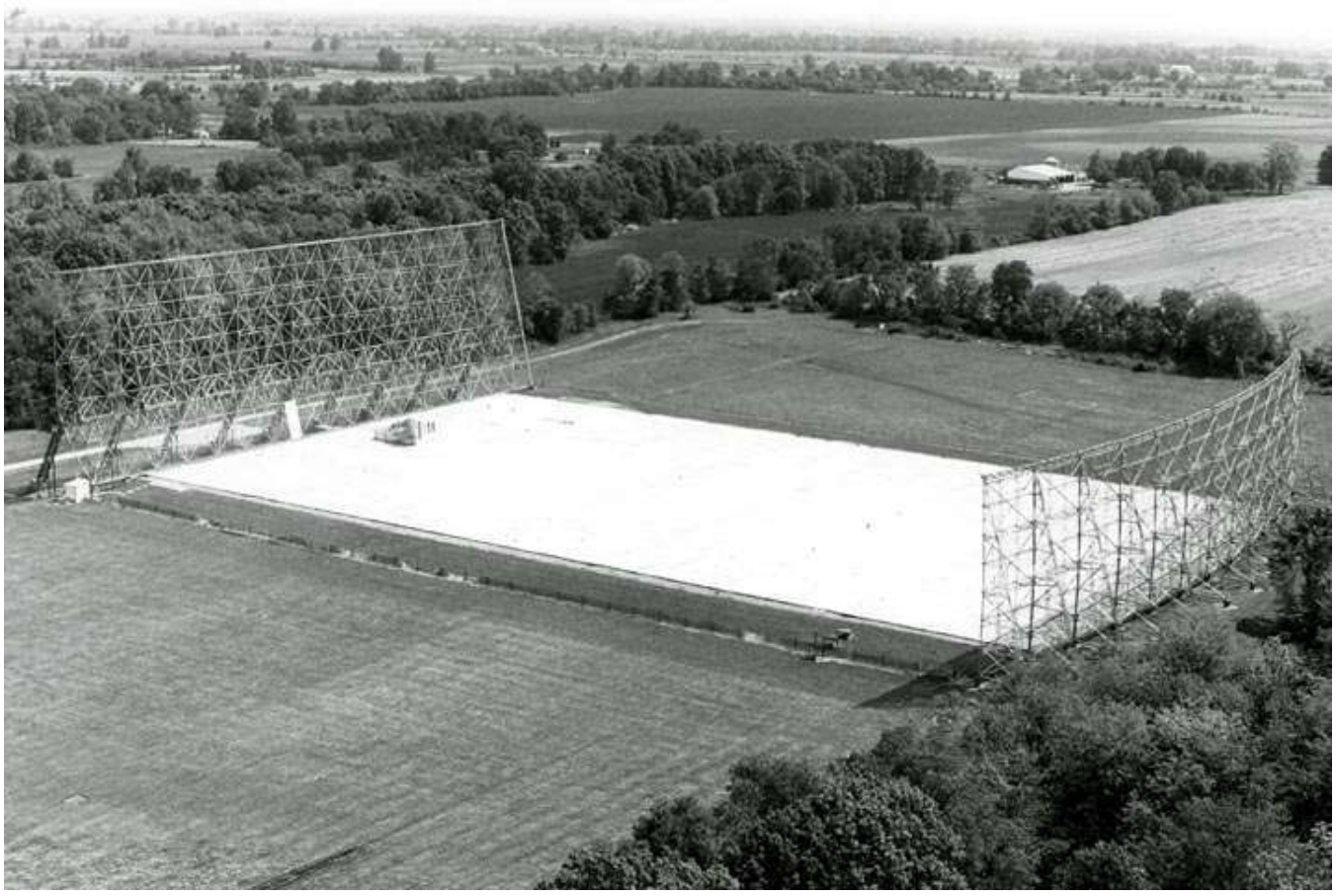

Technical Knowledge & Education: (Jul-Aug 2021)

Evaluation Engineering ~ *2021 Special Report: Signal & Spectrum Analyzers*: https://www.evaluationengineering.com/instrumentation/signal-spectrum-analyzers/article/21223201/evaluation-engineering-2021-special-report-signal-spectrum-analyzers-empower-advanced-wireless-system-development

Centre for Astrophysics and Supercomputing

Colloquia Series: https://astronomy.swin.edu.au/research/colloquia.php

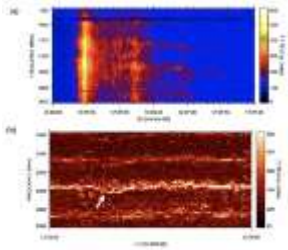

Community of European Solar Radio Astronomers (CESRA) ~ *Narrowband Spikes Observed during the 2013 November 7 Flare*: http://www.astro.gla.ac.uk/users/eduard/cesra/?p=2972

Research Notes of the AAS ~ *An Arecibo 327 MHz Search for Radio Pulsars and Bursts in the Dwarf Irregular Galaxies Leo A and T*: https://iopscience.iop.org/article/10.3847/2515-5172/ac0c1d

National Telecommunications & Information Administration (NTIA) Institute for Telecommunication Sciences (ITS) ~

Have you ever wondered how a spectrum analyzer works, how to properly adjust all of the analyzer's parameters, or why a stair-step pattern initially appears on a spectrum analyzer screen when you turn it on? Do you know how to precisely calculate the analyzer's sensitivity in your head, merely by glancing at the screen display without any signal present? Are you uncertain about how much gain, and how low a noise figure, you ought to specify when you are ordering a low-noise amplifier (LNA) for a radio receiver? Do you want to know the difference between noise figure and noise factor? Do you wonder how to diagnose and solve radio interference problems?

If you have questions about how to make good radio spectrum measurements or how to diagnose interference problems, you will find the answers in the NTIA Seminar Series on Spectrum Measurement Theory and Techniques. In this series of talks, an NTIA engineer at the Institute for Telecommunication Sciences (ITS) laboratory in Boulder, CO, discusses the fundamentals of radio spectrum measurements. The speaker, Frank Sanders, who has nearly thirty years of experience in this field, recognizes that even for many engineers who routinely use spectrum analyzers, the fundamentals of how they work and how to use them may be a bit murky; even in university lab classes the instructors do not always understand these machines very well themselves.

Most of the talks, which are 80-100 minutes long, are divided into two parts. In the first portion of each video, Sanders explores a particular aspect of radio spectrum measurement technique or theory with a whiteboard lecture. In the second part, the lessons of the whiteboard discussion are implemented with actual measurement hardware and radio signals. A few of the talks, which for example involve large numbers of photographs of radar systems, are videos of his Microsoft Powerpoint presentations.

In this series, Sanders explains spectrum analyzer functionality in terms of convolution bandwidth and shows how, when convolution is understood along with the mechanics of analyzer design, spectrum analyzer operations and outputs become easy to understand and use. Other topics include (1) what you need to know to use spectrum analyzers to examine all types of radio signals, including mobile radios, radars, and digital data links; (2) the use of low noise amplifiers and how to specify the right gain and noise figure for your receiver and measurement applications; (3) how radar systems work, and how to understand and interpret the signals that you see coming from radars; (4) the ways that radio interference can occur; (5) a methodical approach for diagnosing and solving radio interference problems; (6) the math needed to convert spectrum analyzer

measurements into field strengths of radio signals; and (7) the proper conversions for radiation hazard calculations.: https://www.youtube.com/watch?v=wJcSGicDjLw

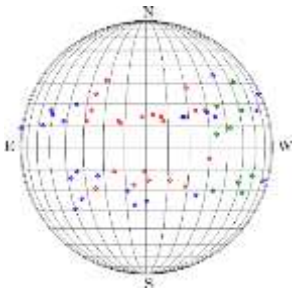

Journal of Space Weather and Space Climate ~ *Halo coronal mass ejections during Solar Cycle 24: reconstruction of the global scenario and geoeffectiveness*: https://www.swsc-journal.org/articles/swsc/full_html/2018/01/swsc170032/swsc170032.html

Cornell University ~ *Fast radio bursts at the dawn of the 2020s*: https://arxiv.org/abs/2107.10113

Ford Motor Company ~ *EMC Design Guide for Printed Circuit Boards*: https://www.emcfastpass.com/wp-content/uploads/2017/04/Ford-EMC-Design-Guide-for-PCB.pdf

Texas Instruments ~ *PCB Design Guidelines For Reduced EMI*: https://www.ti.com/lit/an/szza009/szza009.pdf

edX & EPFLx ~ *The Radio Sky II: Observational Radio Astronomy: This course covers the principles and practices of radio astronomical observations, in particular with modern interferometers. Topics range from radio telescope technology to the measurement equation to radio interferometric calibration and imaging*: https://www.edx.org/course/the-radio-sky-ii-observational-radio-astronomy

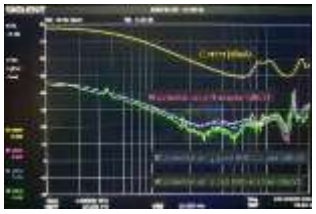

In Compliance magazine ~ *RF Tech Tip: BNC Versus Threaded Connectors*: https://digital.incompliancemag.com/issue/august-2021/rf-tech-tip-bnc-versus-threaded-connectors/

Würth Elektronik - *Function and Design of Coaxial Connectors*: https://www.we-online.com/web/en/electronic_components/extra_pbs/webinars/webinars_midcom/2021_webinars/aug21_connectors2.php

Cornell University ~ *Radio signals from early direct collapse black holes*: https://arxiv.org/abs/2107.11307

For Your Radio Astronomy Bookshelf

(Prices in USD)

- **The Evolution of Radio Astronomy;** Hey, James S.; Watson Publishing International, LLC; 1973; $10.00
- **Amateur Radio Astronomy;** Fielding, John; Radio Society of Great Britain; 7th edition (January 1, 2006); $74.00
- **Radio Astronomy : Observing the Invisible Universe** (2017, DVD); Great Courses Series; 2017; $75.00

SuperSID

Collaboration of Society of Amateur Radio Astronomers and Stanford Solar Center

- ✓ Stanford provides data hosting, database programming, and maintains the SuperSID website
- ✓ Society of Amateur Radio Astronomers (SARA) sells the SuperSID monitors for 48 USD to amateur radio astronomers and the funds are then used to support free distribution to students all over the world (image below as of Fall 2017)
- ✓
- ✓ Jonathan Pettingale at SARA is responsible for building and shipping the SuperSID monitor kits: SuperSID@radio-astronomy.org
- ✓ SuperSID kits may be ordered through the SARA SuperSID webpage: http://radio-astronomy.org/node/210
- ✓ Questions about the SuperSID project may be directed to Steve Berl at Stanford: steveberl@gmail.com
- ✓ Jaap Akkerhuis at Stanford is responsible for the SuperSID software and SARA has provided financial support for his efforts
- ✓ SuperSID website hosted by Stanford: http://solar-center.stanford.edu/SID/sidmonitor/
- ✓ SuperSID database: http://sid.stanford.edu/database-browser/
- ✓ The data is searchable by time, station, date, and multiple plots may be placed on the same graph for comparison.

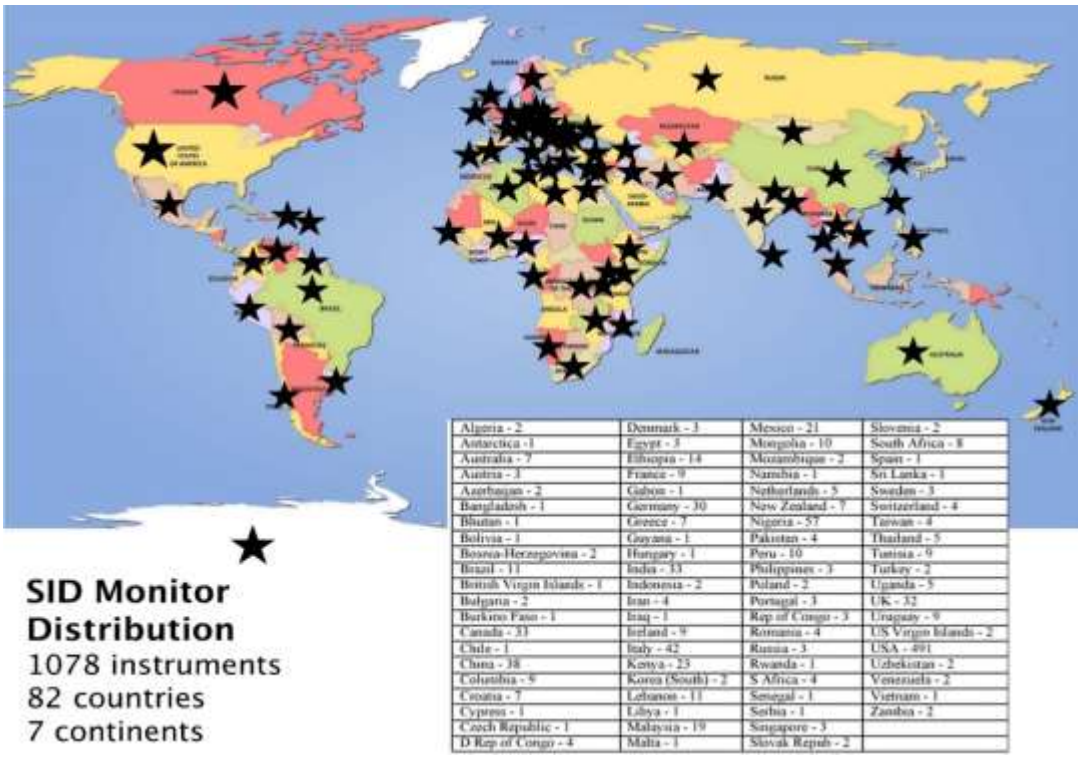

Algeria - 2	Denmark - 3	Mexico - 21	Slovenia - 2
Antarctica - 1	Egypt - 3	Mongolia - 10	South Africa - 8
Australia - 7	Ethiopia - 14	Mozambique - 2	Spain - 1
Austria - 3	France - 9	Namibia - 1	Sri Lanka - 1
Azerbaijan - 2	Gabon - 1	Netherlands - 5	Sweden - 3
Bangladesh - 1	Germany - 30	New Zealand - 7	Switzerland - 4
Bhutan - 1	Greece - 7	Nigeria - 57	Taiwan - 4
Bolivia - 1	Guyana - 1	Pakistan - 4	Thailand - 5
Bosnia-Herzegovina - 2	Hungary - 1	Peru - 10	Tunisia - 9
Brazil - 11	India - 53	Philippines - 3	Turkey - 2
British Virgin Islands - 1	Indonesia - 2	Poland - 2	Uganda - 5
Bulgaria - 2	Iran - 4	Portugal - 3	UK - 32
Burkina Faso - 1	Iraq - 1	Rep of Congo - 3	Uruguay - 9
Canada - 33	Ireland - 9	Romania - 4	US Virgin Islands - 2
Chile - 1	Italy - 42	Russia - 3	USA - 491
China - 38	Kenya - 23	Rwanda - 1	Uzbekistan - 2
Colombia - 5	Korea (South) - 2	S Africa - 4	Venezuela - 2
Croatia - 7	Lebanon - 11	Senegal - 1	Vietnam - 1
Cyprus - 1	Libya - 1	Serbia - 1	Zambia - 2
Czech Republic - 1	Malaysia - 19	Singapore - 3	
D Rep of Congo - 4	Malta - 1	Slovak Repub - 2	

For official use only
Monitor assigned: _____
Site name: _____
Country: _____

SuperSID Space Weather Monitor

Request Form

	Your information here		
Name of site/school *(if an institution)*:			
Choose a site name: *(3-6 characters) No Spaces*			
Primary contact person:			
Email:			
Phone(s):			
Primary Address:	Name School or Business Street Street City Country	 State/Province Postal Code	
Shipping address, if different:	Name School or Business Street Street City Country	 State/Province Postal Code	
Shipping phone number:			
Latitude & longitude of site:	Latitude: _____	Longitude: _____	

I understand that neither Stanford nor the Society of Amateur Radio Astronomers is responsible for accidents or injuries related to monitor use. I will assure that a surge protector and other lightning protection devices are installed if necessary.

Signature: _____ **Date:** _____

I will need:

What	*Cost*	*How many?*
SuperSID distribution USB Power	$48 (assembled)	
USB Sound card 96 kHz sample rate *(or provide this yourself)*	$40 *(optional)*	
Antenna wire (120 meters) *(or you can provide this yourself)*	$23 *(optional) with connectors attached and tested*	
RG 58 Coax Cable (9 meters) *(or provide this yourself)*	$14 *(optional) with connectors attached and tested*	
Shipping	US $12 Canada & Mexico $40 all other $60	
	TOTAL	$

____ **I have included a $**_____ **check** (payable to SARA)

____ **I will make payment thru** www.paypal.com to treas@radio-astronomy.org

or

____ If you are a Minority-serving institution, in a Developing or economically deprived nation, and/or you are using the monitor with students for educational purposes, you may qualify for obtaining a monitor at reduced or no cost. Check here if you wish to apply for this designation. Then tell us how you want to use the SuperSID monitor. Include type of site, number of students involved, whether public or private school, grade levels, etc. and describe your program. The goal of the SuperSID project is to provide as many students with systems as possible. If you are able to pay for a system, even if you qualify for a free one, please do so and help support our goal.

_____

_____

_____

For more details on the Space Weather Monitor project, see: **http://sid.stanford.edu**

To set up a SuperSID monitor you will need:

1. Access to power and an antenna location that is relatively free of electric interference (could be indoors or out)
2. A **PC**** with the following minimal specifications:
    - A sound card that can record (sample) up to 96 kHz, or a USB port to connect such a sound card (for North and South America)
        - All other countries can use AC97 sound card with 48 kHz record (sample) rate. Most computers made after 1997 will have AC97.
    - Windows 2000 or more recent operating system
    - 1 GHz Processer with 128 mb RAM
    - Ethernet connection & internet browser (desirable, but not required)
    - Standard keyboard, mouse, monitor, etc.
3. An inexpensive antenna that you build yourself. You'll need about 120 meters (400 feet) of **insulated** wire. Solid wire is easier to wind than stranded. Magnet wire will work but be more fragile. You can use anything from #18 to #26 size wire. The antenna frame can be made of wood, PVC pipe, or similar materials. We'll provide instructions. You can purchase the wire from us or obtain your own.
4. RG58 coax cable with a BNC connector at one end to run from the antenna to the SuperSID receiver. 9 meters is recommended, but the length will depend on where you place the antenna. You can purchase the coax from us or obtain your own.
5. Surge protector and other protection against a lightning strike

---

Return this form to: SuperSID@radio-astronomy.org
or mail to: SARA
Brian O'Rourke, SARA Treasurer
337 Meadow Ridge Rd,
Troy, VA 22974-3256

The British Astronomical Association
A company limited by guarantee
Registered Charity No. 210769
Burlington House, Piccadilly, London, W1J 0DU
Telephone: 020 7734 4145
Fax No.: 020 7439 4629
Email: office@britastro.org
Website: www.britastro.org
Founded in 1890

Please send all reports and observations to jacook@jacook.plus.com

John Cook's VLF Report

May has been the most active month so far in solar cycle 25, with 26 flares recorded as SIDs including four of M-class. Prior to this, we had just a single M-class in 2020 November, and another in 2020 May. Cycle 24 ended with 12 M and four X-class flares back in 2017 September. The strongest flare was the M3.9 just before sunset on the 7th.

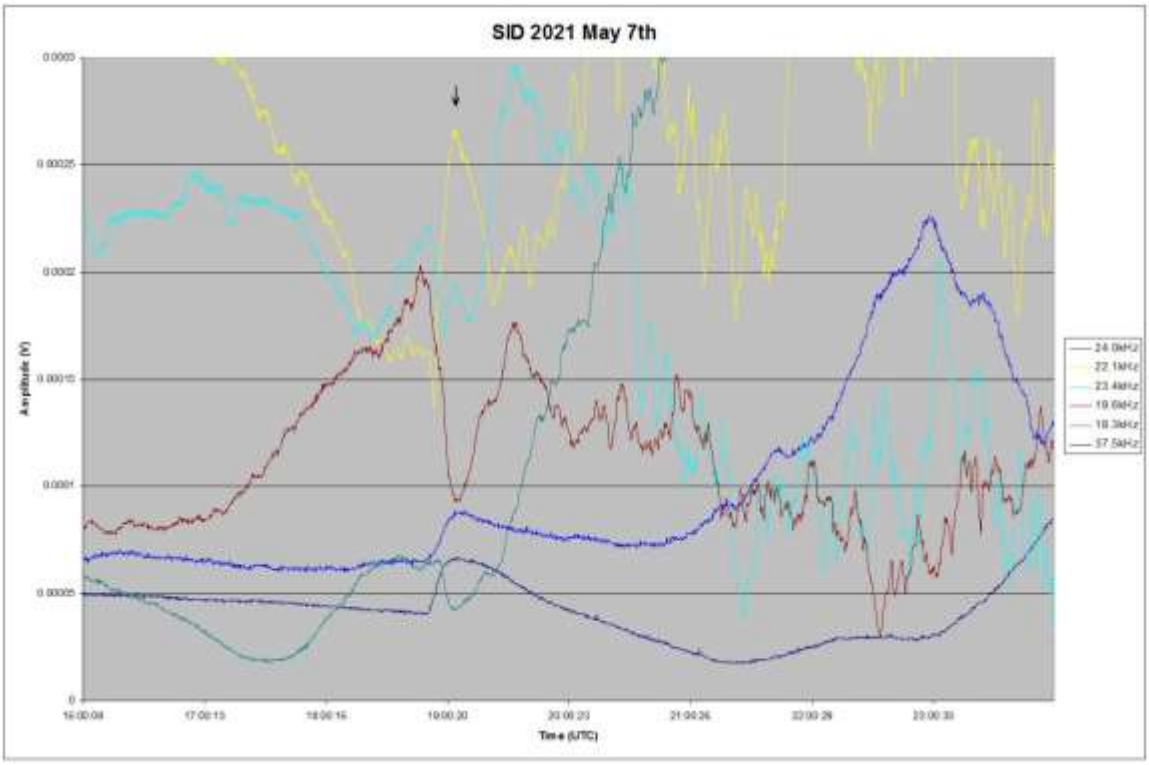

The multiple signals shown in Mark Edwards' recording make it easier to see, particularly on the western paths at 24 and 37.5kHz (black and dark-blue traces). Mark has added an arrow above the 22.1kHz trace (yellow) to identify the SID. Active region AR12822 was responsible for this flare, and continued over the next few days with a few B- and C-class flares as it rotated out of view from Earth.

Most of the activity was later in the month, on the 22nd and 23rd as AR12824 grew and became more active in the northern hemisphere. The first chart on the next page shows the early C6.0 flare recorded by Paul Hyde, even showing a clear SID on the western path at 37.5kHz. The second chart shows the activity later on the 22nd, recorded by Mark Prescott. There is a long break in the 20.9kHz signal, missing the first C3.2 flare.

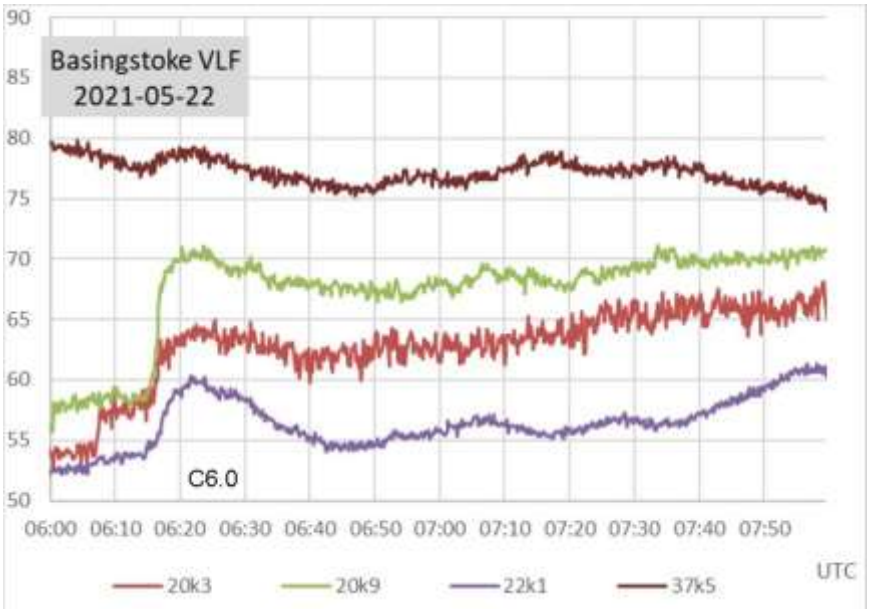

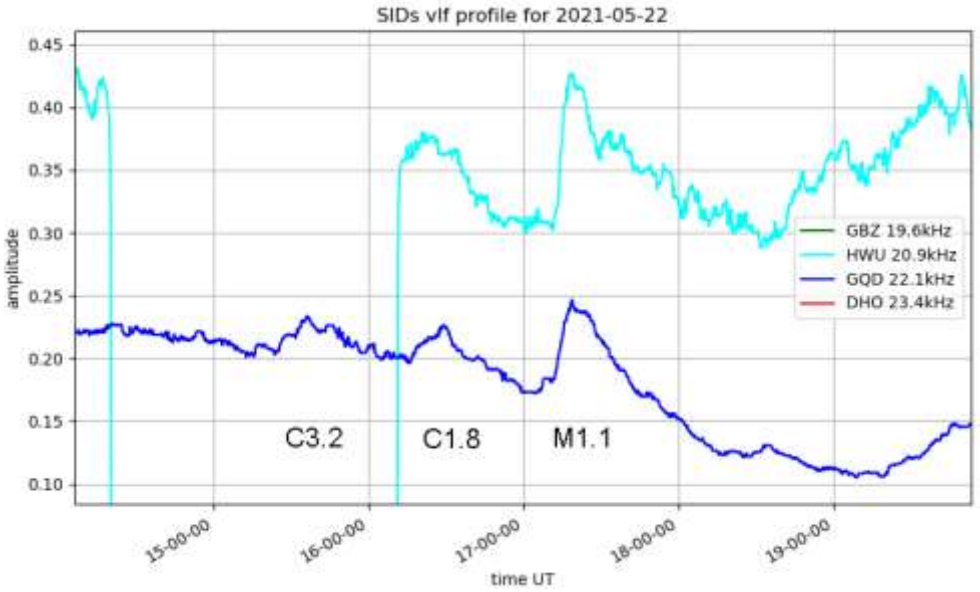

AR12824 continued its activity on the 23rd, with another M1.1 flare close to midday. There were also some HF and VHF radio noise bursts recorded by Colin Briden at 28MHz and Colin Clements at 151, 408 and 610MHz.

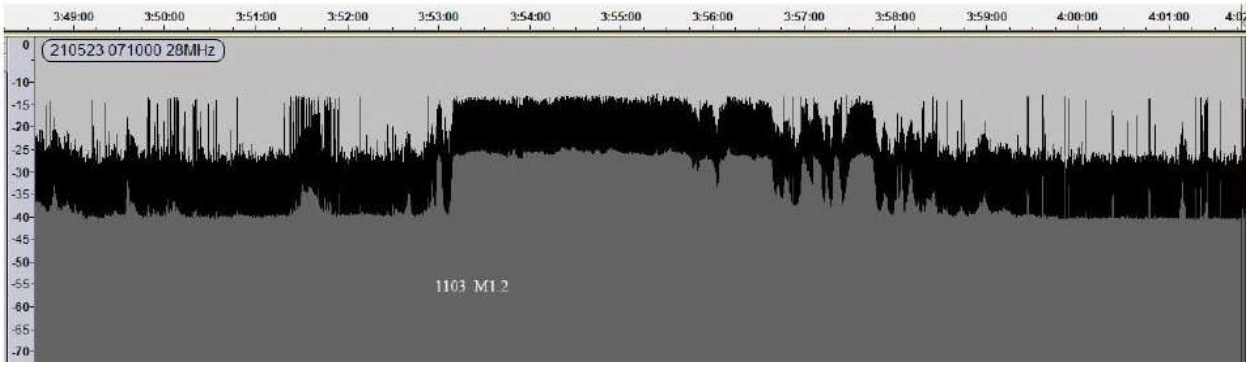

This 28MHz recording by Colin Briden shows the M1.1 flare, starting at 11:03UT, lasting for about 7 minutes. The Black band shows the peaks of the signal.

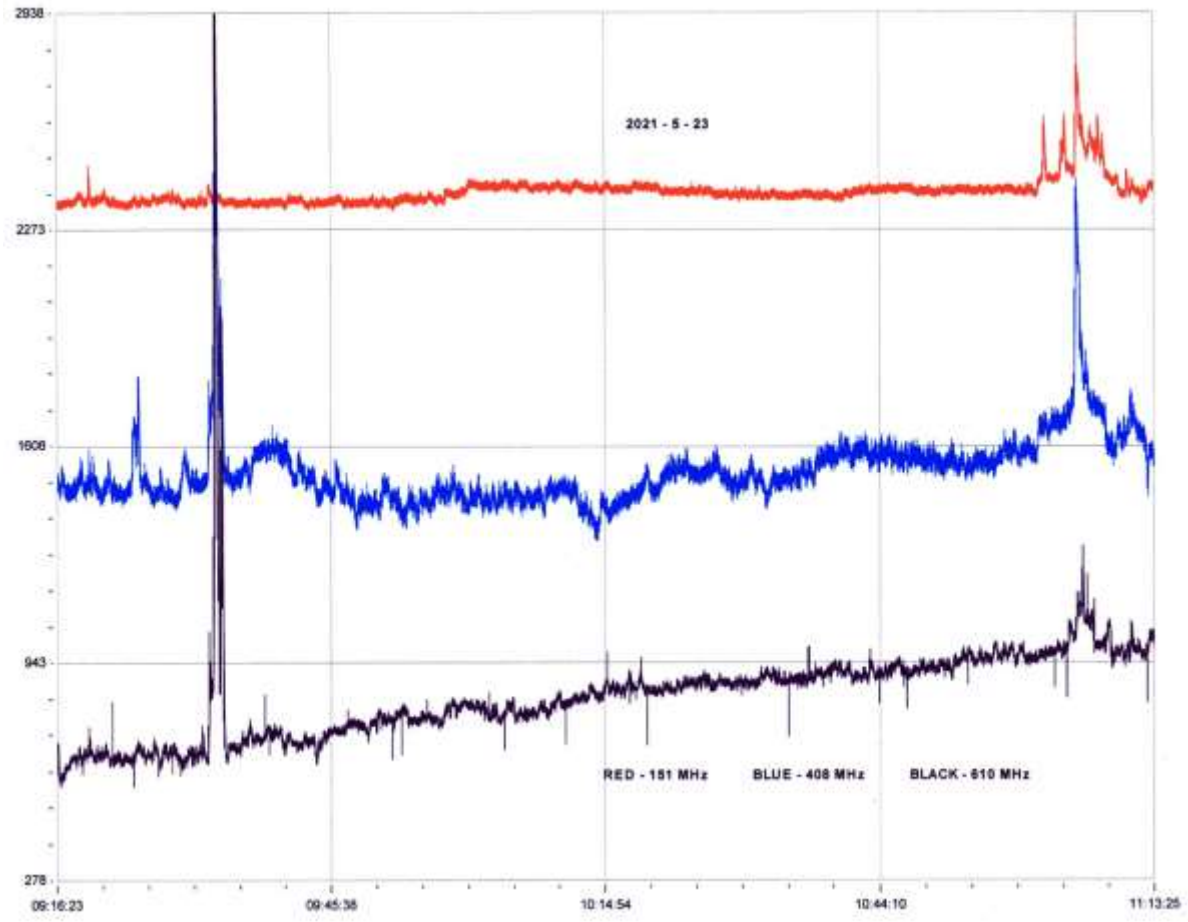

In Colin Clements' recording, above, the M1.1 flare is at the far right, with the C2.4 flare at the left. Mark Edwards' VLF chart is shown below, the 18.3kHz signal (green) also showing a clear SID for the B9.0 flare at 10:50.

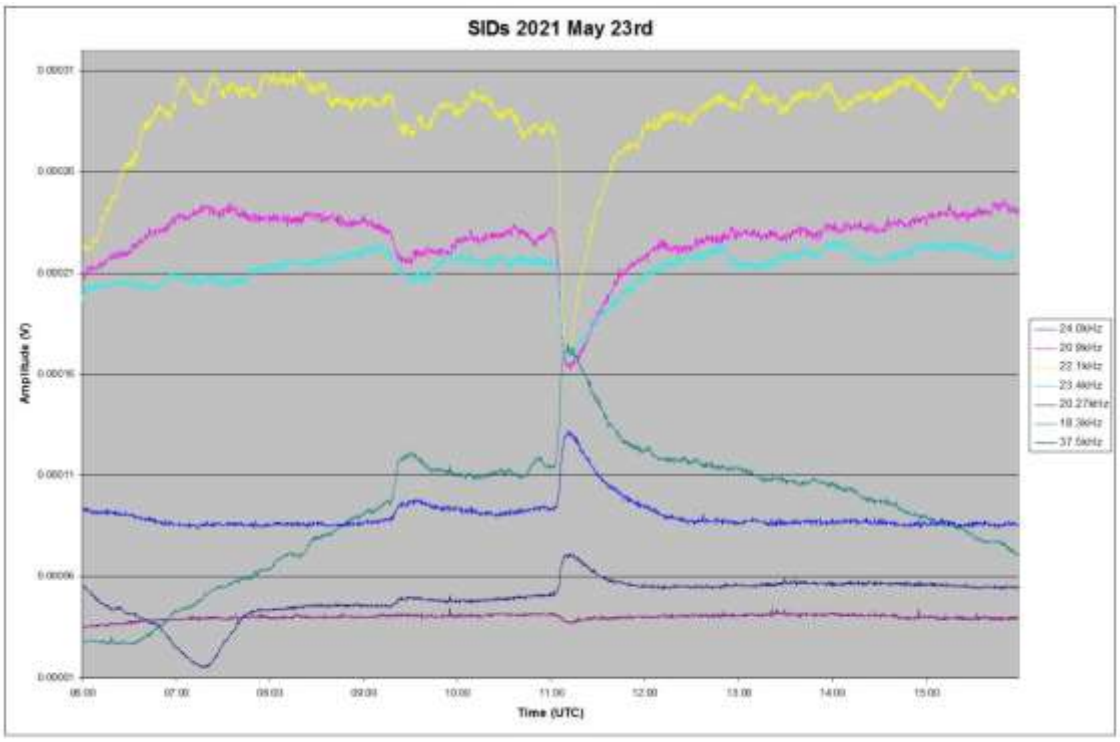

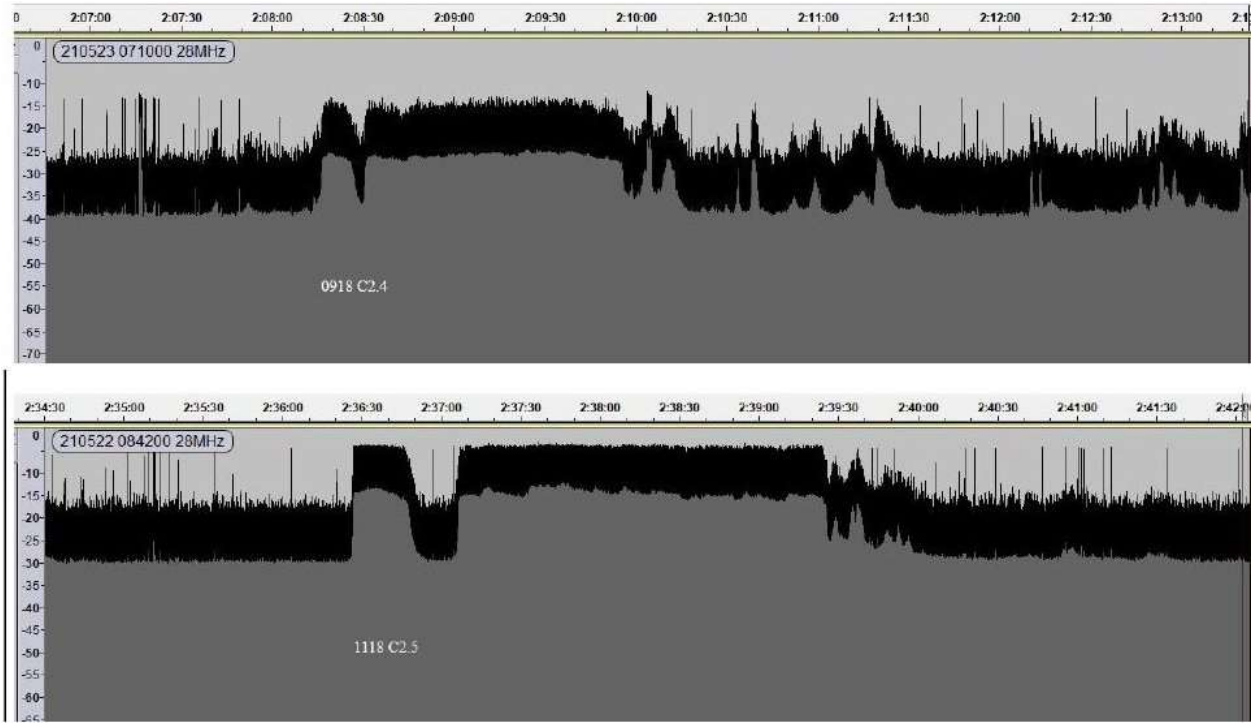

These are the 28MHz recordings by Colin Briden of the C2.4 and C2.5 flares on the 23rd. Note that the horizontal axis shows time since the start of the recording, not actual time. The C2.4 burst lasts for about 2 minutes, while the C2.5 burst is about 3 minutes with a 10dB stronger peak signal. The month ended with a C3.0 flare shown as four well-matched SIDs in Paul Hyde's recording:

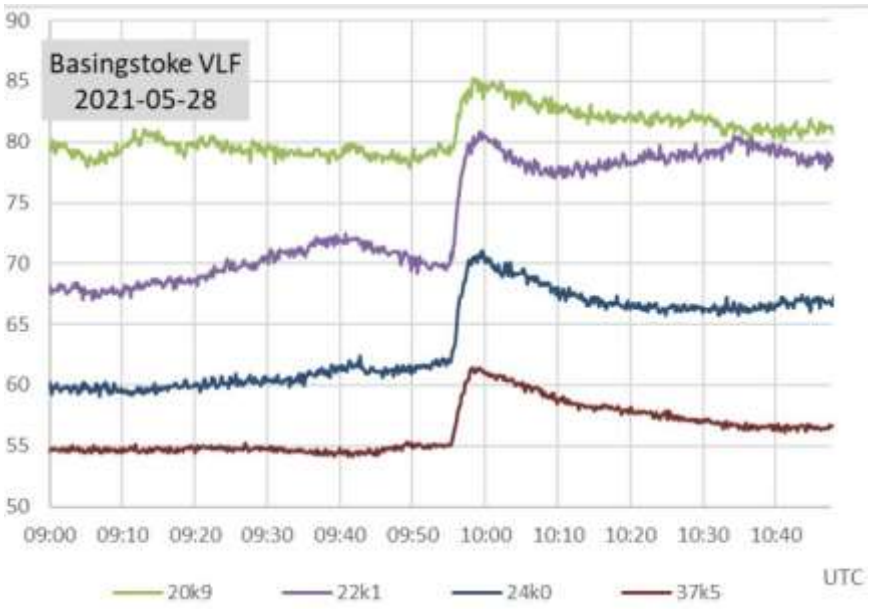

MAGNETIC OBSERVATIONS.

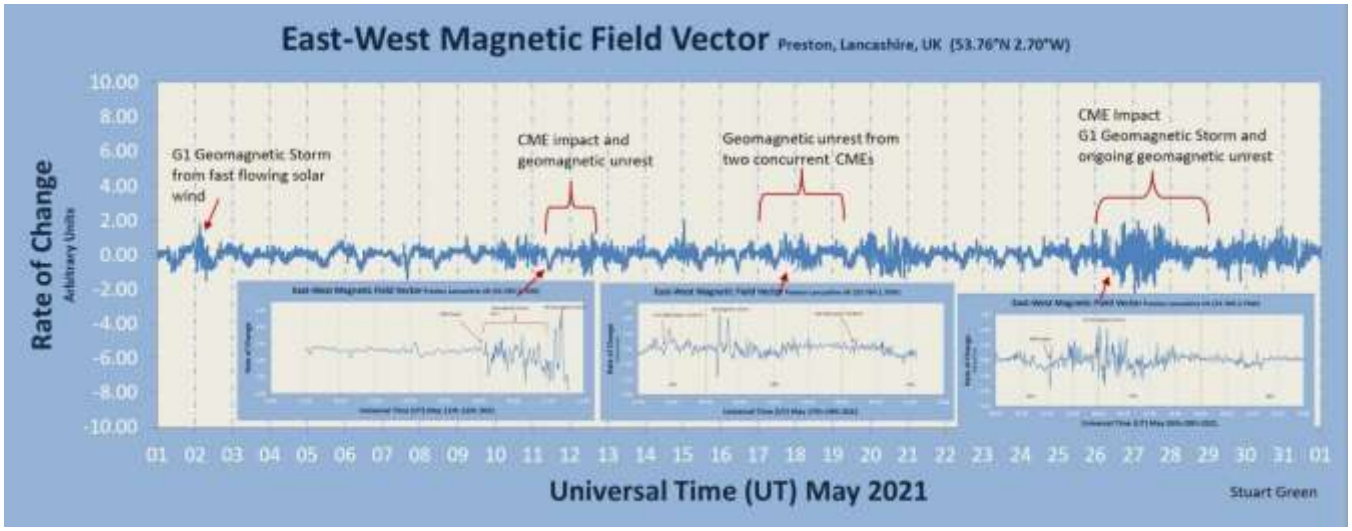

The increased solar activity has resulted in more CME than coronal hole disturbances in May. Stuart Green's chart of the month's activity shows the greatest disturbance at the end of the month with CMEs associated with the M-class flares. Our recordings show a fairly small shock at the CME arrival time around 13:00UT on the 26th, visible in the chart from Nick Quinn:

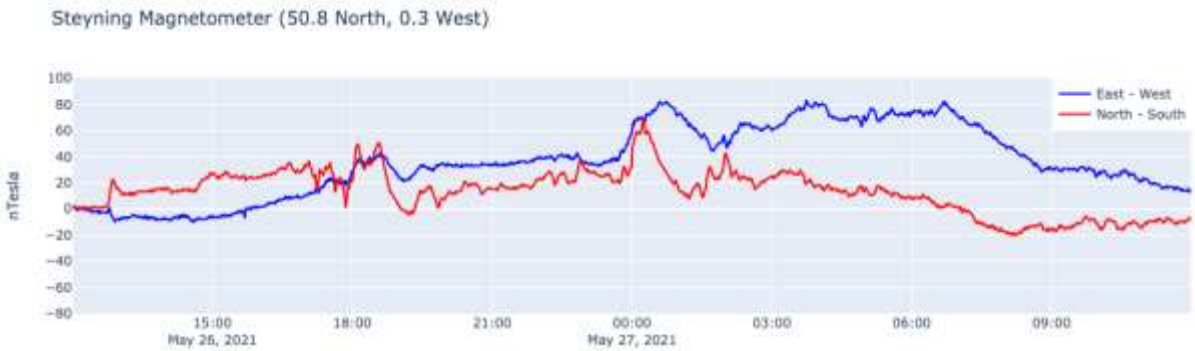

A disturbance of up to 100nT followed into the morning of the 27th, fading out by midday. SOHO images show this to be linked to the flares on the 22nd. A much clearer shock arrival can be seen at 06:39:29UT in Nick's chart from the 12th:

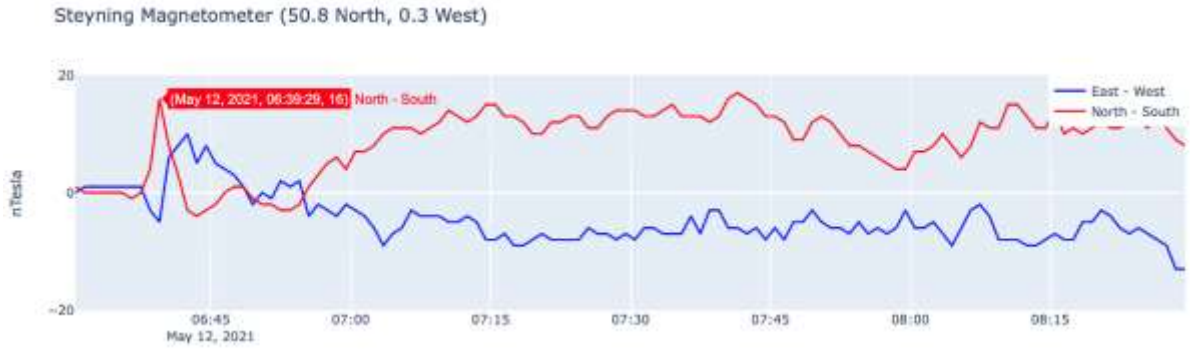

SOHO images first show the CME on May 9th from a filament eruption. The disturbance continued through the day, but had largely faded out by midnight. The activity is shown in Roger Blackwell's recording on the next page:

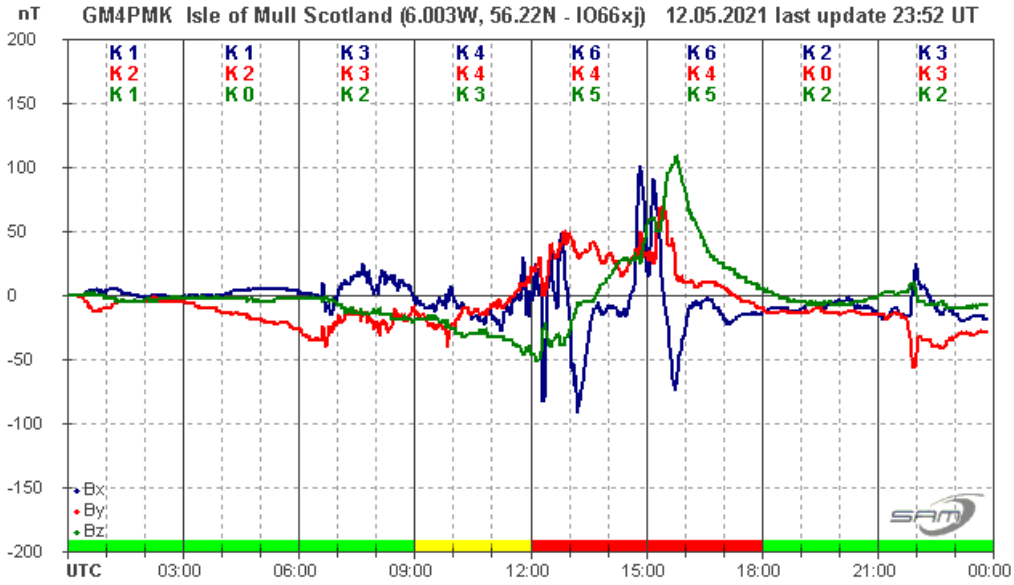

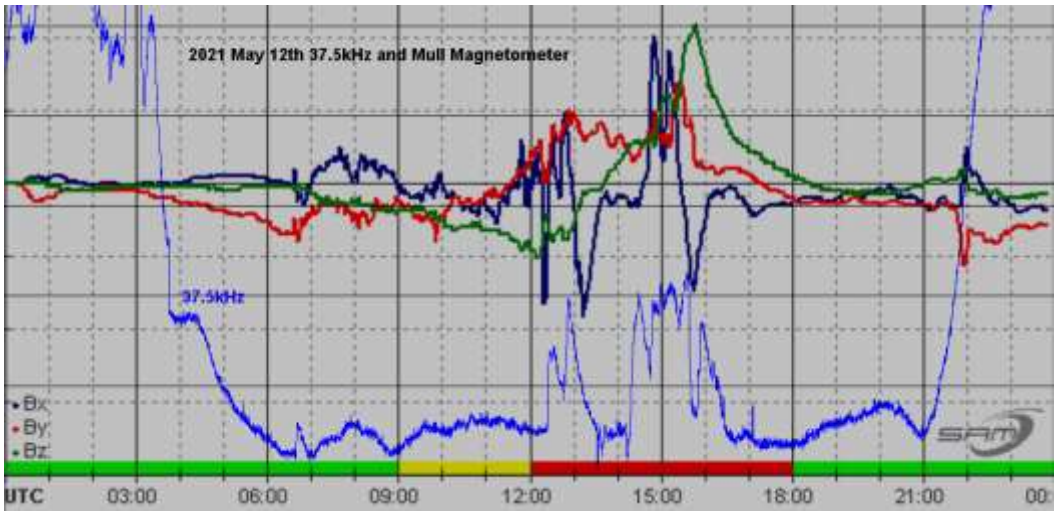

Mark Edwards has added his 37.5kHz recording to Roger's magnetometer, showing some strong VLF activity during the afternoon. The small burst of activity around 22:00 does not appear to be another CME impact, but was too late to cause any VLF disturbance. Also of note is the very small SID-like feature coincident with the initial CME shock. This also shows well in Colin Clements' 37.5kHz recording, timed at 06:40UT.

SOHO images show another strong CME leaving the sun in the evening of the 13th, although no source was given. It produced a very small magnetic disturbance on the 18th. A coronal hole high speed wind became effective late on the 19th, with some fairly mild disturbances through the day on the 20th. Colin Clements' chart on the next page shows this well, despite some local interference between 09 and 10UT.

The Radio astronomy Section webinar series has been very popular, and will be continuing. For full details of the programme and joining instructions, please go to the BAA website where they are listed along with the other BAA events.

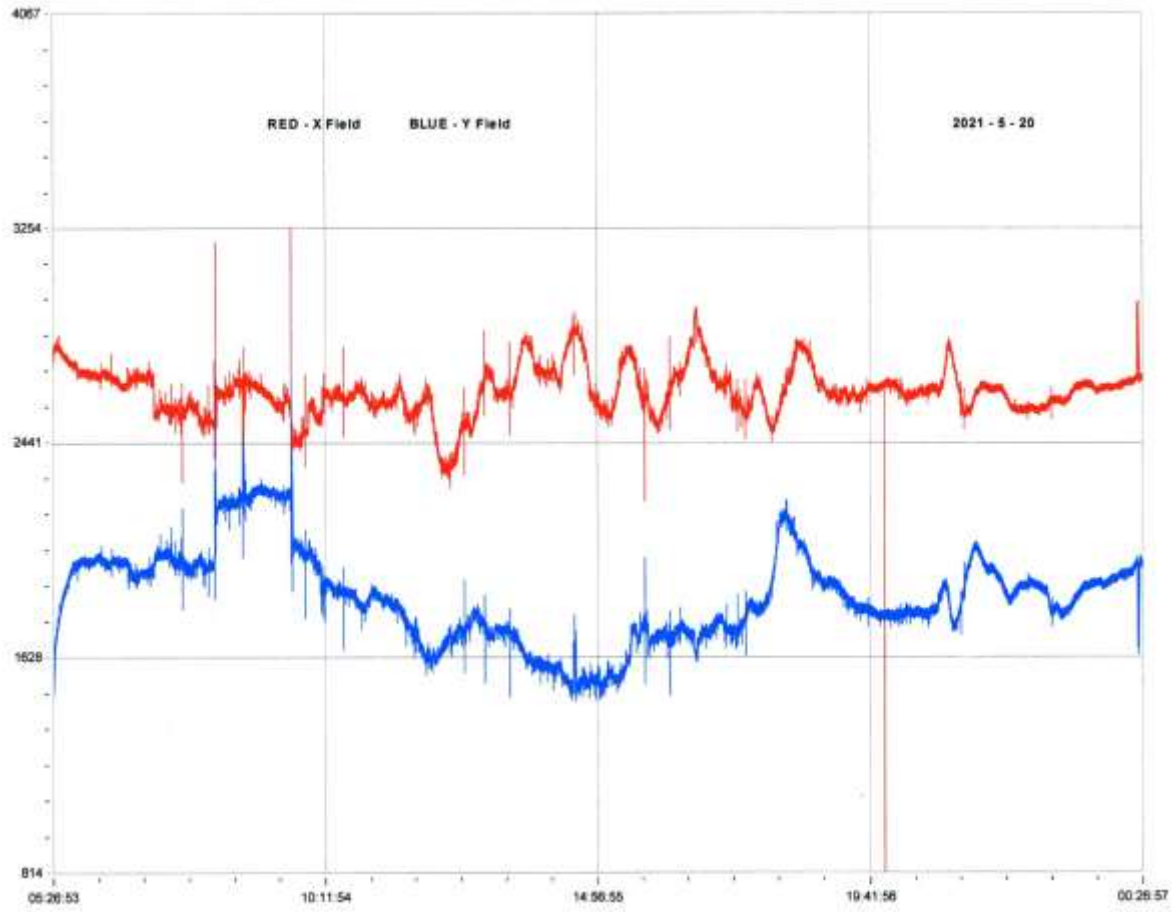

Magnetic observations received from Roger Blackwell, Colin Clements, Stuart Green, Paul Hearn, Andrew Thomas, Nick Quinn and John Cook.

BAA Radio Astronomy Section **2021 JUNE**

June flare activity was lower than in May, with no M-class flares recorded. The strongest flare in the X-ray data being the C3.7 flare widely recorded on the 9th. There were plenty of small B-class flares, mostly far too weak for detection as SIDs. The annular solar eclipse on June 10th has created some interesting VLF recordings. The path of annularity was from central Canada through northern Greenland and on to eastern Siberia. Here in the UK it was a small partial eclipse, but its effects were recorded on the 24kHz and 37.5kHz signals.

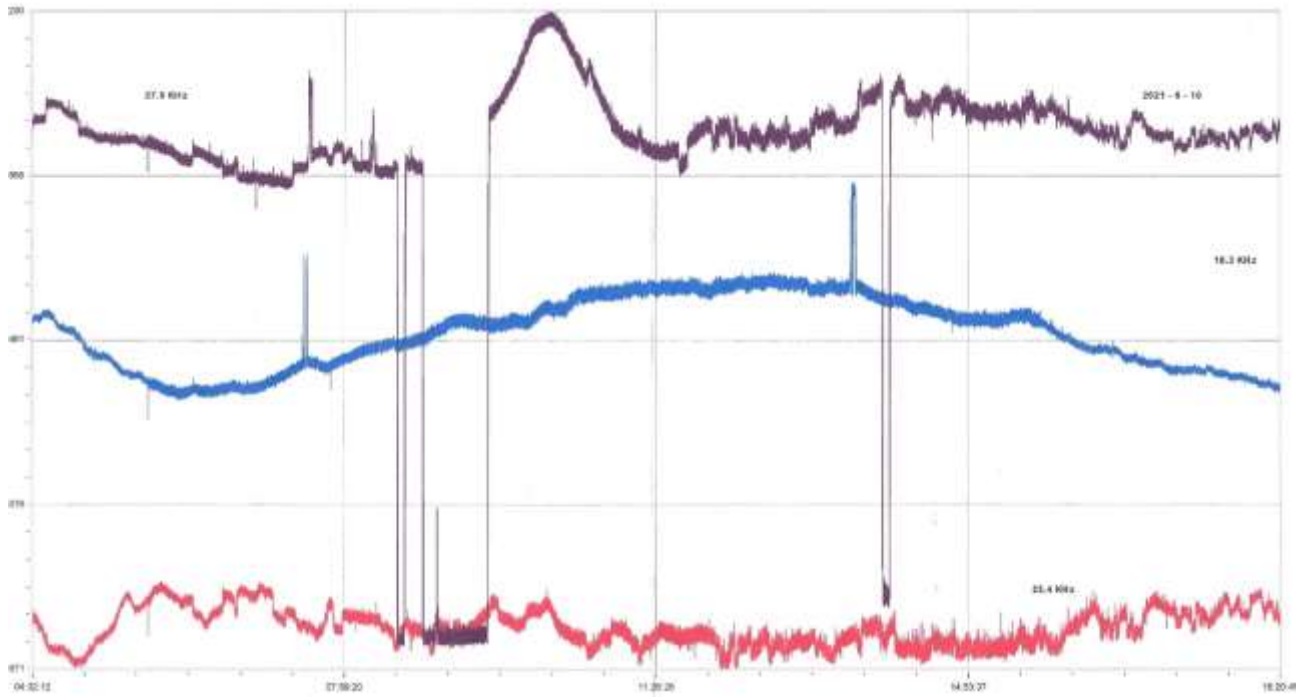

This recording by Colin Clements shows the 37.5kHz signal from Grindavik, Iceland, at the top, with 18.3kHz (blue) and 23.4kHz (red) for comparison. There is a break in the 37.5kHz signal just before a distinct rise in strength during the eclipse. The signal then returns back to normal with another small break in the afternoon. The other two signals remain unaffected during the eclipse period. The centre point of the path to Iceland would have seen a much greater partial phase compared to the other two signals.

Paul Hyde monitored the 24kHz signal from Cutler, USA. The centre point of this path is also much further into the eclipse path, and his recording on the next page shows another rise in signal strength during the eclipse (blue trace). The orange trace shows the same signal on June 8th including the two SIDs present.

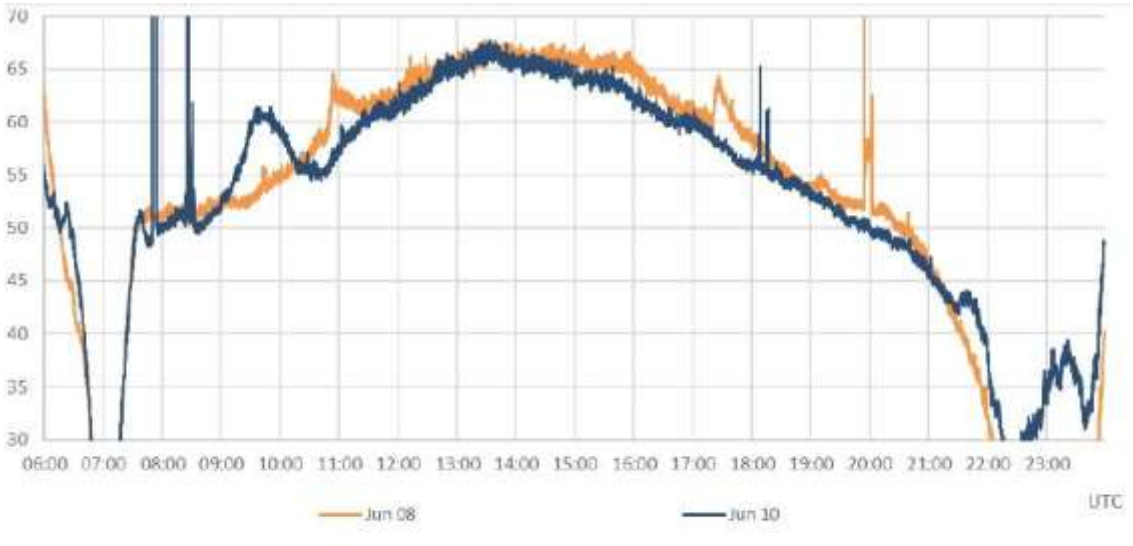

2021 Solar eclipse at 24 kHz from Basingstoke UK

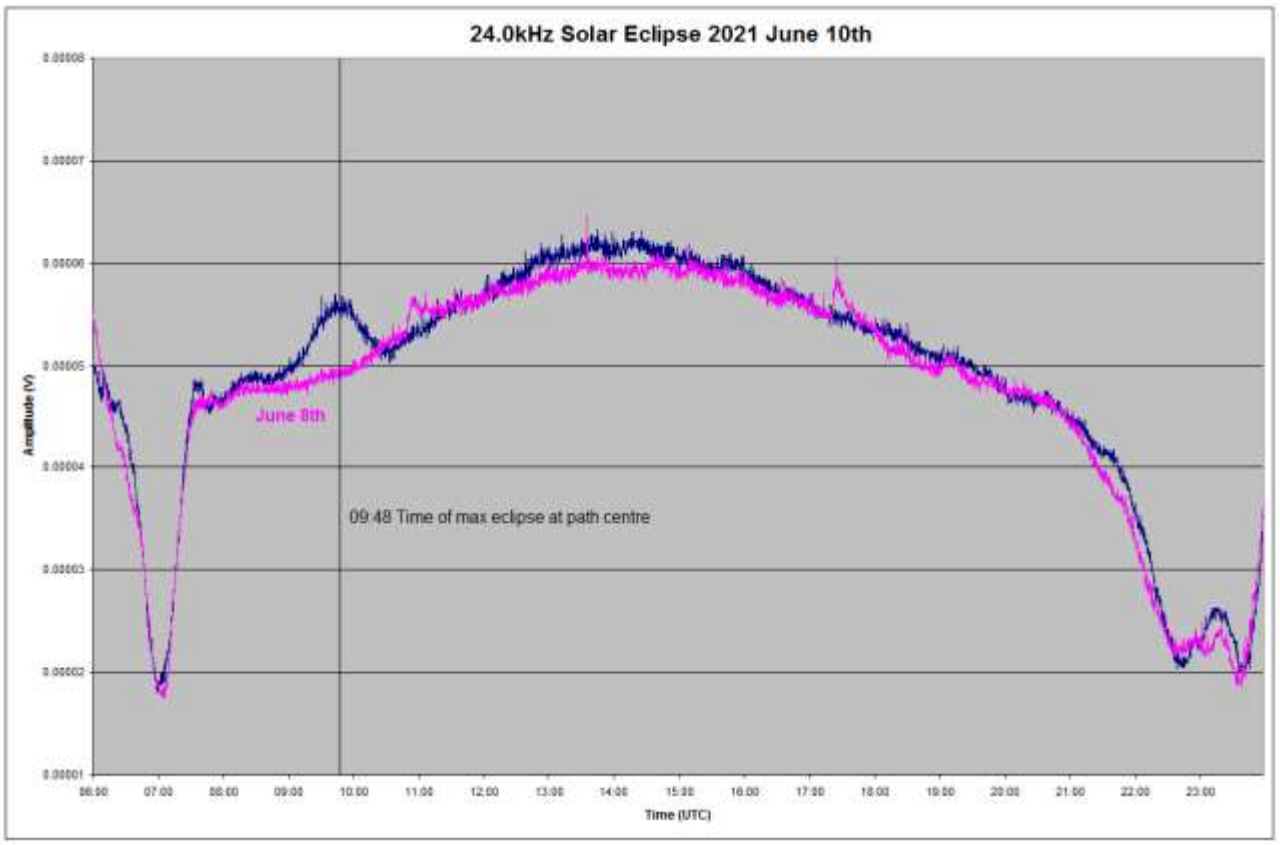

This recording by Mark Edwards again shows a rise in signal strength at 24kHz during the eclipse, with June 8th added for comparison. During a solar eclipse, the ionisation level of the D-region would be expected to decrease, similar to that seen during sunset. The sunset signal strength falls, while it has risen in all three recordings during the eclipse, a result that was not expected. It is interesting comparing this with the much larger partial eclipse of 2015 March 20th. An analysis of observations from that eclipse was published in the section's ragazine Volume 2 issue 4 from 2015 May. It can be downloaded from our pages on the BAA web site. Some recordings were also included in the 2015 March Summary.

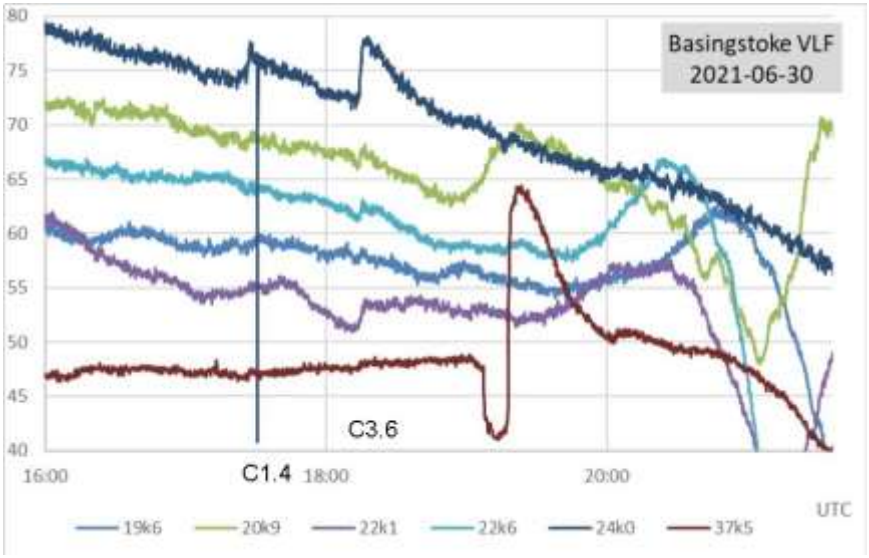

This recording by Paul Hyde shows activity on June 30th, both SIDs showing clearly at 24kHz. The other signals are far less clear, the flares occurring as they fade towards sunset. They do not show at all at 37.5kHz, with just a very odd transient visible around 19:00 - 19:30.

MAGNETIC OBSERVATIONS.

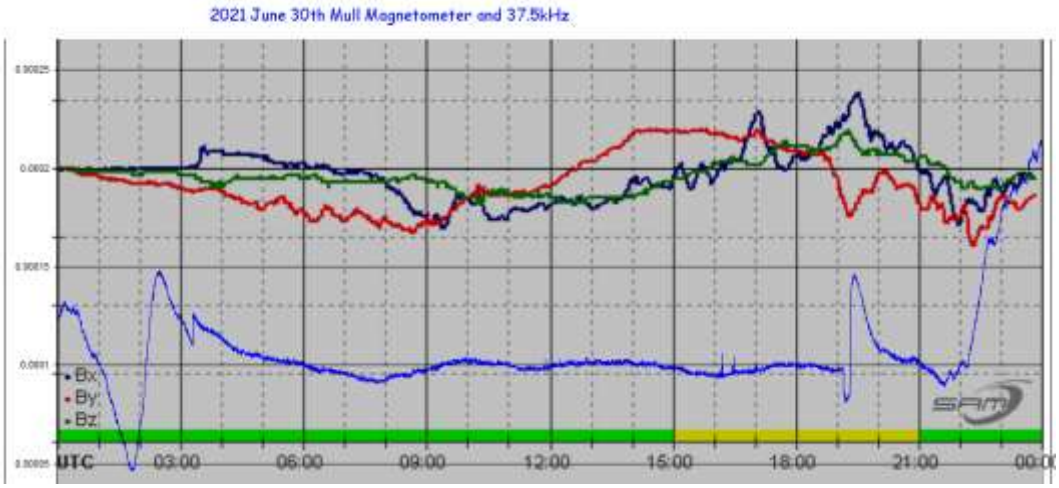

Mark Edwards has overlaid his 37.5kHz signal from the 30th on the magnetometer recording by Roger Blackwell. This also shows the unusual transient seen in Paul's recording above. The peak of the transient aligns well with the dip in the By magnetic signal. There is also a sharp rise in the signal at 03:18, occurring before the small Bx magnetic signal. This 37.5kHz rise matches the amplitude of the fall just after 19:00, giving the impression of a transmitter change. Subtracting that change leaves a much clearer magnetic effect on the VLF signal, similar to those seen before.

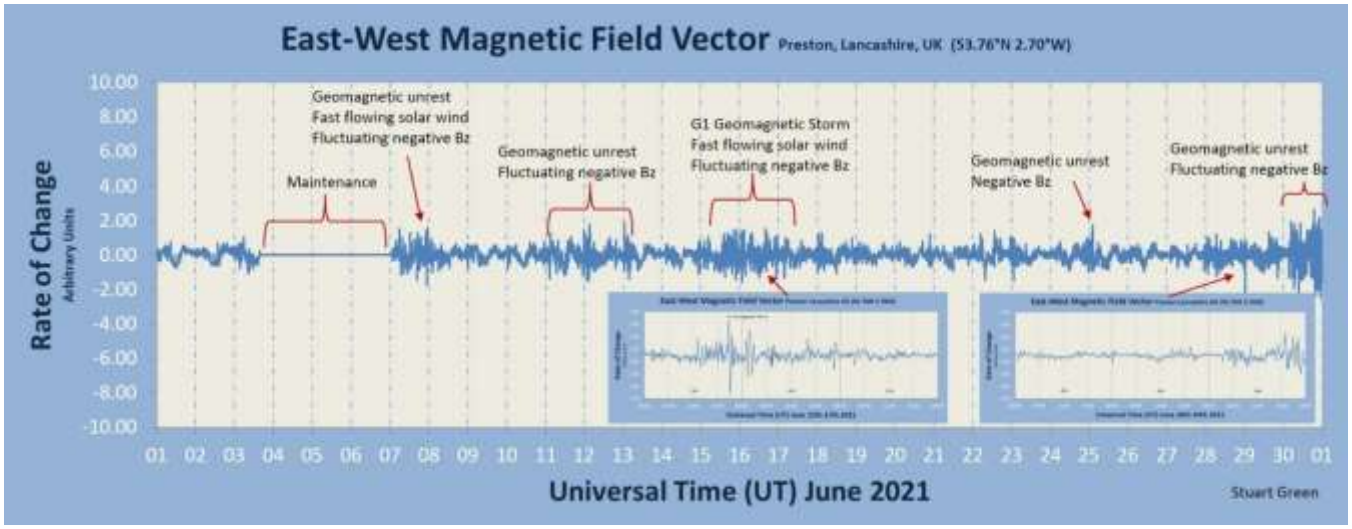

Stuart Green's summary for June shows a lower level of activity compared to previous months. There was a three day break for maintenance early in the period, but nothing of interest seems to have been missed. The most active period was on the 30th, already illustrated above. The Bx transient at about 03:30 in Roger Blackwell's recording appears to be the arrival shock of a CME seen in satellite data from the 27th. Its source is not clear, but may have been a glancing blow from an eruption on the solar limb as seen from Earth. The build-up of activity can be seen through the day, and continued into the morning of July 1st. Another CME arrival shock can be seen in this recording by Nick Quinn at about 13:30 on June 2nd:

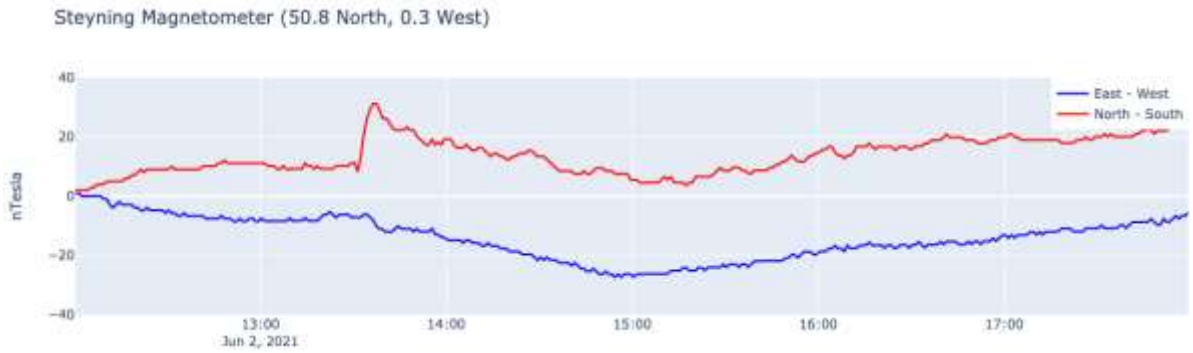

Satellite data links this to a CME on May 28th, but it produced no further significant magnetic disturbance.

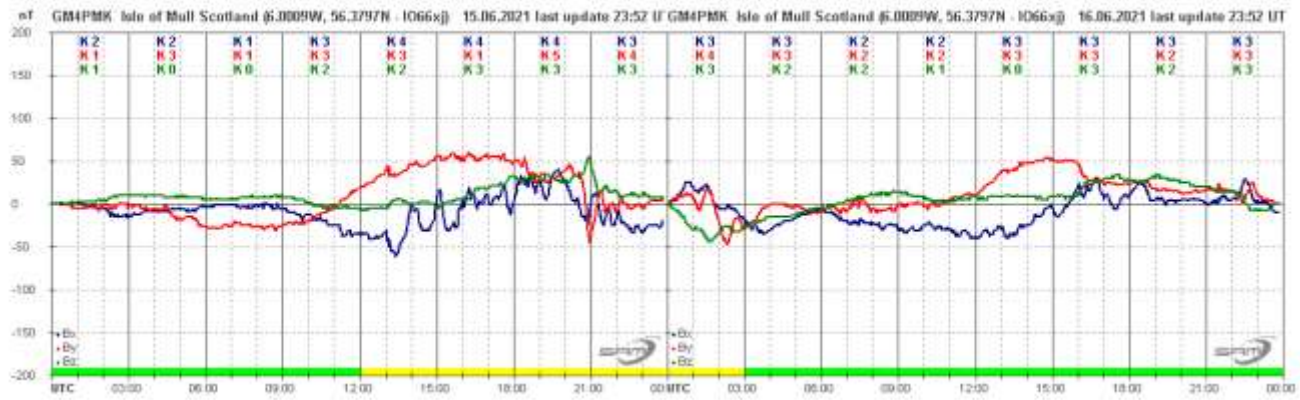

Coronal holes have been much less frequent over the last few months as sunspot activity has increased. A large south pole to equator coronal hole was present around mid-month, its high speed winds producing the disturbance shown in this recording of June 15th and 16th by Roger Blackwell. It may well be a reappearance of the coronal hole seen on May 19th.

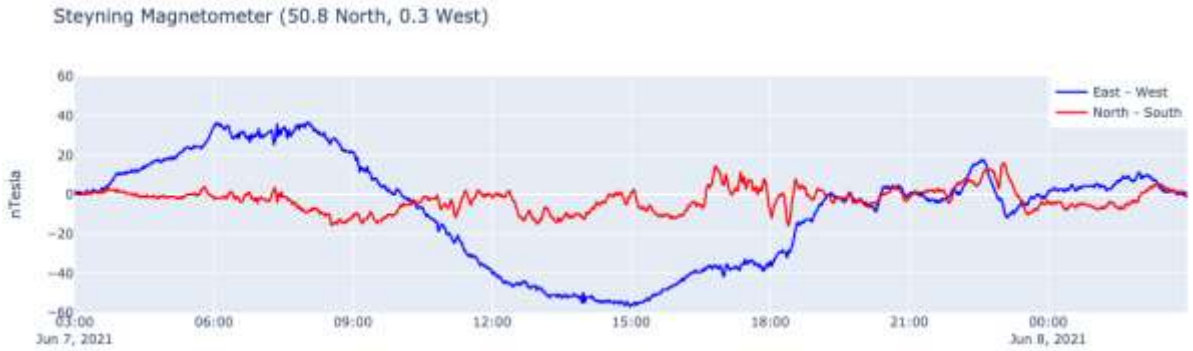

This recording by Nick Quinn shows a large swing in the east-west component of the field through the day on the 7th, the north-south component showing more rapid variations. The source appears to have been a high speed wind as noted by Stuart Green.

Magnetic observations received from Roger Blackwell, Colin Clements, Stuart Green, Nick Quinn and John Cook.

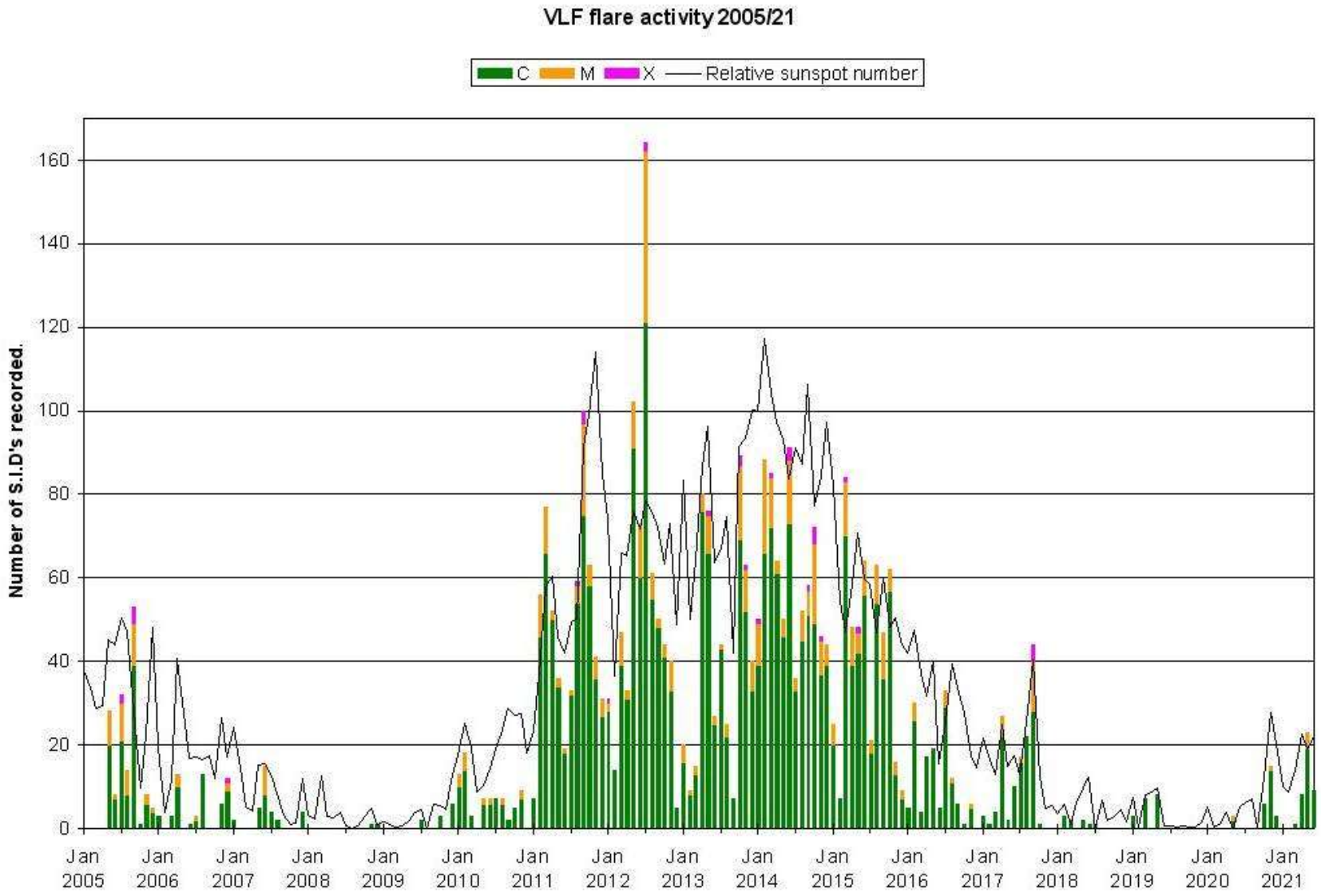
VLF flare activity 2005/21
C
M
X
Relative sunspot number
Number of S.I.D's recorded.
0
20
40
60
80
100
120
140
160
Jan 2005
Jan 2006
Jan 2007
Jan 2008
Jan 2009
Jan 2010
Jan 2011
Jan 2012
Jan 2013
Jan 2014
Jan 2015
Jan 2016
Jan 2017
Jan 2018
Jan 2019
Jan 2020
Jan 2021

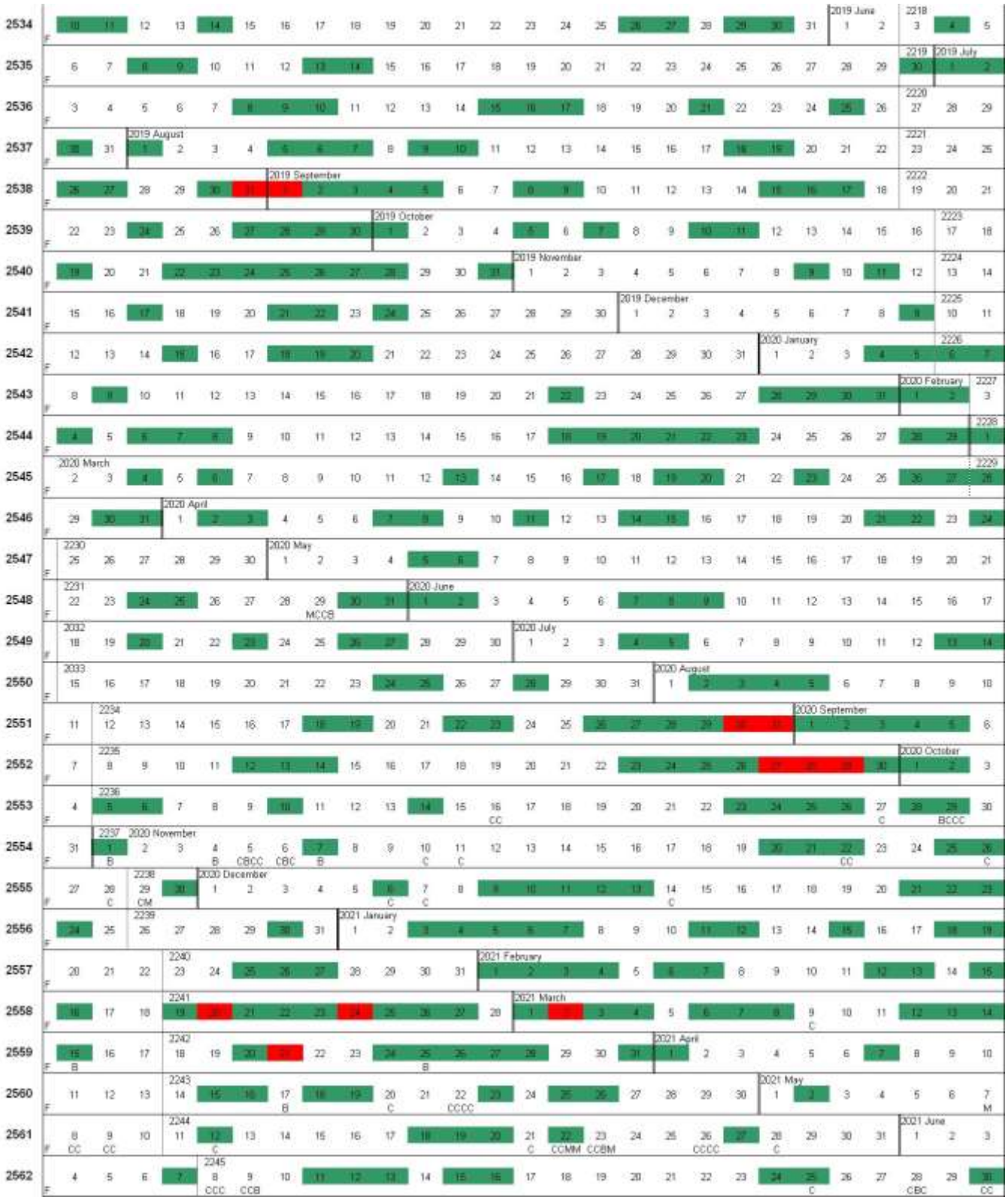

INTERNATIONAL EARTH ROTATION AND REFERENCE SYSTEMS SERVICE (IERS)

SERVICE INTERNATIONAL DE LA ROTATION TERRESTRE ET DES SYSTEMES DE REFERENCE

SERVICE DE LA ROTATION TERRESTRE DE L'IERS
OBSERVATOIRE DE PARIS
61, Av. de l'Observatoire 75014 PARIS (France)
Tel.: +33 1 40 51 23 35, e-mail: services.iers@obspm.fr, http://hpiers.obspm.fr/eop-pc

Paris, 05 July 2021

Bulletin C 62

To authorities responsible for the measurement and distribution of time

INFORMATION ON UTC - TAI

NO leap second will be introduced at the end of December 2021. The difference between Coordinated Universal Time UTC and the International Atomic Time TAI is:

from 2017 January 1, 0h UTC, until further notice: UTC-TAI = -37 s

Leap seconds can be introduced in UTC at the end of the months of December or June, depending on the evolution of UT1-TAI. Bulletin C is mailed every six months, either to announce a time step in UTC, or to confirm that there will be no time step at the next possible date.

Christian BIZOUARD, Director
Earth Orientation Center of IERS
Observatoire de Paris, France

_____

Earth rotation acceleration: the length of day (LOD) since decreases in average by 0.3 ms/year since 2016:

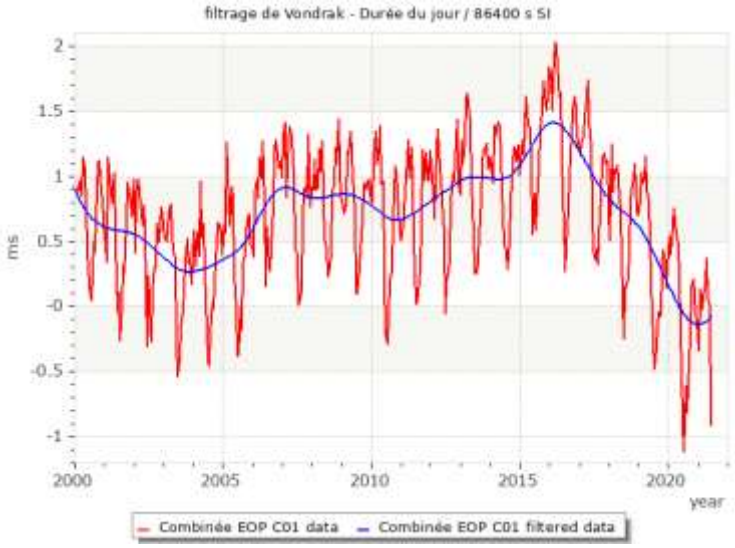

Special Article

Experiences of Attu Expedition ~ by Grote Reber ~ 9/3/1950 through 9/13/1950

Transcribed from 15 pages of notes hand-written by Grote Reber while he prepared to make radio observations at 465 MHz (65 cm wavelength) of the solar eclipse on 12 September 1950. Initial comments in italics and transcription by Whitham D. Reeve, Anchorage, Alaska.

Reeve comments: A total solar eclipse took place on 12 September 1950 but the eclipse path only crossed United States territory at Attu Island, the outer-most island in the Alaska Aleutian Island Chain. An expedition to Attu was conceived and organized by John. P. Hagen of the Naval Research Laboratory (NRL) to observe the eclipse. Ten people participated in the expedition including Grote Reber, who worked for the National Bureau of Standards (NBS) at the time. Radio observations were made at 0.8, 10, 20 and 65 cm wavelengths (37.5 GHz, 3 GHz, 1.5 GHz and 465 MHz). The expedition even setup an 8 inch eclipse camera/telescope, a fool's errand considering the Aleutian Islands' notoriously and persistently poor weather. The Korean War was well underway by September 1950, so it is quite amazing this expedition – primarily involving Navy personnel – even took place.

The expedition personnel spent almost a month on Attu installing equipment at Alexai Point on Attu and preparing for the eclipse. At the time, Attu was inhabited only by about 25 Navy and Coast Guard sailors who operated and maintained a weather (aerological) station and a LORAN-A station. During World War II, two sets of runways were built at Attu, one adjacent to Casco Cove and Massacre Bay, the site of a wartime Naval Air Station and submarine repair facility (among other things), and another at the Army Air Forces base at Alexai Point. During the war both airfields were used to launch bombing campaigns against the Kurile Islands of northern Japan. The Alexai Point facilities were abandoned at the end World War II.

Reber kept hand-written notes of his time on Attu, and I obtained them through {NRAO}. My transcription includes, to the extent possible, Reber's (mis)spelling, capitalization, (lack of) punctuation and (questionable) grammar. Reber refers to the Navy's weather station at Massacre Bay, where the group was housed, as an "Aerological Station". The notes are interesting reading about a time when everything was done by hand the hard way. Apparently, no scientific papers were produced because of all this work except one by Reber (see References).

It is obvious from his notes that Reber did a lot of bellyaching (maybe from being around sailors, who, according to a sailor friend, have a sacred duty to bellyache). It also is obvious that the expedition was poorly planned in spite of a preparatory trip made to Attu by two NRL personnel prior to the expedition itself. Reber refers to Mauna Kea, Hawaii and Washington DC – Sterling, Virginia several times in his notes. These apparently were locations for some type of future work not associated with the solar eclipse observations at Attu but that he hoped would incur better planning. Reber's notes say nothing about the radio observations themselves or the electronic equipment, but several photographs of the equipment are in the NRAO archives {NRAO-Phto} and a few are included here in no particular order (see Credits).

Based on other archival information (NRAO-Arc}, the group of scientists traveled to Attu by air (probably on a Navy plane). Their equipment apparently went by sea and was carried at least part of the way (Adak to Attu) on the Navy tug USS Tawasa. The actual amount of equipment was not recorded, but it appears that at least 10 tons was transported and setup.

Reber commented on the weather each day of his visit to Attu and those comments are also transcribed here. Poor weather – rain and strong winds – blew through the area on eclipse day. Because of the weather and all the other problems, the data obtained were not very good according to a member of the group on Attu, Cornell H. Mayer {Mayer}.

I first visited the Aleutian Islands as a 5-year-old in 1953 and then flew there frequently in the late 1950s and throughout the 1960s. Given the extensive wartime activity during World War II, the Aleutians were always fun to visit and explore, especially before the government "cleaned up" their huge wartime and post-war environmental calamities. I never saw it, but I was told about a sign at the Attu airport that read "Attu is not the end of the world, but you can see it from here." Attu also is known as "The last place on earth."

Following is a transcription of Reber's notes with his photographs interspersed:

Apparatus viewed from northwest, Attu, Alaska, eclipse expedition site

Road: The road from aerological station to Alexai Point is very bad. The airline distance across Massacre Bay is only about six miles. The shortcut route along edge of bay is about ten miles. However, detours bring the distance up to about twelve miles. The total elapsed time of transit is about 80 to 95 minutes. The original road built by army engineers in 1944 wound its way along edge of bay. Numerous cuts were made thru sides of hills which run down to water. This material was used to build up the intervening beaches to a sufficient height. Apparently the last detachment of troops left Attu in the summer of 1948. Since then the roads have deteriorated due to neglect. Floods due to melting snow last spring and heavy rains washed out several places in the road and particularly around bridge structures. These were not fixed at all, or done very badly. Several places the grades are over 30% for short distances where the trail dips down into and climbs out of washouts. Thus the vehicle must operate in low gear about half the time. Four wheel drive is imperative. None of the road is paved. The surface merely being crushed rock. While the drainage is excellent and no puddles exist in the road, a very bad dust is setup behind each vehicle. This not only covers any following vehicle but also may be blowing into originating vehicle by strong winds which are nearly always present. Some oil or asphalt covering is necessary to settle the dust. The was apparently built on a basis of expediency. Thus it winds around a great deal. This prevents any speed being attained on even the good parts. Since a considerable number of cuts were made where the ridges of the hills went right down to the sea, it was false economy not to enlarge these, or tunnel, in order to straighten out the road. Since both sides of the road are near sea level and it follows the shore, the maximum altitude of the road is less than 100 feet. Thus, there is no reason for steep grade.

To the occasional traveller, a bad road is merely an irritation. However, to one who must traverse it two or more times a day the matter is intolerable. The price paid for a bad road is

(1) Time of transit three times what is necessary. Transport done on paid time which is waste of salaries.
(2) Great wear and tear on vehicles. Trucks not available due to times for repair. High repair cost.
(3) Very poor gas mileage due to much use of low gear.
(4) Bad effect on personnel who are all worn out by continuous bouncing and in a very bad humor when they arrive at job.
(5) All merchandise must be securely tied down in vehicle to prevent shifting or falling out. This wastes time at both loading and unloading.
(6) Merchandise is broken by bouncing.
(7) Merchandise and personnel covered with dust at end of trip. Cleaning of both is a nuisance, aggravation and waste of time.

Loading crates of eclipse expedition equipment onto truck, Attu, Alaska

(8) More vehicles needed due to greater use, large times out for repairs.
(9) Increased possibility of accidents on road. This is particularly true in wet or freezing weather.
(10) A poor road will require more costly maintenance of (way?).

All the above effects are visible on run between Washington and Sterling which has a high use factor. The same are even more visible on the run between Massacre Bay and Alexai Point which has a lower use factor but much worse condition. All the above must be considered in relation to any venture on Mauna Kea. Since no personnel will be housed at top, the run must be made twice a day or more. The price of the above inconvenience may easily be $10,000 per year. If money is worth 7% it will be profitable to spend $150,000 on road to reduce operating expenses.

Shelter: The only shelter at Alexai Point is an old quonset hut with one end knocked out. Part of it has a cement floor but the windows and rear door are gone. These were closed with celotex and an improvised lighting system installed. No heat whatever is provided. A few benches were installed to hold equipment. No chairs were provided. The open end of the hut was partially closed with celotex; but no front steps or porch was provided. This bad set of circumstances was due to poor planning and no realization of the consequences. The price paid for this situation is

(1) Personnel not anxious to go to work because it will be a long cold day. Working at a cold job where it is possible to warm up for ten minutes every hour at all is something else.
(2) The dampness is worse than the cold or exposure and wind. By raising temperature from 50° at 100% to 70° at 50% is a tremendous improvement merely by applying heat.
(3) Dampness causes tools to become slippery and hard to handle also processes of rust are hastened. Work is delayed.
(4) Even a slight drizzle will cause the personnel to be (irritable?) because there is no possibility of drying out.
(5) The old quonset was adequate shelter from wind except when it came from direction of open end.
(6) No plumbing facilities were available. Therefore it was impossible to even wash when hands became dirty or greasy.

Transport: The only transport available was an old ten wheel truck of about 5 ton capacity with an open body having sides about 2 feet high but no tail gate; and a jeep with metal top and doors of homemade local vintage.

Both were in poor order in that the doors didn't shut. Where tied shut no ventilation was provided, fumes from leaky exhaust was insufferable, the odometer didn't work and they were hard to shift plus a long series of flat tires. One wheel came off from truck because studs on brake drum broke off. The short wheel base of jeep made it very rough on the roads. While the truck had a longer wheelbase and more wheels it rode roughly also due to stiff springs. Once we had it loaded with about 6 tons of equipment and it rode much more smoothly. It was necessary to haul most (8 to 10) of the party in the truck because the commander wanted to use the jeep. The wind, rain and dirt made the trip miserable. Some mattresses were put in bottom of truck and this helped a bit. However, there was nothing to hold on to inside the truck and the personnel banged around badly, after 45 minutes of this treatment the rider was in no mood to do constructive scientific work. It was found that the truck rode quite a bit better if all the air was let out of the eight rear tires. This was alright for hauling personnel, but not for hauling heavy merchandise.

Any venture on Mauna Kea will require closed vehicles for hauling personnel. A heavy station wagon such as a Pontiac or Mercury will be satisfactory for scientific personnel and light apparatus. The contractor will need a good bus. It should no be like bus used from Washington to Sterling which is merely an army post bus and having seats which tip the wrong way. It should be like a Greyhound bus with comfortable seats and plenty of room. The drive up Mauna Kea will be 30 to 40 miles which is commensurate with drive from Washington to Sterling. Thus even tho the road is good, comfortable transport will be needed.

465 mc apparatus (10 foot radar mirror) from north, close view, Attu, Alaska, eclipse expedition site

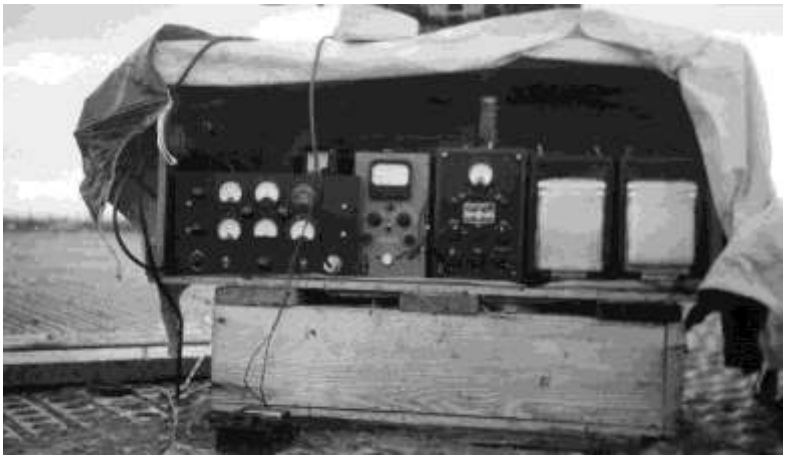

465 mc equipment, Attu, Alaska, eclipse expedition site

Planning: Aside from planning the scientific details of the apparatus for eclipse measures, the planning was practically non-existent. Hagen and Harrison made a trip to Attu for a few days in May. While the former is conscientious and tries hard, the latter is a loud mouthed incompetent. What transpired in May is unknown, but of small consequence. Any arrangements they made with the Aerological Station personnel were purely of the verbal or gentlemans agreement type. Between May and August 29th the Navy replaced all but one or two of the men present in May. The new officer in charge arrived about a week before we did. The new outfit knew nothing about any arrangements made with the old outfit and cared even less. We were provided with one old truck and a jeep plus any amount of gas we needed, provided we pumped it ourselves. This was the extent of cooperation of Aerological Station personnel. Within a few days a memorandum appeared on the bulletin board by the new officer in charge which notified the station personnel that Alexai Point was out of bounds. This effectively squashed any faint interest any of the crew might have had in our work. Thus it was now impossible to recruit any sailors to help on a goodwill basis during off hours. We were entirely on our own.

38,000 mc apparatus from south, Attu, Alaska, eclipse expedition site

Facilities: The island was an immense supply dump at the end of the war, all kinds of equipment were available. About 1947 the Army came and took the best but left a wide variety of stuff. This was allowed to stay outside and rust even tho a great quantity of buildings were available. Thus everything was broken down and nothing would run. All this stuff seems to be written off as war loss because no one is responsible for it. I counted three quite similar motorized cranes. None would run, but all had some of the tires still inflated. Some of the windows were broken and one had a radiator missing. It seems very likely that one good one could have easily been made out of the three by a few days work of interested people. Since we had no crane, all heavy boxes we had to be lifted by us; a stupid result of mismanagement. The situation on cement mixers was the same, a dozen of all sizes were available but none would run. Thus all cement was mixed by hand using shovels. Since no one wanted anymore of this back breaking labor than possible, the foundations were made as small as possible; in fact, too small. A direct consequence was that the eclipse apparatus was rather unstable and quite difficult to get and maintain oriented. It also blew in the wind with considerable vibration. Thus the data somewhat impaired and this of course is the ultimate end of the expedition. A lot of time was wasted trying to bolster up the mountings with little success using planks. The foundations were poured on top of steel landing mat. This mat lay on sand and was quite springy. furthermore it transmitted vibrations over a considerable distance due to people walking (about 10 feet) and trucks moving (about 30 feet). The foundations should have been made directly in the sand with good wide bases. Unfortunately, no cutting torch could be found that would work. We had to dig all our own sand, gravel and boulders by hand because no operating power equipment was available. We hauled water in 50 gallon drums

from the Aerological Station to make the concrete even tho ponds of fresh water were available less than 200 feet away because no pumps could (be) found that worked and no good hose. When we ran out, I even hauled a dozen buckets by hand from the ponds. Hauling water up hill is work! All this heavy work was done by technically skilled personnel which was a great waste and created some ill feelings as the personnel felt they had other more important things to do.

The scientific apparatus arrived in thirty nine cases of various sizes up to 6' x 6' x 9' and weights up to 700 pounds. The cases were numbered for shipping identification but there were no packing lists. since the packing was done by the shipping room at NRL, only a vague idea was had of their contents. Thus the wrong ones were opened first.

Two gas engine generators of 10 kW capacity were available on small two wheel trailers. After the tires were fixed, these were found to be in good operating shape. While both were 60 cycle, one turned out to be 110 V single phase, and the other 220 volt three phase. This complicated the switchover system. Both used spark ignitions but fortunately were not bad when moved 200 feet from electronic equipment. It might have been otherwise. We hauled gas for these in 50 gallon drums. First it was hand pumped from ground to drum on trucks. Then pumped again into tanks of engine driving generator. Both, a lot more work. A bucket of gas was kept handy to wash ones hands in.

3000 mc apparatus from north, Attu, Alaska, eclipse expedition site

A preliminary group should have been sent out with adequate letters of introduction and authority to get affairs in order before the scientists arrived. A minimum of demands should be; one motorized crane in working order to lift heavy pieces; one cement mixer in order to make concrete; one motor shovel to dig sand, gravel and boulders; fix up quonset hut and install heating plant and wash facilities; layout north-south line and pour foundations in accordance with supplied plans; mount tank on truck or fix tank truck for hauling water; get sofas or combined seats for hauling personnel in truck and fix roads at important places. The last is a very important item and was very aggravating. All kinds of road building equipment including scrapers, shovels, drags and pile drivers were available but nothing was in operating shape. Plenty of rock drills and explosives were on hand also if quarrying were to be done. Immense quantities of piles, beams and planks plus hardware were available to fix bridges if necessary. All the makings of a first class construction group were available including at least 50 Caterpillar tractors of all kinds up to 20 or 30 ton jobs with diesel engines. Unfortunately, nobody was interested or cared. The staff at the Aerological Station was charged with running the station only and thats all. They seemed privileged to loot and destroy whatever else they wished on the island. Most were incompetent on matters other than their assigned duty. A Lt. was in charge. He seemed only mildly interested in the station and not at all in other matters. The navy policy is to replace all personnel after six months duty at this station. All hands (25 total) had only one idea in their minds. That was to get out as soon as possible after six months and to do as little as possible while on Attu. The feeling of unimportance and insecurity pervaded the entire establishment.

The question of foundations for telescope mounts was aggravating in more ways than one. Until these foundations were in, no mountings could be setup. With no mountings, no electronic gear could be installed. Until the electronic apparatus was installed nothing could be tried out and thus there was a lot of anxiety to learn what, if anything, was broken; and how much fixing would have to be done. Thus everything depended on the

foundations. Now the foundations had to be installed on north-south line so that the polar mountings would function. The maps were poor and the steel landing mat caused large errors in compass reading. Thus recourse was necessary to solar or stellar observations. A theodolite had been sent but nobody knew which box it was in, because there were no packing lists. When this was found, a long run of cloudy weather started. Altogether, about three days were lost on this mixup before the foundations were poured.

While two engine generators were available, no thought had been given to connections, regulators, etc. These were improvised in a crude way by semiskilled technicians on the job. Since the quonset hut was 300 feet from apparatus some housing was necessary for electronic apparatus. No provisions had been made. Some boxes with looted tarpaulins were erected in a rather unsightly mess and tied down to landing mat with ropes.

Quarters: The quarters for the men were in some ways better and some ways worse than expected. Six of the men (including me) were quartered in one room about 15' x 20' using foldable deck beds. Adequate locker space was available and a table with four chairs was present. Abundant light from overhead fluorescent fixtures was good. Two more men chose to live in a nearby quonset hut where there was more space but less light and heat. The other three lived with personnel of the station at various places. Most of us used the crews wash room. This caused an overload in morning but was reasonably satisfactory otherwise.

The food was good, hearty well cooked and plentiful. Fresh foods were quite lacking and none was groun on island and the ship came with supplies only once a month. Milk was served on average of once a day. Fruit consisted of apples (in not very good condition) and oranges. The milk seems to have come frozen from Seattle. When thawed it contained a lot of fine particles of wax from the cartons. These stuck to inside of ones mouth plus made it taste bad.

Antennas and equipment at Attu, Alaska, eclipse expedition site, viewed from west

Hours of Work: Breakfast was served from 7:00 to 7:30, lunch from 12:00 to 12:30 and supper from 5:00 to 5:30. Since it takes 40 minutes to get out to Alexai Point from Aerological Station, work would not begin much before 8:30 and we had to quit at 4:00 in order to get back to eat. A half hour was taken for lunch. This made a working day of 7 hours which wasn't bad, but a bit short. The main difficulty was that we were operating on Adak time which is about an hour and a half ahead of Attu local time. Thus we were really starting about 7:00 am and quitting at 2:30 pm. The mornings were always cold and wet. Usually the afternoons were much better even tho the sun may not shine because things warm up and dry out a bit. Actually, we often quit just about the time things were best. The work should have started about two hours later and continued about three hours later. This poor timing was brought about by schedule of morning and evening meals.

Any venture on Mauna Kea should adjust the working schedule to the best hours of the day. Work should probably end about sunset, so that a return may be made while still light.

The Attu experience brought out forcibly a situation which is present also at Sterling. Where it is necessary to transport personnel over long distances on paid time (even on unpaid time) it will be much better to work long days. This is because the ratio of working time to total elapsed time increases. If weather conditions permit, a working day of 10 hours with a total elapsed time of 12-1/2 hours should not be a hardship on anyone (1 hour each way and 1/2 hour for lunch). On such a schedule it will be best to work 4 to 6 days and then take 1 to 3 days off to rest, and repeat. The off periods may be adjusted to bad working weather if suitable forecasts can be secured. Rest days are important.

Weather station at Attu

On Attu we got off on the wrong foot, at first it was attempted to eat all those meals at the Aerological Station. Four truck rides a day were killing and the day was so short that little work was done. Then they started sending out sandwiches for lunch. This was also bad. Finally they brought hot food which was luke warm by time it arrived. They never did get up to hot coffee for lunch. The situation was still poor.

Any venture on Mauna Kea will require a really good <u>hot</u> lunch to be served with <u>hot</u> coffee. Also someone should dish out the lunch to prevent the early and greedy from robbing the rest. A suitable place to work and cleanup is also necessary.

Some of these ideas finally sank in, and for the last five days on Attu we ate two meals at the Point each day. We probably got in ten working hours that way, as we returned to station about 9:00 pm. Nobody complained much but it was obvious people were becoming very tired. It would have been better to be able to rest a few minutes after cleaning up and then eating the evening meal at the station.

Reber in parka and mittens on day of eclipse, September 12, 1950, Attu, Alaska

The idea of days off didn't seem to occur to the management. Some people worked every day we were there. I took two days off, the 10th and the 13th. Continuous work without rest is poor, because peoples minds begin to get dull and wrong decisions are made and the work is not expedited. Even tho the person doesn't spend the day off resting, he has an opportunity to go elsewhere and see other things and places. This is refreshing in itself.

Toward the end the management must have realized the party was in no mood to do a lot more heavy manual labor because they secured the help of some sailors to load and unload the boxes onto trucks. We, however, packed and closed all the boxes plus repaired or made new ones, as was needed.

<u>Weather Comments at Attu 50° 50' N 173° 11' E</u>:

Aug 24th Arrived at 1200 noon scattered clouds with sunshine at times. No (?), need Parka

Aug 25th Cloudy in morning with rain and thunder. Partly clear with little rain in afternoon. Parka in morning, Sweater in afternoon. Rainbows in morning and evening.

Aug 26th Partly cloudy in morning. Clear and sunny in afternoon. Warm north light breeze. Light sweater needed.

Aug 27th Clear and sunny all day. Warm light breeze. Took long walk (10 miles) in afternoon. Beautiful day. Took off shirt for heavy work in afternoon.

Aug 28th Clear in morning. Partly cloudy in afternoon. Nice day. Only shirt or light sweater needed.

Aug 29th Cold drizzle all day. Heavy clouds, light wind. Miserable day. Used Parka all day with hood up.

Aug 30th Clear and sunny all day. Blue sky. Little wind. Only shirt needed for hard work.

Aug 31st Faint (?) at times in morning. Afternoon wet and drizzle. Heavy clouds. Can't tell where sea ends and sky begins. Steady SW wind all day. Parka needed at all times mostly with hood up.

Sept 1st Cloudy in morning. Need Parka because of ground fog. Afternoon sunny and (?), light breeze. Work in shirt sleeves.

Sept 2nd Cold wind all day. Used Parka at all times mostly with hood up. Morning cloudy with ground fog and drizzle, afternoon sunny and cold.

Sept 3rd Cool & cloudy all day. Little wind, damp. Use Park then & hood to keep warm because no sun, except when doing heavy labor a sweater is adequate.

Sept 4th Cold & cloudy all day. Calm in morning. Windy and rain afternoon. Used Parka and rain coat all day. Most miserable day yet. Got soaked returning in open truck.

Sept 5th Cloudy all day. Little wind. Used parka with hood down all day except for heavy work a sweater was sufficient.

Sept 6th Cloudy and drizzle all day. Used rain parka. Considerable wind. Saw rainbow for few minutes in late afternoon.

Sept 7th Cloudy all day except for a few hours near noon. Drizzle in morning & evening. Used parka with hood due to wind except in sunshine near noon when a sweater was adequate.

Sept 8th Morning cloudy & rain. Afternoon considerable sun. Slight wind. Took off parka when sunny. Rainbows in morning. First day in more than a week there was sun at 4:30 (totality time).

Sept 9th Cloudy & rain showers most of day. Sun peeked thru faintly at times. Used parka all the time except when wind died down & rain stopped. Remained at Alexai Point until after sunset. The sun set across Massacre Bay behind some mountains which had black clouds above their tops. The rays of the sun were cut off on bottom side by mountain peaks and displayed against clouds a perfect rising sun emblem of Japan in red orange (?).

Sept 10th Stayed at Aerological Station all day. Sun faintly visible thru clouds. Too much wind outside to use only a sweater unless working hard.

Sept 11th This is day of the eclipse. Atrocious weather. Morning heavily overcast; by noon a wind started and by 3:30 there was a howling gale from south with a lot of rain. Used rain parka and was nice and dry except for feet which got wet because forgot to bring rubber overshoes. The moderate exercise of cranking azimuth wheel of mounting most of afternoon kept me quite warm. The rain (?????...????). The wind at Point probably above 30 mph and gusts to 50 mph.

Sept 12th Cloudy all day. Rain until 3 pm. Used rain parka outside. Worked inside in unheated quonset hut most of time packing boxes. Sweater was satisfactory.

Sept 13th Cloudy in morning. Considerable wind. Used Parka outside. By noon the sun came thru weakly. Afternoon cloudy again. Need Parka because of wind.

Sept 14th Reasonably clear and sunny, cool. Need Parka when just standing around. Left on Tawasa at 10:00 am.

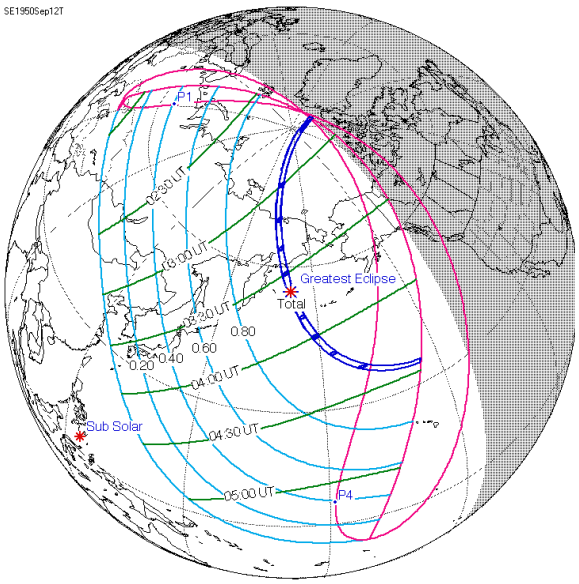

Image: By Attribution: Eclipse Predictions by Fred Espenak, NASA's GSFC - http://eclipse.gsfc.nasa.gov/ , Public Domain, https://commons.wikimedia.org/w/index.php?curid=17086184

References:
Reber, Grote, and E. Beck. The measurement of 65 centimeter radiation during the total eclipse of September 12, 1950. Available at: https://ui.adsabs.harvard.edu/abs/1951AJ.....56Q..47R/abstract

Alaskan Eclipse Expedition, National Bureau of Standards, Technical News Bulletin, Vo. 35, No. 2, February 1951. Available at: https://www.nrao.edu/archives/files/original/80f001c262b3171eb4e6f0927cb56e66.pdf

{Mayer} Interview with Cornell H. Mayer on 30 September 1971: https://www.nrao.edu/archives/items/show/15047

Credits:
{NRAO} Papers of Grote Reber: “Expedition to Attu, Alaska, to view solar eclipse of September 12, 1950,” *NRAO Archives*: https://www.nrao.edu/archives/collections/show/269

{NRAO-Phto} NRAO Images: Papers of Grote Reber, “Expedition to Attu, Alaska, to view solar eclipse of September 12, 1950,” *NRAO Archives*, accessed June 21, 2021: https://www.nrao.edu/archives/collections/show/450

{NRAO-Arc} List of Pictures of Trip to Attu: https://www.nrao.edu/archives/items/show/13123

Feature Articles

Passive Equalizer

Christian Monstein

A passive equalizer (figure 1) can be used to compensate for the high-frequency roll-off in low loss in coaxial cables, such that a whole band will have a more or less flat frequency response. For very long lossy cables one could even add two equalizers in series. The goal is to attenuate the lower frequencies in the equalizer about the same as the higher frequencies in the cable, so that the dynamic range of the receiver or spectrometer can be used for measurement and NOT to cope with the spectral slope of the system.

Fig. 1: Equalizer shown with open cover. It consists of only five SMD components, one capacitor, two resistors and two inductors. Connectors at each end are type SMA-female. Dimensions are 42 mm x 32 mm x 12 mm.

A simulation was performed with RFSim99 [1] software and available standard SMD (surface mount device) R, L and C components (figures 2 and 3). Actual measurements are comparable to the simulations (figure 4 and table 1).

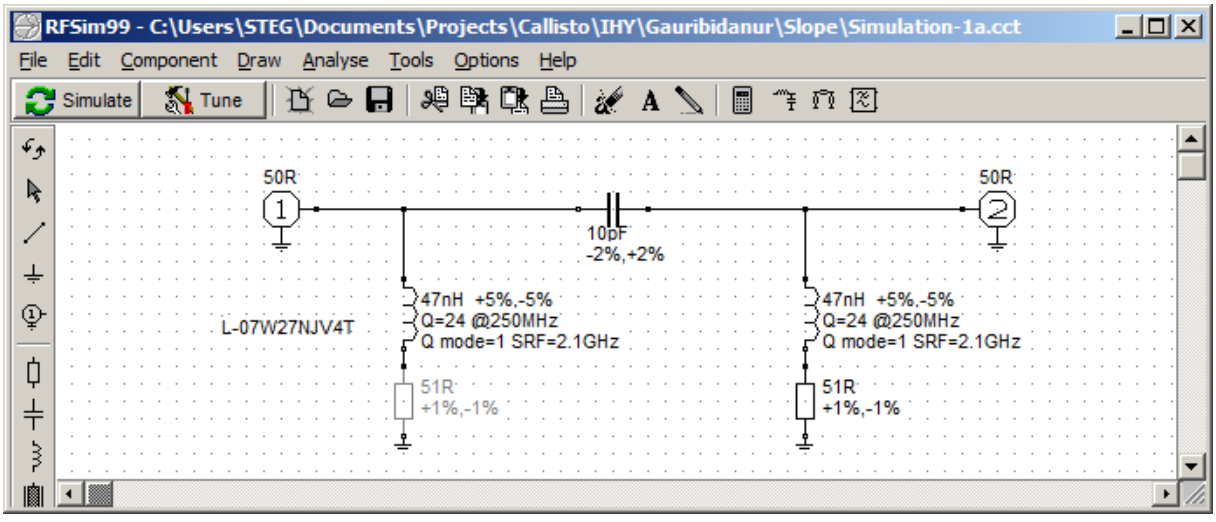

Fig. 2: Two-port model used for simulation in RFSim99.

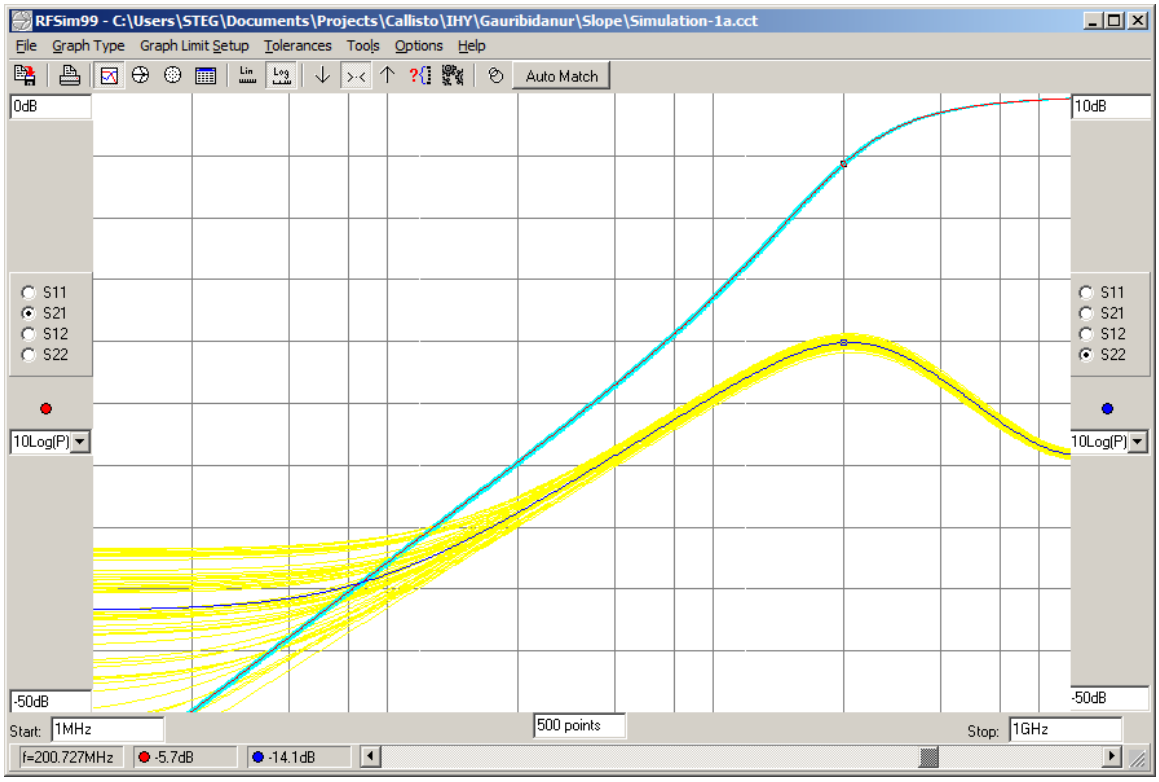

Fig. 3: Result of simulation for RFSim99. The black line outlined in yellow is the transmission coefficient S21 (left vertical scale). The yellow area accounts for component tolerances. The turquoise line is S22 reflection loss (right vertical scale). The frequency range shown on the horizontal scale is 1 MHz to 1 GHz.

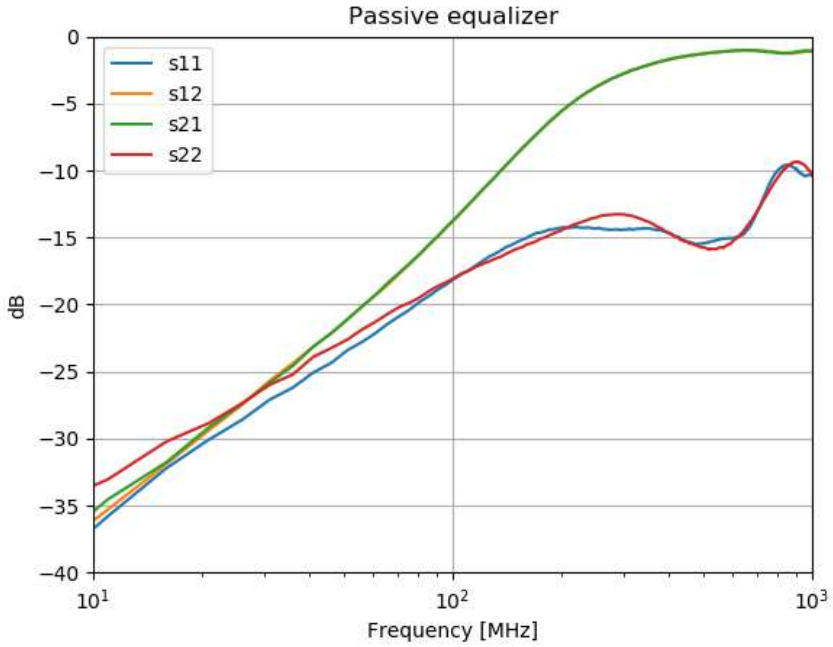

Fig. 4: Measured s-parameter of the prototype circuit from 10 MHz to 1 GHz. S21 (green) and S12 (orange) are almost identical. Port matching s11 and s22 are slightly different but always below - 10 dB.

Table 1: Key measurement points versus simulation. Measurement includes a 15 cm long SMA connection cable.

Frequency [MHz]	SImulation s21= s12 [dB]	Measured s21= s12 [dB]
10	-35.8	-36.0
100	-13.8	-13.7
200	-5.6	-5.5
400	-1.5	-1.6
800	-0.5	-1.2

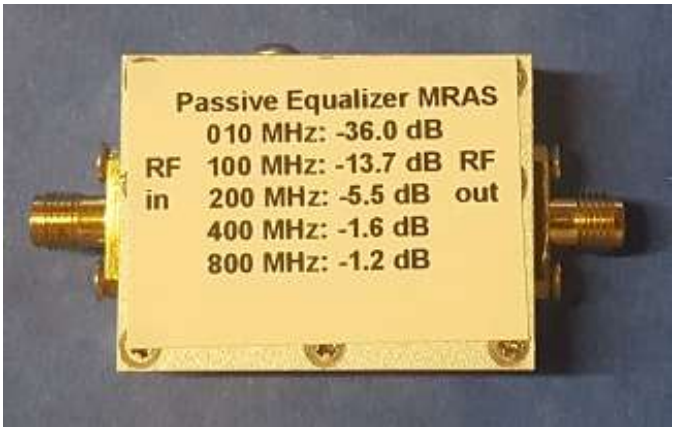

Fig. 5: Final product with cover mounted, a passive equalizer. Attenuation is on the order of –20 dB per decade.

A practical experiment with the equalizer shown in figure 5 is illustrated in figure 6 and is based on a 42 m long RG-58 coaxial cable [2]. This might be typical for a scanner antenna on the roof and a receiver or spectrometer down in the living room or office. The combined attenuation (RG-58 plus equalizer) only requires an additional dynamic range of ~16 dB compared to the high frequency end while the RG-58 by itself requires additional dynamic range of ~25 dB.

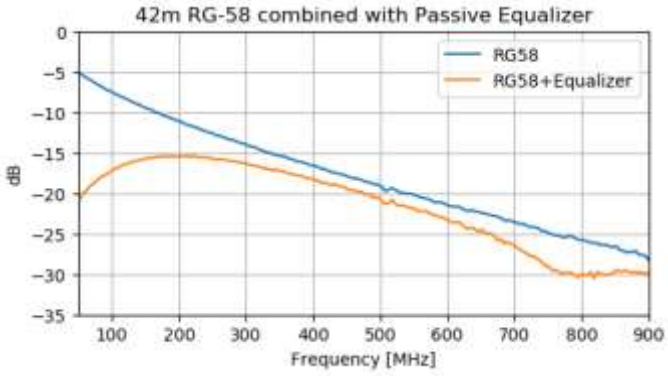

Fig. 6: Comparison of the attenuation of 42 m of RG-58 cable alone (blue) and in combination with the passive equalizer (red) over a frequency range of 50 to 900 MHz. Note that the combination introduces slightly higher attenuation at higher frequencies than the RG-58 cable.

Assuming an 8-bit digitizer such as in a Software Defined Radio (SDR) receiver or CALLISTO), with a dynamic range of $(2^8)^2$ = 48.2 dB, the 'left-over' dynamic range in the case of RG-58 by itself is only 48.2 dB – 25 dB = 23.2 dB, while in combination with an equalizer, the 'left-over' dynamic range is 48.2 dB – 16 dB = 32.2 dB. This is not a significant problem if one only observes weak signals near the instrument noise floor; however, if there is strong RFI from local transmitters or even self-produced RFI, the remaining dynamic range might not be sufficient to avoid saturation effects. Of course, the slightly higher attenuation of the combination RG-58 cable plus equalizer

requires additional gain, in this example (figure 6) several dB of additional gain is required depending on sensitivity of the attached receiver or spectrometer.

References:

[1] RFSim99: https://www.electroschematics.com/rfsim99-download/

[2] RG-58: https://www.koax24.de/en/product-info/coaxial-cable/koaxialkabel-50-ohm/49-61-mm-size4/rg58.html

Christian Monstein is a native of Switzerland and lives in Freienbach. He obtained Electronics Engineer, B.S. degree at Konstanz University, Germany. Christian is a SARA member and is licensed as amateur radio operator, HB9SCT. He has 21 years of experience designing test systems in the telecommunications industry and is proficient in several programming languages including C++, IDL and PYTHON. He has worked at ETH-Zürich on the design of a noise transmitter as payload on a drone and is responsible for the hardware and software associated with the e-CALLISTO Project. He plays also the role of a coordinator of SetiLeague in Switzerland and he is also representing Switzerland within CRAF. He is a member of the ISWI steering committee at UN office for outer space affairs in Vienna (UNOOSA. He is also a member of COSPAR and SCOSTEP.

Email contact: christian.monstein(at)irsol.usi.ch

Summary of Solar Radio Emission Types and Characteristics

Whitham D. Reeve

Solar cycle 25 began in December 2019 and already has produced many radio bursts and magnetic disturbances in the 20 months since then. The cycle is in full swing, and it is time to review the types and characteristics of radio emissions that might be detected throughout a solar cycle. Geomagnetic effects will be reviewed in a future article.

Figure 1 illustrates the frequency-time characteristics of solar radio phenomena. Table 1 provides a general description of the spectral classifications that correspond to figure 1, and table 2 provides more detailed descriptions of the major characteristics for each burst type. For actual spectrographic images of the various solar radio phenomena, see {Catalog} and {Reeve13). On a very broad basis, solar radio emissions consist of radio bursts or radio continuum, or a combination of the two. Bursts sweep through a range of frequencies while continuums are broadband noise phenomena that sometimes have a bursty nature but do not sweep.

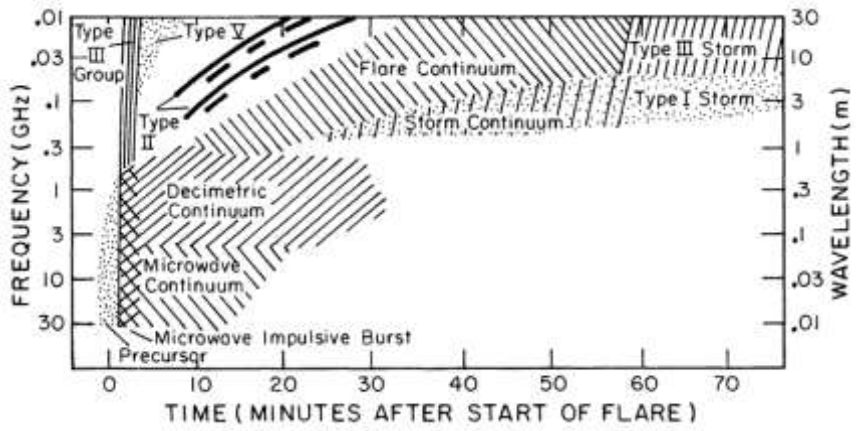

Figure 1 ~ Solar Radio Bursts ~ Frequency-Time Characteristics. Source: Figure 11, [Dulk]

Solar radio emissions associated with flares have the highest received power level of all celestial radio sources. Some of the emissions can be received with just about any shortwave receiver and a simple antenna such as a dipole. Solar radio emissions generally are easy to recognize in the narrowband audio output from ordinary high frequency receivers or in the wideband spectral signatures displayed by software defined radio (SDR) receivers and radio spectrometers.

When a burst is received, the background noise heard in the receiver output increases in volume, peaks and then decreases. The audio output may be connected to a PC soundcard and plotted, for example with Radio-SkyPipe software (figure 2). The plots often (but not always) show a characteristic *shark fin* shape with a more rapid rise than decay. If the received emissions are processed by an SDR receiver or spectrometer, the signal intensities displayed on a spectrogram brighten during the burst (figure 3). Generally, solar radio emissions received on Earth are strongest and most common in the high frequency band; however, Earth's ionosphere blocks solar radio emissions below 10 to 15 MHz.

Although solar radio emissions cannot be received directly at frequencies below about 15 MHz, solar flares can be detected indirectly by LF and VLF receivers and a modest loop antenna. In this case, it is the flare x-ray and extreme ultraviolet radiation that causes the effect, not the radio radiation. The flare radiation enhances the ionization in Earth's lower ionosphere (D-region), which affects the propagation of the low frequency transmissions from high-power transmitters used for submarine communications or time-frequency

dissemination. When the output from a VLF or LF receiver is plotted, the flare usually is seen as an enhancement in the signal level, and this is called a sudden ionospheric disturbance, or SID (figure 4).

Table 1 ~ Solar Radio Burst Spectral Classifications: General (see also table notes below)

Type	Characteristics	Duration	Frequency Range (MHz)	Associated Phenomena
I	Short, narrow-bandwidth bursts. Usually occur in large numbers with underlying continuum	Single: ~1 second Storm: hours – days	80 – 200	Active regions, flares, eruptive prominences
II	Slow frequency drift bursts. Usually accompanied by a second harmonic	3 – 30 minutes	Fundamental: 20 – 150	Flares, proton emission, magneto-hydrodynamic shockwaves
III	Fast frequency drift bursts. Can occur singularly, in groups, or storms often with underlying continuum. Can be accompanied by a second harmonic	Single: 1 – 3 seconds Group: 1 – 5 minutes Storm: minutes – hours	0.01 – 1000	Active regions, flares
IV	Stationary Type IV: Broadband continuum with fine structure	Hours – days	20 – 2000	Flares, proton emission
	Moving Type IV: Broadband, slow frequency drift, smooth continuum	0.5 – 2 hours	20 – 400	Eruptive prominences, magneto-hydrodynamic shockwaves
	Flare Continua: Broadband, smooth continuum	3 – 45 minutes	10 – 200	Flares, proton emission
V	Smooth, short-lived continuum. Follows some type III bursts. Never occurs in isolation	1 – 3 minutes	10 – 200	Same as type III bursts
VI	Series of Type III bursts over a period of 10 minutes or more, with no period longer than 30 minutes without activity	> 10 minutes	See Type III	See Type III
VII	Series of Type III and Type V bursts over a period of 10 minutes or more, with no period longer than 30 minutes without activity	> 10 minutes	See Type III and Type V	See Type III and Type V

Table notes:
1. Drifting bursts almost always drift from high to low frequencies
2. Frequency range is the typical range in which the bursts appear and not their bandwidth
3. Sub-types of Type IV are not universally agreed upon

For continuously updated information on the progress of the current solar cycle, see {NOAA}. The Space Weather Prediction Center (SWPC, part of NOAA) provides daily reports of solar activity, or *Events*, which include radio bursts. The Events reports are ASCII text files that may be downloaded at {SWPCEvnt}. These reports use many abbreviations, which are defined at {README} (also a text file) and essential to understanding the reports. SWPC provides many other space weather *products*, all free, that may be downloaded or viewed; a good place to start is their homepage at {HOME}. From there, various dashboard may be accessed as well as reports, forecasts, and archived data.

Additional important sources of information are fellow radio astronomers, especially those who observe at the same time and frequency. Time correlation of radio emissions received at two or more geographically separated locations is an excellent verification method because it eliminates local radio frequency interference (RFI) as a possible source for the event. Some solar radio emisisons are indistinguishable from RFI.

Table 2 ~ Solar Radio Bursts: Summary of Major Characteristics
(Source: Table 1, [Dulk])

Burst type	Duration at 100 MHz or 10 GHz	Temperature (K)	Polarization (circular)	Frequency range/ bandwidth	Height range/ magnetic topology	Association	Emission mechanism
I	≤ 1 s	≥ 10^{10}	50 – 100%	50-300 MHz/ ~1 MHz (burst)	0.1 – 0.6 R_0/ closed	large sunspots	fundamental plasma
I storm	days to weeks	≥ 10^{10}	o-mode	~100 MHz (storm)			
III storm	days to weeks	≥ 10^{10}	o-mode	50 MHz – 30 kHz/	0.6 R_0 – 1 AU/ open	Type I storms	fundamental and/or harmonic plasma
II	≥ 10 min	10^8 – 10^{11}	usually unpolarized	200 → 1 MHz/ 10 MHz	0.2 – 200 R_0/ open	flare shockwave	fundamental and harmonic plasma
III	few seconds	10^8 – 10^{12} (to 10^{13} at ~ 1 MHz)	fundamental: 30% harmonic: 10% o-mode	200 → 1 MHz/ 10 MHz 2 harmonics	0.2 – 200 R_0/ open (closed for U or J burst)	c/3 electron stream	fundamental and harmonic plasma
IV moving	~ 30 min	10^8 – 10^9	low → high x-mode	200 → 10 MHz/ > 10 MHz	0.5 - few R_0 / plasmoid	small flare	gyrosynchronous and/or plasma
IV flare continuum	~ 20 min	10^8 – 10^{12}	0 – 40% o-mode ?	200 → 10 MHz/ 100 MHz	0.1 – 1 R_0/ closed ?	moderate to large flare, initial phase	plasma ?
IV storm continuum	few hours	> 10^8	60 – 100% o-mode	50 – 300 MHz/ 100 MHz	0.1 – 0.6 R_0/ closed ?	flare, late phase	fundamental plasma
V	> 1 min	10^8 – 10^{11}	< 10% x-mode	100 → 10 MHz/ 50 MHz	0.5 – 2 R_0/ open ?	follows some Type IIIs	harmonic plasma
Microwave impulse	> 1 min (at 10 GHz)	10^7 – 10^9	~ 30% x-mode	3 – 30 GHz/ 10 GHz	~ 10^4 km closed	small to large flares hard x-rays	gyrosynchronous (Maxwellian or power law)
Microwave IV	~ 10 min	10^7 – 10^9	~ 10% x-mode	1 – 30 GHz/ 5 GHz	10^4 – 10^5 km closed	large flares with shocks	gyrosynchronous (power law)
Microwave postburst	minutes to hours	~ 10^7	low	1 – 10 GHz/ 5 GHz	10^4 – 10^5 km closed	flare, late phase	thermal bremsstrahlung
Microwave spike burst	~ 10 ms (burst) ~ 10 min (group)	> 10^{13}	~ 100% x-mode ?	~ 0.5 – 5 GHz/ few MHz	10^4 – 10^5 km closed	flare, hard x-rays	cyclotron maser

Solar radio emissions will increase over the next several years as the solar cycle progresses. Radio activity will continue even after the solar cycle peaks, but there is no better time to start monitoring than now.

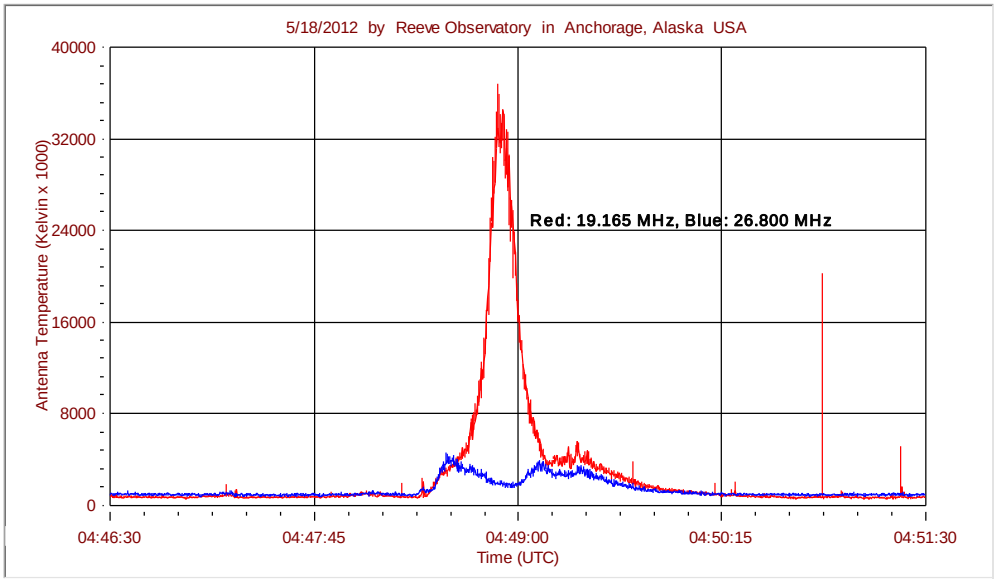

Figure 2 ~ Narrow slices of spectrum at two frequencies plotted over a 5-minute period with Radio-SkyPipe software at Anchorage, Alaska on 18 May 2012 during solar cycle 24. The peak received power (antenna temperature) of this solar radio burst at 19.2 MHz was about 35 million K. The descending frequency sweep of this burst is apparent – note that the blue trace (26.8 MHz) peaks before the red trace (19.165 MHz).

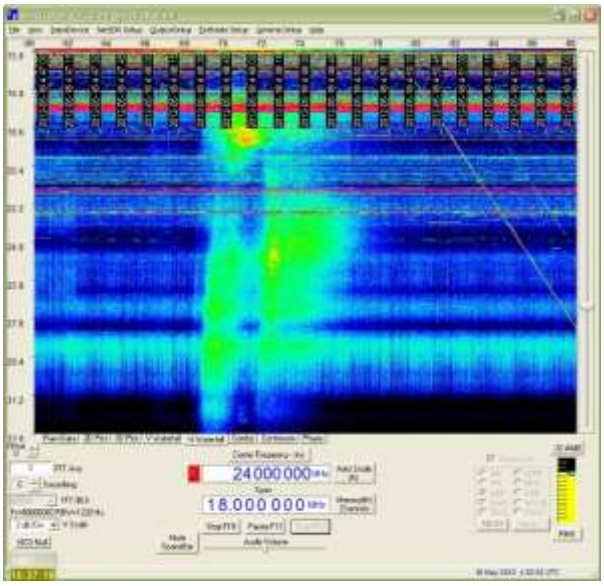

Figure 3 ~ Horizontal waterfall spectrogram of the 18 May 2012 solar radio burst over a 5-minute period received with an SDR receiver and associated software at Anchorage, Alaska. This spectrogram shows a wideband representation of the burst plotted above over the frequency range 15 to 33 MHz. Frequency is labeled on the left vertical scale (increasing top-to-bottom). Time from 0447 to 0452 is on the horizontal scale at top (left-to-right). The plot of the intensity of a horizontal line of pixels at 19.165 MHz would show a trace similar to the red trace in the above plot. The slanted yellow lines on the right side are *sweepers* from ionosondes or over-the-horizon radars. The diffuse horizontal turquoise swaths are radio interference. The other horizontal features include radio interference and radio stations.

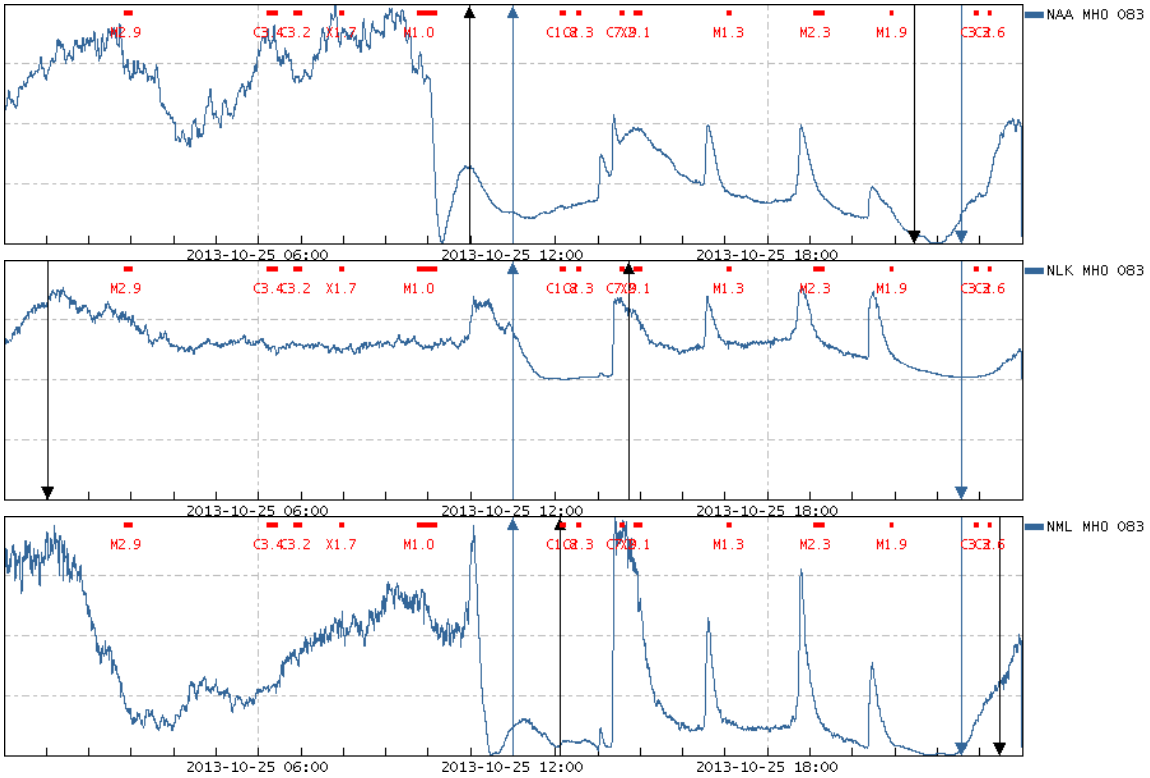

Figure 4 ~ Three plots for 25 October 2013 during solar cycle 24 of low frequency received signal level (vertical scale) with respect to time (UTC, horizontal scale). The transmitter sites are, top-to-bottom, NAA (24.0 kHz) in Maine, NLK (24.8 kHz) in Washington and NPM (21.4 kHz) in Hawaii; all are in USA. The receiver site is in Michigan USA and maintained by Tom Hagen. The black up-arrow indicates sunrise and the black down-arrow indicates sunset at the transmitter site in each plot. Similarly, the blue up- and down-arrows indicate sunrise and sunset at the receiver site. Relatively high, short-term signal variations occur during the night at the receiver site, especially between about 0000 and 1100 UTC. Except for station NLK, the received signal levels rise at night. Numerous solar flares are marked along the top of each plot, including several M-class (moderate) and one X-class (extreme) flares; some flares overlap. The corresponding SIDs with their signature shark-fin shape can be seen in the traces immediately below the flare labels. Images source: Stanford Solar Center {SSCData}.

Weblinks & References:

[Dulk] Dulk, G., Radio emission from the Sun and Stars, 1985, available at: http://adsabs.harvard.edu/abs/1985ARA&A..23..169D

{Catalog} http://www.e-callisto.org/GeneralDocuments/BurstCatalog.pdf

{NOAA} https://www.swpc.noaa.gov/products/solar-cycle-progression

{README} ftp://ftp.swpc.noaa.gov/pub/indices/events/README

{Reeve13} http://www.reeve.com/Documents/CALLISTO/Reeve_SolarRadioBurstCatalog_SARA2013West.pdf

{SSCData} http://sid.stanford.edu/database-browser/

{SWPCEvnt} ftp://ftp.swpc.noaa.gov/pub/indices/events/

1420 MHz Phase Switched Interferometer

Shef Robotham

Abstract:

This paper describes the construction, and resulting data, of a Phase Switched Interferometer using one Software Defined Radio, sdr. I constructed the interferometer with hopes to gain more sensitivity and angular resolution over my single antenna radio telescope. The interferometer, with its electronics reside in a 50 Caliber AMMO can with power and control over CAT5/6. I use a single sdr, controlled with GNU Radio running under a Raspberry Pie 4B. The LNA is my design with the added capability of phase and amplitude control. The basic hardware used in this project is readily available and at a very reasonable cost.

Overall:

This paper will describe a Phase Switched Interferometer using a NooElec, NESDR Smart version 4s rtl-sdr. Figure 1 shows the concept of the Phase Switched Interferometer, PSI. GNU Radio provides control of the rtl-sdr, data acquisition and raw data processing.

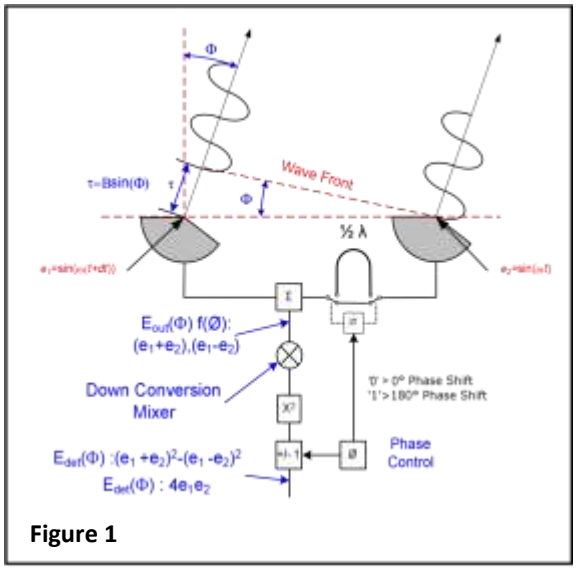

Figure 1

Section 1, Total Power Radio Telescope, the Baseline:

The basis of this interferometer is the GNU Radio flowgraph and a Python application taken from Apostolos's 'VIRGO Radio Telescope'. I have expanded Apostolos's Virgo Python code to write the data in a csv text file for further processing in a Spread Sheet. I have also added calculations for the Local Mean Sidereal Time, Right Ascension, Declination and Galactic Latitude and Longitude as a function of location, time, the Antenna Azimuth and Elevation. The final addition to Apostolos's code was allowing the user to define a specific data acquisition start time and add 'Session Notes'.

Figure 1.1

My continuum, Total Power, VIRGO Radio Telescope resides in a '50 Caliber AMMO can' and uses a Raspberry Pi 4B, Rpi, as the controller as shown in Figure 1.1. The Rpi communicates and gets power over CAT5/6 using PoE technology. Waterproof 'N' and CAT5/6 RJ connectors are used for AMMO Can I/O. This allows the main electronics to be close to the antennas minimizing any feedline losses. The LNA, a pre-production NooElec 1.42 GHz LNA, is housed in die-cast box and is placed at the antenna. I use PuTTY and FileZilla to control and extract the data files from the Rpi. GNU Radio is launched for a time such

that the target will traverse the 3 dB, Half Power Beam Width [HPBW] of the antenna over the drift scan time. This can be related to astro-imaging without guiding. I am using a modified 5.8 GHz, 1m dish with a HPBW of approximately 20 degrees which relates to 1.3 hours needed for the target to traverse the beam pattern. The antenna modification was published in a past SARA journal.

I have expanded the AMMO Can internals to implement the PSI, shown in Figure 3.2.

Section 2, Phase Shift Interferometer as a Radiometer:

The Phase Switch Interferometer uses 2 LNAs with one that has a 0° and 180° phase control as shown in Figure 1. The LNAs do not have the same exact gain and the phase inversion may not be exactly 180°. A sensitivity analysis was done to see how the LNA Gain and Phase error affected the total interferometer performance. The 0° and 180° times of the Phase Control Command also have an effect if not equal. The sensitivity analysis looked at the LNA gain imbalance, the LNA 0° and 180° phase inversion error and unequal 0° and 180° command times. The Phase Control Command signal is generated within GNU Radio running on the Rpi.

The basic analysis subtracts the LNAs output power's, with the variable under analysis, which should result in a null, without errors. The error is expressed as temperature. Figure 2.1 shows a screen snippet from MathCAD showing the set-up. P_{LNA1}-P_{LNA2} yield the 'Power Error' due to unequal gains, or the variable being analyzed. The 'Power Error' can then be related to the equivalent Temperature. The same reasoning is used when looking at the other variables.

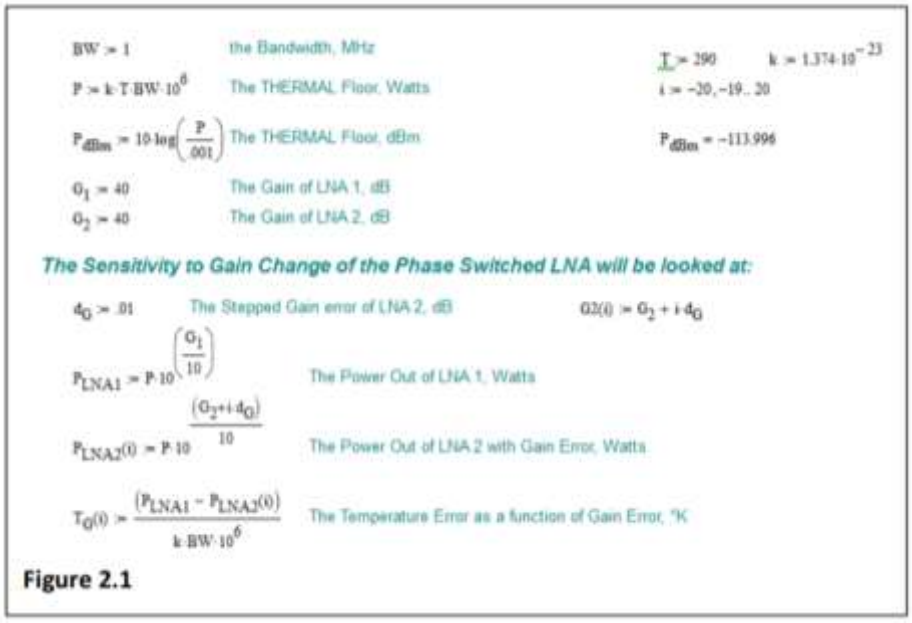

Figure 2.1

Figure 2.2 shows the temperature error with LNA gains of 40 dB with the gain of LNA2 stepped in .01dB increments. The temperature error increases with increased LNA gains. This can be explained as .01 dB on 40 dB has a greater gain factor increment than a .01dB increment on 30 dB.

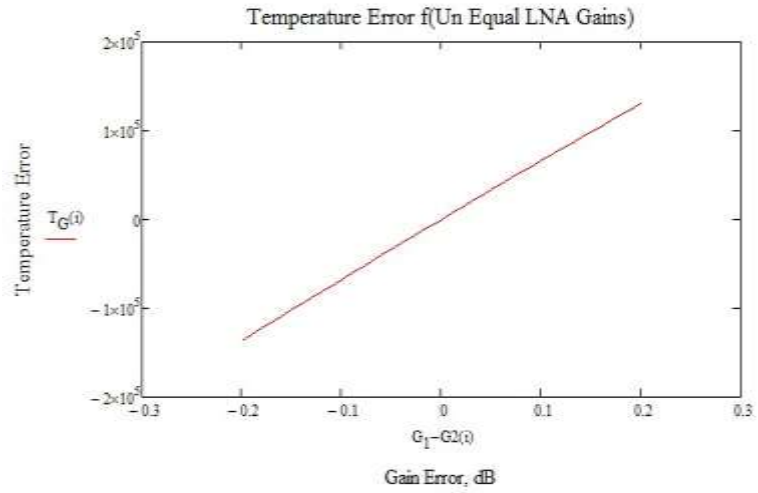

Figure 2.2

Figure 2.3 shows the temperature error if LNA2 does not have an exact 180 Degree phase inversion.

Figure 2.4 shows the temperature error resulting from unequal 0 and 180 phase times, or command Duty Cycle.

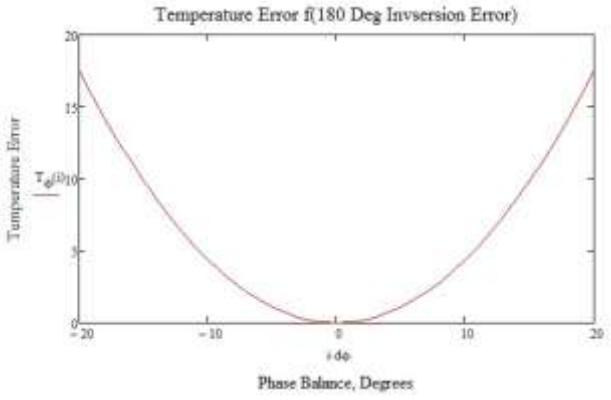

Figure 2.3

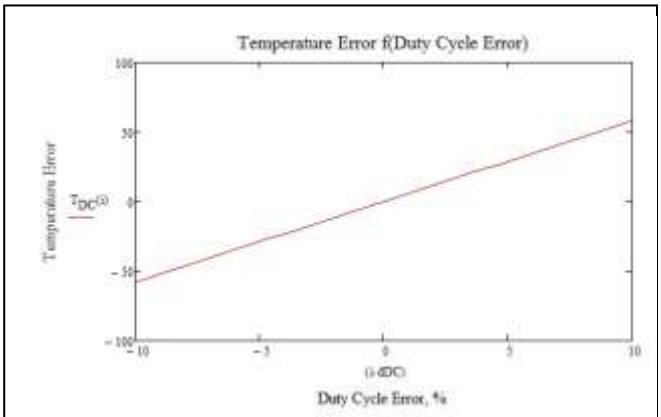

Figure 2.4

The analysis shows the biggest error in the Phase Switched Interferometer is due to unequal LNA gains with the phase command times, Duty Cycle, second.

This fact drove my 'Second Iteration' of my Phase Switched LNA as the first did not address unequal gains. The second iteration uses a 9036, 9037, ERA-3, a Voltage Variable Attenuator, VVA, and a Double Balanced Mixer, DBM. I added +4V and -4V regulators which are used for the ERA-3, DBM and VVA.

The Gains are matched using a signal generator and spectrum analyzer. The LNAs were both powered using the system configuration shown in Figure 3.2 accounting for bias tee and summer port variances and under actual

PoE supplied power. The MiniCircuits combiner does not have equal port losses so the LNA gains were set after the combiner. Each LNA was then assigned a channel or RF path. In addition, the LNAs were powered ON for 30 minutes so that thermal drifts were settled out. The Spectrum Analyzer Δ marker shows the gain of the LNA under test. Video Averaging was used to average the marker amplitude data to achieve a stable reading. Each LNA had its 0° and 180° Gains set to 40.0 dB.

Section 3, Phase Shift Interferometer and the Raspberry Pi 4:

Implementing a PSI, requires a signal to set the phase of one of the LNAs. Getting a 'bit-out' from GNU Radio was a problem that, it appears, nobody has done. I am using Rpi's Python 'led.on' and 'led.off' to output a bit which is embedded in a GNU Python Block. The LED uses GPIO 17 and is readably available on the Rpi header. The result is a square-wave with a 50% duty cycle at a switch frequency of 1Hz. The 1Hz is limited by the Rpi capabilities running GNU Radio.

The ability to output a bit can also be used to control a front-end antenna switch to switch a matched resistive load to the input to the LNA making a Dickie Switched Radiometer. The matched resistive load provides thermal noise power as a function of its temperature. The detected power then provides a calibration of the receiver's total gain. An alternative RF front end could also be switched allowing multiple wavelength data acquisition.

This Phase Switched Interferometer uses one SDR eliminating the need for synchronizing multiple clocks and dealing with multiple data streams. The GNU Radio flowgraph is not rtl-sdr dependent as any other SDR using the Rpi's USB interface can be used. I have 2 Bias-Tee's, from Amazon/eBay, and a MiniCircuits ZFSC-2-2500 Power Splitter/Combiner. All the hardware is mounted on a K&S 6" x 12" x .125" aluminum plate that mounts to the inside of a 50 Caliber AMMO Can. The AMMO Can provides a weather tight enclosure that certainly generates conversation from the neighbors.

Figure 3.1 shows the block diagram of the complete interferometer. The Bias Tees are from ebay, the summer is a MiniCircuits as described above, the 1.42 GHz InterDigital BandPass Filter is a 7-element 'home-brew' while the 30db Gain block, the noise floor into the dynamic range of the rtl-sdr.

Getting the Rpi to run 'Headless' requires some settings within the Rpi. Headless configuration allows a boot-up without a keyboard/Mouse and Monitor. Set the following: Figure 3.1 shows the block diagram of the complete interferometer.

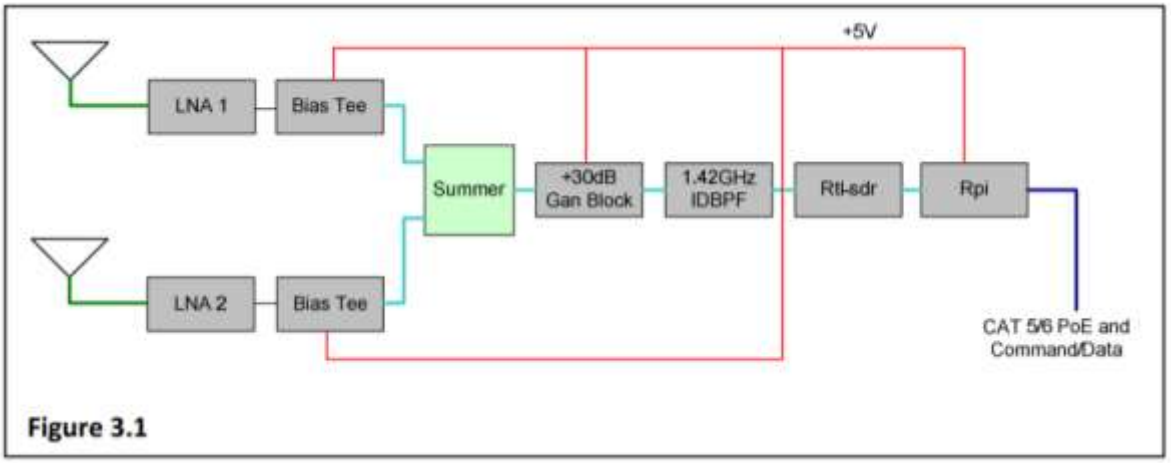

Figure 3.1

The Bias Tees are from ebay, the summer is a MiniCircuits as described above, the 1.42 GHz InterDigital BandPass Filter is a 7-element 'home-brew' while the 30db Gain block, also from eBay, gets the noise floor into the dynamic range of the rtl-sdr. The hardware is shown in Figure 3.2, 3.3 and 3.4. Figure 3.2 does not show an additional gain block needed to bring the noise floor into the sdr's dynamic range.

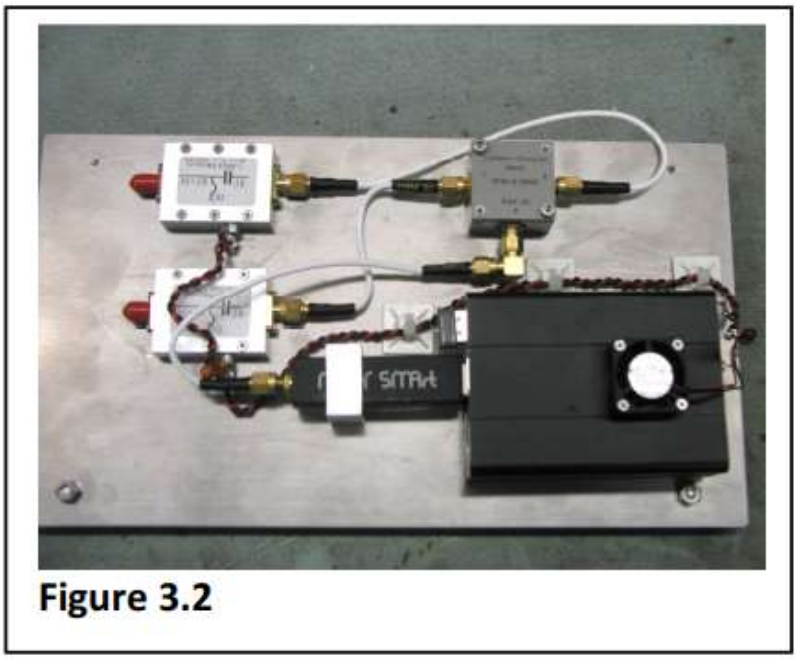

Figure 3.2

Figure 3.3 shows the Rpi's case and the feedthrough capacitors for the +5V, Ground and the Bit-Out. The power uses 1000pF while the Bit-Out uses 100pF feedthrough capacitors. I had to add ferrite common mode chokes prior to exiting the AMMO can as I still saw RF noise from the Bit-Out Phase Command.

Figure 3.3

Figure 3.4 shows the internal of the Rpi case and the +5V common mode choke as well as the GPIO connection for the bit-out. The case with the POE 'Hat' would not allow mounting of the included fan on the inside but is mounted externally. The case did need some 'Dremeling' so the covers would go on. The area around the video monitor jack also needed clearing as the mini-HDMI connector would not completely insert causing the RPi not to boot. The end plates, and their mounting surfaces, were cleaned as an attempt to make a RF tight enclosure. The case modifications are unique to this case only but are highlighted for information only. A concern with the Rpi was its ability to execute the GNU code and output a bit such that the actual outside-world bit was time aligned with the internal software bit. The GNU code generates a +1 and -1 signal applied to a multiplier which implements the phase inversion. To 'see' the time alignment, I added a times 20 Multiply block, to add gain to the raw I/Q data from the sdr, a Complex_to_Real and a QT_Time_Sink blocks. The GNU flow graph was also modified to run stand-alone verses the variables defined by the calling python program. This allowed looking at the internal timing and the actual real time rtl-sdr signals to verify time alignment with a slightly more software load due to the added blocks.

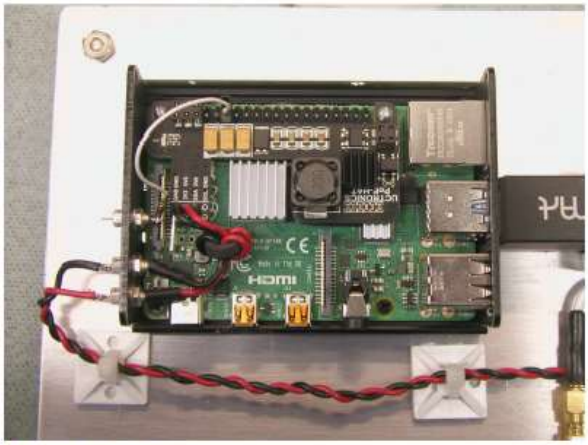

Figure 3.4

The QT_Time_Sink acted like an oscilloscope, shown in Figure 3.5 and 3.6. Figure 3.6 is a close look at the internal bit falling edge relative to the sdr's 'real data'. Both Figures 3.5 and 3.6 verify there is no time misalignment between the internal multiply and the phase flipped signal output to the LNA.

Getting the Rpi to run 'Headless' requires some settings within the Rpi. Headless configuration allows a boot-up without a keyboard/Mouse and Monitor. Set the following:

Rashberry/Prefereneces/Rashberry Pi Configuration
Boot Command Line

You may also need to comment out the HDMI information, in the ***'boot/config.txt'*** file, uncomment ***'hdmi_force_hotplug=1'***. This should allow the Rpi to boot up remotely.

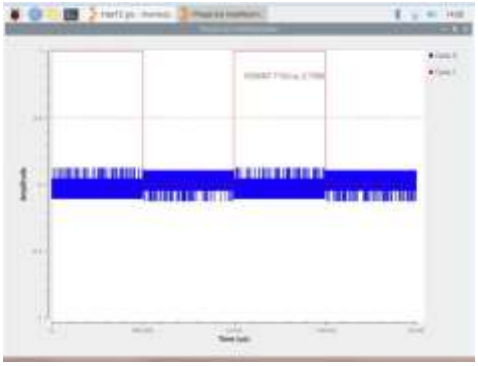
Figure 3.5

The Network address also needs to be identified by using ***'ifconfig'*** at the command line. The Network address will be displayed.

I use ***PuTTY***, from a Windows environment, to execute the python code. Launch ***PuTTY***, enter the network address from above, the username, default is ***'pi'*** and your password which you defined on the initial Rpi power up. Once logged on, you will need to navigate to the proper directory and type ***'python RAIntF(x).py'*** { may change due to code revision } to launch the controlling interferometer program and follow the user prompts as in Figure 5.1.

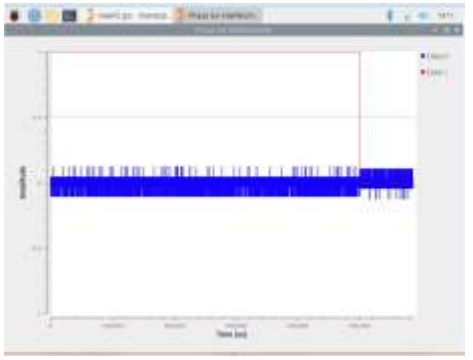
Figure 3.6

I use ***'FileZilla'***, also from a Windows environment, to push/pull code and data to/from the Rpi. This program does not require a log-in procedure. Enter the network address and ***'Connect'***.

To get back to the Rpi Graphical User Interface, at the command line:

Sudo raspi-config
Select 'Boot Options'
'Desktop'
'AutoLogin as' pi
'OK'
'startx' { launches GUI }
Raspberry/Preferences/Raspberry Pi Configuration
Boot set to 'Desktop'
Enable 'Splash Screen'

To shut-down the Rpi:

'sudo shutdown' The unit will shut down in 1 minute

The above took some digging but is available from many websites.

Section 4, Phase Switched LNA:

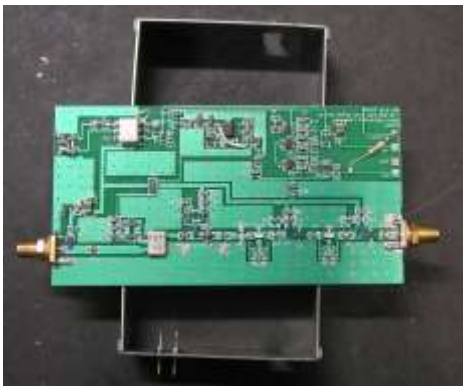
Figure 4.1

I designed the LNA using Qorvo's TQP3M9036 and TQP3M9037. The 9036 has a better match and NF for 1.42GHz when compared to the 9037. I used Genesys to design the LNA which is composed of 9036, 9037, an ERA-3, a Voltage Variable Attenuator, VVA and a Double Balanced Mixer, DBM. The VVA allows for precise Gain control of the
LNA while the DBM allows phase selection. I used 2 Mini-Circuits BFCN-1445+ SMT Bandpass filters to 'somewhat define' the bandwidth.

Genesys predicts a +42.8 dB total gain, input VSWR of 1.109:1 and a NF of .585 dB. The +43dB gain dominates the following receiver chain therefore the Total Receiver can be considered to have a NF of 0.59 dB which relates to a T_{sys} of 42 ° K.

I investigated making the PCB out of Rogers materials, but the additional cost verses the slight performance improvement over FR4 is not worth the ROI. This IS a hobby. I used ExpressPCB with the cost of 4 boards being $128.

The phase switch command is fed through 2 EMI filters to an Opto-Isolator keeping the LNA environment as clean as possible. The 'opto' is biased for 0/3.3V, the Rpi output levels. Figure 4.1 shows my 'first iteration LNA' circuit board, with some 'dynamic engineering', sitting on its case. Figure 4.4 shows the current schematic.

Figures 4.2 and 4.3 show the completed LNA in the enclosure. The Phase Inversion signal is routed through the enclosure with a pair of 100pF feedthrough capacitors as shown in Figure 4.3.


Figure 4.2


Figure 4.3

Assembling the board, especially the LNA MMIC's was challenging due to their size as I used solder paste working under a microscope. On my second iteration I used a Hot-Plate with solder paste to solder the small MMICs and caps which resulted in a 'Home-brew SMT' process. The solder paste melts at 268F which was easily achieved with the Hot-Plate and an aluminum heat spreader block.

Referring to Figure 4.4, the 5V to -4V circuit inverts the +5V to a -4V regulated source needed for the DBM drive and VVA control. I was very skeptical of using anything with rising and falling edges in a sensitive circuit, consequently a separate ground plane with internal and external decoupling and inductive isolation is used in generation of the -4V. A +4V regulated source is used for the DBM drive and ERA-3 bias. The completed LNA

requires +5V at approximately 280 mA which is supplied via the LNA output COAX. Over Voltage protection is done using a 5.2V Zener diode.

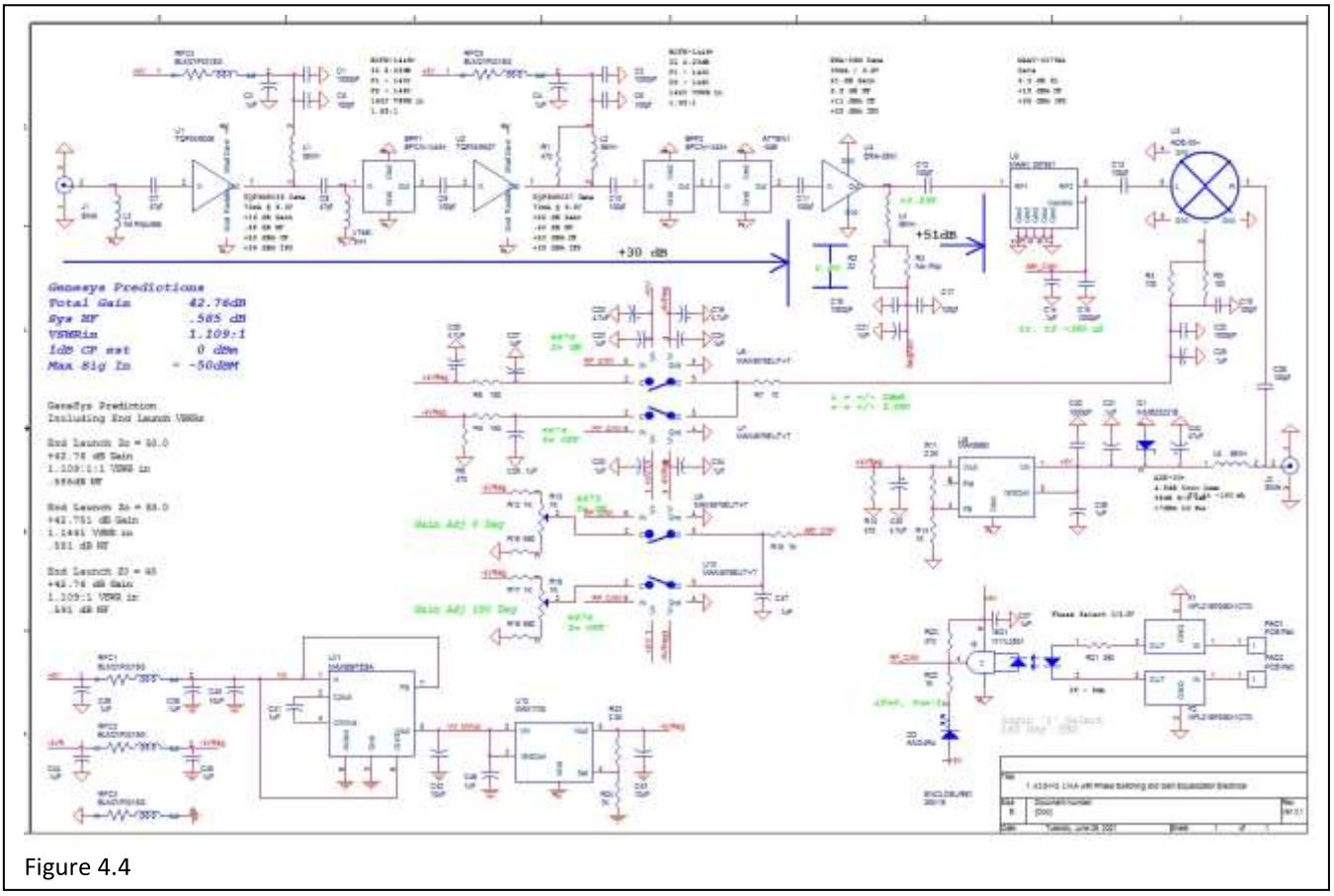

Figure 4.4

The measured Gain, Input VSWR and Noise Figure at 1420.0MHz are detailed in Table 1.

Unit	Gain	VSWR	Noise Figure
S/N 1	40.0dB	1.397:1	.61dB
S/N 2 0°	40.0dB	1.390:1	.63dB
S/N 2 180°	40.0dB	1.418:1	.63dB

Table 1

The Table 1 was data taken after a 30-minute stabilization period with gains set as described in section 2 above.

Figures 4.5, 4.6 and 4.6B show the typical Input VSWR and Gain using a HP8753C for both LNAs. Figure 4.5 is LNA S/N 1 and is not phase switched while Figure 4.6 is S/N 2, the phase switched LNA at 0 ° and 4.6B is at 180°. The measured phase inversion for S/N 2 is 175.50° at 1420.0 MHz. Figures 4.7, 4.8 and 4.8B show the typical Noise Figure and Gain using a HP8790B with similar notations.

Genesys does not have a model for the SMA End Launch. I obtained these from DigiKey, a Cinch, 142-07601871, DigiKey # J610-ND, and had a spec sheet is available. I took detailed physical dimensions of the end launch ; cross checked a calculated Zo and placed the model into Genesys. The schematic shows the predicted performance with different end launch Zo's, a function of the VSWR. I did find a manufacturer that has a PCB edge mount N connector but did not have detailed attenuation and impedance mis-match data.

Testing the Phase Inversion command is shown in Figures 4.9. The unequal duty cycle is showing the Rpi phase inversion signal errors over a 10s time period. The square wave DBM bias voltage is measured at the junction of U6, U7 and R7 as seen in Figure 4.4.

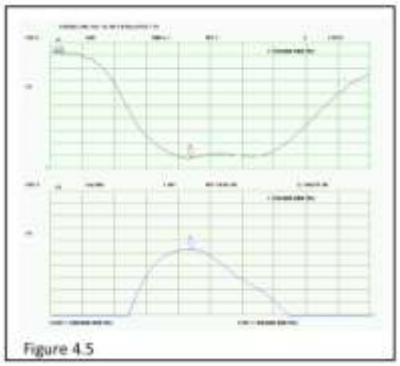
Figure 4.5

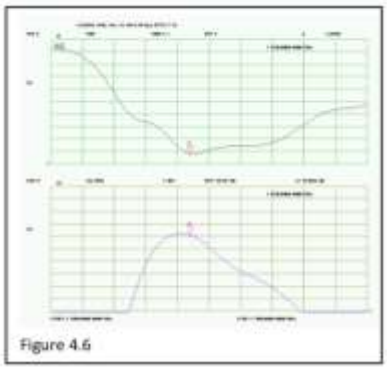
Figure 4.6

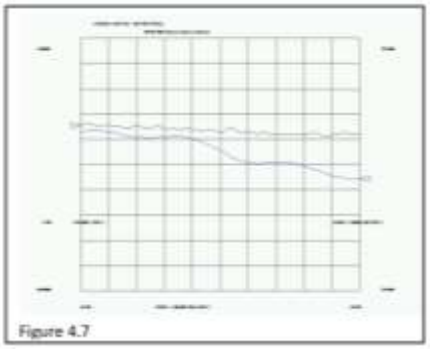
Figure 4.7

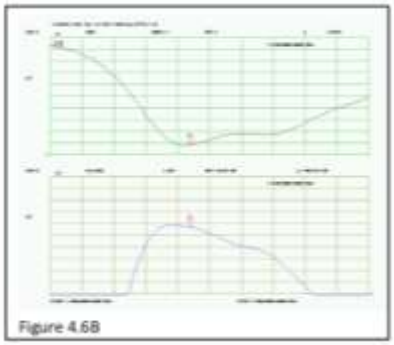
Figure 4.6B

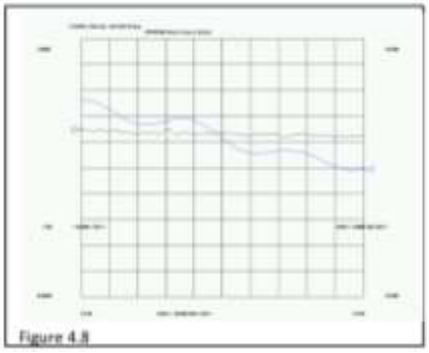
Figure 4.8

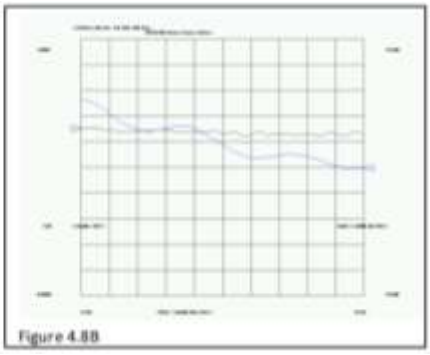
Figure 4.8B

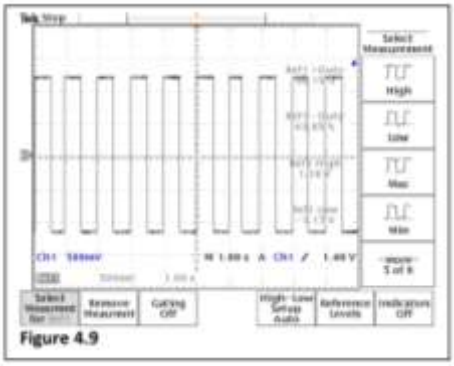

Figure 4.9

Section 5, Python Code and Operation:

The Python code for the Phase Switched Interferometer prompts the user for the usual data as shown in the upper portion of Figure 5.1. Note the valid range of rtl-sdr sample rates referred to as Bandwidth. Using a BW outside the allowed range will result in BOGUS data.

The antenna baseline is defined as 90°/270°, East/West, and they are looking 180°, South. The antenna's Azimuth and Elevation inputs are checked, and the input rejected if outside a 0° to 360° azimuth or a 0° to 90° elevation.

In the shown example, the suggested elevation is 93° so the azimuth should be 0°.

If have added RF and I/Q gain controls inside GNU Radio. These ensure the signal is within the dynamic range of the sdr and the raw I/Q data is valid. The RF Gain controls the front-end gain of the sdr while the I/Q gain is a multiply block within GNU amplifying the I/Q data from the sdr. I have an Auxiliary GNU flowgraph that shows a histogram of the data which allows setting the RF gain such that the signal is not saturated.

Figure 5.1

The ability to configure the interferometer as an Adding or Phase Switched is also available. This controls the GNU multiply block multiplier, either +1 for an Adding interferometer or +/- 1 for a Phase Switched Interferometer.

The middle to lower portion of Figure 5.1 is a check area where the input parameters are displayed. The interferometer antenna HPBW is expressed as time relative to a Drift Scan. The Antenna HPBW, the site longitude and latitude are entered in the front of the python program. The targets Fringe period is calculated, and the number of fringes shown within the antenna HPBW drift scan time. A suggested Data Block write time is shown so that the fringe structure can be detected. The Data Write time is the signal integration time for a data point.

There is a trade off between data write time, fringe period and the time the target is withing the HPBW of the antenna. The data check area provides some insight to these parameters.

Figure 5.2 is a continuation of input displays. The integrator factors are shown and were used in my code development. The lower portion of 5.2 asks for session notes which are included in the csv file header information. The user is then prompted to start immediately or at some future time. I have entered an example start of 7/5/2021 at 1300 LOCAL. The python code checks the computer time in 10 second intervals and if equal, or greater than, launches GNU Radio.

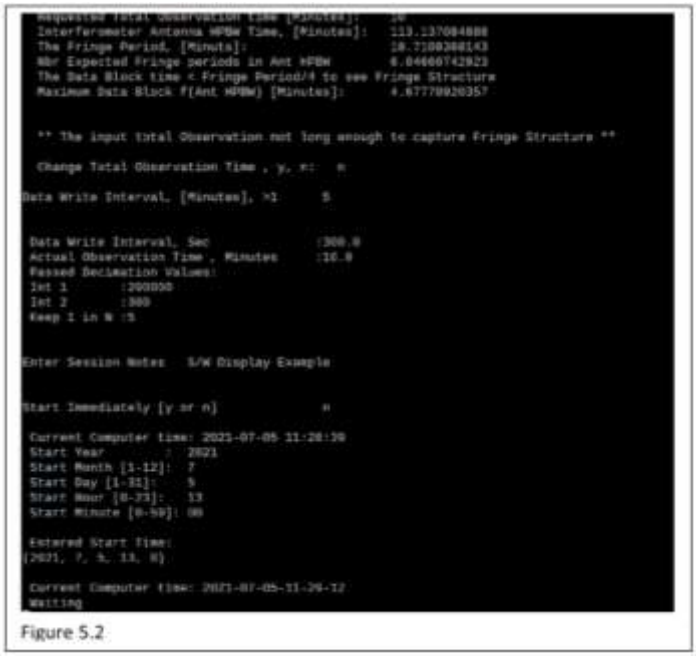

Figure 5.2

I found several challenges waiting for me during this project. GNU Radio and Python were unfamiliar to me. I am NOT a LINUX user and have no experience with Python. The resulting code is from help from my son, in IT, and Google.

The GNU Radio Flowgraph is shown in Figure 5.3. The greyed-out blocks are in-active and were used for debug and stand-alone operation.

The ‘Parameter’ blocks are populated by the calling Python code. The flowgraph is minimum to reduce the software load so that the 1Hz output bit has a 50% Duty Cycle.

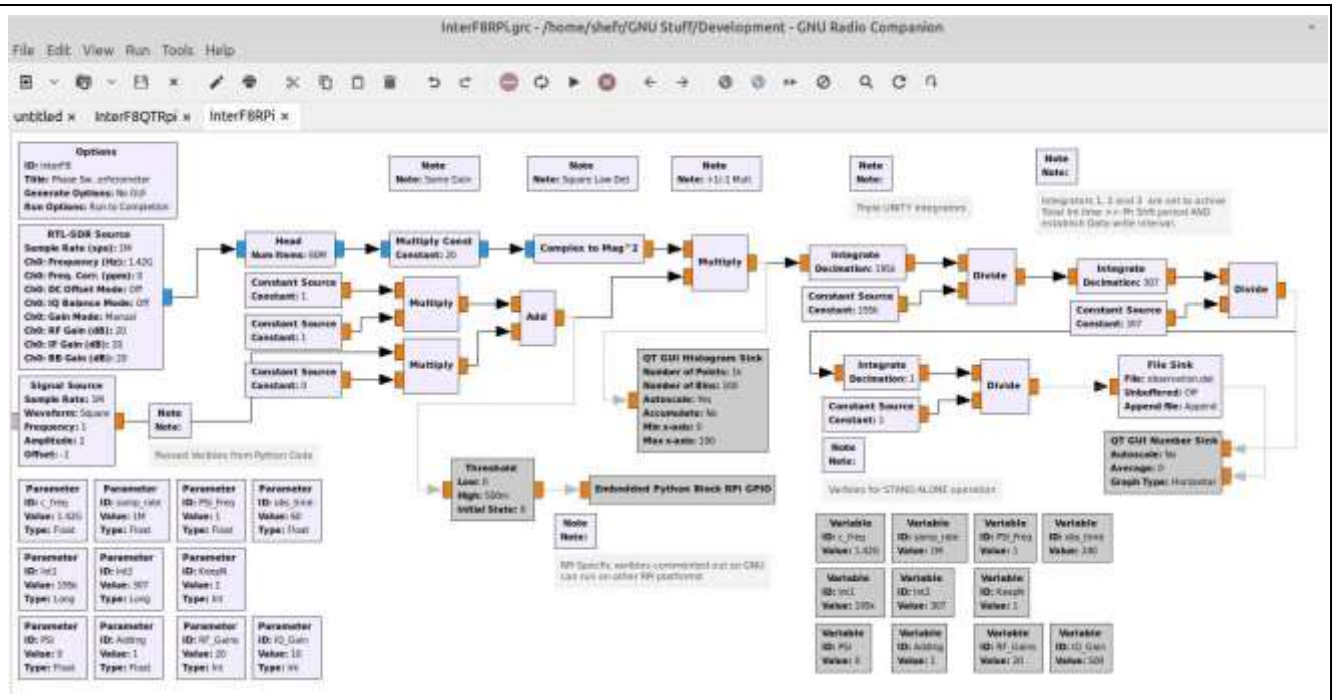

Figure 5.3

Figures 5.4 and 5.5 show some statistics of the Phase Switching command Duty Cycle. The data taken from the Rpi 'Bit-Out' Feed-Through over a 40s window. The Duty Cycle data shown is essentially 50%.

The code behind 'Embedded Python Block Rpi GPIO' is shown as a screen snippet in Appendix A-1. Stated above I am not fluent in Python or Object Orientated Programming consequently; the code probably lacks any sophistication and may cause nausea. The code in Appendix A-1 needs editing before it will run on the Rpi. Appendix A-2 shows the edits required in red text. I used the i7 laptop for overall system development as debugging ANYTHING on the Rpi is painfully slow.

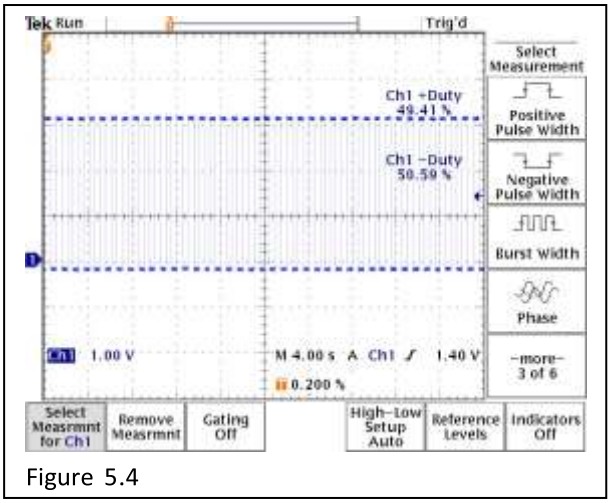

Figure 5.4

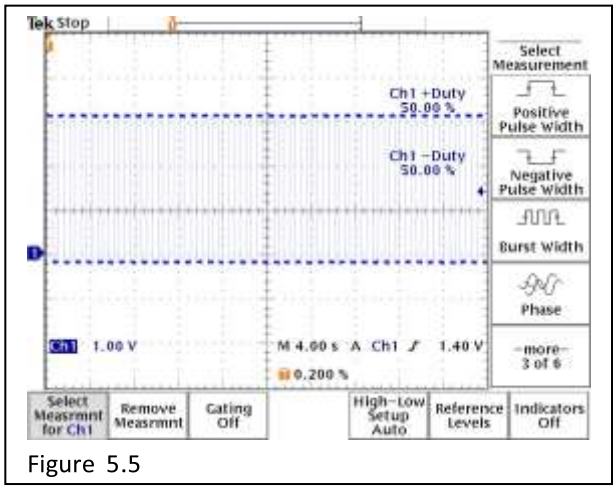

Figure 5.5

Section 6, Data Format:

The python code generates a csv text file that can be postprocessed. The file contains the data and information on the data set. The session information header, shown in Figure 6.1, is adequate for post session reconstruction.

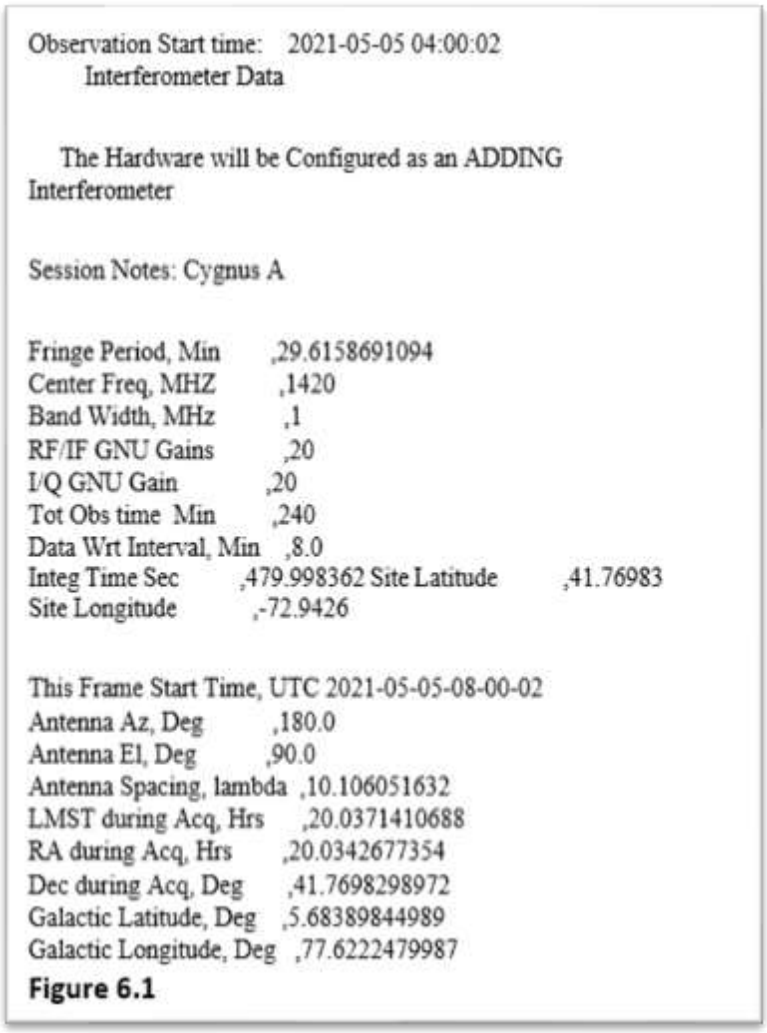

Observation Start time: 2021-05-05 04:00:02
Interferometer Data

The Hardware will be Configured as an ADDING Interferometer

Session Notes: Cygnus A

Fringe Period, Min ,29.6158691094
Center Freq, MHZ ,1420
Band Width, MHz ,1
RF/IF GNU Gains ,20
I/Q GNU Gain ,20
Tot Obs time Min ,240
Data Wrt Interval, Min ,8.0
Integ Time Sec ,479.998362 Site Latitude ,41.76983
Site Longitude ,-72.9426

This Frame Start Time, UTC 2021-05-05-08-00-02
Antenna Az, Deg ,180.0
Antenna El, Deg ,90.0
Antenna Spacing, lambda ,10.106051632
LMST during Acq, Hrs ,20.0371410688
RA during Acq, Hrs ,20.0342677354
Dec during Acq, Deg ,41.7698298972
Galactic Latitude, Deg ,5.68389844989
Galactic Longitude, Deg ,77.6222479987

Figure 6.1

The actual SDR's data is written at user specified intervals. The data write interval should be some fraction of the Fringe period so that the fringe structure can be seen. The Center Frequency, Band Width, Total Observation Time, Site Latitude and Longitude are self-explanatory. The RF Gain is set while watching a histogram of the detected signal to ensure the data is not saturated. I developed an Auxiliary GNU flowgraph utility however it requires a monitor at the Rpi so that the histogram can be seen, and sliders adjusted correctly. In most cases the I/Q gain adjustment is not needed. It is possible to run the Rpi as a remote desktop however I have not investigated this. Using a remote desk-top would allow setting the RF and I/Q gains without sitting at the Rpi.

GNU uses 3 Integrate_Blocks to affect the long integration times. The Integrate block has a maximum decimate factor of 200000 which is not long enough. The decimate factors passed from the python code are integers. The requested sample_rate may not be possible due to rtl-sdr limitations but will be as close as requested. The total integrate time is the actual sample_rate * (Int1_Decimate * Int2_Decimate * Int3_Decimate). A problem arises when the actual sample rate multiplied by the decimate factors winds up more than the observation time such that the last data point in the csv file is not written. To solve this, I decrease Int1 Decimate factor slightly to insure all the data points are written.

The remainder of the information in Figure 6.1 shows the Antenna Azimuth and Elevation, the Antenna Spacing in λ, the observation mid-way LMST, Right Ascension, Declination and Galactic Latitude and Longitude.

Figure 6.2 shows a screen snippet of the data. The time stamp heading is defined as; the day, UTC hour and minute. I inserted an Index during post processing making plotting easier. The last line is the actual power detected at the end of the current write interval.

5:08:24	5:08:32	5:08:40	5:08:48	5:08:56	5:09:00
4	5	6	7	8	9
1.17675	1.19207	1.18931	1.18790	1.19385	1.18758

Figure 6.2

Section 7, Actual Data:

Figure 7.1, 7.2 and 7.3 shows the interferometer hardware set up in my Wife's Backyard! Figure 7.2 shows the phase controlled LNA and Antenna while Figure 7.3 the ammo can I/O. The 'driveway sealer pail' was chosen for its dielectric constant.

Figure 7.1

I learned there are many compromises to be considered with interferometry. The goal is to detect the objects fringe patterns which requires observation integration or time. The Fringe patterns, and maxima, provides a more accurate determination of the target's RA however the integration time will dominate the time resolution. The Fringe Period is a function of the objects Declination and the base line length:

$$t = \frac{\lambda}{b_y \omega_e \cos\delta}$$

Where λ is the wavelength in meters, b_y is the baseline length in meters, δ the object's Declination and t in seconds. ω_e is the Earth's sidereal day expressed as radians/second, 7.29212 e-5 rad/sec. The cos(δ) adjusts for the Earth's effective rotation as at the celestial pole, the apparent sky is not rotating.

GNU integrates the signal for some (tbd) time and the data point is then written to the data file. The integration time must be long enough to generate some S/N but short enough such that the data points show the fringe patterns.

The Antenna's 3dB beam width, HPBW, affects the time the object is in the pattern during the drift scan. A larger antenna will result in more gain, larger signal, a smaller, tighter beam reducing the time the object will be in the beam patten.

Figure 7.2

Figure 7.3

The interferometer compromises are:

A. the object's declination
B. the RF frequency, the baseline length
C. Antenna's HPBW related to drift scan time D. data point write interval

My interferometer uses two 5.8 GHz, 1m antennas which were modified for 1.42 GHz operation. Their temperature is ~ 85°K which could be optimized at a later effort. The 3 dB HPBW is ~20° or 1.33 hours of drift scan time.

I chose Cygnus A for my first target as 'my sky' has numerous trees. Cygnus A does have a large 'cloud' following in ~ 30 minutes which adds some data confusion. I chose 1 MHz of Bandwidth for data uniformity.

Data Run 7-24:

Figures 7-24-1 to 7-24-3 show Cygnus A captured in the Phase Shift Interferometer configuration. Figure 7-24-2 shows the complete 4 hours of data with transit marked. Figure 7-24-3 shows a linear curve fit to straighten out the data with the +/- Antenna HPBWs, the +/- Fringe peaks and Transit marked. The fringe period is 17.5 minutes with a data write interval of 4 minutes making the interval at ~ 4 data points. The data seems to show peaks at the expected times. The baseline is 17.3 λ causing the Fringe spacing to be 17.5 minutes which limits the integration time per data point limiting the detected signal.

Observation Start time:	2021-07-24 02:42:06	
Interferometer Data		
The Hardware will be Configured as a PHASE SHIFT Interferometer		
Session Notes:	Cygnus A New LNA Design	
Phase Switch Freq	Hz	1
Fringe Period	Min	17.53066
Center Freq	MHZ	1420
Band Width	MHz	1
RF GNU Gain	dB	26
I/Q GNU Gain	#	40
Tot Obs time	Min	240
Data Wrt Interval	Min	4
Intag Time	Sec	60
Site Latitude	41.76983	
Site Longitude	-72.9426	
This Frame Start Time	UTC 2021-07-24-06-42-06	
Antenna Az	Deg	180
Antenna El	Deg	90
Antenna Spacing	lambda	17.32466
LMST during Acq	Hrs	23.99037
RA during Acq	Hrs	23.98749
Dec during Acq	Deg	41.76983
Galactic Latitude	Deg	-19.8805
Galactic Longitude	Deg	113.1649

Figure 7-24-1

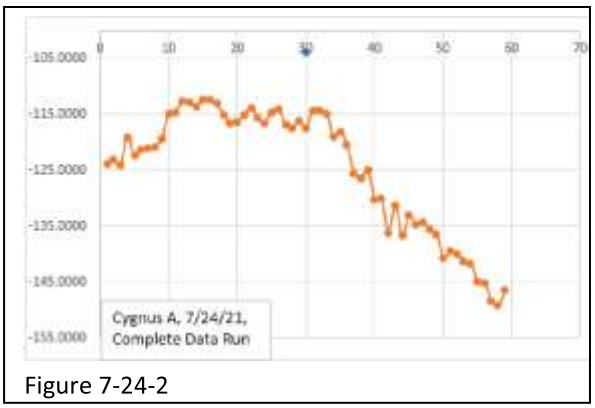

Figure 7-24-2

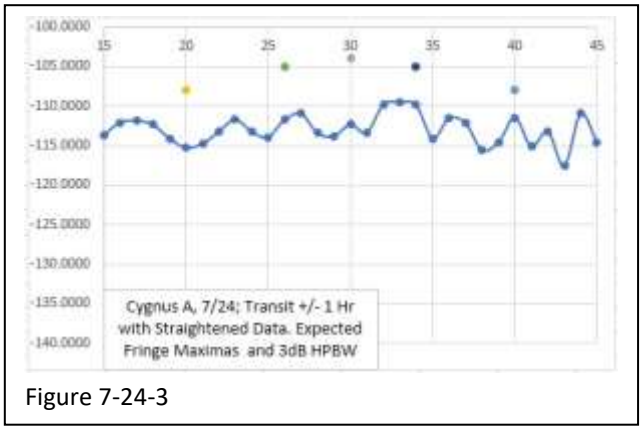

Figure 7-24-3

Data Run 7-26:

Figures 7-26-1 to 7-26-4 show Cygnus A captured in the Phase Shift Interferometer configuration. Figure 7-26-2 shows the complete 4 hours of data with transit marked. The data was pasted into Sigma Plot for curve fitting which resulted in a cubic polynomial, also seen in 7-26-2. Figure 7-26-3 shows the difference between a linear curve fit and the cubic polynomial. The polynomial curve fit was not worth the effort as the linear curve fit provided straightened data. Figure 7-24-4 shows the linear curve data with +/- Antenna HPBWs, +/- Fringe peaks and Transit marked. The fringe period is 17.5 minutes with a data write interval of 4 minutes making the interval at ~ 4 data points again set by the baseline spacing. The '+' Fringe is obvious. Is the '-' Fringe attenuated due to the trees as Cygnus transits?

Observation Start time: 2021-07-26 02:36:08
Interferometer Data

The Hardware will be Configured as a PHASE SHIFT Interferometer

Session N	Cygnus A	New LNA	RF Gain Slight Inc	
Phase Swi	Hz	1		
Fringe Per	Min	17.53066		
Center Fre	MHZ	1420		
Band Widt	MHz	1		
RF GNU Ga	dB	27		
I/Q GNU G	#	40		
Tot Obs ti	Min	240		
Data Wrt I	Min	4		
Integ Time	Sec	60		
Site Latitu	41.76983			
Site Longi	-72.9426			
This Fram	UTC	2021-07-26-06-36-08		
Antenna A	Deg	180		
Antenna E	Deg	90		
Antenna S	lambda	17.32466		
LMST duri	Hrs	0.021514		
RA during	Hrs	0.01864		
Dec during	Deg	41.76983		
Galactic La	Deg	-19.95		
Galactic Lo	Deg	113.5281	Pnts/Fring	4

Figure 7-26-1

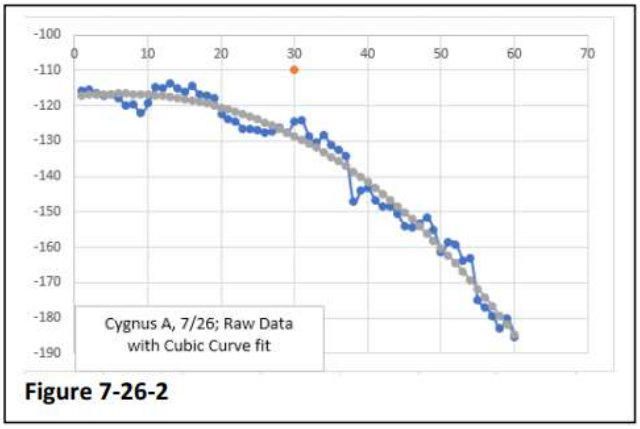

Figure 7-26-2

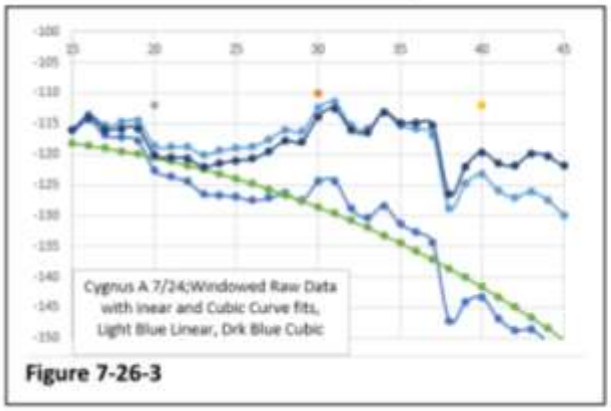

Figure 7-26-3

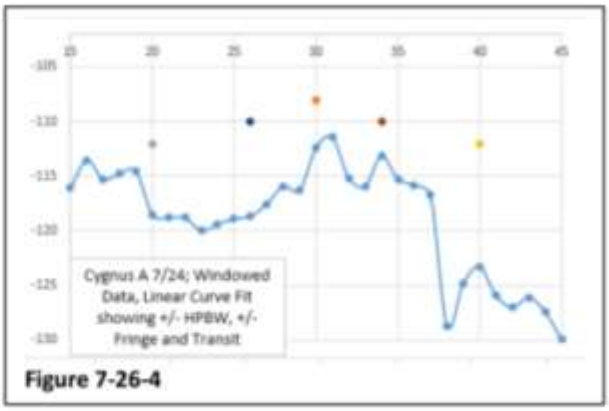

Figure 7-26-4

Data Run 7-31:

Figures 7-31-1 to 7-31-3 show Cassiopeia A captured in the Phase Shift Interferometer configuration. Figure 7-31-2 shows the complete 4 hours of data with transit marked with a simple linearization. Figure 7-31-3 shows the linear curve data, the +/- HPBWs, +/- Fringe peaks and Transit marked. The fringe period is 24.5 minutes with a data write interval of 4 minutes making the interval at ~ 6 data points. The Fringe peaks can easily be seen. Cassiopeia's declination drove the baseline spacing as the previous 10 λ would make the fringe period 42 minutes which is to long relative to my 3dB antenna HPBW in a drift scan.

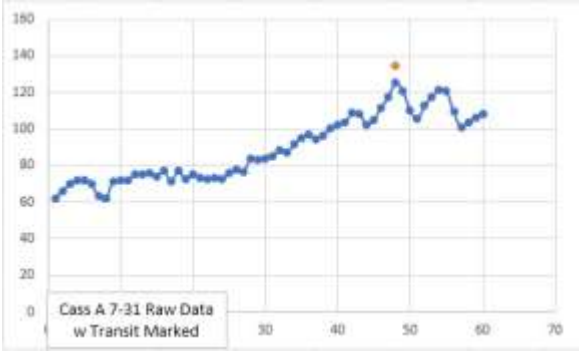

Figure 7-31-2

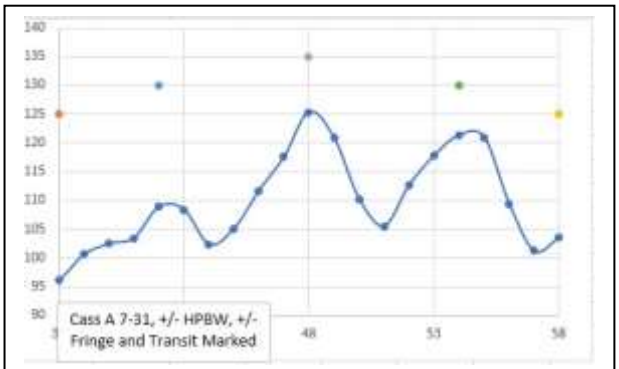

Figure 7-31-3

Data Run 8-1:

Figures 8-1-1 to 8-1-3 show Cassiopeia A captured in the Adding Interferometer configuration. Figure 8-1-2 shows the complete 4 hours of data with transit marked with a simple linearization. Figure 8-2-3 shows the linear curve data, the +/- HPBWs, +/- Fringe peaks and Transit marked. The fringe period is 24.5 minutes with a data write interval of 4 minutes making the interval at ~ 6 data points. The Fringe peaks can be seen however the S/N is marginal. I set the RF Gain to 27dB which is 3dB to high which may explain the attenuated Fringe pattern.

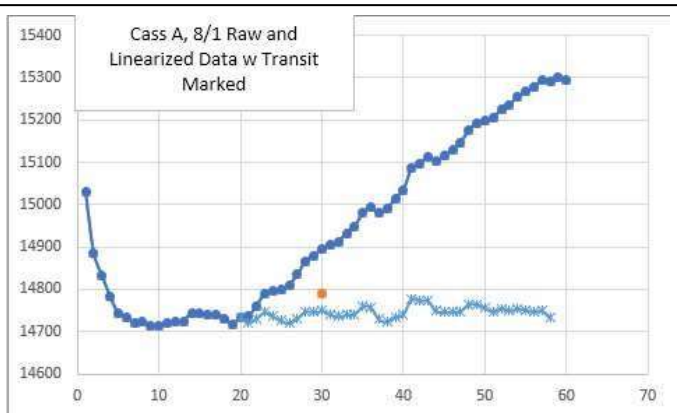

Figure 8-1-2

Observation Start time: 2021-08-01 01:36:04

Interferometer Data

The Hardware will be Configured as an ADDING Interferometer

Session Notes:	Cass A	New LNA Design	Location Clegr of Trees
Fringe Period	Min	24.89548065	
Center Freq	MHZ	1420	
Band Width	MHz	1	
RF GNU Gain	dB	27	
I/Q GNU Gain	#	40	
Tot Obs time	Min	240	
Data Wrt Interval	Min	4	
Intag Time	Sec	240	
Site Latitude	41.76983		
Site Longitude	-72.9426		
This Frame Start Time	UTC 2021-08-01-05-36-04		
Antenna Az	Deg	0	
Antenna El	Deg	73	
Antenna Spacing	lambda	17.32465994	
LMST during Acq	Hrs	23.41303486	
RA during Acq	Hrs	23.41590799	
Dec during Acq	Deg	58.7698301	
Galactic Latitude	Deg	-2.074147012	
Galactic Longitude	Deg	112.2791793	

Figure 8-1-1

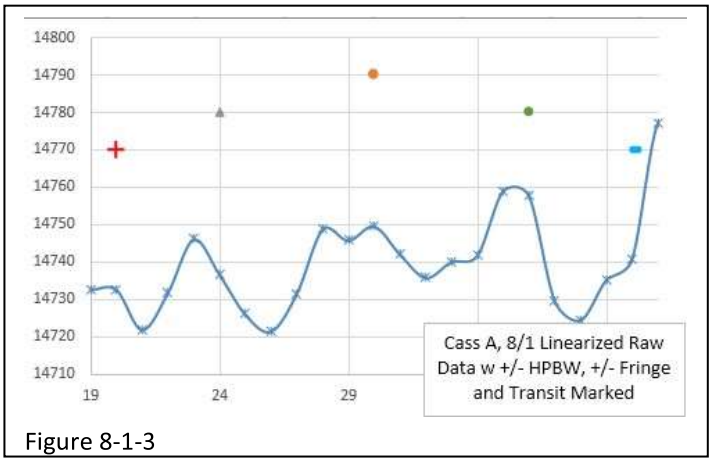

Figure 8-1-3

Data Run 8-3:

Figures 8-3-1 to 8-3-3 show Cassiopeia A and with a strange phenomenon that the fringes appear to be minima's verses maxima's. This could be due to the instantaneous phase relative to the phase inversion command, but this is not verified. The S/N is next to nothing. Increasing the bandwidth would raise the detected signal however the noise bandwidth also increases yielding the same power levels relative to the noise floor.

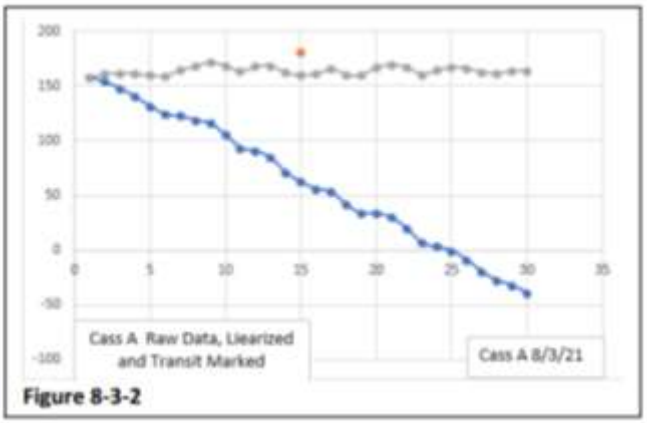

Figure 8-3-2

Observation Start time:	2021-08-03 02:00:08	
Interferometer Data		
The Hardware will be Configured as a PHASE SHIFT Interferometer		
Session Notes:	Cass A	Clear of T New LNA
Phase Switch Freq	Hz	1
Fringe Period	Min	25.24905
Center Freq	MHZ	1420
Band Width	MHz	1
RF GNU Gain	dB	27
I/Q GNU Gain	#	40
Tot Obs time	Min	180
Data Wrt Interval	Min	6
Integ Time	Sec	360
Site Latitude	41.76983	
Site Longitude	-72.9426	
This Frame Start Tim	UTC 2021-08-03-06-00-08	
Antenna Az	Deg	0
Antenna El	Deg	73
Antenna Spacing	lambda	17.32466
LMST during Acq	Hrs	23.44418
RA during Acq	Hrs	23.44702
Dec during Acq	Deg	58.76983
Galactic Latitude	Deg	-2.15049
Galactic Longitude	Deg	112.5092

Figure 8-3-1

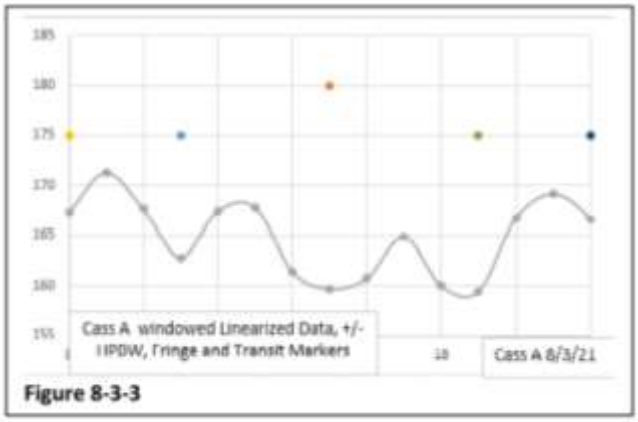

Figure 8-3-3

Data Run 8-4:

Figures 8-4-1 to 8-4-3 show Cygnus A. The baseline was adjusted so that longer integration times, 6 minutes, could be done and still see the fringe structure. The fringe period should be approximately 4 data points. The Fringe and Transit markers appear to be shifted. The data point is the power detected in the previous integration time, or period. The 6-minute data write time may have caused the apparent time slide. The S/N is still in the 'kinda see it' realm. The hope was to show Cygnus with the Adding and Phase Switched configurations showing the phase switched mode would not show the 'RF cloud' that follows Cygnus by ~ 30 minutes. The data just isn't good enough quality to show that benefit clearly.

Observation Start time:	2021-08-03 22:00:02		
Interferometer Data			
The Hardware will be Configured as a PHASE SHIFT Interferometer			
Session Notes:	Cygnus A	BaseLine	New LNA
Phase Switch Freq	Hz	1	
Fringe Period	Min	26.02411	
Center Freq	MHZ	1420	
Band Width	MHz	1	
RF GNU Gain	dB	27	
I/Q GNU Gain	#	40	
Tot Obs time	Min	240	
Data Wrt Interval	Min	6	
Integ Time	Sec	360	
Site Latitude	41.76983		
Site Longitude	-72.9426		
This Frame Start Time	UTC 2021-08-04-02-00-02		
Antenna Az	Deg	180	
Antenna El	Deg	90	
Antenna Spacing	lambda	11.54977	
LMST during Acq	Hrs	20.00031	
RA during Acq	Hrs	19.99743	
Dec during Acq	Deg	41.76983	
Galactic Latitude	Deg	6.033686	
Galactic Longitude	Deg	77.40327	

Figure 8-4-1

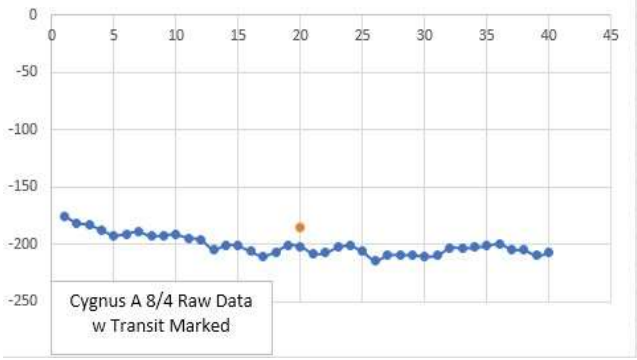

Figure 8-4-2

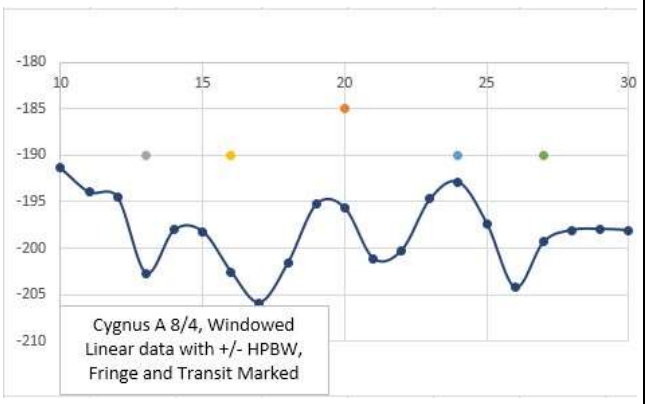

Figure 8-4-3

Section 8, Conclusion and Lessons Learned:

This is HARD!

The data shown here validates that a single sdr can be used successfully in either an Adding or Phase Switched interferometer. The data is marginal with 7-31 being the best. Much of the data has minimal S/N however in Radio Astronomy our targets are well below the noise floor which reinforce the amazement in the results of NRAO and others. The tradeoffs necessary to obtain good data is a balancing act. I used 3 baselines as my antennas are on heavy duty photo tripods. Adjustable baselines with bigger antennas will be mechanically large and costly.

I did not meet my goal of more sensitivity due to the bandwidths I used. My continuum system uses an FFT where the noise bandwidth is the bin width, typically 1 Hz. A 1 MHz to 1 Hz bandwidth reduction relates to a 60dB noise floor reduction. A 'dugh' moment!

The LNA development is a flash back to when I worked in LASER RADAR designing and building LADAR receivers. My second iteration LNA included regulated +4V and -4V used for the DBM drive and VVA attenuation settings. After running dGain/dV tests, I configured the ERA3 to be powered off the +4V. A current source would have been a better choice but would require another PCB iteration and parts. Assuming identical parts in the LNAs have the same temperature coefficients also open to consideration. The Rpi PoE 'Hat' 5V output is not 5V at the LNA internals due to the actual PoE +5 V regulator and the IR loss through the bias Tees. The LNA 5V is closer to 4.8V which is supplied to the Qorvo parts. Genesys uses the *.s2p files for the parts which were done under +5V operation. A new LNA correcting the power problem and still be powered over the LNA output COAX will require the input power to be 'boosted' then applied to the linear regulators generating the required voltages. This results in a lot of 'electronics overhead' and consequently, additional power dissipated. During testing the PCB around the 9036 was 90F. I did try using a TE cooler under the first MMIC confirming my lack of experience in thermal design.

My second LNA build did prove that 'home builders' can do SMT PCB assembly. I used a hot plate, coarsely temperature controlled, to affix the small parts to the PCB. The PCB, with solder paste and parts, were placed on a large chunk of aluminum to act as a heat spreader. This opens building sophisticated electronics at home. I used ExpressPCB, and their software, for PCB fabrication resulting in inexpensive boards. The dielectric constant and loss tangent are NOT tightly controlled. Sunstone Circuits supposedly can take ExpressPCB data using FR4 with tighter specifications, but the cost structure not the same; 4 boards with 5 day turn cost $128. Multiple material PCB stack ups is beyond the hobbyist cost.

My antennas, a modified 5.8 GHz dish written up in a past SARA Journal, need to be improved however their area marginal. My radio telescope resides in my wife's backyard. My previous 408 MHz system is referred to by my wife as 'the monster' which sets my environment! I used one of the modified antennas with Apostolos's VIRGO code and I did repeatably detect the hydrogen doppler in the Perseus arms of our galaxy. The Phase Shift Interferometer goal is to use one sdr and to capture more signal and gain some spatial resolution.

My spin on Python it is like BASIC. I cut my teeth on Radio Shack Level 2 Basic. I am still looking for a book that states a command, its syntax and command description. TRSDOS was a breeze! I am not a python user but used Google for help. I wasted money on 'Python Crash Course' and 'Learning Python' possibly looking for the Level 2 Basic type manual.

GNU Radio is another learning process as, again, I was looking for my 'Level 2 manual'. GNU documentation is almost non-existent. Maybe I was looking in the wrong place. I am NOT a python or LINUX programmer which may explain my unsophisticated coding. I did most of the debug of GNU Radio on an i7 laptop as ANYTHING on the Rpi slow, PAINFULLY SLOW. The problem with the i7 platform is the hardware was not available forcing code transferring.

My sensitivity analysis brings some questions. I know my gain adjustments are not to the hundredths of dB indicated by the analysis results. I used a HP8657B and HP8594E, signal generator and spectrum analyzer, set up with a Δ marker. I can assume my gains to be +/- .5 to 1dB the same. Was my approach correct in assessing the temperature error and is the gain error causing the apparent low, nonexistent, SNR? Gain imbalance introducing an increased noise floor masking the true signal. Is a correlation interferometer subject to the LNA gain in balance?

I want to thank Marcus Leech and Ken Tapping for their help and Bruce Randall's paper on his 408 MHz analog interferometer.

When I was working, I purchased the test equipment necessary to pursue the development on LNAs specifically for Radio Astronomy. My software reside on a Windows 7 machine and I will continue to experiment with Radio Astronomy until this machine dies. There is no way to substantiate the expenditures for replacement software. Again, this is a hobby; but a hobby is defined to take all your spare time and money.

My wife will be glad to see me again as she says I have spent waaay to much time 'in the shed', a backyard 10x20 building that has my HAM station, electronics and astronomy library, main computing and electronics development. She says she doesn't keep track,,,,, RIGHT!

I will assemble the software, LNA schematic and parts list in a ZIP file. It would be possible to extract the VVA and DBM, and support electronics, into a PCB so that other LNAs could be used at other frequencies. The code used here is 'pretty' stable however Murphy is alive and well.

Lastly, I have kept this paper on the serious side, except for this section. I look forward to comments.

Later,

Shef.. WA1RHT
shefrobotham@comcast.net

Appendix:

```
"""
Embedded Python Blocks:

Each time this file is saved, GRC will instantiate the first class it
finds to get ports and parameters of your block. The arguments to __init__
will be the parameters. All of them are required to have default values!
"""   import numpy
as     np     from
gnuradio import gr
from  time  import
sleep
  class  blk(gr.sync_block):    #  other  base  classes  are  basic_block,
decim_block, interp_block


    """Embedded Python Block, Test SquareWave State """
     def __init__(self):                                  # No Passed
Var's          gr.sync_block.__init__
        (              self,             name='Embedded Python Block RPi
GPIO',        # will show up in GRC                in_sig=[np.float32],
out_sig=None
        )
     def      work(self,      input_items,
output_items):
         global
PhSwBitOut
         if
input_items[0].all()==1:
            BitOut=1
            Mult=1
            PhSwBitOut(stat=1)                 # Call external PhSwBit Function w
Stat==1         else:             BitOut=0
            Mult=-1
            PhSwBitOut(stat=0)             # Call external PhSwBit Function w Stat==0
         return
len(input_items[0])



# This function will Control RPi GPIO 17 used for Phase Switching in a
# Phase Switched Interferometer
#
# from gpiozero import LED
# led=LED(17)                        # May cause a crash if not RPi

def PhSwBitOut(stat):               # the actual function
    #global  led
     if
stat==1:
        i=1                           # just some bogus statement to
#led.on()                   # prevent from crashing w/o RPi     else:
        i=2                            # just some bogus statement to
#led.off()                  # prevent from crashing w/o RPi     return
```

Appendix A-1

```
# from gpiozero import LED
# led=LED(17)                          # May cause a crash if not RPi
 def PhSwBitOut(stat):                 # the actual function
    #global  led
     if
stat==1:
        i=1                             # just some bogus statement to
#led.on()                        # prevent from crashing w/o RPi     else:
        i=2                              # just some bogus statement to
#led.off()                        # prevent from crashing w/o RPi
    Return
```

Appendix A-2

Shef Robotham lives in New England and has worked in electronics since high school. Previous positions at United Technologies Research Center and Optical Systems divisions specializing in laser radar. He is a co-founder of DeMaria Electro-Optic Systems, a RF excited CO_2 laser manufacturer, later purchased by Coherent Inc. Shef has an 'above average' home electronics capability, with a focus on Radio Astronomy LNA and receiver projects. An abundant 'junk box', and parts inventory, aides in project completion, He presented a 408 MHz Radio Telescope at a SARA conference several years ago, is very active with astro-imaging with an observatory from a converted a storage shed. A radio amateur, WA1RHT, can be contacted at : shefrobotham@comcast.net.

On the Local Standard of Rest

Wolfgang Herrmann

Abstract

This article deals with the Local Standard of Rest (LSR) which is the commonly used reference frame for giving velocities in particular for spectral measurements in our own galaxy. Such a reference frame is of importance when observations from different observatories, different times, or towards different directions are compared. This article explains the background and demonstrates why this is important also for amateur observations. Code is provided to do the necessary calculations.

What is the issue?

Velocities can be measured when an astronomical object emits (or absorbs) radiation from a well-known transition between different energy levels. This manifests itself in the occurrence of a distinct spectral lines. The most prominent example in radio astronomy is the 21-cm line (1420.405 MHz). But many other lines are also observable in the radio regime and the study of these give detailed information of the dynamics involved. For the amateur radio astronomer, observations of the 21-cm line of neutral hydrogen can easily be achieved. But amateurs have also been successful in observing maser emission lines from OH, methanol and water. With larger instruments radio recombination lines of hydrogen and carbon become observable.

The velocity of the observed objects become apparent by the Doppler shift of the line, i.e. a deviation of the observed frequency from the frequency of the transition, the so-called rest frequency.

The amount of the Doppler shift is determined by the velocity between the observed object and the observer. This immediately shows that there is an issue: The observer itself moves as the earth rotates around the sun and around itself. This will result in different Doppler shifts at different times and even between different observatories. This makes observations difficult to compare to each other. Furthermore, observational results are difficult to interpret with respect to the motions of the observed regions when the observer motion is included in the data. The solution to this problem is to define a standard reference frame, to which all observations are related. By using such a reference frame, observational results become independent of time and location of the observations.

Reference frames: ICRS

In order to provide a common ground, the International Astronomical Union (IAU) [1] has defined a reference frame, the International Celestial Reference Frame (ICRS) [2]. This reference frame is centered at the barycenter of the solar system. The exact definition is refined from time to time. Some links to this subject matter which may be of interest are [3][4][5].

The position of the earth and other objects of our solar system with respect to this reference frame is represented by a solar system ephemeris. A widely adopted ephemeris are the JPL DE430/DE431 models [6]. With this ephemeris, the position and velocity of the earth with respect of the ICRS frame can be calculated for any point in time. Then of course, the motion of the observer location in respect to the center of the earth due to the rotation of the earth needs to be considered as well. Referencing all observations to the ICRS reference frame will eliminate all such variations caused by the motion of the observatory in the solar system.

Reference frames: From ICRS to the Local Standard of Rest

The ICRS reference frame is used for many observations as the standard reference frame. There is one limitation of this standard, though: It takes the solar system barycenter as the point of reference. Obviously, our solar system will also move within our milky way. So, any observation which is intended to learn about the dynamics of our galaxy will be influenced by this motion. It has been found, that our solar system has a peculiar motion with respect

to the stars in the local vicinity, the so-called Local Group. In order to eliminate this motion, an additional correction is introduced which accounts for this. This reference frame is called Local Standard of Rest (LSR).

Determining the peculiar motion of the sun, however, depends on which stars in the neighborhood are taken into account and how the measurements are done. Therefore, over time several different results have been achieved and consequently different definitions have bee drafted. Fortunately, it seems that in the radio astronomy community there is a common ground which is using the following definition based on work by Gordon [7]:

The peculiar solar motion is 20 km/s in direction RA 18 h , Dec +30° at epoch 1900.
This is equivalent to the definition at epoch 2000:
20.0 km/sec towards RA 18h03m50.29s, Dec +30°00'16.8"

This definition is also called the kinematic LSR. It has been verified that this definition is in use at the observatories Effelsberg[8], Jodrell Bank[9], Green Bank[10] and the ATNF telescopes [11]. Since our (Stockert) data using this definition agrees with data from the Nancay telescope it can safely be assumed that the same definition has been adopted there. Therefore, it is highly recommended that this definition should also be applied in the amateur community.

How to calculate the LSR correction
Calculating the LSR correction is a complex task as it needs to take the various motions into account. Fortunately, there are now routines available as part of the AstroPy package. However, there is a big caveat: Astropy routines do not use the kinematic LSR as defined above as default. Therefore, it is required to set the parameters to override the default settings of Astropy.

With this article I am providing Python code to implement the kinematic LSR calculation based on Astropy. The code with the file name lsr_calc.py contains a function vlsr_calc which does all the needed calculations based on the coordinates of the telescope, the equatorial coordinates of the observed sky location and the time of observation. It provides both the Local Standard of Rest velocity and the barycentric velocity. The code also contains examples how to use this function. These examples are:

- Calculate the observer's velocity with respect to the Local Standard of Rest and Barycenter for a given observatory, sky coordinate and time
- Calculate the frequency of the Hydrogen line at rest for the observing parameters as above. This is useful for determining to which frequency the receiver must be set in order to record directly in the LSR frame
- Calculate the LSR-velocity for an observed hydrogen line for the observing parameters as above.

Please note that using this code requires Python 3 and a fairly recent version of Astropy. It has been tested with Astropy 4.2. The code is available on https://github.com/Astropeiler/vlsr_calc.

There is some other code available from Tammo Jan Dijkema on gitlab [12] which works fine and is using the kinematic LSR standard. This code is also based on Astropy.

How about online-calculators? There is one available at [13] which is based on previous work by Steve Olney from the HawkRAO observatory. He himself does no longer provide an online calculator. There used to be a few more around in the past. At the time of writing these seemed to have disappeared or are not functional any more. Any hints to the author about additional calculators are welcome.

Correction applied during data capture or post processing?
One of the questions inevitably come up: Should one correct for the LSR immediately when recording the data or should one record topocentric data and then correct it later in the further process? Both options are viable. The typical approach at professional observatories is to record data in the LSR reference frame. The main argument is that one should take out any observatory specifics and provide data which is independent of the location and time. One can always convert this data into other reference frames without any additional information required. The only thing which needs to be known what reference frame has been used for recording.

In contrast to this, any recording in a local reference frame will need to keep additional information such as location of the observatory and time of observation in order to be able to convert this to other reference frames later on.

In certain cases, when very high-resolution data is recorded with very long integration times (weak maser sources for example) it may be needed to adjust the frequency during the observation. The Doppler shift might vary during the observation time enough to broaden the recorded line. In this case, this can only be avoided by adjusting the frequency of observation from time to time. This is only doable when recording directly in the LSR frame. This scenario, however, will hardly ever occur in an amateur observatory so may be not so relevant here. In particular, it is not required for any Hydrogen line observations as these lines are fairly broad.

Does it matter for the amateur community?
The simple answer is, yes it does. The difference between an uncorrected spectrum and a spectrum referenced to the Local Standard of Rest can be quite significant. Below in fig. 1 are examples of the Hydrogen spectra at galactic latitude 90° / galactic longitude 0°. One spectrum (black) is referenced to the local standard of rest whereas the other (red) is without correction.

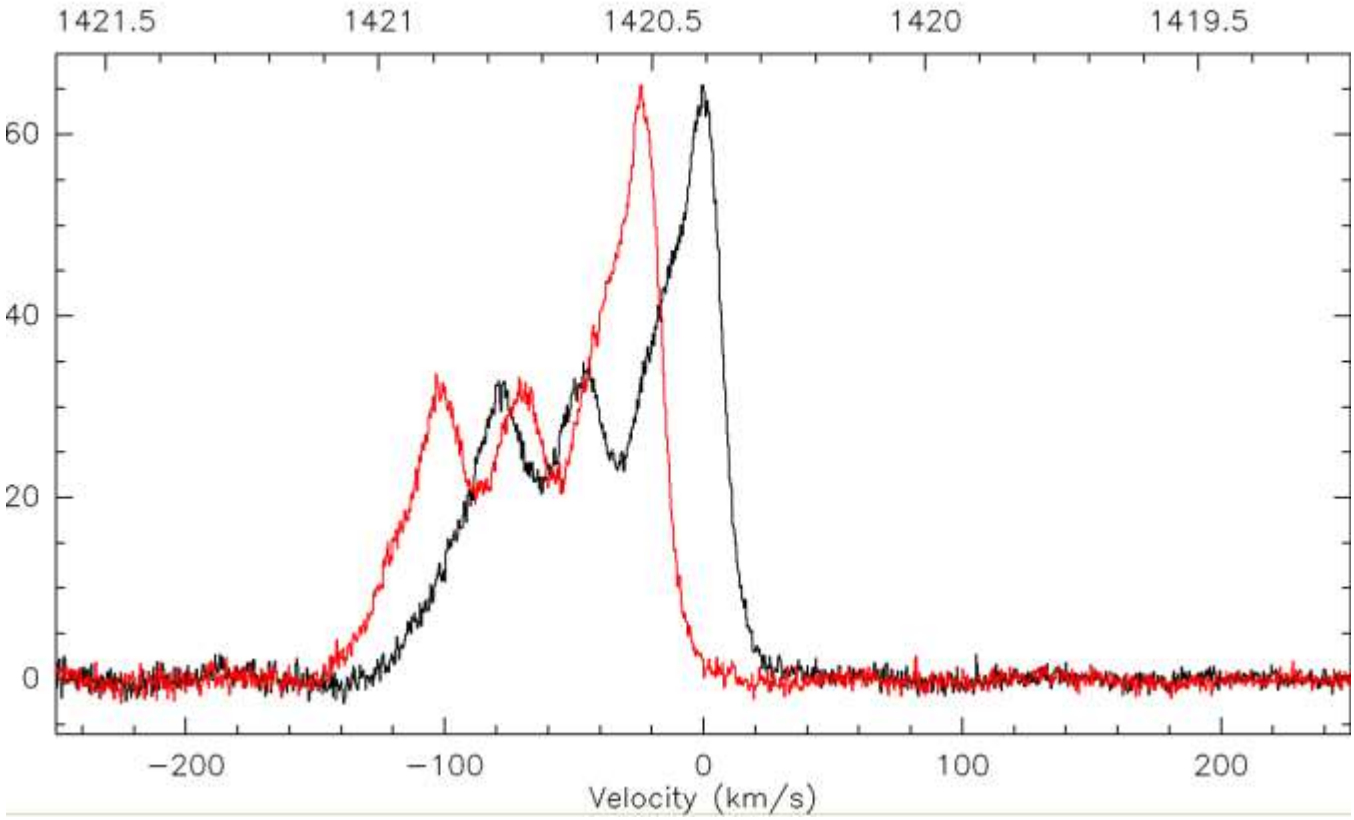

Figure 1: Hydrogen Spectra at l=90°, b=0° with and without LSR correction

The spectra were taken with one of the smaller instruments of our observatory, a 2.3-m dish. Data was recorded at Aug. 6th at approx. 16:07 UTC with 20 seconds integration time each. The difference in velocity at that time was 23.5 km/s km/s. This is certainly a significant difference which cannot be neglected.

A frequent experiment done by amateurs is to record the spectra at various galactic latitudes in the galactic plane and derive the rotation curve from that data. The result will be erroneous if the spectra are not referenced to the LSR as an additional Doppler shift is introduced due to the motion of the observer.

In conclusion, it is recommended that also amateurs adopt the practice to record data in the LSR reference frame.

References

[1] https://www.iau.org/
[2] https://en.wikipedia.org/wiki/International_Celestial_Reference_Frame
[3] https://www.iau.org/static/science/scientific_bodies/commissions/a1/icrf-annual-report-2018.pdf
[4] https://www.iau.org/static/resolutions/IAU2018_ResolB2_English.pdf
[5] https://www.iers.org/IERS/EN/Science/ICRS/ICRS.html
[6] https://naif.jpl.nasa.gov/pub/naif/generic_kernels/spk/planets/de430_and_de431.pdf
[7] “Methods of Experimental Physics: Volume 12: Astrophysics, Part C: Radio Observations", ed. M.L.Meeks, Academic Press 1976.
[8] Private communication with Jürgen Kerp and Benjamin Winkel, University Bonn
[9] Private communication with Sandra Etoka, Manchester University

[10] https://www.gb.nrao.edu/~fghigo/gbtdoc/doppler.html
[11] https://www.narrabri.atnf.csiro.au/observing/obstools/velo.html
[12] https://gitlab.camras.nl/dijkema/HPIB/blob/185d241ad9bd7507ed90c9fa91fe0a63009d3eee/vlsr.py
[13] http://f4klo.ampr.org/vlsrKLO.php

About the Author: Dr. Wolfgang Herrmann is the president of the "Astropeiler Stockert e.V.", the organization which operates the Stockert radio observatory.

He received his PhD in Physics from the University of Bonn. He has spent most of his professional career in the telecommunication industry. At retirement age, he now enjoys learning as much as possible about radio astronomy, doing observations and improving the instruments at Astropeiler.

Contact the author at messbetrieb@astropeiler.de

Comparison of Signals from South and West VLF Stations During June 2021

Whitham D. Reeve

1. Introduction

It is known that the solar terminator (gray line) and other diurnal variations in the spherical earth-ionosphere waveguide affect VLF propagation. Plots over time of the signal power received from distant VLF transmitters have a characteristic pattern and are used to verify receiver and antenna operation and the receiver noise environment and to detect sudden ionospheric disturbances (SID) and other effects associated with solar flares.

The signals propagate along what are known as *short* and *long* paths. The short path is the most direct great circle path between the transmitter and receiver, and it involves one or, possibly, more waveguide modes depending on its length and other conditions. On the other hand, the long path usually is not a single, simple great circle path but is much more complicated because of its greater length, possible non-great circle routing over Earth's surface and mode changes at land, water, and ice interfaces. The various paths and waveguide modes may interfere with each other, both constructively and destructively. Thus, variations may exist in the received signal levels due not only to diurnal solar effects but also to propagation path characteristics. For more information on VLF propagation, see {Reeve19-1}

To investigate these effects, I recorded the received signal levels on two disparate propagation paths, one from a VLF transmitter located south of Cohoe Radio Observatory (CRO) and another from a VLF transmitter located west of CRO (figure 1). Both paths are predominantly over water. Data were recorded during two separate sessions in June 2021. It is shown that the daily signal variations for the south path are significantly different than the west path. While that is not surprising, the data form the basis for further study. Also, it happened that during data collection on the south path, an annular solar eclipse occurred on 10 June. The eclipse was not visible from the path being recorded that day; however, eclipses are known to affect VLF propagation so the characteristics of the data plot for that date are briefly analyzed.

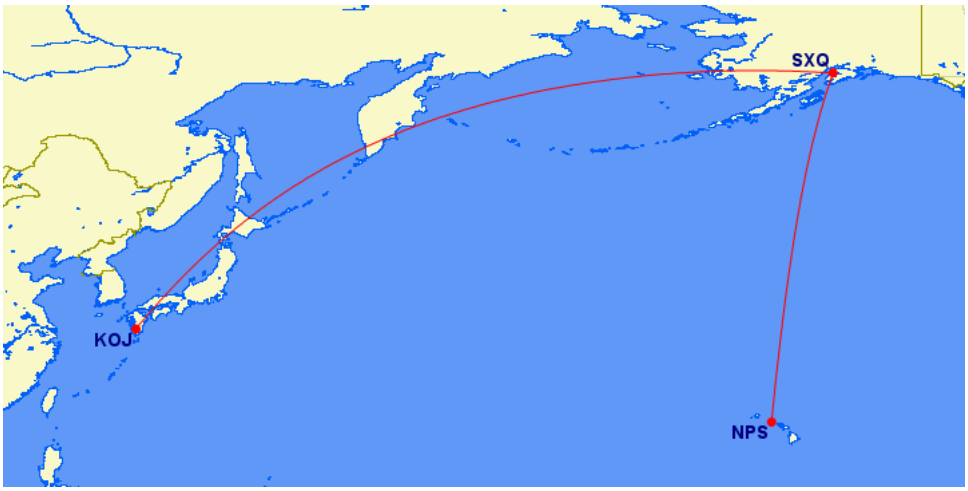

Figure 1 ~ Short paths from Hawaii and Japan to Cohoe Radio Observatory in Alaska. For path mapping purposes, the end points are indicated by the nearest airports: SXQ (Soldotna Municipal Airport near CRO), KOJ (Kagoshima Airport near the JJI transmitter location) and NPS (Ford Island NALF Airport near the NPM transmitter location). Image source: Great Circle Mapper {GCM}

In the case of the south transmitter station, NPM in Hawaii, the solar terminator crossed the short propagation path twice each day at a sharp angle during the times investigated. For the west station, JJI in Japan, the short and long propagation paths and terminator vary from almost parallel to crossing at wide angles. The signal level measurements for the two transmitter stations and solar terminator maps are detailed in section 2 with additional

discussion of this and future work in section 3. Instrumentation is described in section 4 and references and weblinks are listed in section 5.

---

2. Measurements

The information below includes signal level plots and maps showing both the short and long propagation paths. The long path, as shown, is idealized and may not be the actual VLF propagation path in the spherical waveguide but it is sufficient for visualization.

NPM → CRO summary of characteristics:
Transmitter station name, frequency and coordinates: NPM, 21.4 kHz, 21° 25′ 13.38″N, 158° 09′ 14.35″W
Nearest town: Lualualei, Oahu, Hawaii USA
Relative location: South of CRO
Short/long path distance and direction from CRO to NPM: 4364/35 660 km, Azimuth 190° True
Receiver antenna azimuth setting: 000°/180° True
Dates observed: 03 – 13 June 2021

The following discussion is focused on one day, 10 June; all other days were similar. As the solar terminator (figure 2) marched west on 10 June, it intersected NPM with sunset at 0521 UTC (7:21 pm local Hawaii) and then CRO with sunset at 0729 (11:29 pm local Alaska). The next sunrise at CRO was 1238 UTC (4:38 am local Alaska) followed by NPM at 1555 UTC (5:55 am local Hawaii). Since the measurements were near the summer equinox, the sunrise and sunset times varied by only about 1 minute throughout the study period. These sunrise and sunset times are at ground level and would be slightly different for the upper boundary of the earth-ionosphere waveguide, which can vary from approximately 60 to 90 km altitude.

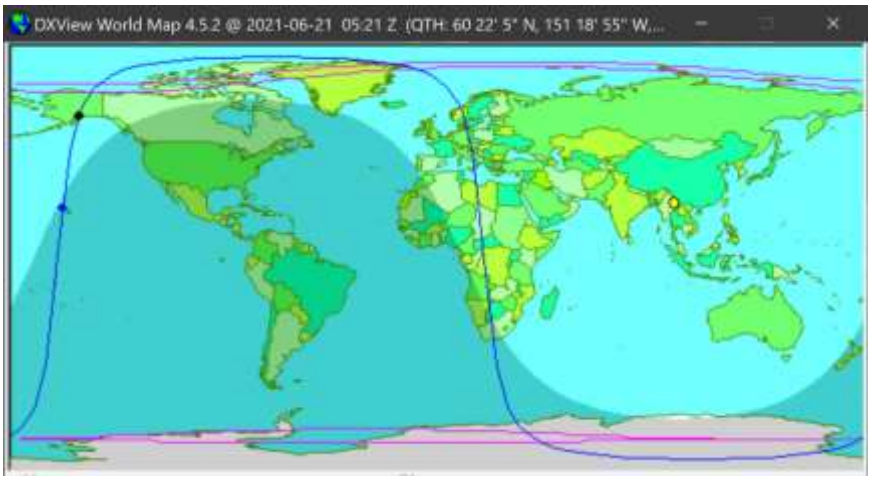

Figure 2 ~ Solar terminator and propagation paths (blue line) at 0521 UTC on 10 June when the Sun rises at station NPM. The receiver and transmitter stations are marked by small solid black circles (left side of image) and the Sun is the small solid yellow circle to the east in the middle of the daylit area. The shaded area, which indicates darkness, moves right-to-left as the day progresses. Image from DXView.

A plot of the received signal levels for the full 10-day study period (figure 3) shows a textbook repeating pattern. The received signal levels increase at night due to more favorable propagation conditions and then fall during the day as D-region absorption increases the propagation losses. Also, there are sunset and sunrise dips in the signal levels (figure 4) as the solar terminator crosses the path. However, in this case, there are two dips at sunrise. The two dips occur 1 hour apart at about 1400 and 1500 UTC, and fall between sunrise at CRO and sunrise at NPM.

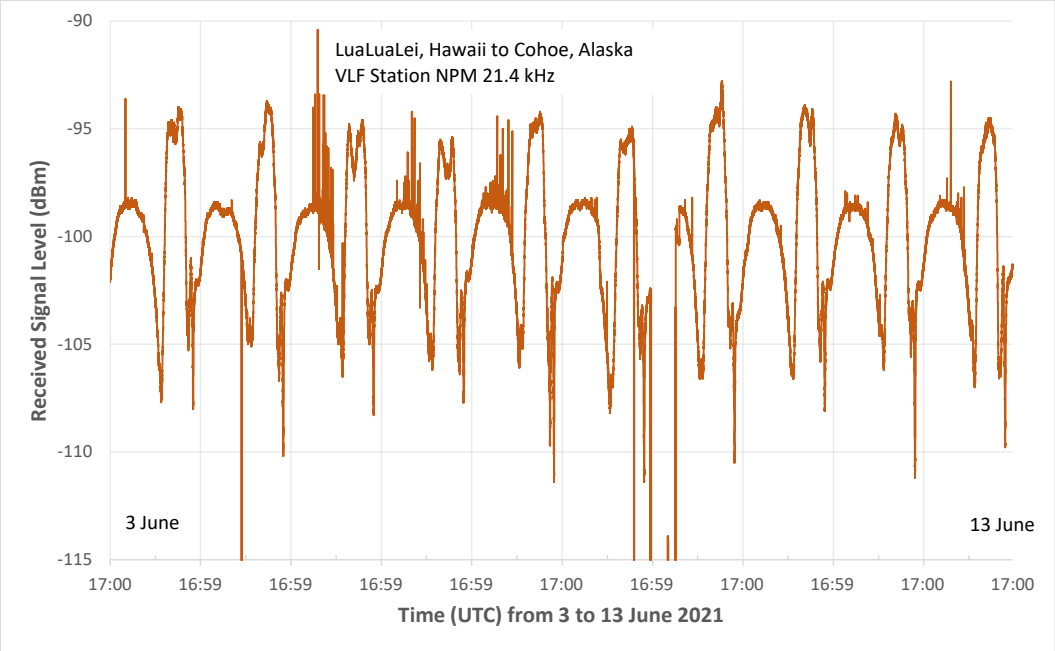

Figure 3 ~ Received signal level at CRO for the 10-day period between 3 and 13 June 2021 from station NPM in Hawaii. Note the short signal dropout on 4 June and a longer dropout on 9 June. These probably are due to transmitter maintenance or failures. There were no known receiver problems.

Another interesting phenomenon is the signal level dip at about 1045 UTC, at which time both the transmit and receive stations and the short path were in darkness (figure 5). However, the Sun was directly over the long path, and the dip may be due to destructive interference between the short and long paths at the receiver. Examination of the data for each of the 10 days shows that the dip does not appear every night.

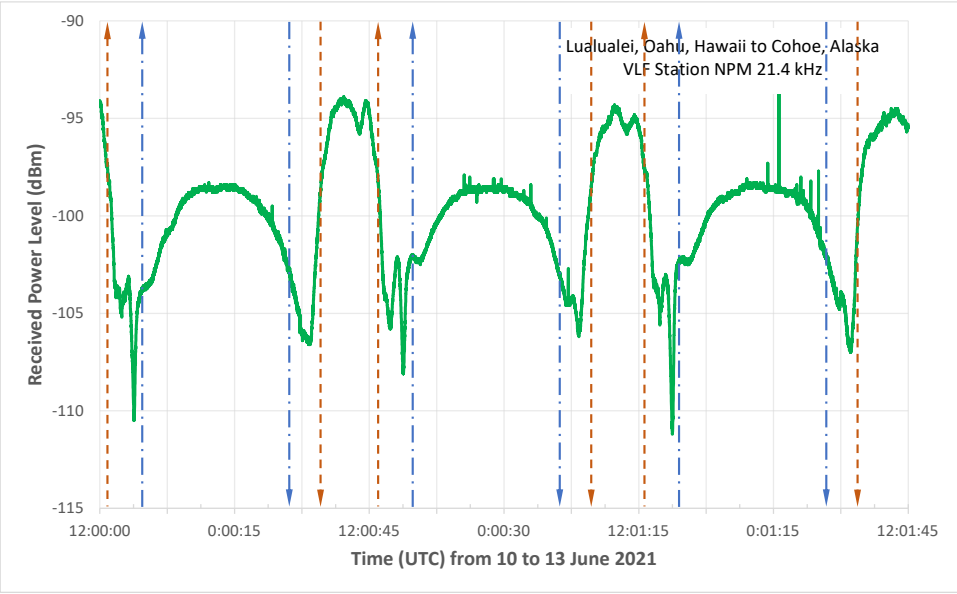

Figure 4 ~ Plot of received signal level for the 3-day period from 10 to 13 June 2021 on the path from NPM to CRO. The repeating pattern is caused by varying propagation conditions during each day and night. The dashed arrowed lines indicate sunset (down arrows) and sunrise (up arrows). The blue lines are for the VLF transmitter at NPM and the orange lines are for the receiver at CRO.

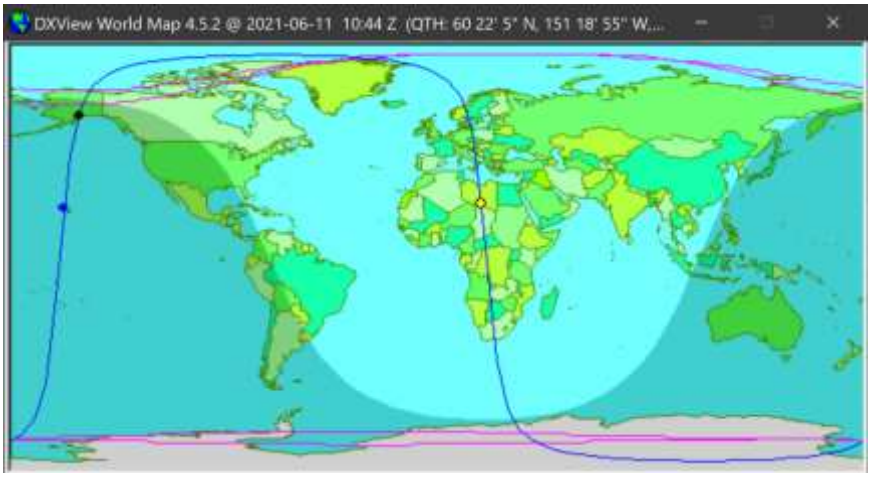

Figure 5 ~ Short and long paths between NPM and CRO (blue line) with solar terminator at 1045 UTC on 11 June 2021, corresponding to the time of the dip seen in the received signal level plot for 11 and 12 June. Image from DXView

Solar eclipse: The solar eclipse on 10 June occurred while the NPM transmitter and CRO receiver locations and short path were in darkness. However, the eclipse annularity path as well as the broader path of the partially eclipsed Sun (figure 6) crossed the long propagation path. Signal level plots for the days before and after the eclipse appear similar to eclipse day (figure 7), but the signal peak near 1200 UTC on 10 June has a slightly higher level than the same time on other days (table 1). This may be unrelated to the eclipse but worth noting.

Table 1 ~ Measured peak signal level during each day near 1200 UTC. Note that the level on eclipse day 10 June is higher than any other day and about 2 dB higher than the average of all other days.

Date	Peak level (dBm)	Remarks
4 June	–94.2	
5 June	–94.3	
6 June	–94.7	
7 June	–95.4	
8 June	–94.6	
9 June	–95.1	
10 June	**–92.9**	Eclipse day
11 June	–94.3	
12 June	–95.0	
13 June	–95.6	
Average	–94.8	All days except 10 June
Std Dev	0.48	All days except 10 June

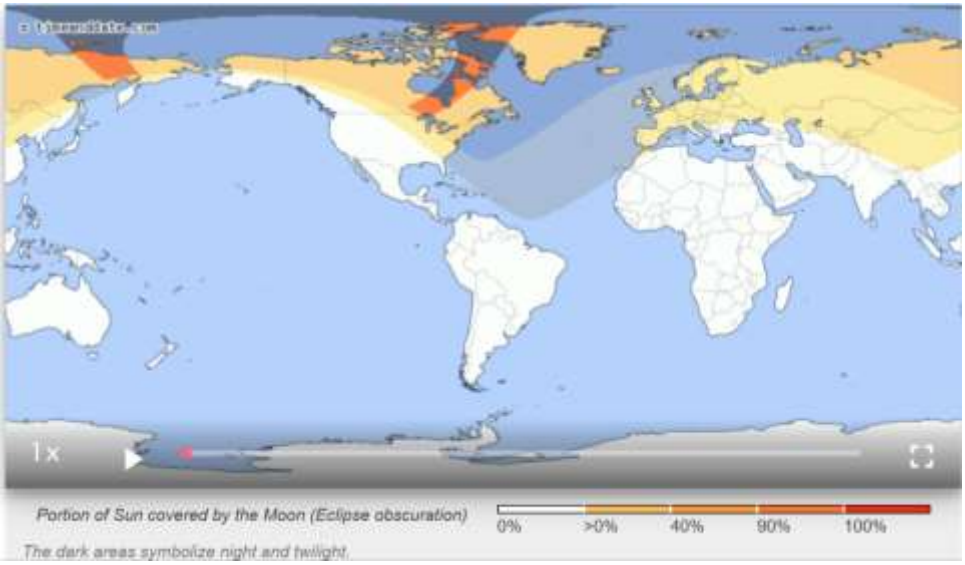

Figure 6 ~ Annular solar eclipse on 10 June 2021 shown by the dark orange swath over Canada, Greenland and Siberia. The maximum occurred at 1042 UTC over Naires Strait near the northwest coast of Greenland. Annularity occurred approximately 1 hour before and 50 minutes after maximum. Comparison with the great circle propagation path above shows the eclipse path did intersect the long path between NPM and CRO. Image source: {TimeDate}

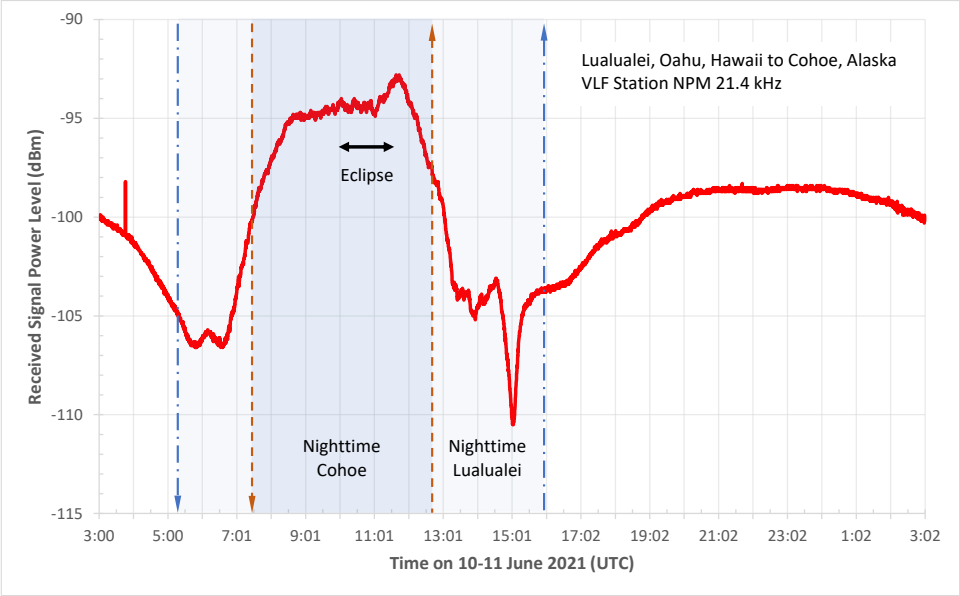

Figure 7 ~ Plot of received signal level on the path from NPM to CRO for the 24-hour period from 0300 UTC on 10 June to 0300 on 11 June 2021. The time range of the solar eclipse is shown. The variations in signal level at eclipse time are not markedly different than the days before and after except the peak just before 1200 is a couple dB higher.

JJI → CRO summary of characteristics:
Transmitter station name, frequency and coordinates: JJI, 22.2 kHz, 32° 04' 58"N, 130° 49' 33"E
Nearest town: Ebino, Miyazaki, Japan
Relative location: West of CRO
Short/long path distance and direction from CRO to JJI: 6299/33 725 km, azimuth 277° True
Receiver antenna azimuth setting: 090°/270° True
Dates observed: 14 – 24 June 2021

The propagation conditions from the VLF station JJI near Ebino in Japan are quite different from the station in Hawaii in that, at times, the solar terminator is almost parallel to the propagation path and other times crosses the short and long paths at wide angles (figure 8). The sunrise and sunset times for 21 June are 1236 and 0737 UTC (4:36 am and 11:37 pm local Alaska) at CRO and 2011 and 1026 UTC (5:11 am and 7:26 pm local Ebino) at JJI,

respectively. Note that, as with the NPM path, these sunrise and sunset times vary by only about 1 minute throughout the 10-day study period.

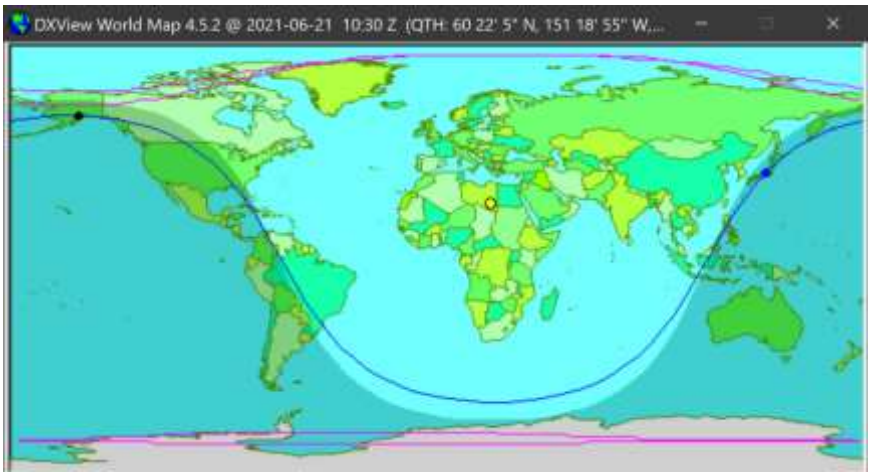

Figure 8.a ~ Solar terminator for the JJI to CRO path at 1030 UTC on 21 June on the path from the west station JJI to CRO. The terminator and great circle propagation paths (blue line) are very close to the same at the time shown. Image from DXView.

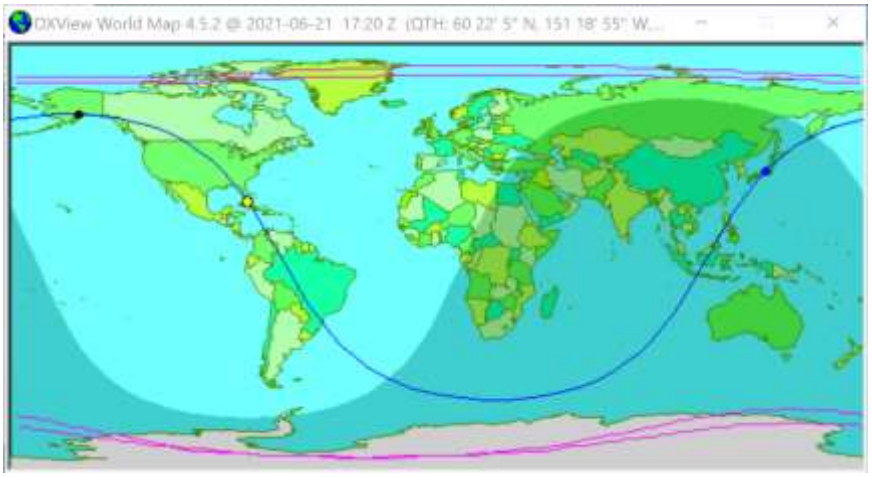

Figure 8.b ~ Solar terminator for the JJI to CRO path at 1720 UTC on 21 June, 7 hours later than the previous image. At the time shown, the solar terminator crosses the short path at nearly a right angle and the Sun is directly over the long path. Image from DXView.

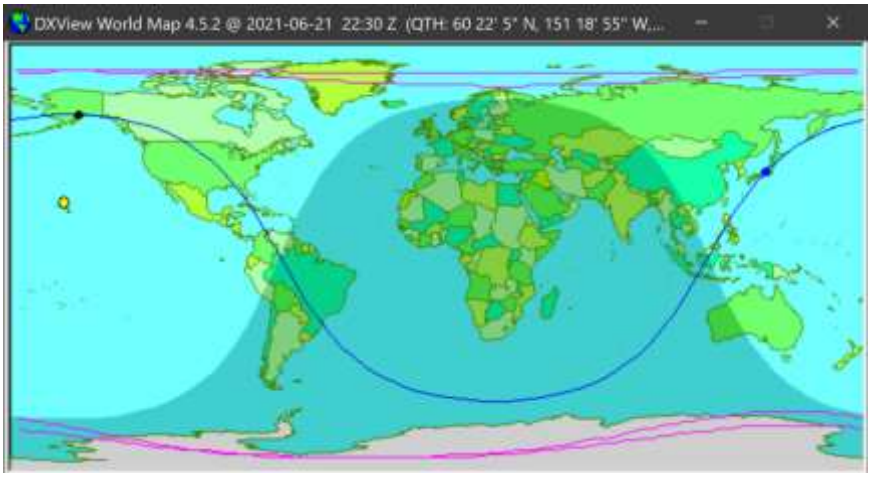

Figure 8.c ~ Solar terminator for the JJI to CRO path at 2230 UTC on 21 June, 5 hours later than the previous image. At the time shown, the solar terminator crosses the long propagation path twice at wide angles. Image from DXView.

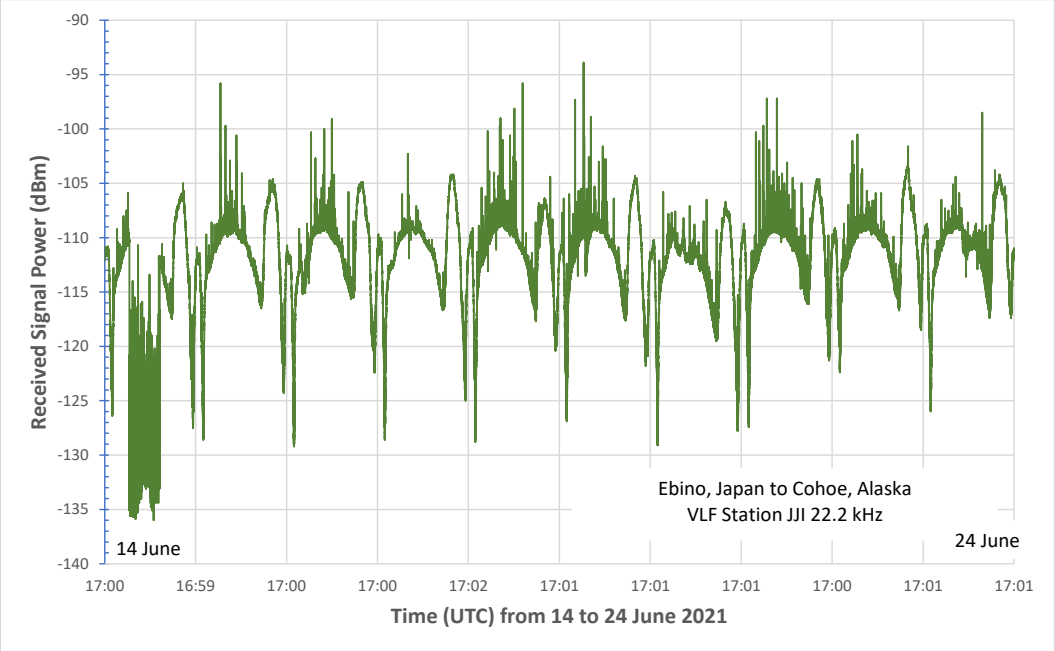

Figure 9 ~ Received signal level at CRO for the 10-day period between 14 and 24 June 2021 from VLF station JJI in Japan. The peak signal levels are about 10 dB lower compared to the NPM path and the daily pattern is different but still recognizable as VLF propagation.

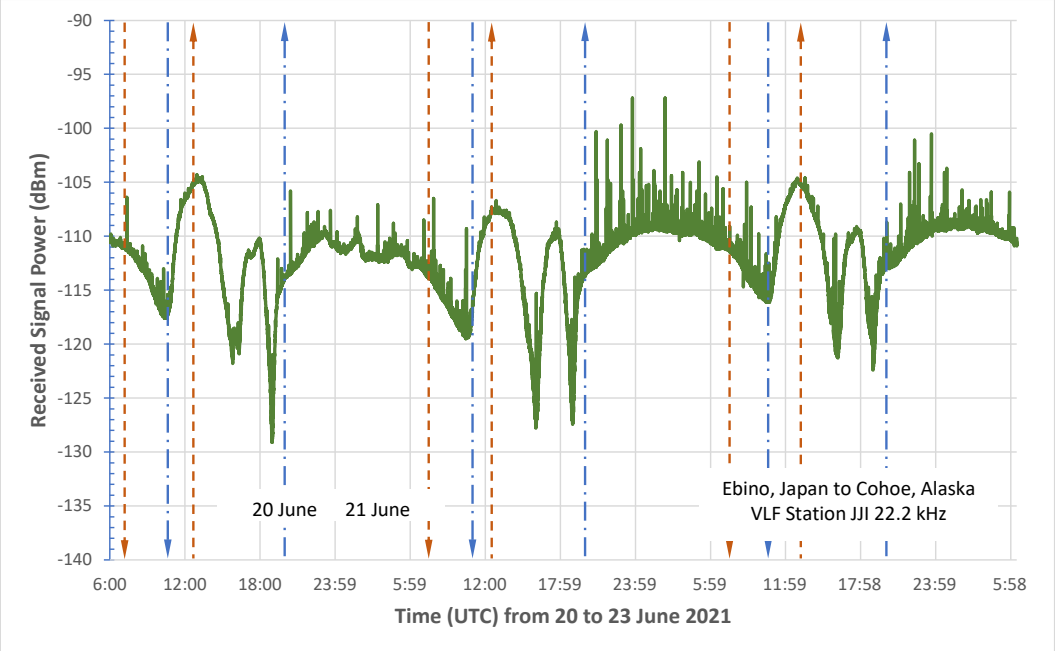

Figure 10 ~ Plot of received signal level for the 3-day period from 20 to 23 June 2021 on the path from JJI to CRO. The dashed arrowed lines indicate sunset (down arrows) and sunrise (up arrows). The blue lines are for the VLF transmitter at JJI and the orange lines are for the receiver at CRO. Note the noise increase between sunrise and sunset at the transmitter station.

The signal level plot for a single 24-hour period on the JJI to CRO circuit shows two signal peaks and three dips that are quite different than those seen on the NPM to CRO circuit (figure 11). On the NPM to CRO circuit, the nighttime signal power has a small dip as previously explained. On the other hand, on the JJI to CRO circuit, there are two substantial peaks and two dips that occur during darkness at JJI. The first dip near 1030 UTC corresponds to when the solar terminator is almost parallel with both the short and long propagation paths; the time is coincident with sunset at JJI. The first peak near 1300 UTC is close to sunrise at CRO. The second dip near 1600 UTC occurs about 1 hour before the Sun crosses the long propagation path. At that time, the terminator crosses both the short and long paths about midway along their lengths. The second peak near 1800 UTC occurs about 1

hour after the Sun crosses the long propagation path. Finally, the third dip near 1900 UTC occurs just before sunrise at JJI.

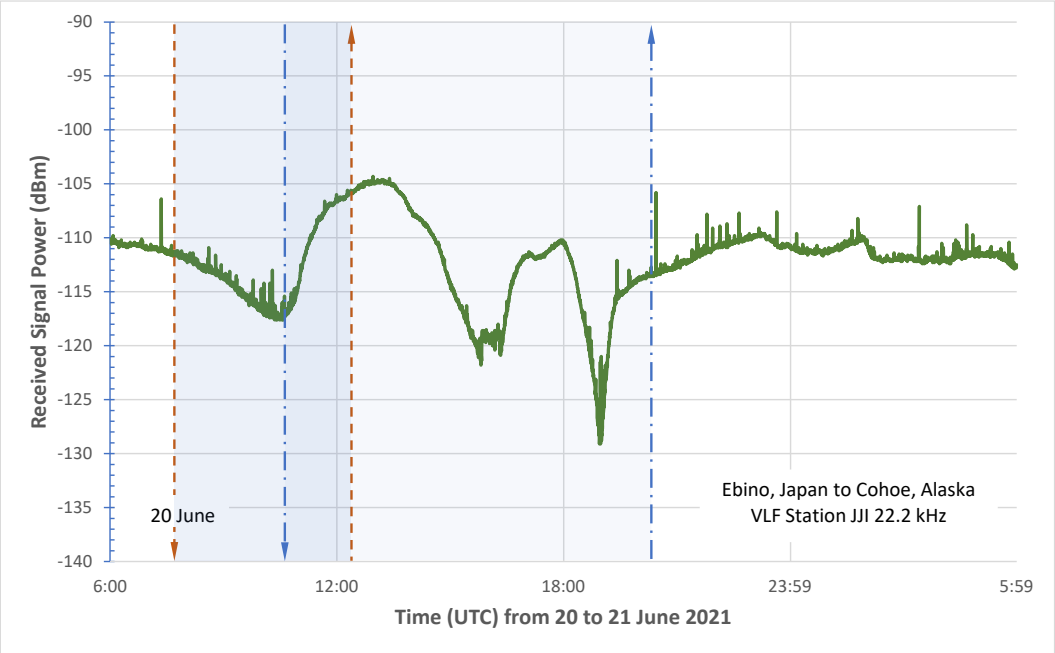

Figure 11 ~ Plot of received signal level on the path from JJI to CRO for the 24-hour period from 0600 UTC on 20 June to 0600 on 21 June 2021.The dashed arrowed lines and shaded area are the same as in previous plots. See text for timing of the various signal peak and dip features.

3. Discussion & Future Work

The data represents only two radio circuits recorded near the summer equinox. The path from the west Japanese station is longer than the path from the south Hawaiian station by almost 2000 km and the received signal levels were about 10 dB lower. The repeating signal level patterns for the two paths during the study periods showed significant differences.

At least some of the pattern differences were due to the interaction of the paths with the varying ionization associated with the solar terminator and other daily variations that normally occur on north-south as opposed to east-west propagation paths. Magnetic field variations and disturbances will affect propagation but this aspect has not been explored. There may be evidence of short and long path interference on the circuits.

For future work, the signal variations from VLF stations to the north and east of CRO will be investigated. The signals from any north station would propagate over land and the North Pole or Greenland (and ice) as opposed to the south overwater path from Hawaii. Similarly, the propagation from some east stations would follow overland paths as opposed to the west overwater path from Japan.

Another factor that is known to affect VLF propagation and will be studied are the effects on specific propagation paths by the solar cycle progression. At the time of this writing, solar cycle 25 has been underway for 1½ years. Recording signal level data on the same two paths every six months or one year throughout the cycle likely would reveal any long-term changes.

Finally, although the solar eclipse on 10 June produced no verifiable indications on the NPM to CRO path, future eclipses are worth monitoring. A little online research quickly reveals what, when and where VLF propagation paths will be crossed by an eclipse path over the next few years. For example, a good place to start is {NASA}.

---

3. Instrumentation

The CRO receiver station is located at 60°22'4.68"N, 151°18'55.14"W. A shop-built square loop antenna and SDRPlay *RSPduo* software defined radio (SDR) receiver are used for VLF work. *SDRuno* software, which is native to the SDRPlay SDR products, was used to gather reception data. A block diagram shows the basic setup (figure 12). More details are given at {Reeve19-2}.

The *PWR & SNR to CSV* function in SDRuno was used to save the measured signal level every 15 seconds to Comma Separated Variable (.csv) files over the two 10-day study periods. Excel was then used to plot the data for various time periods as seen in the previous section.

The main spectrum and waterfall displayed by SDRuno shows all received signals within the configured bandwidth. For the measurements discussed in this article the receiver was set to Zero Intermediate Frequency (ZIF) mode with a sample rate of 2 MHz and factor 8 decimation. These settings provide 250 kHz maximum displayed bandwidth. I used the zoom function to reduce the displayed range to 10 to 40 kHz with 3.81 Hz resolution (FFT bin size of 65 536) (figure 13). The receiver IF gain was set to Auto. The RF gain was adjusted to provide the best signal-to-noise ratio on each of the paths.

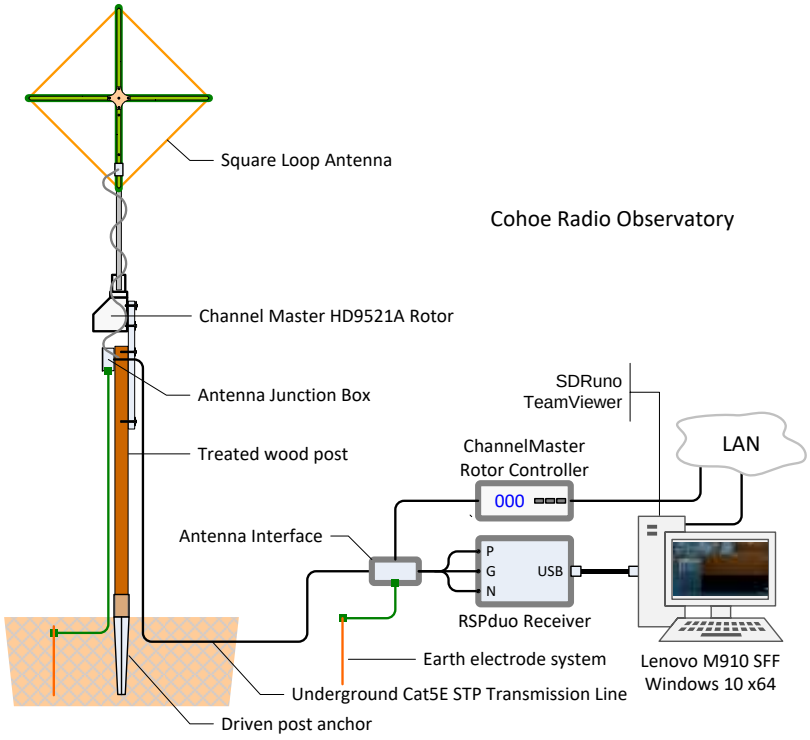

Figure 12 ~ Block diagram of Cohoe Radio Observatory VLF receiver and antenna setup. The diagonal dimension of the loop antenna is 1.2 m and its center is 3.5 m above ground level. The balanced high-impedance (HI-Z) antenna input of the receiver is connected to the antenna through Cat5E STP DB (direct burial) cable. The rotor controller has been modified to enable control over the local area network. Image © 2021 W. reeve

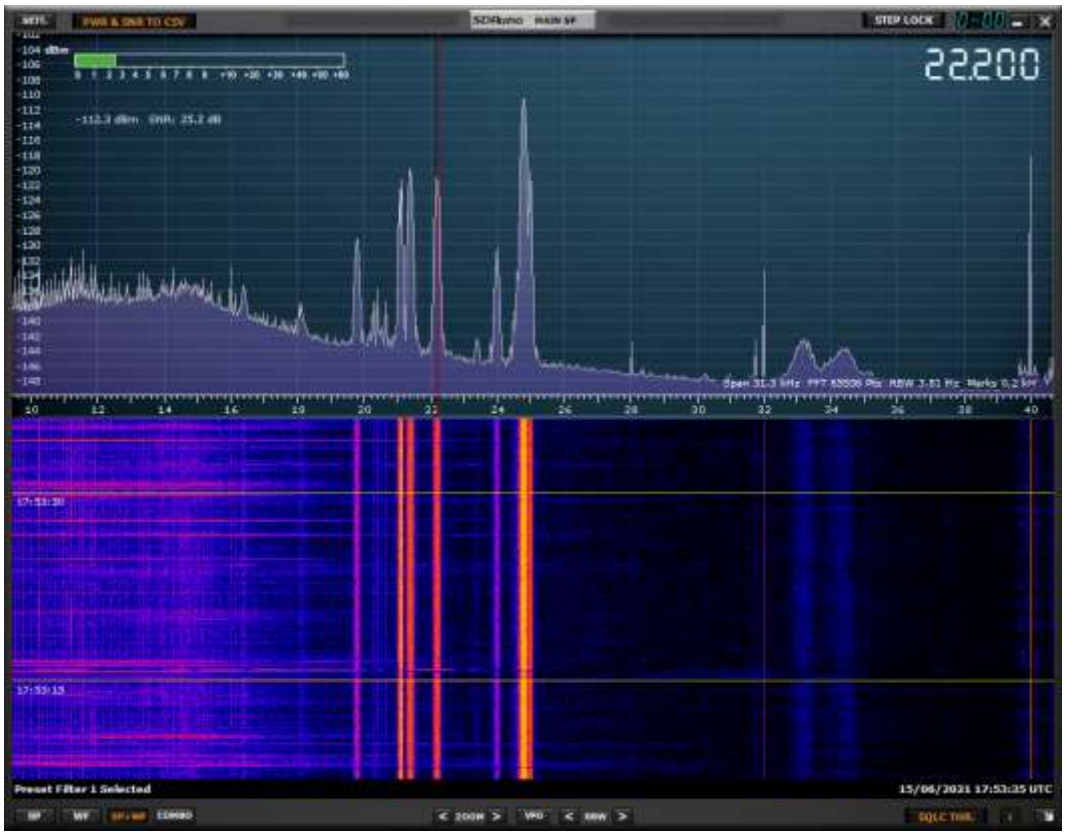

Figure 13 ~ Spectrum and waterfall for 15 June 2021 showing receiver tuned to the JJI station on 22.2 kHz (marked by the red vertical line in the upper panel). The loop antenna was oriented east-west. Many VLF signals are present including NPM to the south. The strongest signal is station NLK in Washington USA to the east at 24.8 kHz. Other identified signals are (with presumed station name in parentheses): 16.4 (JXN), 18.1 (RDL), 21.1 (RDL), 21.4 (NPM), 23.4 (DHO38), 24.0 (NAA), 24.8 (NLK), and possibly 25.0 and 31.9 kHz. There may be an additional signal at 24. 6 kHz hidden behind the strong signal at 24.8 kHz. The very narrow spectrum spikes seen at 16, 32 and 40 kHz are spurious signals at 8 kHz intervals; the spike at 24 kHz is hidden by a signal. The wide double-hump signal at 33-34 kHz is unknown and not visible with the antenna pointed north-south.

---

5. References & Weblinks

{Reeve19-1} Reeve, W., Monitoring Low Frequency Propagation with a Software Defined Radio Receiver, Part I ~ Concepts, 2020, available at: http://www.reeve.com/Documents/Articles%20Papers/Propagation/Reeve_LFProp-ConceptsP1.pdf

{Reeve19-2} Reeve, W., Monitoring Low Frequency Propagation with a Software Defined Radio Receiver, Part II ~ Observations, 2019, available at: http://www.reeve.com/Documents/Articles%20Papers/Propagation/Reeve_LFProp-ObsvP2.pdf

{GCM} http://www.gcmap.com/mapui?P=NPS-SXQ-KOJ

{NASA} https://eclipse.gsfc.nasa.gov/SEgoogle/SEgoogle2021.html

{TimeDate} https://www.timeanddate.com/eclipse/solar/2021-june-10

Author: Whitham Reeve obtained B.S. and M.S. degrees in Electrical Engineering at University of Alaska Fairbanks, USA. He worked as a professional engineer and engineering firm owner/operator in the airline and telecommunications industries for more than 40 years and now manufactures electronic equipment used in radio astronomy. He also is a part-time space weather advisor for the High-frequency Active Auroral Research Program (HAARP) and a member of the HAARP Advisory Committee. He has lived in Anchorage, Alaska his entire life. Email contact: whitreeve@gmail.com

Getting the Best out of PRESTO - Part 3: Waterfalls and Conclusions

Peter East

Abstract

This article completes an investigation into replacing the Chi-square statistic with the peak SNR (signal-to-noise ratio) measure in the PRESTO *prepfold* processes; in this case, to the waterfall graphic [1,2]. With this small change, improved recognition confidence is possible for lower SNR intercepts. Better target visibility is achieved by reducing the number of waterfall time sections and/or applying an accumulating folding algorithm. Finally, a complete low SNR comparison *prepfold* plot is offered based on the information in all three articles. A MathCad program duplicating the *prepfold* processes to produce this completed plot is presented in Appendix 2. Some additional pulsar recognition/confirmation features are also described.

Introduction

The PRESTO *prepfold* software tool rapidly carries out a number of processes on a data file and outputs a graphical plot as shown in Figure 1 [3,4]. The various processes normally combine to provide sufficient information for an operator to confidently confirm the acquisition of a real pulsar; except if, as in this case, the pulsar signal-to-noise ratio (SNR) is below about $\sqrt{\sqrt{2}P/W}$:1 (where *P* is the pulsar period and *W* the half-height pulse width - in the same units).

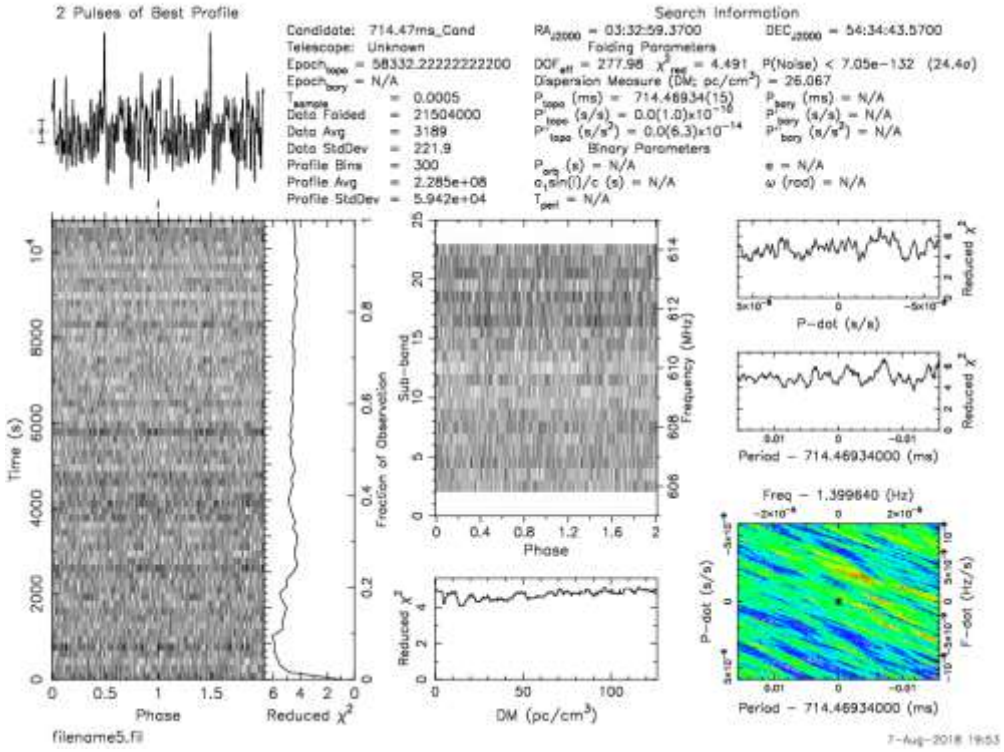

Figure 1. Typical 5:1 SNR Example PRESTO *prepfold* plot using the Chi-square amplitude statistic.

The sub-plots and normal recognition features identified, are summarized below,

1. Pulse profile plot (located top-left of PRESTO plot)

   Pulse profile and amplitude on folded noise base - two periods shown to improve visibility at phase extremities.

2. Waterfall and Reduced-Chi-square running value plots (located left side).

   For large SNRs, vertical dark lines or vestiges directly below the pulse profile plot (none visible here) with possible dropouts indicate the intercept of a regular, but scintillating pulse train. Not always clear for even quite large SNRs. Most *prepfold* runs appear to split the data into 64 sections, effectively reducing the observed SNR by a factor of 8, which may limit the pulse train visibility. The Reduced Chi-square section to the right of the waterfall should indicate a cumulative growth of the statistic from a starting value of one and then to exhibit a continuous, mainly rising, amplitude trend. In this case, there appears an anomalous offset at the beginning and no evidence of the measure growth.

3. Frequency sub-band plot - (located in center).

   Again for large SNRs semi-continuous vertical lines consistent with the pulse profile phase position (again, not visible here) indicating scintillating frequency components in all sub-bands as expected from the broad-band nature of pulsar signals.

4. Dispersion Measure sub-plot - (located center bottom).

   A peak is expected at the known dispersion measure (DM) of the pulsar source (not visible here) implying that the signal is extra-terrestrial and typical of traveling a distance through interstellar space. Note that all other plots require the data to be correctly de-dispersed.

5. P-dot, period search and correlated p-dot/period search plots - right-hand side.

   Peaks are expected at zero search error in all three plots. Also, a peak (red) elliptical feature is expected at zero error in the p-dot/period graphics plot; signifying expected accurate pulsar period with negligible frequency or period rate drift. The ellipse is normally extended and slope should equate to -2/N, where N is the number of pulsar periods in the data sample.

** Note on Chi-square interpretation: The reduced chi-square statistic value should increase with both pulse amplitude and duty cycle and be equal to unity for pure Gaussian noise. RFI that impacts the Gaussian distribution will increase the statistic value and tend to obscure any pulsar present until the pulsar SNR becomes significant. This situation is clear in the Figure 1. running Chi-square plot beside the waterfall. The reduced Chi-square value immediately rises to between 5 and 6 indicating significant non-Gaussian initial offset and further, the pulsar signal present fails to overcome this throughout the data duration. When judging the effectiveness of DM, period and p-dot search plots, the effect of residual noise distortion is to reduce the statistic discrimination.*

Positive evidence in all five cases (seven plots) builds the required recognition confidence (see Table 1.). Normally, depending on the pulsar duty cycle, intercept SNRs well above 12:1 (for 1% duty cycle) are required. The 5:1 SNR example in Figure 1, shows that at this SNR level, apart from the pulse profile, the other sub-plots provide no positive recognition information at all.

Earlier articles have indicated the data peak SNR statistic improves the majority of these sub-plots. The present article applies peak data SNR tracking to point 2. above; the waterfall and associated confidence plots.
Amateurs have been satisfied with just a large value SNR result and in some cases correct period and DM search peaks. It is known however that in modest to low SNR cases, that this is insufficient and that other pulsar properties may need to be evaluated to improve analysis confidence.

There is now a trend for amateurs to require this evidence only from professional software which may not have been intended for this task. This third article offers a considered response to this criterion by showing that by

duplicating PRESTO algorithms but applying the peak SNR measure, pulsar validation confidence can be extended to much lower target SNRs.

PRESTO Recognition Summary

Table 1 Checks on Essential Pulsar Properties

Sub-plot	**Property**
Profile	pulse shape/width
Time Waterfall/cumulative plot	scintillating pulse train
Frequency Waterfall	scintillating wide band noise
DM Plot	correctly dispersed - interstellar source
Period Search	accurate matched period
P-dot Search	negligible spin-down
Period/P-dot Plot	high stability pulse train

Positive indications in the Table 1 sub-plots confirms the presence and matching of the listed pulsar properties. All should be satisfied for sufficient evidence to prove a correct intercept.

The Final Folded Pulsar Profile

Figure 2 shows the final folded result of 10,000 periods producing modest SNR with the data bandwidth reduced to pass the expected pulse profile [5].

All large transient spike RFI and other RFI spectral harmonics have been blanked. The central candidate is obvious but the varying folded noise base has very similar characteristics and there is a small chance that the central peak could also be an unusual noise peak. This conclusion becomes more likely in cases where the integrated peak is lower.

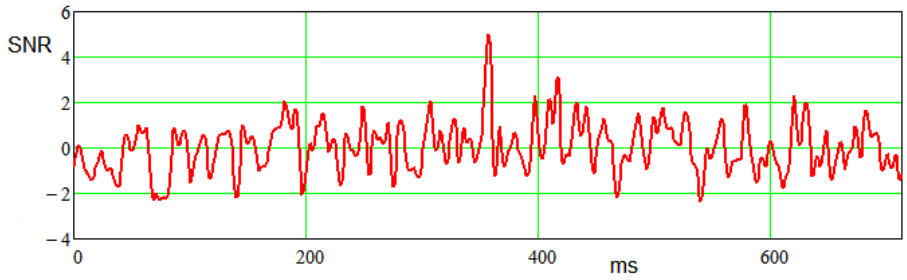

Figure 2. 5:1 SNR B0329+54 Example Matched-Period Fold of 10000 Periods.

This particular plot is the result of integrating some 150 billion samples of data down to just 714 points and whilst it is acknowledged that the folding algorithm is the optimum for maximizing the best signal-to-noise ratio, other valuable validation information may still reside in the recorded data. A relevant sub-fold correlation method to minimize noise ambiguities and highlight strong candidates is discussed later.

Spectral recognition methods are not viable at this low SNR level as, once folded, the noise occupies and obscures the same harmonic line structure as the wanted pulsar spectrum. The pulse bandwidth-limited fold algorithm provides the best pulsar SNR possible.

The Waterfall Plot

Figure 3 shows a 'waterfall' plot (flowing upwards). For this plot the data file of Figure 2 was divided into four equal sections and folded separately before combining in the contour graphic (red strong positive, blue strong negative). The central pulsar signal fills each section as expected but, as discussed above, some noise peaks remain present for two or more sections. When dividing into many more sections, the central pulsar feature reduces by the square root of the number of sections and eventually drops below the mean noise peaks noise and so to invisibility.

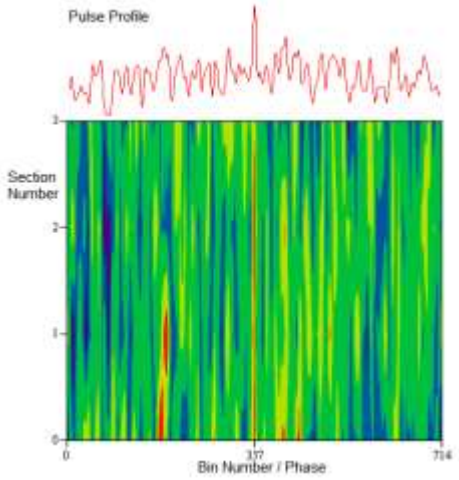

Figure 3. 5:1 SNR B0329+54 Example Matched-Period 4-Section Fold of 10,000 Periods.

In this example the Figure 2 pulsar peak SNR is reduced by one half (1/√4 for four sections).
It is this reduction in component SNR with increased waterfall sections that is responsible for the poor visibility of pulsar presence in the Figure 1 time-waterfall plot. In general, for a waterfall plot, a reasonable goal is to limit the number of sections '*S*' so that the section expected SNR does not drop much below 2.5:1; with this proposed constraint the candidate integrated fold SNR should be greater than $2.5\sqrt{S}$.

Cumulative SNR Plot (Analysis and Software in Appendix 2)

This section investigates using the cumulative SNR measure instead of the *prepfold* cumulative Chi-square statistic. For this plot, the data is again divided into a number of equal sections (now 100), each section is folded, but in this case, the sections are accumulated sequentially before folding and the SNRs calculated for the increasing section sums and plotted.

In Figure 4, the brown plot follows the cumulative peak SNR; this may report either the maximum noise peak or, if significant, any pulsar pulse amplitude whichever is largest. It also shows the central bin pulsar candidate's SNR (red); which appears to increase roughly as the square root of the number of sections, as is predicted. The variations may also be expected due to base noise, source scintillation and/or random effects of residual RFI features along the data record. The red curve shows that the pulsar candidate takes over from random noise peaks as the accumulated SNR exceeds about 3:1. This is a powerful tool for not only differentiating pulsar candidates and noise, but to recognize the impact of scintillation and/or sporadic RFI; ignoring/removing these sections can improve the final pulsar SNR (see Appendix 1).

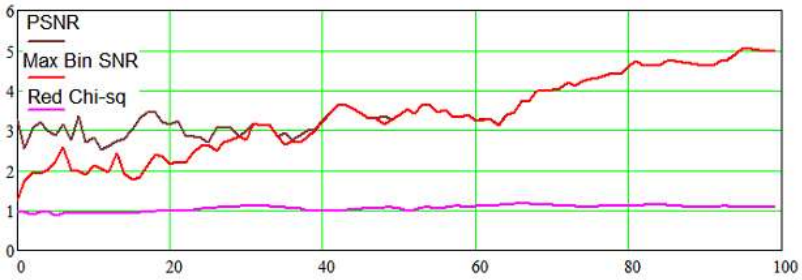

Figure 4. 5:1 SNR B0329+54 Example Accumulated Section SNR

The presence of scintillation means that the cumulative integration pattern will be different depending on whether the integration is carried out from beginning to end or, from end to beginning. The end results of both will always be the same but the path to get there will be different and hint at the stronger scintillation regions. For completeness in Figure 4, the Chi-square cumulative statistic is calculated for the data and plotted in magenta. As discussed in earlier articles it starts with a value of 1 indicating the base noise is closely Gaussian/Normal and rises very little being relatively insensitive to the low-level, low duty cycle pulsar candidate and non-presence of significant RFI (see Reference 1).

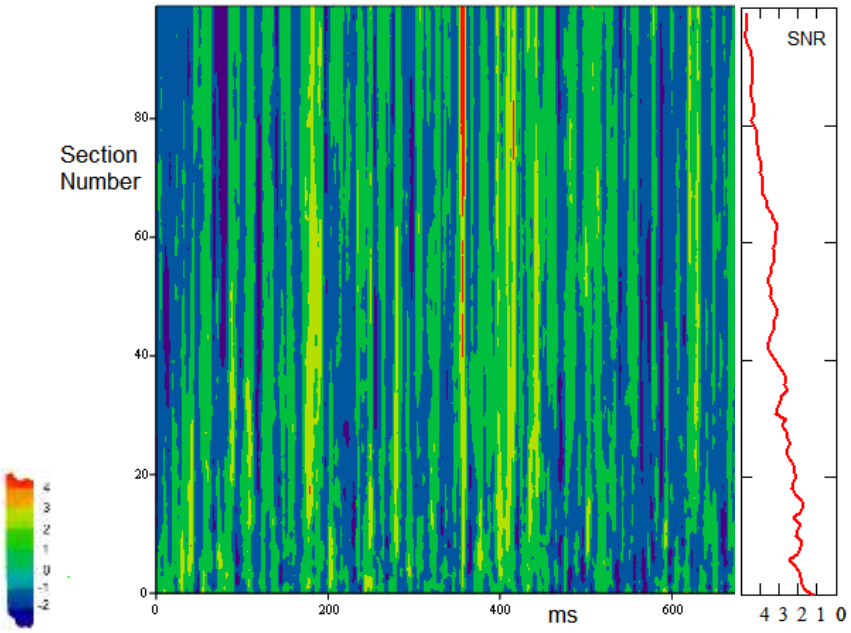

Figure 5. 5:1 SNR B0329+54 Example Accumulated SNR Waterfall

A more instructive PRESTO comparison approach is to plot this accumulated SNR as a waterfall plot showing all the data as in Figure 5. In this method, instead of displaying a few sub-section fold results, a larger number of accumulating folds, such that by the final section, the sum fold of all the data is presented.

Figure 5 shows much more clearly the suppression of random noise components and the final dominance of this low SNR pulsar candidate's response (red). There are some drop-outs of the integrating signal possibly indicating the effects of scintillation, but the final pulsar line width is in keeping with its pulse width/period ratio. The vertical lower-level noise features (green bands) show that the final noise peaks appear present throughout the record but tend not to integrate as does the true pulse train; This appears a memory effect, not evident in the standard time section waterfall of Figure 3; once a strong peak section is accumulated, it appears to take many sections to

get washed out and is susceptible to being re-invigorated by subsequent section peaks. Expected randomness only appears in the initial 5-10 sections. It is not obvious why this occurs but it appears due to the fine harmonic frequency filtering property of the folding algorithm.

Combined Data Comparison Plot

Combining the information discussed above with the results of the earlier articles, it is now possible to compare the results of using SNR rather than Chi-square to sense the pulsar presence [1,2].

Figure 6 shows the PRESTO *prepfold* SNR look-alike plot. An extra inclusion is the frequency spectrum (center) plot; the data used was recorded using a 3-band RTL receiver, each of 2 MHz bandwidth centered on 609, 611, and 613 MHz [5]. The detailed MathCad data analysis and algorithms are given in Appendix 2.

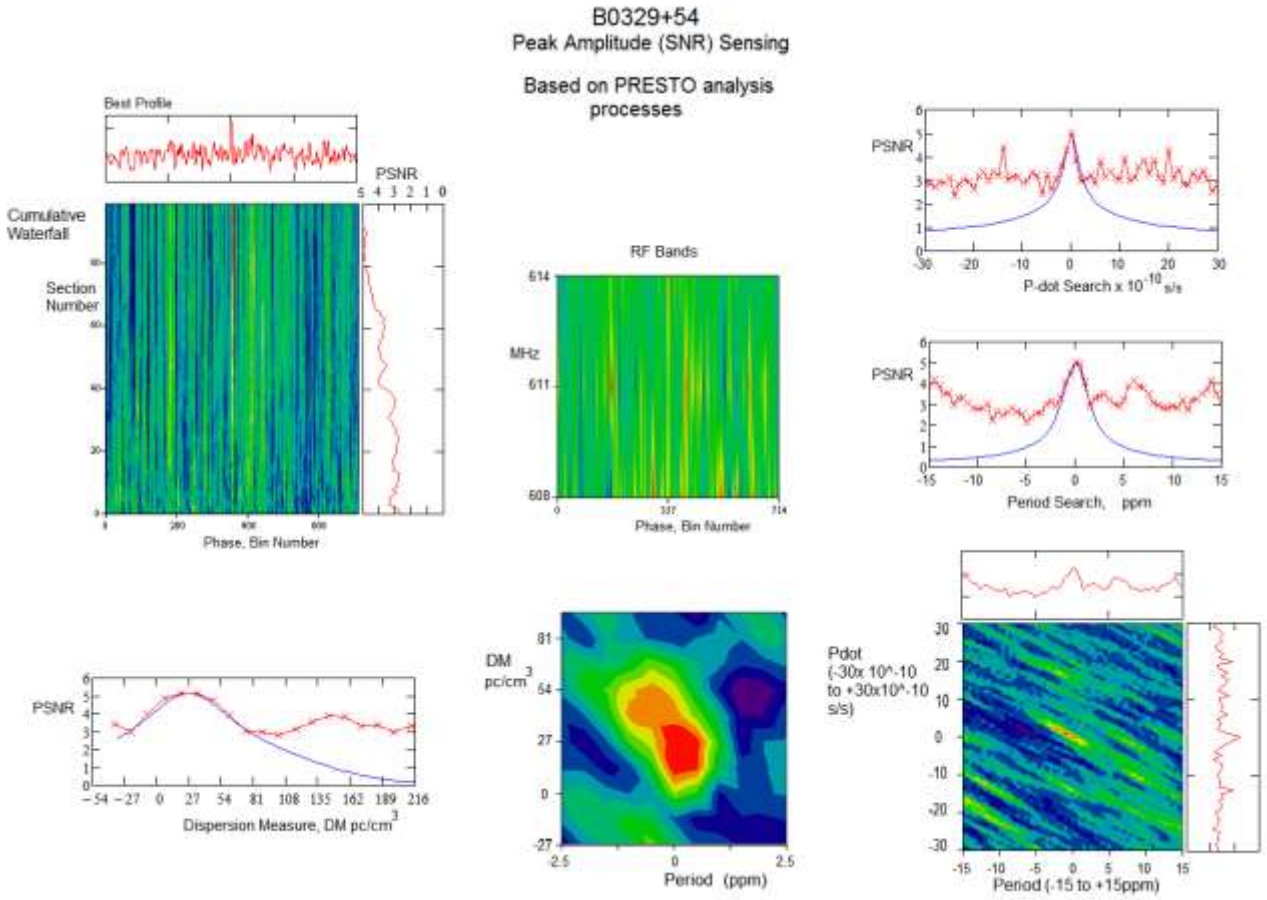

Figure 6. 5:1 SNR B0329+54 Example PRESTO *prepfold* Comparison Plot

Comparing Figure 6 with the 5:1 SNR *prepfold* plot in Figure 1 it is concluded that all PRESTO-approved pulsar recognition features are now clearly evident; just by using the maximum SNR rather than the Chi-square statistic. To improve clarity, the *prepfold* time waterfall plot has been replaced with the accumulated 100-section waterfall. For the DM, period search and p-dot search plots, the blue curves included are those calculated for an ideal noise-less pulse train matching the pulse characteristics of the target pulsar [6]. The calculated curves have been normalized to the measured data peaks and in the case of the DM plot, the peak was adjusted by half the data sample time; again to match peaks and to accommodate the data timing coarseness. The close match of data and theory is an additional strong indicator of the pulse train-like characteristic of the candidate pulsar. Included for

interest, as it is offered in other professional software, is the 2-D DM/Period plot showing maximum correlation about DM=27 and zero period error. It should be admitted that there was a large time penalty to obtain the detail of Figure 6; the plots were assembled manually from MathCad for this exercise but it would seriously benefit from the power of a Python GUI!

Noise Rejection by Cross-Correlation

Pulsar identification information used by PRESTO, listed in Table 1, looks only at the essential pulsar parameters. The parameter search routines described in Reference 6 utilize more detailed search prediction features to add weight to pulsar recognition; specifically, calculated changes in bin position and pulse width. The time and frequency waterfalls can confirm an extensive pulse train and a broadband source with scintillation present in both parameters. In all, this represents convincing evidence of a true pulsar acquisition. All of these techniques exploit the pulse-train-like and intrinsic properties of pulsars. Three other techniques have been investigated that exploit noise properties throughout the recorded data to add weight to the recognition process especially at very low SNR levels; these are the cumulative SNR plot described in this paper, the multi-bin folding algorithm extension evaluated in Reference 8, and the half-fold multi-correlation procedure described in Reference 7. This is by no means the end of the list of anticipated features that add recognition confidence; there is the simple check in drift-scan mode, for increased level and density of pulsar data on the antenna boresight for example.

A demonstration of multi-fold correlation using the data file of Figure 6 is shown in Figure 7. In the upper part of Figure 7 is shown the overlaid results of the example data file divided into 8 sections which are individually folded. It is clear from this that the central section containing the pulsar candidate (separated and magnified to the right) exhibits variable, but positive co-located peaks (ranging from 0.8:1 SNR to 2.8:1 SNR). The remaining 'noise' components appearing random. Summing these section results, with suitable scaling, produces the expected all-data fold appearing in red in the lower plot.

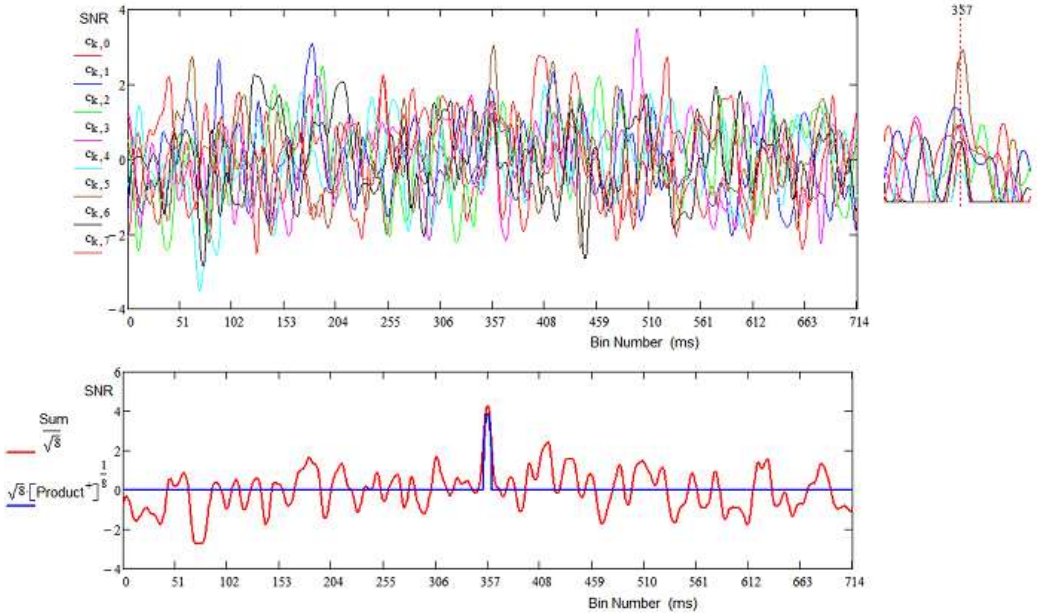

Figure 7. 8-Section Data Correlation

The correlation algorithm multiples the positive folded excursions together and in this case, takes the eighth root and factors as indicated on the left side of the lower plot to produce the blue curve shown.

This algorithm appears to zero the noise but pass the regular pulse train pulsar shape with minimal amplitude reduction. Providing scintillation does not zero a section, this technique will always preferentially display the pulsar pulse region. Experimentation, either with number of sections or combining randomized data half-folds may be necessary in general to fully zero all noise peaks [7]. It is considered that randomized data half fold combining would be somewhat more robust. The algorithm is an extension of the two variable near identity: $\sqrt{2\ a\ b} \approx (a+b)/\sqrt{2}$, unless *a* or *b* approach zero.

Conclusions

This is the latest article in a series studying the problem of recognizing and identifying a weak pulsar in recorded data collected by amateur radio telescopes. The key indicator and problem is the powerful epoch folding algorithm. This reduces gigabytes of collected data to a few hundred bytes, optimally matched to the wanted pulsar pulse width and repetition period. This maximizes the pulsar signal to noise ratio. For weak SNRs it is superior to any spectrum technique. However, the final fold signal and noise pattern is now fixed; noise frequency components occupy the same frequency harmonics as the wanted pulsar signal and all may be simply considered as pulsar-like signals of different phases.

The three articles have explored the benefit to amateurs of using the maximum SNR measure rather than the reduced Chi-square statistic as is used in the PRESTO *prepfold* pulsar processing tool. The benefit is much better visibility of low SNR pulsar acquisitions below 12:1 (1% pulse duty cycle). PRESTO uses the Chi-square statistic for good reasons; firstly it requires less computing power and hence much faster and secondly, the primary aim of PRESTO is to search for new pulsars of unknown pulse width, period and dispersion; it is very efficient at searching this wide triple-parameter range. Amateurs are unlikely to be in the same class for discovering new pulsars but will know the target parameters. They can optimize data processing bandwidths and may have more time on their hands for extracting pulsar-recognition detail.

The techniques described in these three articles duplicate the PRESTO *prepfold* tool processes and provide much more recognition information detail and can prove more useful for validating weak, but genuine, pulsar intercepts for either small or large antenna systems. In short, a straight comparison between Figures 1 and 6 shows that with this change, a much more amateur-friendly pulsar recognition plot results.

Postscript

Detection and recognition of the loudest pulsars is definitely within the capability of all amateurs with modest but well-designed and tuned antenna/receiver systems; certainly in drift-scan observation mode. There may be problems, however, with RFI and emitter scintillation that need to be addressed possibly causing some failed observations. Detection verification is stated by some players as only being acceptable using professional astronomer's pulsar software. This is misleading as none provide a yes/no answer and new pulsar search rather than recognition is their primary role. In analysis mode, *prepfold* examines the data and provides a visual display of some of the pulsar characteristic properties but offers only limited discrimination at low levels. It is only a proper scientific interpretation and confirmation of Table 1 characteristics and others, easier the larger the received pulsar amplitude, that inspires satisfactory recognition confidence. Just because a low SNR pulsar data set is recorded, it doesn't mean that it is not there. The challenge for amateurs is to apply these and other analytic processes to extract the pulsar signal from noise/RFI and not to be put off by detection statistics.

References

[1] PW. East, Getting the Best out of the PRESTO Pulsar Search & Analysis Tools., Journal of the Society of Amateur Radio Astronomers. January-February 2021.

[2] PW. East, Getting the Best out of PRESTO - Part 2 The PRESTO Period/P-Dot Search Graphic., Journal of the Society of Amateur Radio Astronomers. March-April 2021.

[3] PRESTO Home, https://www.cv.nrao.edu/~sransom/presto/

[4] SM Ransom. Searching for Pulsars with PRESTO https://www.cv.nrao.edu/~sransom/PRESTO_search_tutorial.pdf

[5] PW East, A Minimal Pulsar Detection System. Journal of the Society of Amateur Radio Astronomers. January-February 2018. p36. http://www.y1pwe.co.uk/RAProgs/MiniPulsarRx.pdf

[6] PW East. An Analytical Method of Recognizing Pulsars at Moderate SNR., Journal of the Society of Amateur Radio Astronomers. November-December 2018.

[7] PW East, A Correlation Method for Low SNR Pulsar Search and Recognition. Journal of the Society of Amateur Radio Astronomers. July-August 2019.

[8] PW East, Getting the Best Out of the Pulsar Folding Algorithm. Journal of the Society of Amateur Radio Astronomers. May-June 2021.

Appendix 1. **Improving Folded SNR**

The brown plot in Figure 4 reports the maximum peak SNR from the accumulated sections. The red plot reports the accumulated peak level at the known bin containing the pulsar signal. A method of determining this bin number is to scan the bins, in groups or singly, to find the bin whose response matches the upper part of the brown plot. This function is incorporated in the Appendix 2 MathCad program.

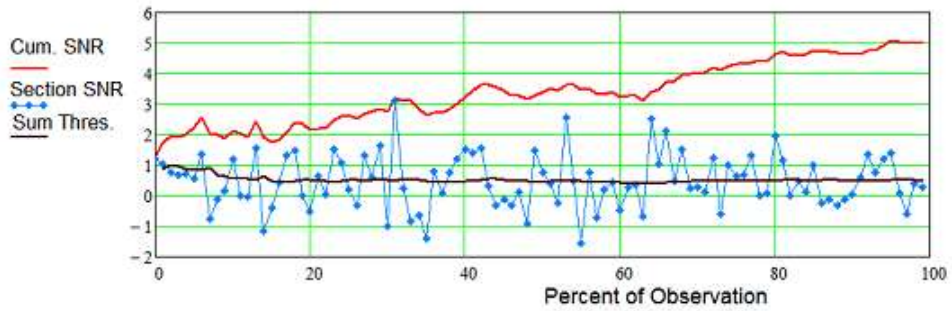

Figure A1. Accumulated Section SNR (red), block SNR (blue), SNR Threshold (black)

Inspecting Figure A1, it is evident that there are three obvious regions between sections 33 and 64 where the accumulating SNR (red) fails to increase. Close inspection of the section SNRs (blue points) reveals groups of SNRs that fall below the expected mean section SNR (black) curve. Possibly due to natural scintillation or some spurious RFI effects. In either case, it is possible to remove these sections and process the remaining sections. The result of this on the cumulative SNR plots is shown in Figure A2 after removing sections 32-35, 43-48, 55-63.

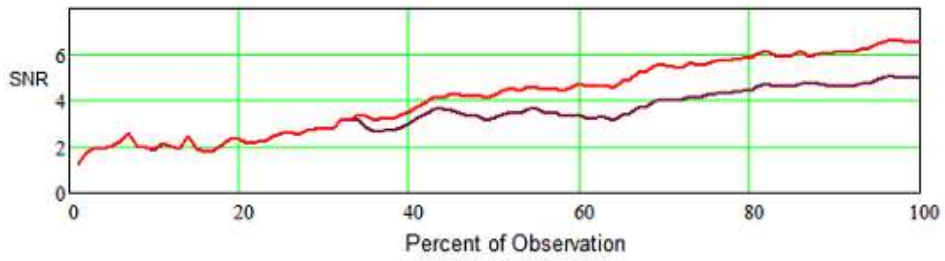

Figure A2. Accumulated Section SNR (red) with 3 Weak Sections Removed

This has had quite a significant effect in improving the final SNR showing a 30% improvement from just under 5:1 to 6.5:1. The resulting final fold is shown in Figure A3 (red) and can be compared to the original result (blue).

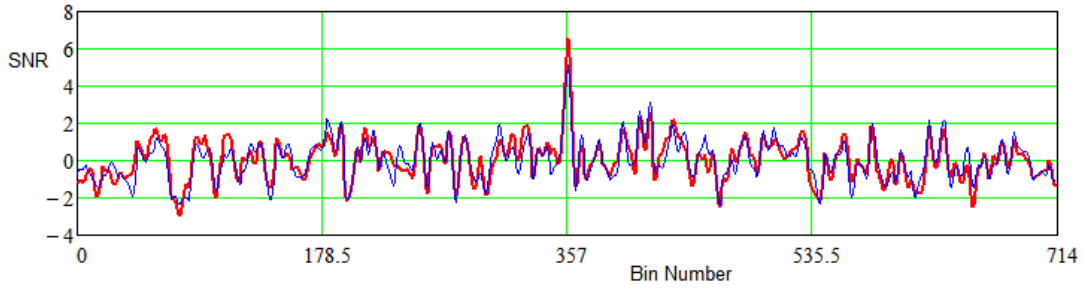

Figure A3. Final SNR (red) with 3 Weak Sections Removed Compared to All of the data SNR (blue)

It may be thought that removing data to improve the observed SNR is akin to data manipulation, but this choice is up to the user; in reflection, is this any different to RFI mitigation?

Appendix 2. MathCad Data Analysis Software

Pulsar Data Analysis and Recognition PWE May 2021

$B1 := READPRN("B311.txt")$

$B2 := READPRN("B312.txt")$ Bands 1-3 data (1ms samples)

$B3 := READPRN("B313.txt")$ Bands 1 and 3 de-dispersed relative to Band 2

$Min := 0 \quad Max := 7260000$ Number of data file samples

$i := Min .. Max - 1$ Data range

$Pt \equiv 714.4794809425$ B0329 data topocentric period (ms)

$P(p) \equiv Pt\left(1 + \frac{p}{10^6}\right)$ Pulsar Period change in ppm (ms)

$pw \equiv 6.5$ Pulsar Pulse width (ms)

$N := floor\left(\frac{Max}{Pt}\right)$ Number of periods in data file

$N = 1.016 \times 10^4$

$K := 714$ Standard Number of Fold Bins ~ 1ms time resolution

$q := 0 .. K - 1$ Fold bin range

$Nn := 100$ Number of data sections

$n := 0 .. Nn - 1$

$Bt_i := B1_i + B2_i + B3_i$ Combined de-dispersed data

$secfold_n := Stfoldpp\left(K, Pt, 0, Bt, n \cdot \frac{Max}{Nn}, \frac{n+1}{Nn} \cdot Max, pw\right)$ Data section folds

$cumsecfold^{\langle n \rangle} := \left[\sum_{x=0}^{n} \left(secfold_x\right)\right]$ Accumulating section folds

$cumsecsnr_{q,n} := snrcs\left(q, K, cumsecfold^{\langle n \rangle}\right)$ Accumulation section SNR calculation

$maxpeak_n := max\left(cumsecsnr^{\langle n \rangle}\right)$ Maximum Peak SNR in accumulated section folds

$secsnr_{q,n} := snrcs\left(q, K, secfold_n\right)$ SNR of individual section folds

$maxsnr := mx(K, Nn, cumsecsnr)$ Maximum Peak SNR in accumulated section folds + bin number

Running SNR Plot

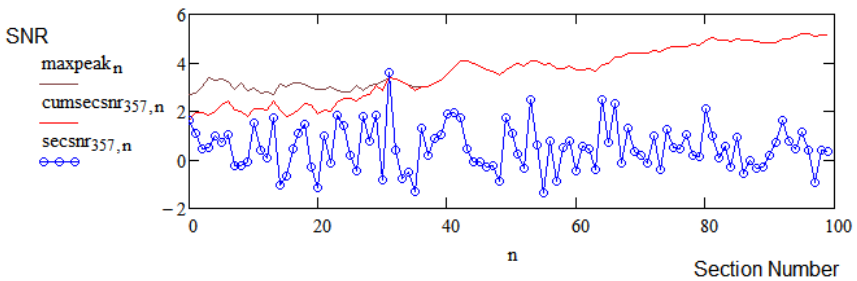

B0329 Dispersion Measure $DM := 26.7$

$$D := 4.15 \cdot DM \cdot \left[\frac{1}{(.611 - .002)^2} - \frac{1}{(.611 + .002)^2} \right]$$

Dispersion between Band1, Band 3 centres (ms) $D = 3.886$

Search Defining Equations - see Reference 6.

$$ptheory(p, N, w, P) := \frac{1}{N} \cdot \sum_{n=1}^{N} e^{-4 \cdot \ln(2) \cdot \left[\frac{p \cdot \left(1 - \frac{n}{N}\right)}{\frac{2 \cdot w \cdot 10^6}{N \cdot P}} \right]^2}$$

period search amplitude profile
peak value v period p in ppm

$$pdtheory(t, N, w, pd, P) := \frac{1}{N} \cdot \sum_{n=1}^{N} e^{-4 \cdot \ln(2) \cdot \left[\frac{t + (n-1) \cdot (n-2) \cdot \left(\frac{pd}{10^{10}} \right) \cdot \frac{P}{2}}{w} \right]^2}$$

p-dot search amplitude profile
amplitude profile v time for
p-dot value in parts/10^-10 s/s

$$distheory(d, B, w) := \frac{1}{B} \cdot \sum_{n=1}^{B} \left[e^{-4 \cdot \ln(2) \cdot \left(\frac{n}{B} \cdot d - \frac{d}{2} \right)^2} \right]$$

DM search amplitude profile
peak value v dispersion across
pulse at offset 'x'

Band Folds and frequency waterfall plot

$vV1 := Stfoldpp(K, Pt, 0, B1, Min, Max, pw)$ Band 1 609MHz band centre

$vV2 := Stfoldpp(K, Pt, 0, B2, Min, Max, pw)$ Band 2 611MHz band centre

$vV3 := Stfoldpp(K, Pt, 0, B3, Min, Max, pw)$ Band 3 613MHz band centre

$Vf_{q,0} := vV1_q$ $Vf_{q,1} := vV2_q$ $Vf_{q,2} := vV3_q \cdot .5$

SNR

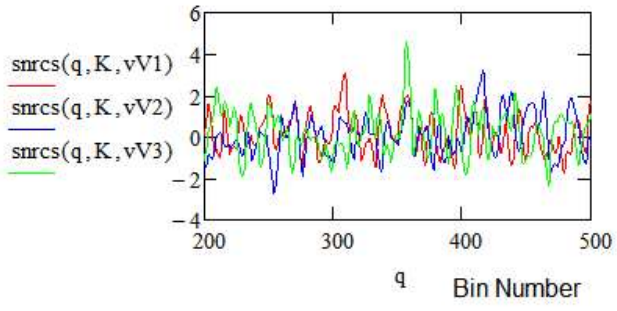

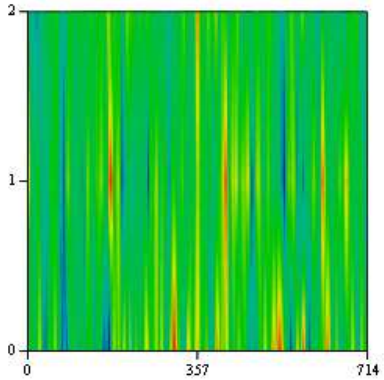

Vf Frequency Waterfall Plot

Best profile fold

$vV := Stfoldpp(K, Pt, 0, Bt, Min, Max, pw)$

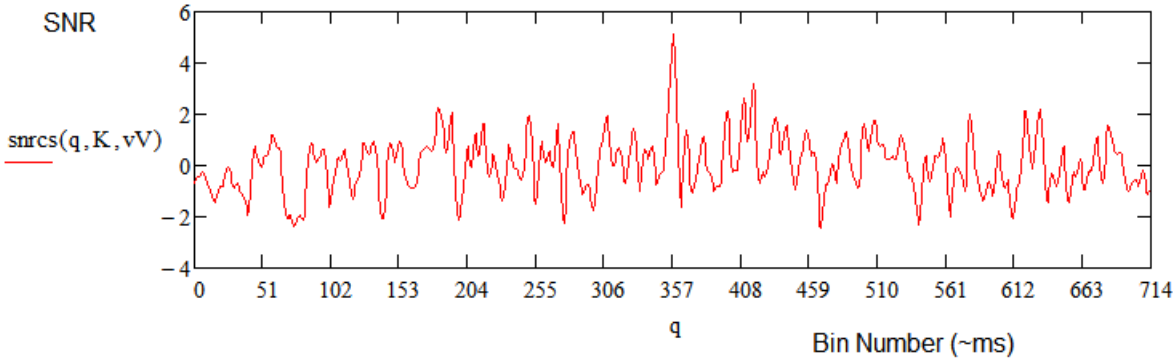

Cumulative Waterfall

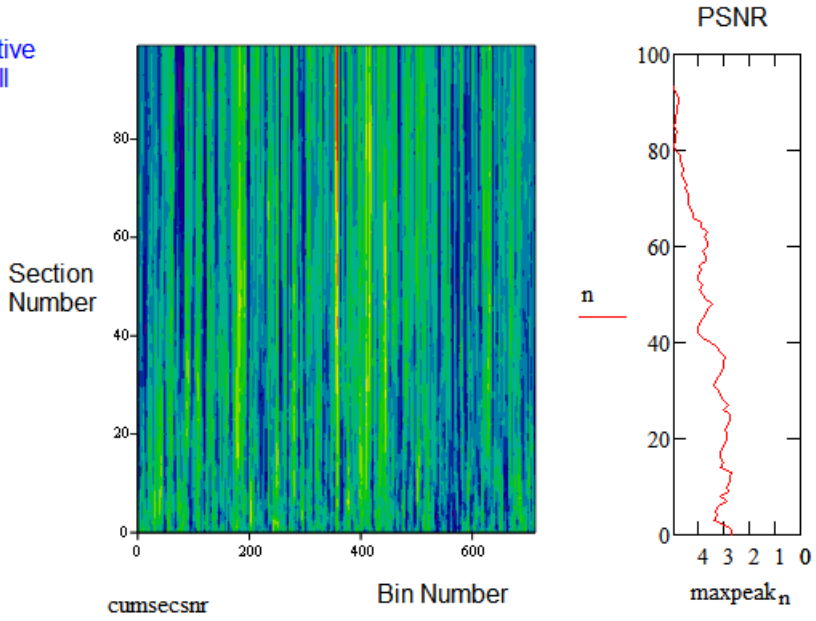

Bin Position of Peak Fold Response

$maxsnr_{0,99} = 5.128$

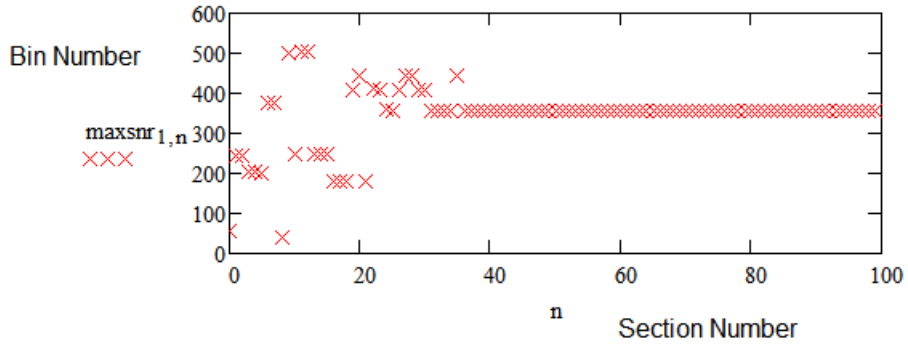

Dispersion Search

$q := 0 .. K - 1$

$d := 0, 1 .. 24$ Dispersion search range (ms)

Dispersion band combiner

$Vd_{q,d} := vV1_{mod(q+K+4-d,K)} + vV2_{mod(q+K+0,K)} + vV3_{mod[(q+K)+d-4,K]}$

Note: range 'd' offset by +4 and -4 ms

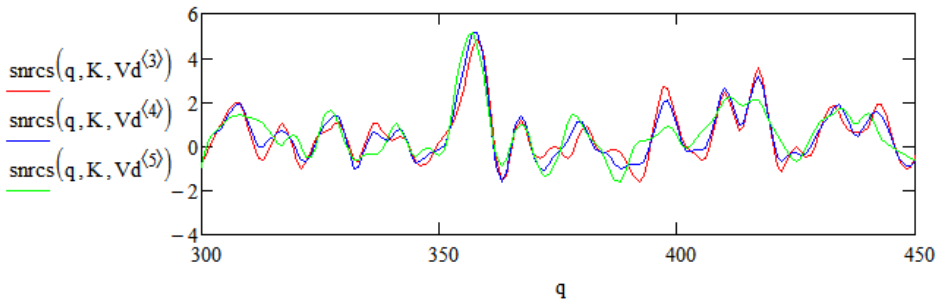

$dm_{q,d} := \left(snrcs\left(q, K, Vd^{\langle d \rangle}\right)\right)$ Actual dispersed fold SNR over search range

DM = 26.7

D = 3.886

Comparison of theoretical and practical SNR as a function of dispersion

$dd := -2, -1.9 .. 9$ Dispersion data range (ms)

SNR

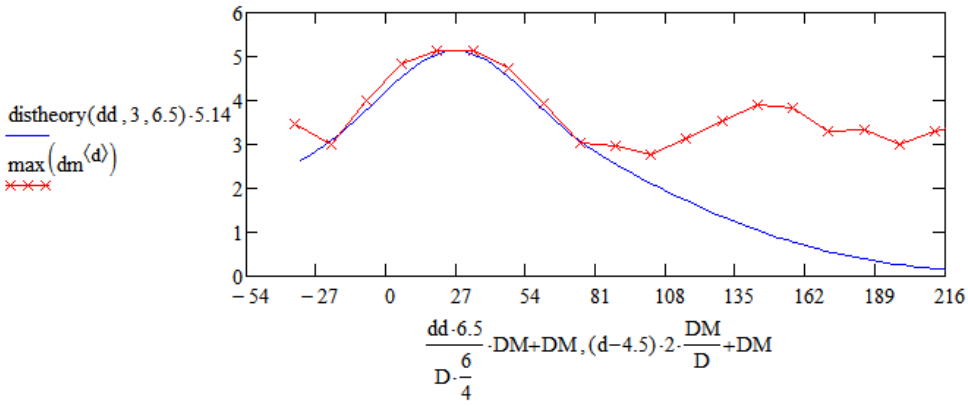

Notes:-

Data normalisation:

For the real-data plot, the x-axis should be 2(d-4)DM/D + DM as d=4, represents de-dispersed data. However, as the data is in 1ms increments and only 3 bands, the accuracy is limited. The 0.5ms offset for the real-data plot enabled an improved data symmetrical match with the theory.

For the theoretical plot, dd is indicated as a multiplier of Dp/W, where Dp is the total dispersion across the pulse (=6D/4), and W is the pulse width. When Dp/W =2 the pulse amplitude drops by one half.

Period+Pdot Search

P-dot 'zz' and period 'z' data ranges,

$zz := 0..60 \quad z := 0..60$ period in 0.5ppm and p-dot in 0.5x 10^-10 s/s, offset by 15ppm and 30x10^-10

$PPd_{z,zz} := \max[Stfoldpp[K, P[.5\cdot(z-30)], [0.5\cdot(zz-30)], Bt, Min, Max, pw]]$ 2-D PSNR calculation

$norm := \frac{maxsnr_{0,99}}{PPd_{30,30}}$ Peak SNR/amplitude normalizing factor

Comparison of theoretical and practical period search SNR over period ppm range

SNR

$\frac{ptheory\left(\frac{z-30}{2}, N, pw, Pt\right)\cdot maxsnr_{0,99}}{(PPd_{z,30})\cdot norm}$

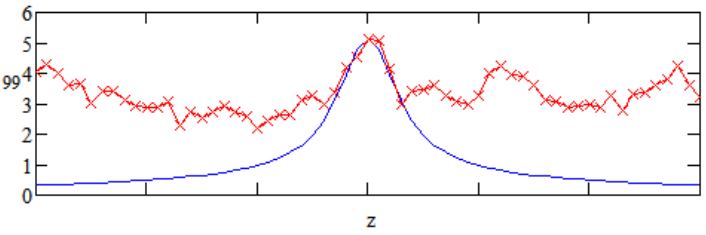

Period range: -15ppm to +15ppm

$px := 0..30$ P-dot value range to find peak

$hpk_{zz,px} := pdtheory(zz, N, pw, px, Pt)$ Search theoretical response to encompass the fold peak value over the p-dot range px and zz

$hk_{px} := \max\left(hpk^{\langle px \rangle}\right)$ Find p-dot search response peak value for each p-dot search value

Comparison of theoretical and practical p-dot search SNR over p-dot value in range range

SNR

$\frac{hk_{zz-30}\cdot 5.}{hk_{30-zz}\cdot 5.}$

$PPd_{30,zz}\cdot norm$

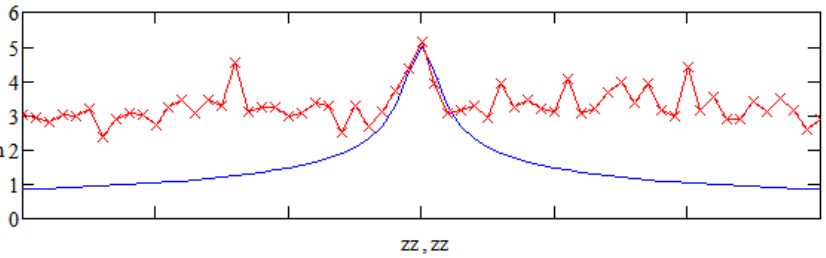

2-D period search/p-dot search plot

Pdot range: -30x 10^-10 to +30x10^-10 s/s

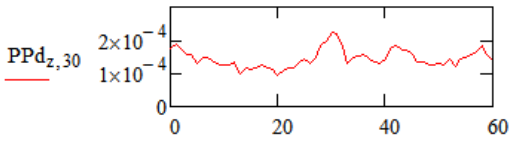

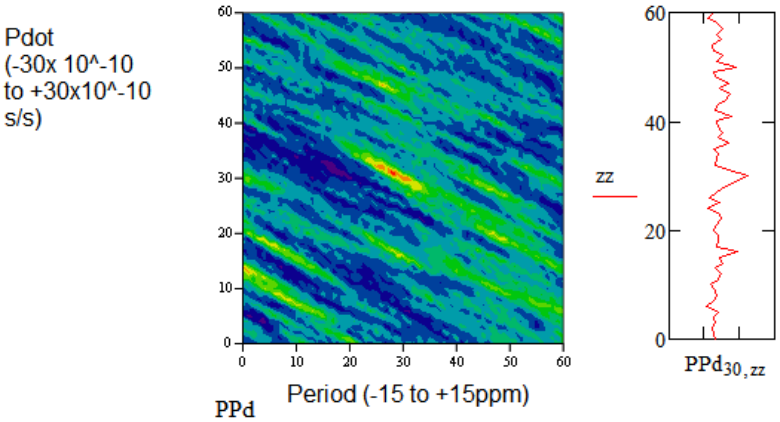

Folded data SNR calculation

$$
\begin{aligned}
&\text{snrcs}(s, n, \text{dat}) := \\
&\quad mn \leftarrow 0 \\
&\quad rms \leftarrow 0 \\
&\quad mnr \leftarrow 0 \\
&\quad rmsr \leftarrow 0 \\
&\quad mx \leftarrow 0 \\
&\quad d \leftarrow \text{floor}\left(\frac{n}{40}\right) \\
&\quad nx \leftarrow 0 \\
&\quad \text{for } x \in 0..n-1 \\
&\quad\quad mn \leftarrow mn + \text{dat}_x \\
&\quad\quad rms \leftarrow rms + (\text{dat}_x)^2 \\
&\quad\quad \text{if } \text{dat}_x > mx \\
&\quad\quad\quad mx \leftarrow \text{dat}_x \\
&\quad\quad\quad nx \leftarrow x \\
&\quad n1 \leftarrow \text{floor}(nx - d) \\
&\quad n1 \leftarrow 0 \text{ if } n1 < 0 \\
&\quad n2 \leftarrow \text{floor}(nx + d) \\
&\quad n2 \leftarrow n - 1 \text{ if } n2 > n - 1 \\
&\quad \text{for } x \in n1..n2 \\
&\quad\quad mnr \leftarrow mnr + \text{dat}_x \\
&\quad\quad rmsr \leftarrow rmsr + (\text{dat}_x)^2 \\
&\quad mn \leftarrow \frac{mn - mnr}{n - (n2 - n1) - 1} \\
&\quad rms \leftarrow \frac{rms - rmsr}{n - (n2 - n1) - 1} \\
&\quad rms \leftarrow rms - mn^2 \\
&\quad out \leftarrow \frac{\text{dat}_s - mn}{\sqrt{rms}} \\
&\quad out
\end{aligned}
$$

2-D data peak/position calculation

$$
\begin{aligned}
&mx(q, n, \text{dat}) := \\
&\quad \text{for } x \in 0..n-1 \\
&\quad\quad nx_{0,n} \leftarrow 0 \\
&\quad\quad nx_{1,n} \leftarrow 0 \\
&\quad \text{for } x \in 0..n-1 \\
&\quad\quad \text{for } y \in 0..q-1 \\
&\quad\quad\quad \text{if } \text{dat}_{y,x} > nx_{0,x} \\
&\quad\quad\quad\quad nx_{0,x} \leftarrow \text{dat}_{y,x} \\
&\quad\quad\quad\quad nx_{1,x} \leftarrow y \\
&\quad\quad nx \\
&\quad nx
\end{aligned}
$$

2-D Bandwidth - matched fold algorithm for period and p-dot search

$$\text{Stfoldpp}(B, P, p, Dat, Min, Max, w) :=$$

for $fs \in 0 .. B - 1$

$\quad bdat_{fs} \leftarrow 0$

$\quad bcount_{fs} \leftarrow 0$

for $x \in Min .. Max - 1$

$\quad P2 \leftarrow P \cdot \left(1 + \frac{2 \cdot x \cdot p}{1000000 \cdot Max}\right)$

$\quad s \leftarrow \text{floor}\left[\left(\frac{x}{P2} - \text{floor}\left(\frac{x}{P2}\right)\right) \cdot B\right]$

$\quad bdat_s \leftarrow bdat_s + Dat_x$

$\quad bcount_s \leftarrow bcount_s + 1$

for $b \in 0 .. B - 1$

$\quad bindat_b \leftarrow \frac{bdat_b}{bcount_b}$

$\quad cw_b \leftarrow .1 \cdot \exp\left[-4 \cdot \ln(2) \cdot \left(\frac{b - \frac{B}{2}}{\frac{w}{1.5} \cdot \frac{B}{P}}\right)^2\right]$

$fdat \leftarrow \text{cfft}(bindat)$

$fdat_0 \leftarrow 0$

$fc \leftarrow \text{cfft}(cw)$

for $b \in 0 .. B - 1$

$\quad ffda_b \leftarrow fdat_b \cdot \left|\frac{fc_b}{fc_0}\right|$

$tdat \leftarrow \text{icfft}(ffda)$

$\text{Re}(tdat)$

PWE 2021

Appendix 3 SNR - Ratio or dB?

Signal-to-noise ratio is officially defined as a power ratio which is measured by a power meter and converted to a decibel (dB) measure by taking its logarithm to the base 10 and multiplying this by 10. This is fine until the signal plus noise is demodulated/detected, either by a square-law detector or the components squared and summed as for digital I/Q samples. Strictly, these outputs are now equivalent voltages so to convert this voltage ratio to dB, the logarithm of this voltage ratio should be multiplied by 20. Often in amateur radio astronomy, the x10 multiplier is used and this is OK if it is remembered that this figure now refers to the signal-to-noise power ratio at the RF input, not at the measurement point. To prevent this confusion, it is generally agreed that for pulsar work the SNR measure is always presented in its linear ratio form, as throughout this article.

Peter East, *pe@y1pwe.co.uk* is retired engineer from a career in radar and electronic warfare system design. He has authored a book on Microwave System Design Tools, is a member of the British Astronomical Association since the early '70s and joined SARA in 2013. He has had a lifelong interest in radio astronomy; presently active in amateur detection of pulsars using SDRs, and researching low SNR pulsar recognition. He encourages free information exchange in the amateur community and is keen to widen interest in radio astronomy generally. He maintains an active RA website at *http://www.y1pwe.co.uk*

Radio interference reduction in interstellar communications: methods and observations

William J. Crilly Jr

Green Bank Observatory, West Virginia, USA

***bstract*— The discovery of interstellar communication signals is complicated by the presence of radio interference. Consequently, interstellar communication signals are hypothesized to have properties that favor discovery in high levels of local planetary radio interference. A hypothesized type of interstellar signal, Δt Δf polarized pulse pairs, has properties that are similar to infrequent elements of random noise, while dissimilar from many types of known radio interference. Discovery of Δt Δf polarized pulse pairs is aided by the use of interference-filtered receiver systems that are designed to indicate anomalous presence of polarized pulse pairs, when pointing a radio telescope to celestial coordinates of a hypothetical transmitter. Observations reported in previous work (ref. arXiv:2105.03727) indicate an anomalous celestial pointing direction having coordinates 5.25 ± 0.15 hours Right Ascension and -7.6° ± 1° Declination. Augmented interference reduction mechanisms used in the current work are described, together with reports of follow-up radio telescope beam transit measurements during 40 days. Conclusions and further work are proposed.**

***Index terms*— Interstellar communication, Search for Extraterrestrial Intelligence, SETI, technosignatures**

1. Introduction

The experimental protocol in previous work [1] produced measurements of the Additive White Gaussian Noise (AWGN)-caused likelihood of observations of energy-efficient [2] interstellar coherence hole (ICH) constrained signals, described by Messerschmitt [3]. The hypothesis in [1] predicts that indications at celestial coordinates 5.25 ± 0.15 hours Right Ascension (*RA*) and -7.6° ± 1° Declination (*DEC*), may be explained by an AWGN model. The experiment described in [1] appears to have falsified the hypothesis to the extent measured by the Bayesian posterior probabilities calculated in [1]. The absence of development and testing of auxiliary and alternate hypotheses hampers conclusions. The problem compels the work reported in this paper.

Follow-on work, proposed in [1], to continue single telescope beam transit observations, attempts to further study certain hypothesized ICH-constrained signals, referred to as Δt Δf discovery signals, and polarized pulse pairs. During the course of the follow-on work, four additional Radio Frequency Interference (RFI) amelioration mechanisms were designed and implemented, as additional suspected RFI was observed and excised, and while hypothetical interstellar communication methods were considered.

Due to the change in experimental protocol in the follow-on work, the hypothesis stated in [1] is retained, albeit modified for the current beam transit experiment.

***Hypothesis* [1]:** An AWGN-cause model is expected to explain observations of Δt Δf orthogonal circular-polarized pulse pairs, narrow bandwidth ICH-constrained elements of hypothetical interstellar transmitted signals, while a radio telescope is pointed on and off celestial coordinates 5.25 ± 0.15 hours Right Ascension (*RA*) and -7.6° ± 1° Declination (*DEC*). The term *polarized pulse pair* is used in this work to refer to the hypothetical interstellar signals.

In one argument, the Bayesian posterior probabilities calculated in the current work may include the factor of prior probabilities, posteriors calculated in [1]. In another argument, prior

William J. (Skip) Crilly Jr. is a Volunteer Science Ambassador in Education & Public Outreach of the Green Bank Observatory.
email: wcrilly@nrao.edu

probabilities may be considered as indications of the significance of the 5.25 ± 0.15 hours *RA* and -7.6° ± 1° *DEC* parameters placed in the predictive hypothesis above. The hypothesis may then be subjected to a test with new experimental data, with no explicit Bayesian prior, or with the inclusion of the prior, depending on assumptions.

The remainder of this paper describes four methods of RFI reduction, added to the methods described in [1], summarizes 40-day beam transit observations using the 26 foot radio telescope in New Hampshire, and discusses results, conclusions, and proposed further work.

2. Methods

The RFI filter mechanisms that excise candidate polarized pulse pairs, based on Δt, Δf and polarized pulse pair interarrival time, are described in **Figure 1**.

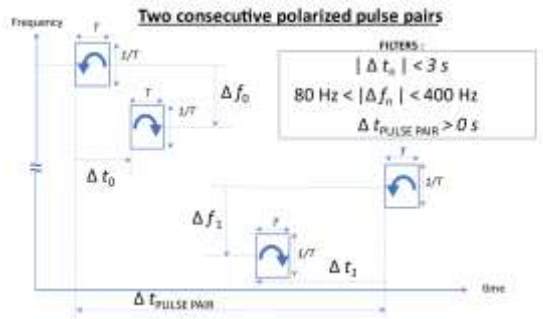

Figure 1: Filters are designed to reduce RFI-caused indications of hypothetical interstellar polarized pulse pair signals. $1/T$ is equal to 3.725 Hz in this work.

In the augmented RFI filters, measured Δt and Δf are constrained to limits, and the interarrival time of candidate polarized pulse pairs, $\Delta t_{\text{PULSE PAIR}}$, is required to be non-zero. RFI amelioration methods implemented in machine post-processing [1], and retained in the current work, are summarized below, together with the description of the four added or changed amelioration methods implemented in the current work.

1. Telescope-specific, pre-observation, spectral segment excision of persistent RFI,
2. Post-processing spectral excision of persistent RFI,
3. Dynamic RFI excision using spectral Infinite Impulse Response filtering of Signal-to-Noise Ratio (SNR) threshold crossings,
4. Harmonically related frequency excision, within ±25 kHz of 500 kHz harmonics, and ±1 kHz of 100 kHz harmonics, (the latter implemented, but not stated in [1]),
5. Observation frequency band edge and in-phase quadrature (IQ) near-zero baseband excision.
6. **Changed:** Δt Δf polarized pulse pairs measuring $|\Delta t|$ less than 3 seconds are included as candidate polarized pulse pairs. Previous work [1] used $\Delta t = 0$ throughout the machine post-processing of observations. Two reasons explain the use of $\Delta t = 0$ in [1]. Synchronized geographically-spaced radio telescope observations in [1] naturally lead to the search for $\Delta t = 0$ polarized pulse pairs, implying a single pulse is propagated to both telescopes. Further, $\Delta t = 0$ polarized pulse pairs have minimum likelihood in AWGN, yet have potentially high flux due to RFI. The increase of the $|\Delta t|$ filter maximum to 3 seconds is hypothesized to increase the non-RFI polarized pulse pair flux, improving statistical properties during relatively short-term beam transit measurements.
7. **Changed:** Δt Δf polarized pulse pairs having $|\Delta f| <$ 80 Hz, are excised, to reduce indications caused by Doppler-spread RFI. Doppler spread of signals is caused by various movements of transmitting antennas, receiving antennas, and various movements of objects located within primary Fresnel zones of the signal propagation paths [4].
8. **Added:** Consecutive Δt Δf polarized pulse pairs having an inter-arrival time of zero are excised. Elements of RFI from a single transmitting source tend to be coincident, within the pulse integration period T, after propagation to the receiver. Possible leakage of RFI through the polarized pulse pair filters, i.e. RFI amelioration methods 1 through 7, may confuse experimental results. The use of a filter having $\Delta t_{\text{PULSE PAIR}} > 0$ is hypothesized to reduce RFI-caused indications, while reducing received true-positive polarized pulse pair flux by a minimal amount, as polarized pulse pairs are hypothesized to be infrequent when transmitted at a single pulse duration T, among other possible values of transmitted pulse duration.

9. **Changed:** Sorting of SNR, high to low, by the lower SNR of the two orthogonal circular polarizations' SNRs, is implemented in the current work. The SNRs of candidate polarized pulse pair elements have a threshold of 13.0 dB for the higher of the two polarized SNRs, and 11.8 dB for the lower SNR. In previous work [1], the higher SNR of the two orthogonal polarizations' SNRs was used in the sort, for reasons that follow. In receiver systems that filter RFI with $\Delta t = 0$, e.g. using geographically-spaced radio telescopes as in [1], a single high SNR pulse received at one telescope is compared to indications at the second telescope. Reduction of threshold SNR at the second telescope seems natural, when seeking a weak signal originating from a single transmitting source, propagated into each telescope's beam pattern. When using a single telescope in beam transit measurements, repetitive polarized RFI near $\Delta t = 0$ is expected to confuse measurement results. RFI is hypothesized to have polarization measurements localized on the Poincare´ sphere, with significant SNR difference indications of orthogonal polarizations. The flux of transmitted polarized pulse pairs is hypothesized to increase at high SNR thresholds of each orthogonal polarization, due to properties of the Ricean to Rayleigh density ratio, described in Appendix B of [1]. Sorting by the lower of the polarized SNRs therefore seems important in this work.

The RFI amelioration methods 2 – 9 above are implemented in the post-processing of telescope raw data. Telescope measurements of 11.8 dB SNR threshold crossing events are saved in files during signal capture, to reduce the risk of corruption of telescope experimental raw data due to post-processing methods.

RA filtering is implemented in beam transit measurements, similar to *RA* filtering used in [1], to correlate anomalous polarized pulse pair flux to a hypothetical celestial direction. In the current work, *RA* is quantized to 0.3-hour intervals, providing 80 *RA* intervals over 24 hours of *RA*, at -7.6° *DEC*. Binomial density likelihood functions use event probability equal to the ratio 0.3 hours *RA* / 24 hours *RA*, as uniform celestially distributed events are expected in AWGN.

3. Observations

A 40-day beam transit measurement was conducted, beginning shortly after a 44-day artificial noise test was completed, the latter described in [1]. Observations were undertaken using the experimental protocol described in [1], modified by the augmented RFI filters, described in **II. METHODS**. The post-processing and presentation of results follows procedures described in Appendix C, Method B of [1], with filter parameters, SNR sorting, and *RA* coverage modified as described in **II. METHODS.**

Figures 2 – 9 describe the binomial density likelihoods of SNR-sorted polarized pulse pairs, given an AWGN cause. Several anomalies are observed within the population of 80 *RA* ranges, suggesting that unexcised RFI might be present in the experimental results. Text below each figure summarizes anomalous measurements in the ten ranges of *RA* plotted in each figure.

In **Figure 3**, the 5.1 **–** 5.4 hour *RA* window indicates a significantly low binomial density calculated value, 0.00063, at 417 SNR trials, perhaps as a result of undiscovered RFI, equipment, and/or another cause. AWGN-caused pulse pair count likelihood, normalized using the expected AWGN-caused binomial density at 417 trials, calculates to 0.0036.

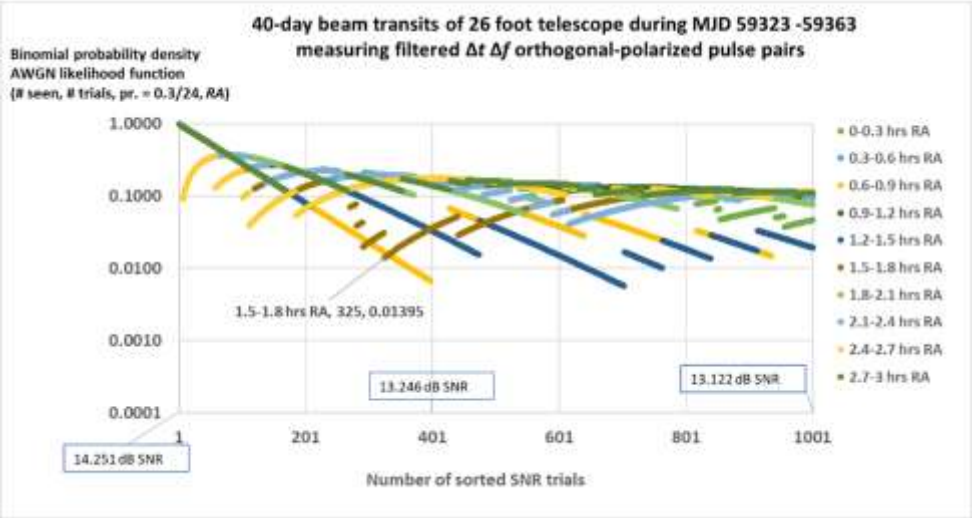

Figure 2: The 1.5 **–** 1.8 hour *RA* range indicates reduced binomial densities. Decreasing density discontinuities in **Figures 2 – 9** indicate anomalous presence of polarized pulse pairs, due to the two-sided binomial density function.

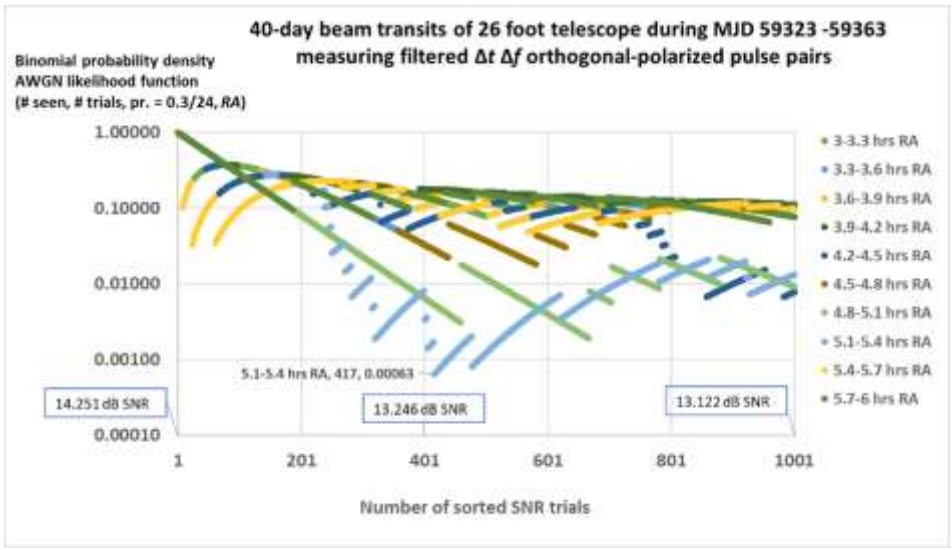

Figure 3: Polarized pulse pairs indicate in the 5.1 **–** 5.4 hour *RA* range, values of parameters of the hypothesis in this work, at a minimum of 0.00063 binomial density due to AWGN, 0.0036 times the density expected in an AWGN-only model at 417 trials. Fourteen polarized pulse pairs were observed, while a mean of 5.2 pulse pairs is expected in AWGN at the 417 SNR trial level. Pulse pairs appear distributed across Modified Julian Days (MJDs) and RF frequency, described in **Figure 12**. Δ*f* vs. Δ*t* are plotted in **Figure 13**. The 5.1 **–** 5.4 hour *RA* pointing direction indicates the third lowest binomial density, in 80 *RA* intervals. The lowest binomial density was observed in a group of anomalous pulse pairs primarily seen on MJD 59332, described in **Figures 9** and **10**.

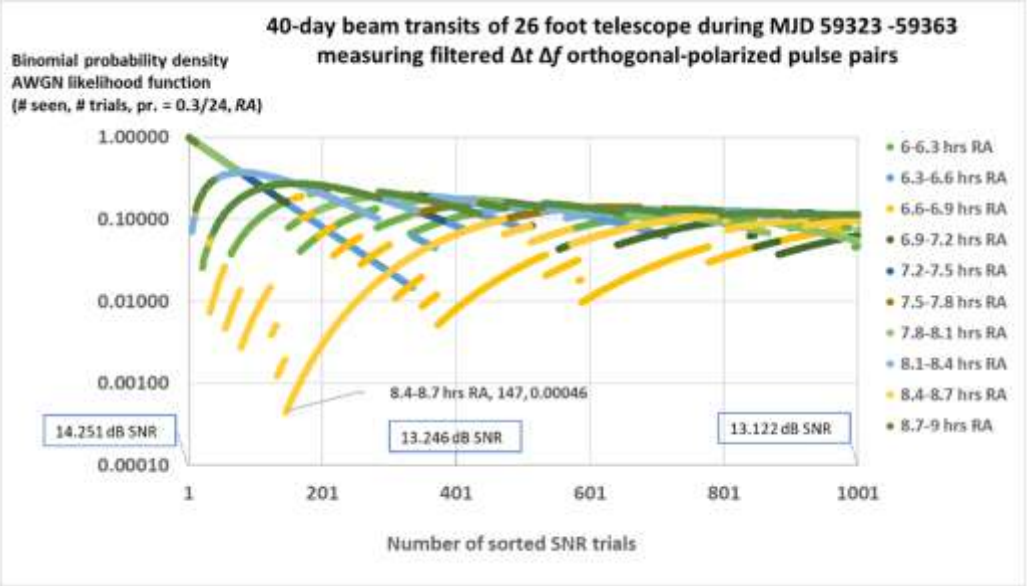

Figure 4: The 8.4 **–** 8.7 hour *RA* range indicates reduced binomial density of excess polarized pulse pairs. Distribution of polarized pulse pairs across MJD and RF Frequency are described in **Figure 11**.

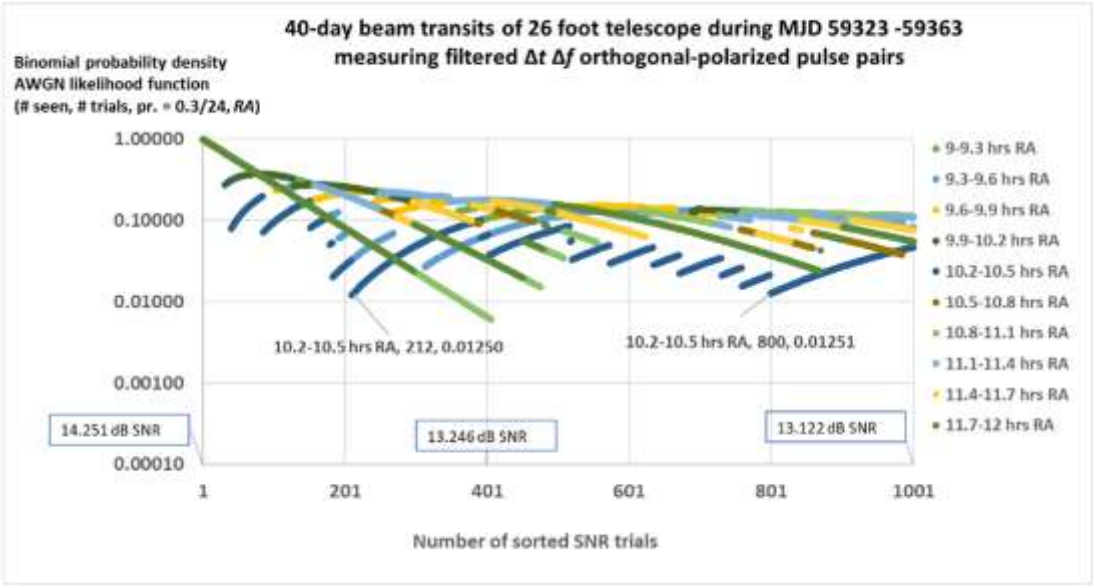

Figure 5: The 10.2 **–** 10.5 hour *RA* range indicates two SNR-sorted regions of reduced binomial density of excess polarized pulse pairs.

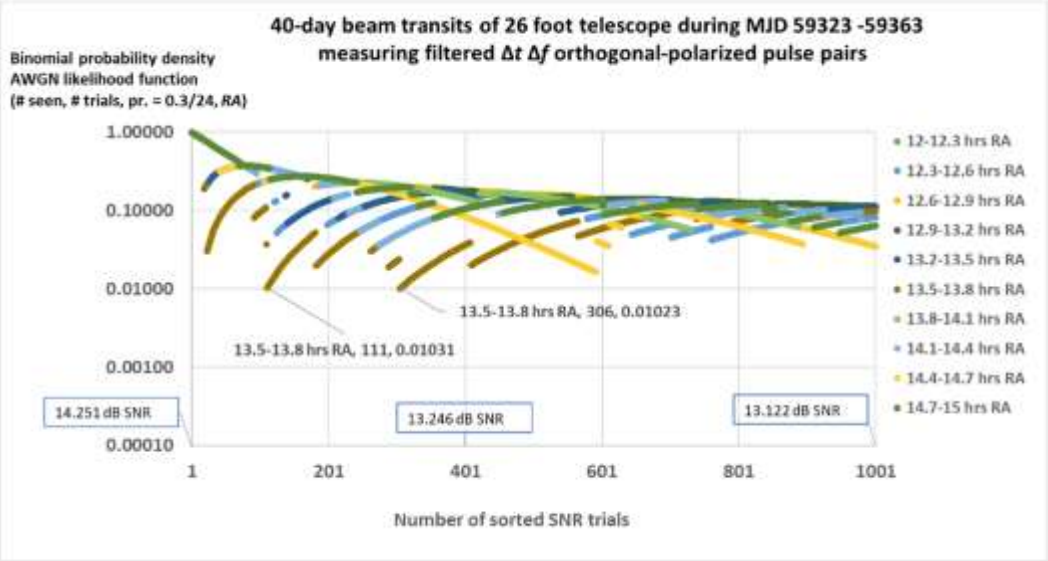

Figure 6: The 13.5 **–** 13.8 hour *RA* range indicates reduced binomial densities, displaying two indications at ≈ 0.01 density.

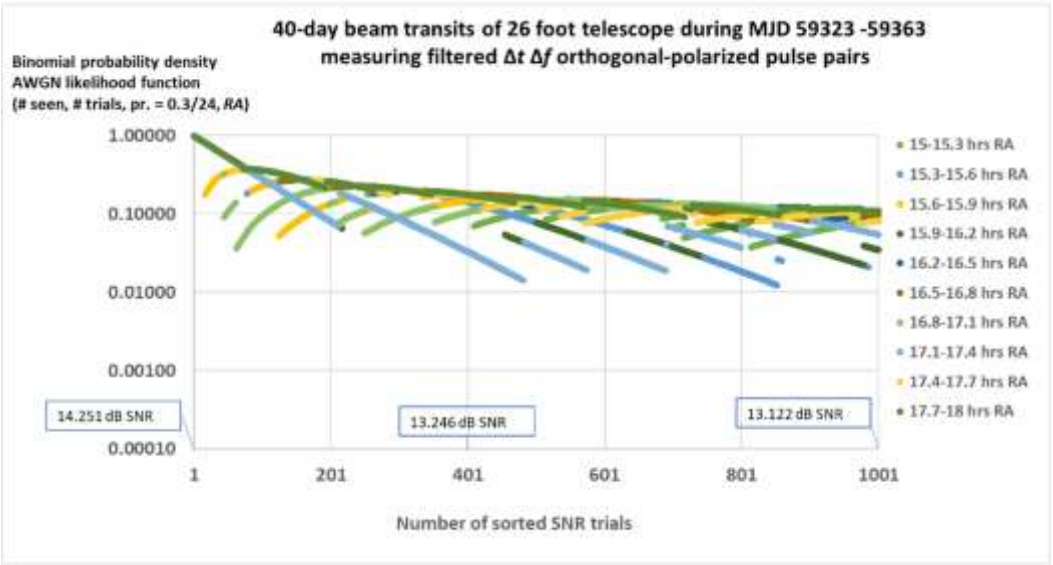

Figure 7: The 15 **–** 18 hour *RA* ranges do not indicate anomalous polarized pulse pairs.

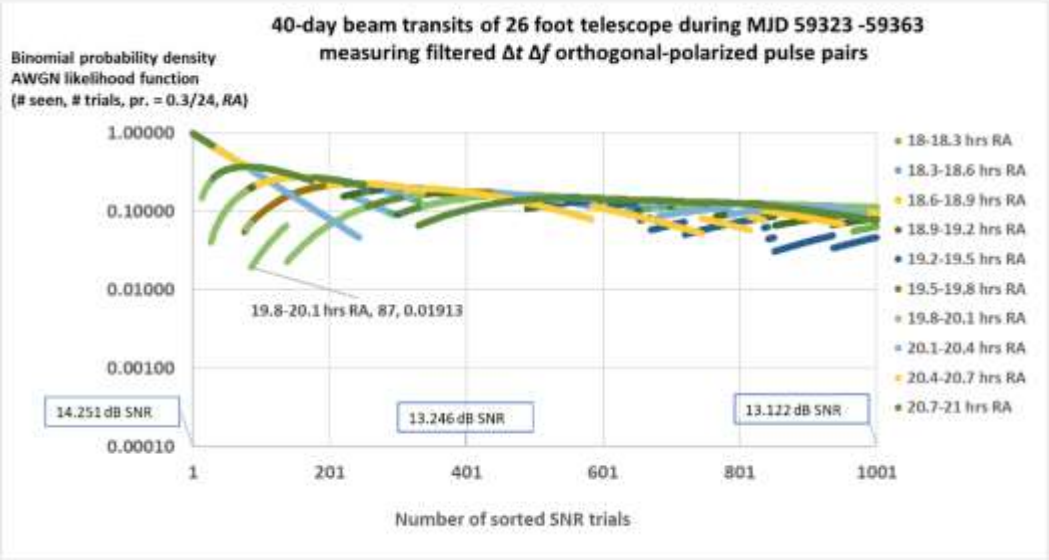

Figure 8: The 19.8 **–** 20.1 hour *RA* range indicates several high SNR binomial density reductions.

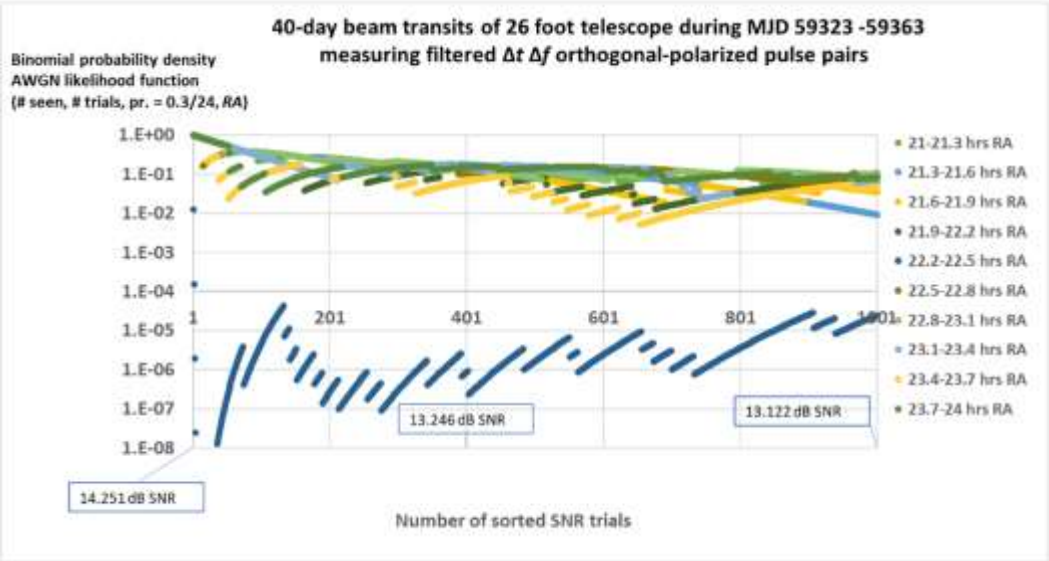

Figure 9: The 22.2 **–** 22.5 hour *RA* range anomalies significantly indicate on a single MJD day, MJD 59332, described in **Figure 10**. The single day presence of these pulse pairs, i.e. during a single beam transit, suggests a possible RFI explanation. Measured wideband distributed RF frequency of 22.2 **–** 22.5 hour *RA* polarized pulse pairs, similar to hypothetical interstellar signals, points to a potential undiscovered and unfiltered RFI source, possibly affecting data in other *RA* directions. A beam transit experiment is now underway (June 2021) to study alternate explanations.

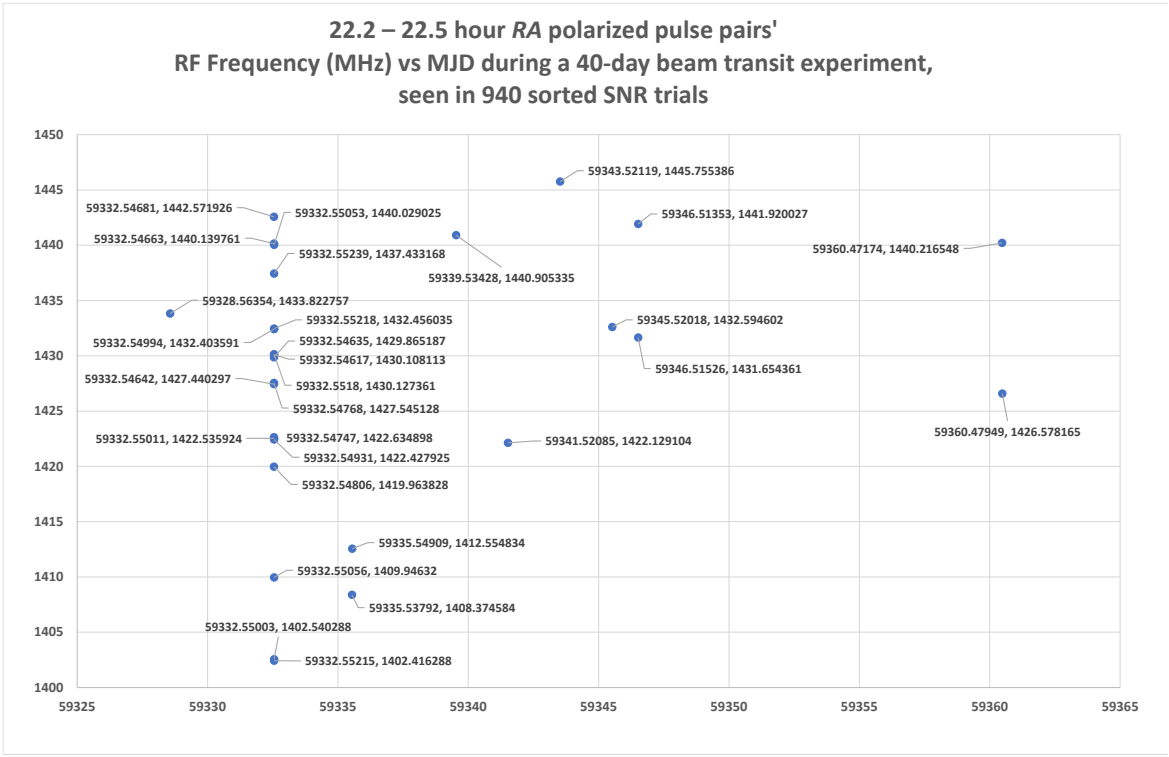

Figure 10: The 22.2 to 22.5 hours *RA* polarized pulse pairs' RF Frequencies, having measured MJD 59332, are concentrated with frequency differences near the fundamental and harmonics of approximately 2.44 MHz.

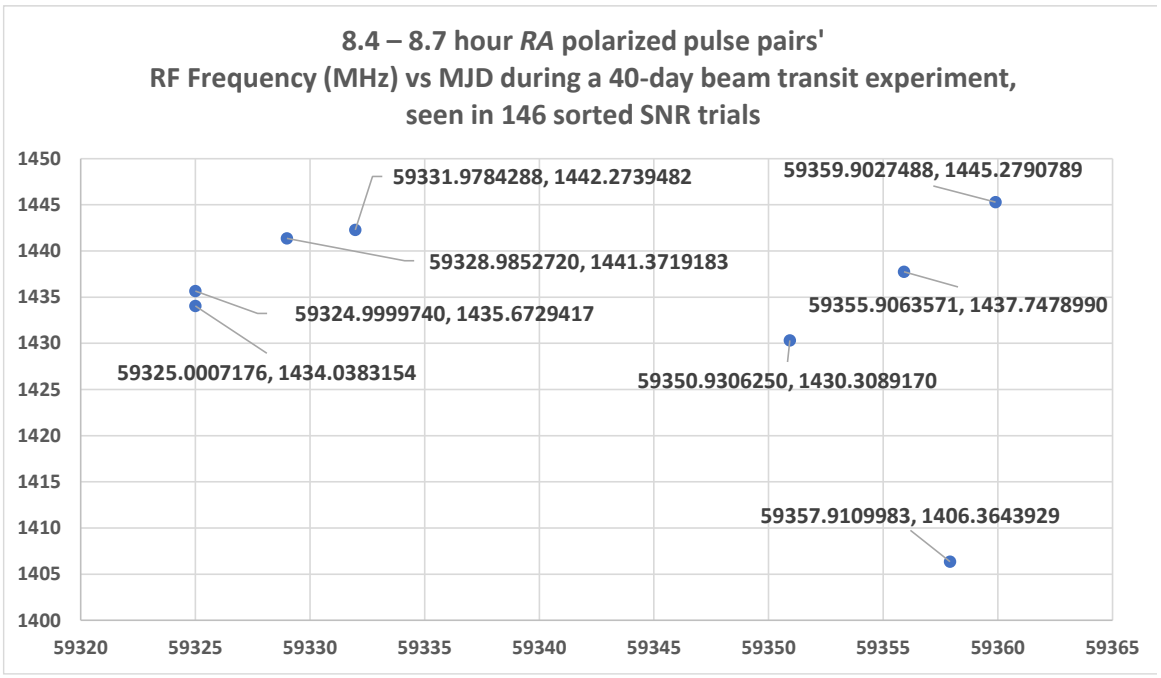

Figure 11: The 8.4 – 8.7 hour *RA* polarized pulse pairs appear distributed in MJD and RF Frequency.

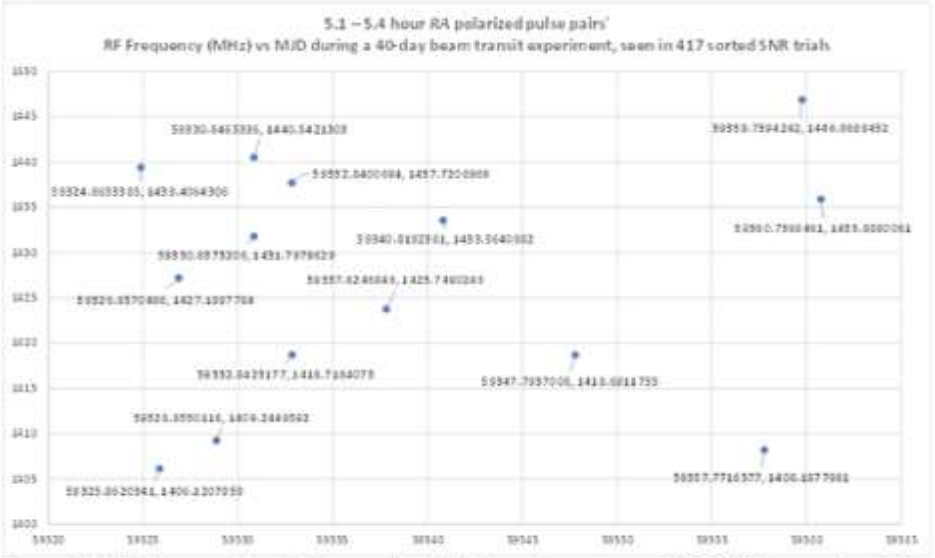

Figure 12: With the exception of the two polarized pulse pair events near 1418.7 MHz, anomalous 5.1 – 5.4 hour *RA* polarized pulse pairs appear distributed in MJD and RF frequency, as expected in an energy-efficient communications signal. Fourteen polarized pulse pairs were observed, while 5.2 polarized pulse pairs are expected, given an AWGN model.

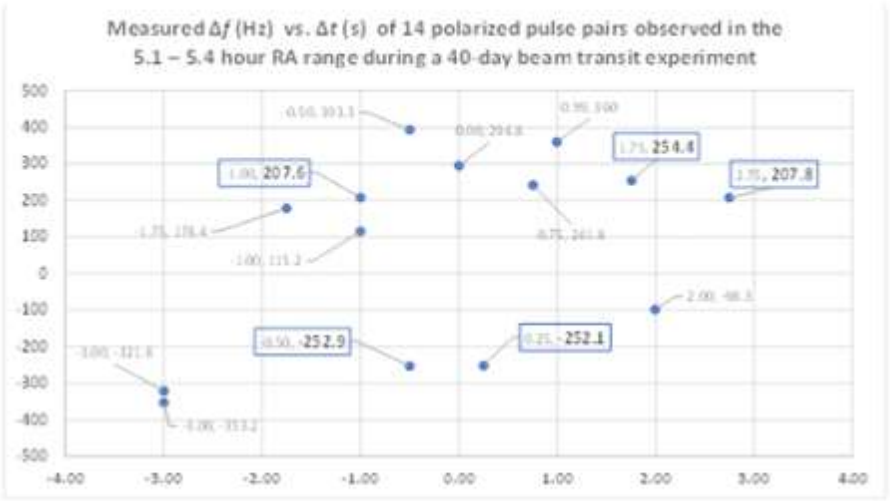

Figure 13: Δ*f* (Hz) vs. Δ*t* (s) of the 14 highest sorted SNR polarized pulse pairs in the 5.1 to 5.4 hour *RA* range. Four of the polarized pulse pairs indicate at nearly the same **Δ*f*** values, near 207.7 and -252.5 Hz. The probability density of similar matching **Δ*f*** pulse pair events, per experiment, calculates and simulates to 0.075, given AWGN. The probability density per experiment of the **Δ*f*** = 254.4 Hz polarized pulse pair, calculates to 0.19, given AWGN, assuming uniform **Δ*f***, and that a near-match | **Δ*f*** | = 254.4 Hz might measure within one FFT bin (3.7 Hz) of ±207.7 Hz, or ±252.5 Hz.

4. Discussion

In Bayesian inference, a tested model inherently includes aspects of the methods used to select the data population that is applied to the model's likelihood function [5].

The AWGN model stated in the hypothesis in this and previous work [1] is considered a model that has intentionally robust RFI filtering, in an attempt to select data that has the properties of AWGN, and consequently, hypothetical AWGN-like polarized pulse pairs. The resulting selection of a studied data population that is a subset of the overall telescope data may confuse the calculation of likelihoods.

To counter this confusion, an assumption is made that the theory underlying human-made RFI phenomena is captured in the algorithms and machine design that reject telescope data. In other words, RFI filters are considered experimental design aspects, similar to the reduction of telescope sidelobes, radio quiet zones, Faraday cages, etc. The model to be tested in this experiment is therefore an AWGN model that has intentionally rejected, in various ways, theoretical human-made radio interference.

The resulting model will be referred to as an AWGN model, given the argument that filters and equipment in an experiment are commonly designed to reject data that is understood to be not relevant, and ignorable to the discovery of the phenomena sought, i.e. AWGN-like communication signals. Design documentation and post-processing output files may be examined to determine if the experimental design and data population selection process are introducing false positives.

The binomial distribution is used in a likelihood function that estimates the probability of an AWGN cause of the measured count of polarized pulse pairs, within one of 80 *RA* ranges, at an SNR-sorted trial number. The underlying assumption that justifies the binomial is that each *RA* range is assumed to be independent of the 79 other *RA* ranges, allowing a binomial distribution to be applied separately to each *RA* range, instead of a multinomial distribution, comprising all ranges. The binomial assumption seems valid if the events in the other 79 *RAs* are adequately independent of events in the *RA* range examined, and adjacency and quantization of *RA* are ignorable.

The presence in the post-processing output file of apparent non-AWGN components, in one or more alternate *RA* ranges, within the binomial trials of a hypothesized significant *RA* range, biases the calculated binomial density likelihoods of the hypothetically significant *RA* range, with bias analyzed as follows. If one considers an intentional and justified elimination of *N* suspected alternate *RA*, non-AWGN components, then the number of trials in the binomial calculation of a hypothetically significant *RA* range is reduced by *N*, reducing calculated likelihood, when pulse pair count is anomalously high. To prevent this type of bias, suspected alternate *RA* non-AWGN components are retained during binomial calculations, understanding that anomalous events in alternate *RA*s might bias otherwise low calculated likelihoods to slightly higher values. The use of the binomial likelihood seems justified if the number of alternate *RA* non-AWGN pulse pairs is low relative to the number of trials in the binomial calculation. This condition is often met when the number of *RA* ranges is large, and when many *RA* ranges appear noise-like.

The AWGN model, associated with its hypothesis and experimental method, appears to have been falsified in previous work, to a Bayesian posterior of approximately 10^{-4} (Figure 12 text in [1]). The current work might use this value as a prior, and calculate a Bayesian posterior at less than 10^{-6}, as a result of the AWGN likelihood of 0.0036, calculated from data in **Figure 3,** using Bayesian inference methods described in Appendix E of [1]. Data invalidity arguably might increase this value significantly. For example, a fortuitous set of pulses may have been present in the 5.1 – 5.4 hour *RA* range, caused by noise, RFI, and/or equipment issues. If these complicating issues are assumed to be present, then the probability that data is valid may be low. The Bayesian posterior probabilities of many models, given invalid data, subsequently increase. Further, a combination of auxiliary and alternate hypotheses might explain the anomalies in **Figures 3, 4** and/or **9**.

A modified experimental step might invalidate the use of Bayesian inference, because, for example, a second model is considered in the Bayesian conditional likelihood function development, while a first model was used in the development of the prior probability. However, if an assumption is made that

augmented RFI filters likely remove, and do not add, non-AWGN anomalies, then the use of a pre-augmentation model's prior in Bayesian inference might be justified, during a falsification. In another argument, almost any change in experimental protocol complicates a prior's subsequent use in Bayesian inference, due to uncertainty of the effect of the protocol change.

Robust RFI filtering presents the problem that hypothetical interstellar communication signals may be rejected by the RFI filters. An interesting outcome of the design and implementation of the robust RFI amelioration in this work is the inherent ability of the RFI filters to reject many types of suspected human-made RFI. Anomalously high counts of $\Delta t\, \Delta f$ polarized pulse pairs might then appear, as either filter leakage of human-made RFI, or signals caused by something other than human-made RFI. In effect, the AWGN model, together with robust RFI filtering in the experimental protocol, seems useful to the discovery of intentionally transmitted $\Delta t\, \Delta f$ polarized pulse pair signals.

In addition to equipment, methodology, and RFI leakage issues, one or more natural objects may explain anomalous results. In general, T duration natural signals having relatively high levels of energy confined to bandwidth $1/T$ = 3.7 Hz are considered rare, due to the Doppler spread of rotating transmitting objects. Continuum measurements recorded during the 40-day beam transit test do not indicate a broadband telescope average power response in the range of 5.1 – 5.4 hours *RA,* at or above the sensitivity of the 26 foot telescope. Natural object measurement work is preliminary and does not include measurements and analysis that might indicate response due to various types of natural objects.

5. Conclusions

The results of this experiment appear to falsify the AWGN model hypothesis, to the Bayesian posterior levels inferred from **III. OBSERVATIONS,** and **IV. DISCUSSION**. The AWGN model is falsified to a lesser extent if the prior from [1] is not considered. Models derived from auxiliary and alternate hypotheses have not been designed and tested to a degree necessary to propose conclusions that might explain the discrepancy between AWGN-caused expectations and observed results. Absent experimental methods, theory and evidence to test various alternate and auxiliary hypotheses, further work is important.

6. Further Work

The further work described in [1] is retained. Prioritization is adjusted to focus on the development of RFI models and tests. Spectrum analyzers with dedicated antennas have been added to the receiver system, continuously measuring suspected potential RFI sources. Beam transit measurements run almost continuously. Examination of the various reduced values of binomial density, RFI files, and associated pulse files, is planned. Repeatability of *RA*-correlated polarized pulse pair anomalies seems important.

II. Acknowledgments

Special thanks are given to Deep Space Exploration Society members, the workers of the SETI Institute, Breakthrough Listen and the U.C. Berkeley SETI Research Center, for work, ideas and helpful guidance. Special thanks are given to the workers of the Green Bank Observatory. Special thanks are given to family and friends for helpful advice.

III. References

[1] W. J. Crilly Jr, *An interstellar communication method: system design and observations*, arXiv: 2105.03727v1, May 8, 2021

[2] C. E. Shannon, W. Weaver, *The Mathematical Theory of Communication*, Urbana and Chicago, IL: University of Illinois Press, pp. 97–103, 1949

[3] D. G. Messerschmitt, *End-to-end interstellar communication system design for power efficiency*, arXiv 1305.4684v2, pp. 26–27, 70–74, 86–106, 201–223, 2018

[4] J. G. Proakis, *Digital Communications*, 4th Ed., New York, NY: McGraw-Hill, pp. 800–809, 2001

[5] A. Gelman, J. B. Carlin, H. S. Stern, D. B. Dunson, A. Vehtari, D. B. Rubin, *Bayesian Data Analysis*, 3rd Ed., Boca Raton, FL: CRC Press, p. 197, 2014

Observation Reports

HF Radio Observations of X1.5 Solar Flare on 3 July 2021 at Anchorage, Alaska

Whitham D. Reeve

Solar Active Region 2838 produced an X1.5 x-ray flare between 1418 and 1429 on 3 July 2021 (figure 1). The Space Weather Prediction Center (SWPC) Events report showed numerous radio emissions associated with the flare including bursts in the UHF and SHF ranges and sweeps in the HF and VHF ranges {SWPCEvnt}. The flare was reported by SpaceWeather.com as the strongest since September 2017 (SpWx). It also was the strongest so far in solar cycle 25.

Figure 1 ~ Solar flare images for 3 July.
Left: SDO/AIA 094 {SDO} image shows the flare near the northwest limb at 1435 UTC shortly after its peak in extreme ultraviolet (EUV) wavelength of 9.4 nm, corresponding to a temperature of 6 million kelvin.
Right: SWAP instrument on {PROBA2} almost simultaneously recorded the flare at 17.2 nm wavelength, corresponding to a temperature of 1 million kelvin. The time of this image is 1433.

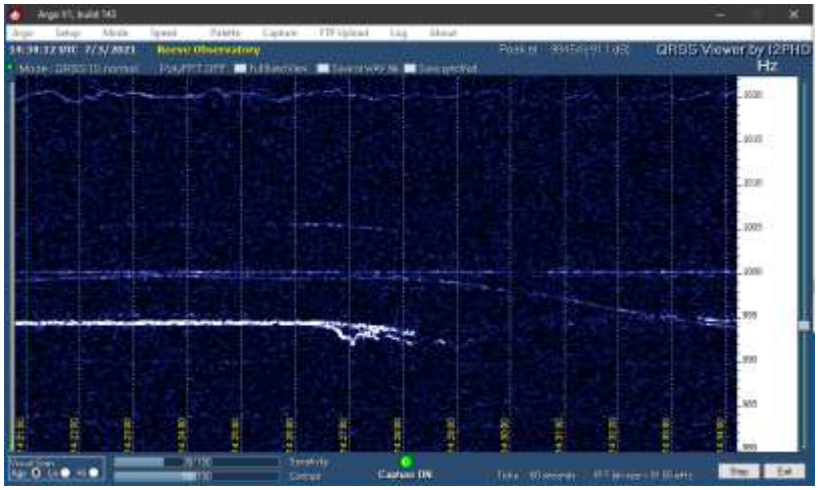

Figure 2 ~ Argo narrowband horizontal waterfall from 1421 to 1434 UTC. The white trace in the lower-left half of the image is the weak WWV or WWVH carrier at 15 MHz that has been demodulated to 995 Hz in LSB mode. A small sudden frequency deviation at 1426:30 indicates the initial disturbance in Earth's ionosphere along the path. The signal disappears entirely at 1428, indicating a radio blackout at that frequency. However, the blackout lasted only several minutes and the signal recovered to preflare levels around 1450 (not shown). The faint traces on this image are spurious signals.

The flare occurred when the Sun was over the mid-Atlantic Ocean and about 2 hours after the Anchorage sunrise. The flare's effects on HF radio propagation at 15 MHz are shown in a narrowband spectrogram waterfall (figure 2). The WWV/WWVH time-frequency transmitters supplied the signal received at Anchorage. It is not known which of the two transmitters was being received, but it probably was WWV in Colorado (about 3800 km away). The initial effect was a small sudden frequency deviation (SFD) of about 2 Hz starting at 1426:30 UTC and lasting 1 minute. The signal then disappeared altogether.

Flare radiation produced heavy D-region absorption (figure 3) leading to the radio blackout. Although propagation across the Atlantic was most affected, the radio blackout also reached propagation paths throughout the lower-48 United States and even Alaska. The flare also produced some minor geomagnetic effects but these were not evident on the Anchorage SAM-III magnetometer because of masking by the natural geomagnetic activity at higher latitudes (Anchorage is 62° N magnetic latitude).

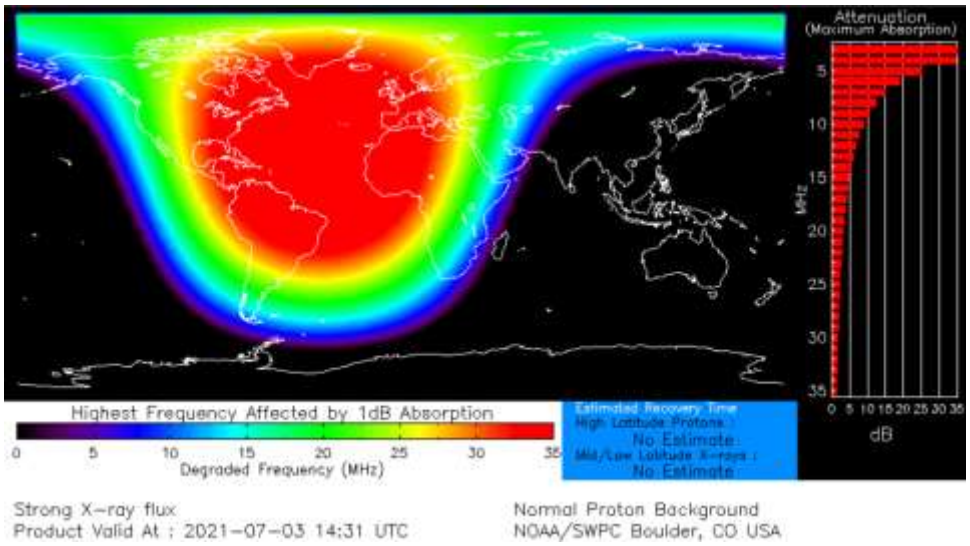

Figure 3 ~ D-Region Absorption Prediction (D-RAP) model results at 1431 UTC on 3 July. The red area shows that the D-region absorption increased at least 1 dB up to 35 MHz; frequencies below 35 MHz in this area experienced higher absorption. The green-turquoise areas along the edges correspond to at least 1 dB absorption at 15 MHz. The path from WWV near Fort Collins, Colorado to Anchorage is within this area. Image source: {D-RAP}

Instrumentation: An Icom R-8600 wideband receiver was used with a rotatable KMA-1832 log periodic dipole array antenna. The receiver was tuned to 15.000 995 MHz in LSB mode with the AGC turned off. Argo software running on an observatory PC produced the narrowband spectrum waterfall shown above.

References:

{D-RAP} https://www.swpc.noaa.gov/products/d-region-absorption-predictions-d-rap
{PROBA2} https://proba2.sidc.be/ssa
{SDO} https://sdo.gsfc.nasa.gov/data/aiahmi/
{SpWx} https://spaceweather.com/archive.php?view=1&day=03&month=07&year=2021
{SWPCEvnt} ftp://ftp.swpc.noaa.gov/pub/indices/events/20210703events.txt

VHF Observations of Type III Solar Radio Bursts on 3 July 2021 at Cohoe, Alaska

Whitham D. Reeve

Solar activity continues to be relatively high compared to a year ago. In early July, the Sun produced numerous flares, coronal mass ejections, radio bursts and radio sweeps. In particular, Type III bursts were observed at Cohoe Radio Observatory in Cohoe, Alaska at 2119 UTC on 3 July {e-CALLISTO} (figure 1). According to Space Weather Prediction Center Event report {SWPC-EVNT}, the events involved solar Active Region 2835, which also produced a small B5.1 x-ray flare. Type VI bursts and a radio blackout also were observed earlier in the day.

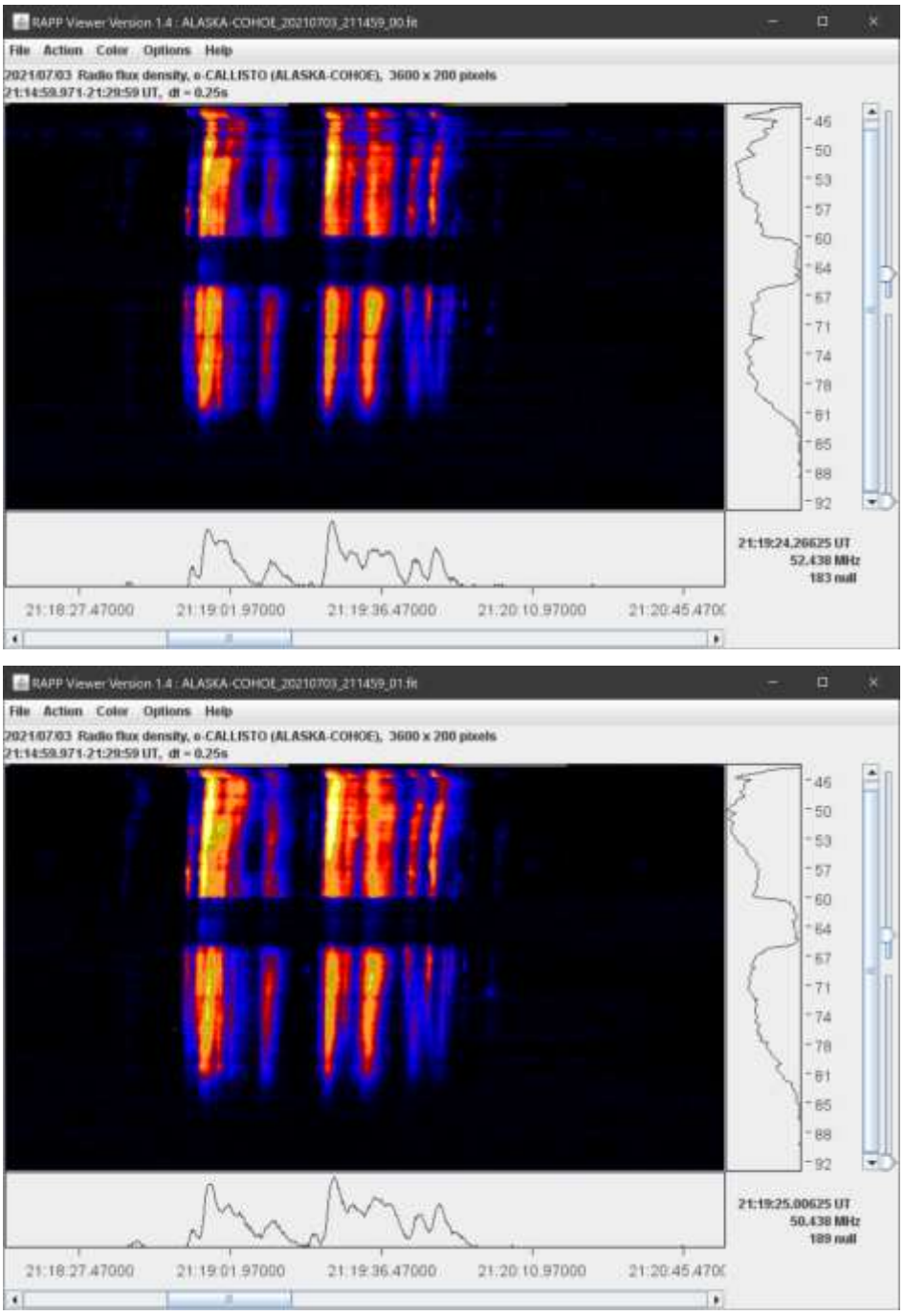

Figure 1 ~ Type III fast-drift radio bursts observed between 45 and 85 MHz.

Upper: Right-Hand Circular Polarization (RHCP).
Lower: Left-Hand Circular Polarization (LHCP).

The gap between 60 and 66 MHz is caused by intermodulation distortion in the antenna active electronics from nearby FM broadcast transmitters.

The lower frequency is limited by the native frequency range of the Callisto instrument (45 MHz). The upper frequency is limited by filters with a high frequency cutoff near 85 MHz.

Frequency in MHz is shown on the right vertical scale and time in UTC is on the horizontal scale at the bottom. The colors indicate relative intensity with black-blue being lower and red-yellow being higher. The text in the lower-right corner indicates the time, frequency and relative power of the cursor location when the image was taken (the cursor is not visible in these images).

These images are screenshots of the RAPP Viewer software.

Type III fast-drift radio emissions are thought to be caused by electron streams launched by magnetic instabilities and plasma turbulence through the solar corona at roughly one-third the speed of light. Type VI bursts are a series of Type III bursts over 10 or more minutes with no gap exceeding 30 minutes. See {SOLAR} for information on the types and characteristics of solar radio emissions.

Instrumentation: An LWA crossed-dipole antenna and two Callisto spectrometers were used for these observations (figure 2). The Callistos have an instantaneous bandwidth of 300 kHz and an integration time of 1 ms. The Callisto software collects data as Flexible Image Transport System (FITS) files, which are stored locally. The files also are uploaded automatically to Fachhochschule Nordwestschweiz (FHNW) University of Applied Sciences & Arts website {FHNW} for permanent archiving.

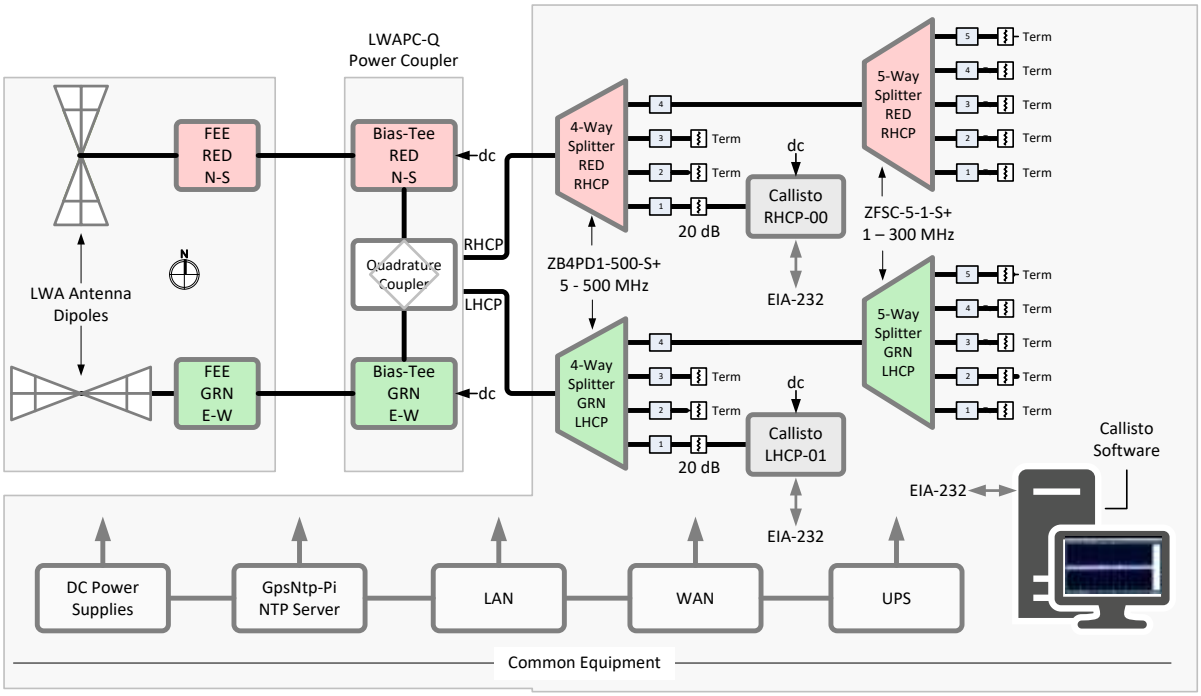

Figure 2 ~ System block diagram shows the components associated with the LWA Antenna and Callisto instruments and the common equipment shared across the observatory. Polarizations are color-coded: Red, RHCP; Green, LHCP. The Callistos are frequency agile and programmed to sweep through 200 channels between 45 and 92 MHz every 250 ms; in this configuration, the frequency resolution is 250 kHz. The data are collected by the Callisto software through EIA-232 serial interfaces and formatted as FITS files for archiving.

References & Weblinks:

{e-CALLISTO} http://soleil.i4ds.ch/solarradio/data/BurstLists/2010-yyyy_Monstein/2021/e-CALLISTO_2021_07.txt
{FHNW} http://soleil.i4ds.ch/solarradio/callistoQuicklooks/
{SWPC-EVNT} ftp://ftp.swpc.noaa.gov/pub/indices/events/
{SOLAR} http://www.reeve.com/Solar/Solar.htm

Radio & Geomagnetic Observations at Anchorage, Alaska on 28 July 2021

Whitham D. Reeve

Spaceweather.com reported rare blue aurora over Edmonton, Alberta Canada on 28 July {SpcWx}. It was caused by the interaction of a coronal hole high-speed stream (CHHSS) with Earth's magnetosphere. The enhanced solar wind from the CHHSS was first intercepted by Earth late in the UTC day on 27 July and continued into the next day. I operate a SAM-III magnetometer and a HF meteor trail and aurora reflections receiver station at Anchorage, Alaska and report here my observations for those two days.

The Anchorage SAM-III magnetometer recorded a disturbance just before 2300 UTC on 27 July but there was no unusual activity seen at that time on the HF reception plots for the WWV/WWVH stations on 15, 20 or 25 MHz. However, as the event continued into 28 July, HF reception started to show anomalous indications. The images on the next page show a horizontal waterfall of the demodulated audio from three receivers tuned to (nominal) 15, 20 and 25 MHz (plot 1) and plots of the X- (plot 2), Y- (plot 3) and Z-components (plot 4) of the geomagnetic field as measured at the surface. These plots cover the time period from 0243 to 0543 UTC on 28 July 2021 (6:43 pm to 9:43 pm AKDT, 27 July).

Plot 1 consists of fifteen 12-minute Argo images spliced together. The composite image has been stretched vertically to exaggerate the frequency deviations. The time scale of the Argo images is too small and distorted to read, so it is necessary to refer to the magnetic flux density plots below for time references. The vertical frequency scale of the Argo plot has a spectral width of 40 Hz. Each of the three received frequencies is plotted at a different horizontal position in the waterfall as described in the next paragraph.

All traces on the Argo plot are carriers received from the WWV or WWVH time-frequency stations that have been demodulated in the LSB mode by the receivers. The receivers were detuned by approximately 1 kHz as follows: Lower =15.000 995 MHz, which provides a trace at 995 Hz, middle = 20.001 005 MHz for a trace at 1005 Hz and upper = 25.001 015 MHz for a trace at 1015 Hz. Vestiges of the WWV-25 (top) trace start about 0400 with peak intensity from 0420 to 0427; the WWV-25 trace disappears completely at about 0433. The WWV/WWVH-20 trace (middle) lasts from approximately 0250 to 0520 with variable intensity and quasi-periodic frequency deviations.

The disturbances seen in the WWV/WWVH-15 trace (bottom) are approximately bounded by the time range of the image; that is, reception at 15 MHz was normal until 0243, disturbed from 0243 until 0543 and then returned to normal at 0543. There is evidence of aurora reflections in the 15 MHz trace at 0345 and 0440 as indicated by the wild Doppler frequency shifts in what appear to be separate traces. The approximate peak frequency deviations of the traces from nominal are: 25 MHz, +1 to –2 Hz; 20 MHz, +2 to –2 Hz; and 15 MHz, +10 to –15 Hz. The negative deviation in the 15 MHz trace is limited by the vertical scale setting and includes the Doppler shifted aurora reflections.

It is interesting that the geomagnetic field was not particularly disturbed at Anchorage during the time period in question – the data show a K-index of 3, which is below storm level. However, the disturbance clearly had some effect on Earth's ionosphere because it enhanced propagation at frequencies above 15 MHz. Whereas no propagation existed at 20 and 25 MHz before the disturbance, signals were received at 20 MHz for about 2 hours and at 25 MHz for about 30 minutes during the disturbance.

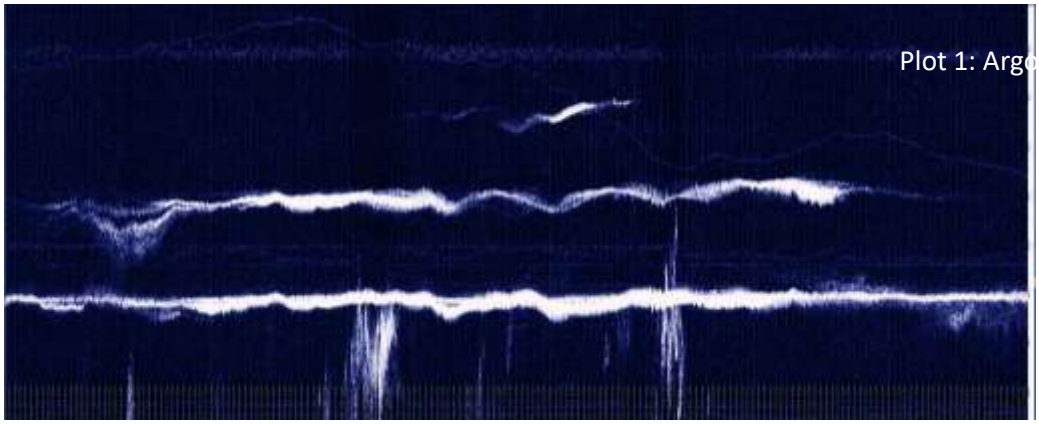

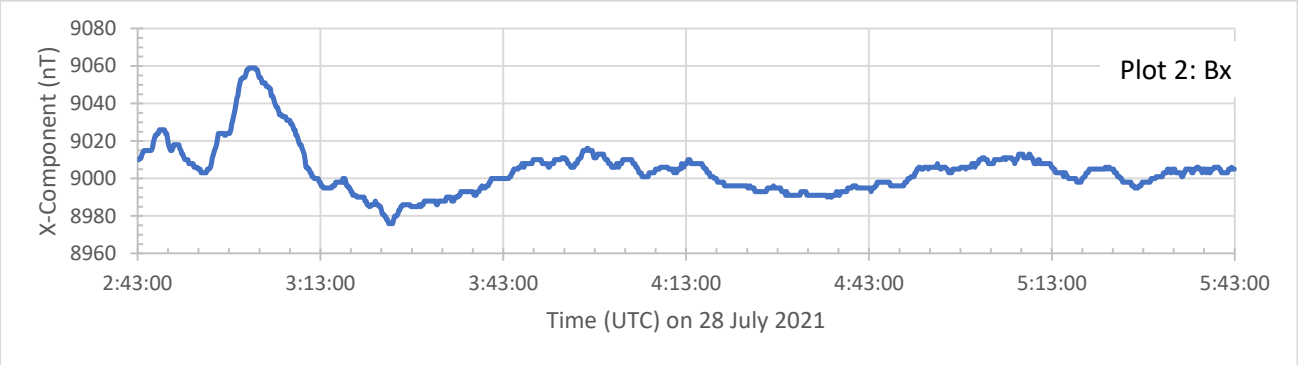

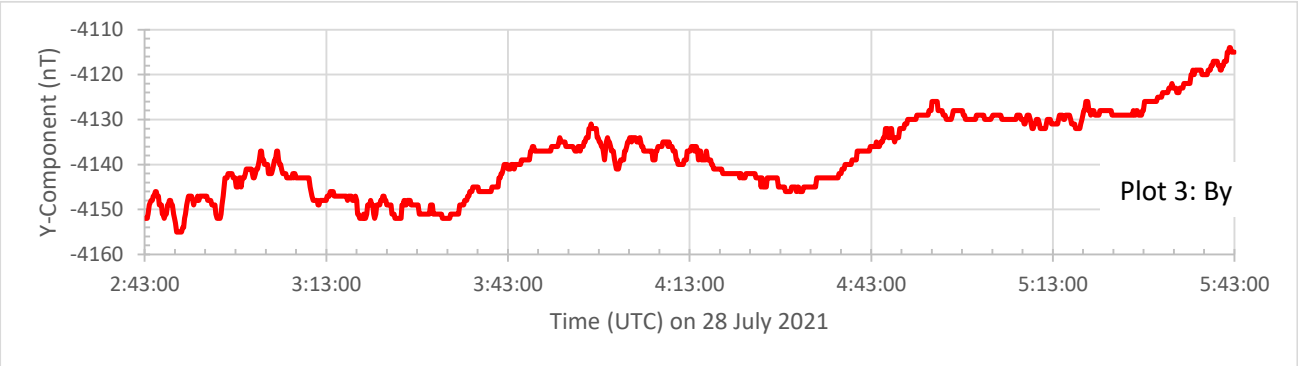

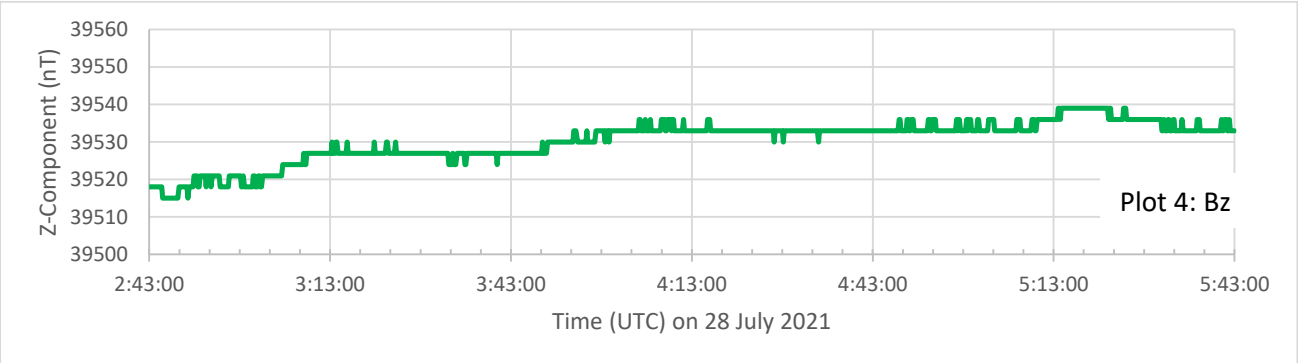

References:
{SpcWx} https://spaceweather.com/archive.php?view=1&day=28&month=07&year=2021

HI Line Observations at Haswell, Colorado: August 6-7, 2021

Richard A. Russel

Source: HI Line (various sources)
Dates: August 6-7, 2021
Radio Telescope: 18m dish (Deep Space Exploration Society) (www.DSES.science)
Location: Haswell, Colorado, USA
Receiver: Spectracyber 1: (www.radioastronomysupplies.com)
Tracking Mode: track/drift scan (track)
Observation Goal: Observe HI line for multiple sources to include in the DSES Observing Guide

Source	Date	RA (J2000)	DEC (J2000)
3C10	8/7/21	0h25m21s	64d8m26s
3C58	8/7/21	2h5m36s	64d49m41s
3C123	8/7/21	4h37m4s	29d40m13s
3C144 (Tau A)	8/7/21	5h34m31s	22d0m52s
DA001	8/7/21	0h2m42s	67d19m59s
DA003	8/7/21	0h5m24s	68d6m59s
DA046	8/7/21	1h30m12s	63d15m59s
DA076	8/7/21	2h25m35s	62d8m48s
CAS A	8/7/21	23h23m24s	58d48m53s
CYG A	8/7/21	19h59m28s	40d44m2s
SAG A	8/7/21	17h45m12s	-28d48m17s
VIRGO A	8/7/21	12h30m49s	12d23m28s
S7	8/7/21	02h06m12.59s	60d32m54.9s
S8	8/7/21	05h47m21.34s	-01d40m18.41s
W10	8/7/21	5h35m17s	-5d25m 0s
W11	8/7/21	5h36m12s	23d12m59s
W12	8/7/21	5h41m42s	-1d54m44s
W13	8/7/21	6h9m39s	20d29m12s

3C10

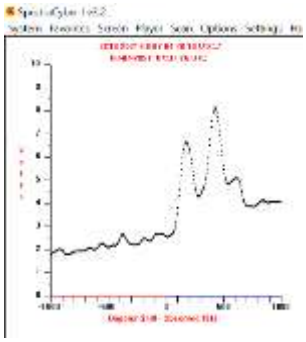

3C58

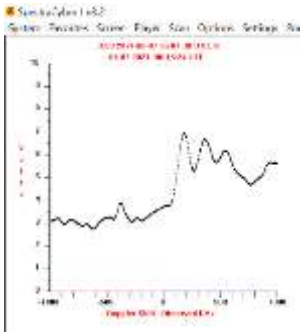

3C123

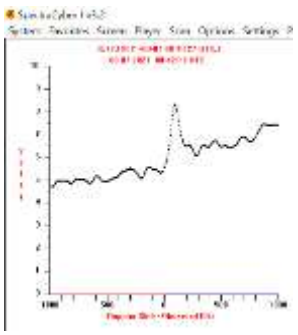

3C144

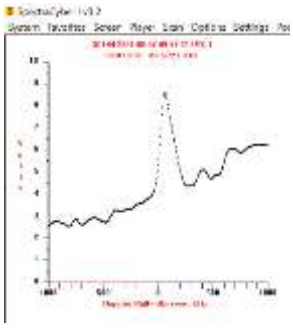

DA001

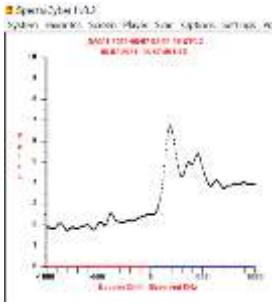

DA003

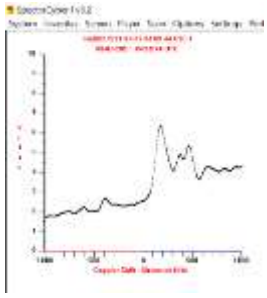

DA046

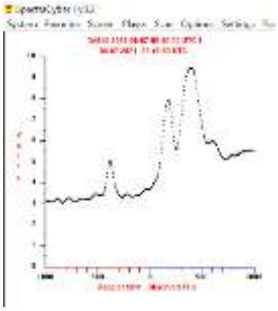

DA076

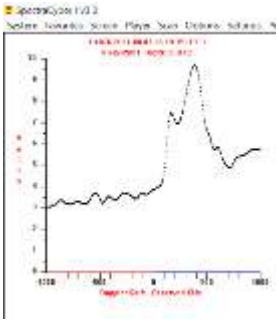

CAS A

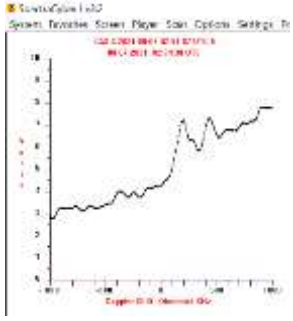

CYG A

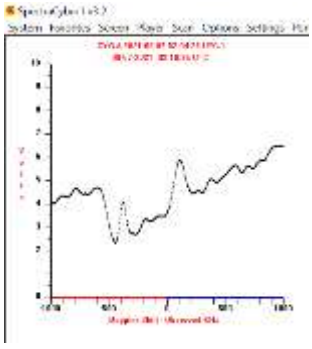

SAG A

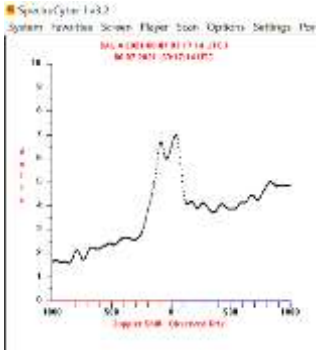

VIRGO A

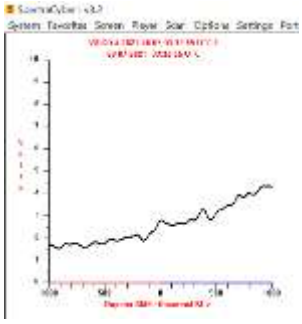

S7

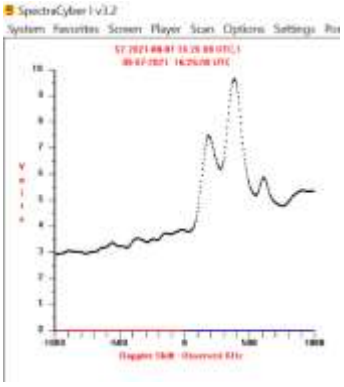

S9

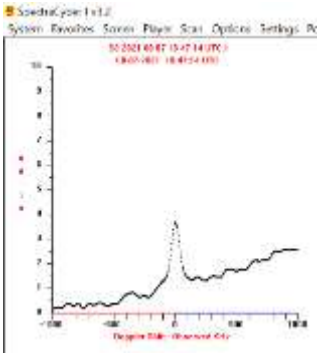

W10

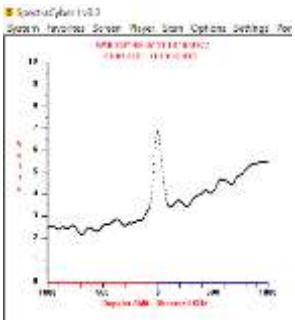

W12

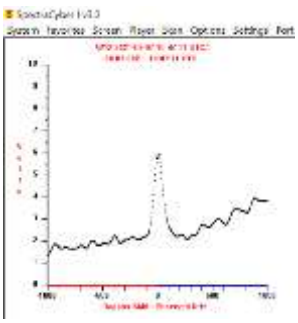

W13

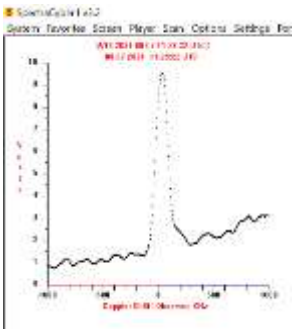

W16

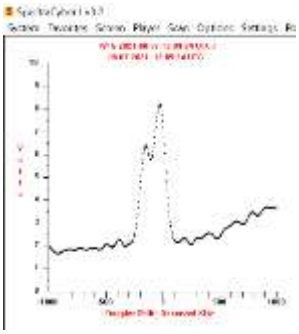

Deep Space Exploration Society Observations of Pulsars PSR B1641-45 and PSR B0329_54 on August 7-8, 2021
Dan Layne

DSES Pulsar Observation Report: B1641-45

Date & Time (UTC): 20210808_015721
Observers: Dan Layne, Ray Uberecken, Richard Russel
Telescope: Deep Space Exploration Society (DSES) 60 ft. dish (18.3 m). Haswell, CO
Feed horn: 1420 Mhz, Single Polarization, Beamwidth = 0.81°
Receiver: USRP B210, Bandwidth = 40 Mhz. Frequency = 1420 Mhz, RF Gain = 44
Computer: System76, 16 core, Ubuntu 20.04
Software: Murmur (planning), GnuRadio (collection), PRESTO (folding and detection)
Run time: 1800 seconds (30 min)
Source name, Flux density: PSR B1641-45 (J1644-4559), S1400 = 300 mJy
Source RA, DEC (J2000): $16^h\ 44^m\ 49.2^s$; -45° 59' 09.7''

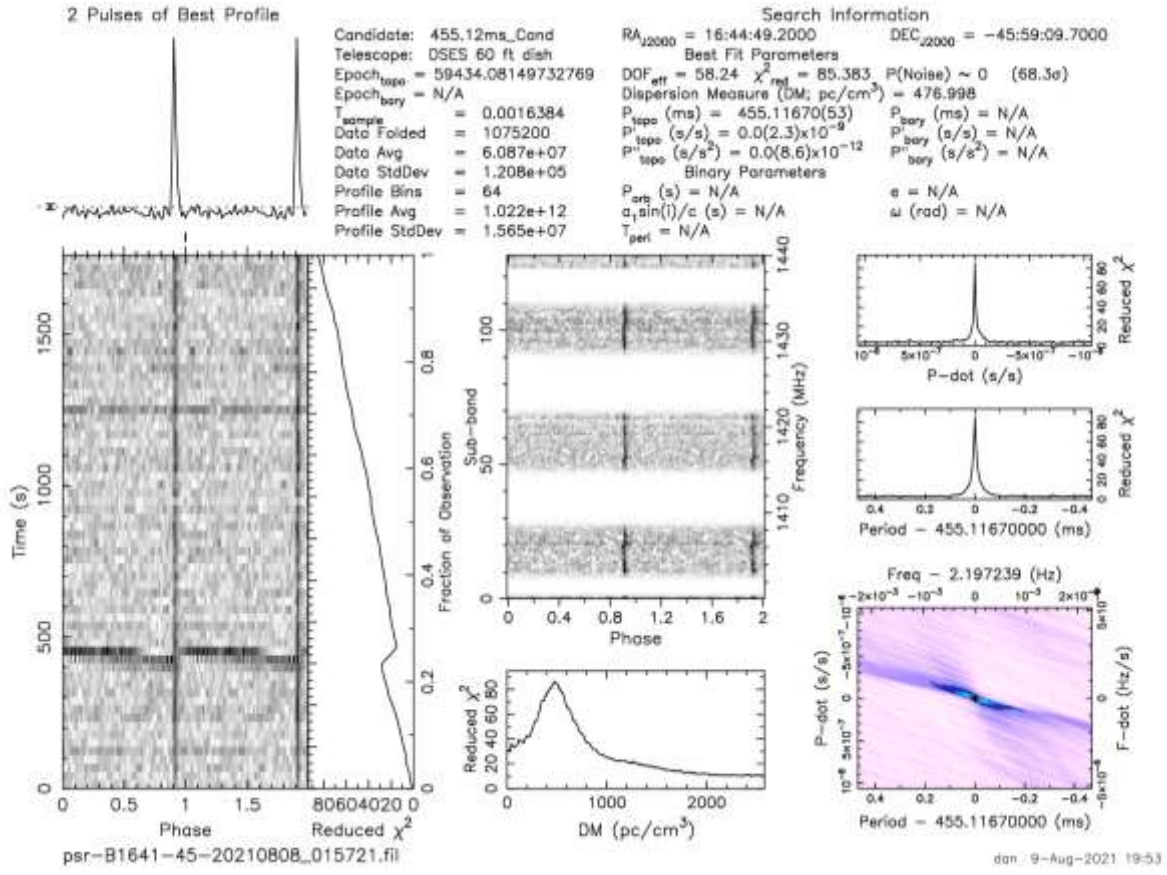

Figure 1: PRESTO plot for B1641-45

Discussion: This bright pulsar was just four degrees about the horizon for a few hours on August 8, 2021. We are tuning the receiving system following extensive repairs and upgrades.

DSES Pulsar Observation Report: B0329+54

Date & Time (UTC): 20210807_215545
Observers: Dan Layne, Ray Uberecken, Richard Russel
Telescope: Deep Space Exploration Society (DSES) 60 ft. dish (18.3 m). Haswell, CO
Feed horn: 1420 Mhz, Single Polarization, Beamwidth = 0.81°
Receiver: USRP B210, Bandwidth = 40 Mhz. Frequency = 1420 Mhz, RF Gain = 44
Computer: System76, 16 core, Ubuntu 20.04
Software: Murmur (planning), GnuRadio (collection), PRESTO (folding and detection)
Run time: 1200 seconds (20 min)
Source name, Flux density: PSR B0329+54 (J0332+5434), S1400 = 203 mJy
Source RA, DEC (J2000): $03^h\ 32^m\ 59.4^s$; +54° 34' 43.3''

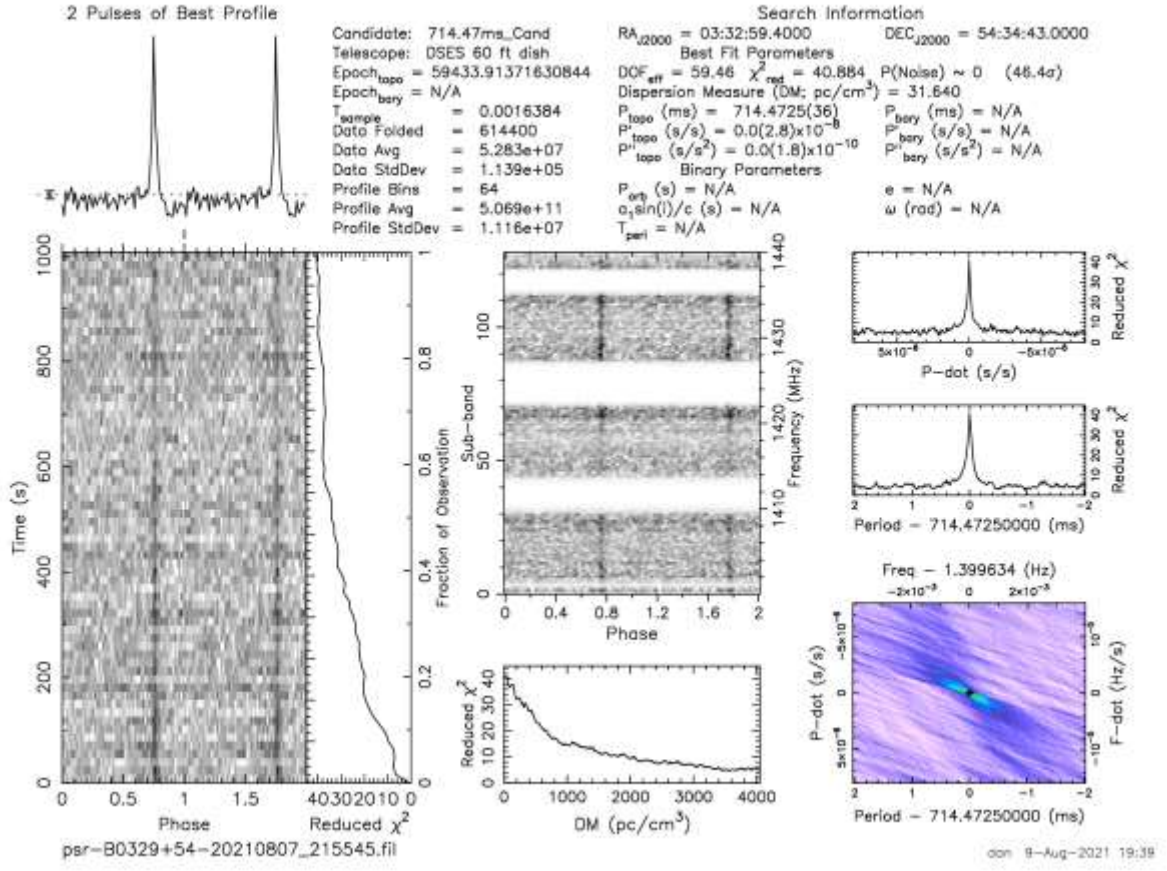

Figure 2: PRESTO plot for B0329+54

Discussion: This pulsar is routinely used to verify system performance. We also successfully detected B0950+08 and B1933+16 on August 8, 2021.

Membership

Administrative

Officers, directors, and additional SARA contacts

The Society of Amateur Radio Astronomers is an all-volunteer organization. The best way to reach people on this page is by email with SARA in the subject line SARA Officers.

President: Dennis Farr, WB4RJK, http://www.radio-astronomy.org/contact/President +1 813 833-3918
Vice President: Dr. Rich Russel, AC0UB http://www.radio-astronomy/contact/Vicepresident
Secretary: Bruce Randall, NT4RT, http://www.radio-astronomy/contact/Secretary +1 803-327-3325
Treasurer: Brian O'Rourke, K4UL, http://www.radio-astronomy/contact/Treasurer
Past President: Ken Redcap, tbd@radio-astronomy.org +1 319-591-1131
Founder Emeritus and Director: Jeffrey M. Lichtman, KI4GIY, jeff@radioastronomysupplies.com +1 954-554-3739

Board of Directors

Name	Term expires	Email
Ed Harfmann	2022	edharfmann@comcast.net
Dr. Wolfgang Herrmann	2023	messbetrieb@astropeiler.de
Tom Jacobs	2023	tdj0@bellsouth.net
Charles Osborne	2023	k4cso@charter.net
Keith Payea	2022	kbpayea@bryantlabs.net
Steve Tzikas	2022	Tzikas@alum.rpi.edu
Jon Wallace	2023	wallacefj@comcast.net
David Westman	2022	david.westman@engineeringretirees.org

Other SARA Contacts

All Officers	http://www.radio-astronomy.org/contact-sara	
All Directors and Officers	http://www.radio-astronomy.org/contact/All-Directors-and-Officers	
Eastern Conference Coordinator	http://www.radio-astronomy.org/contact/Annual-Meeting	
All Radio Astronomy Editors	http://www.radio-astronomy.org/contact/Newsletter-Editor	
Radio Astronomy Editors	Dr. Richard A. Russel	drrichrussel@netscape.net
Contributing Editor	Whitham D. Reeve	whitreeve@gmail.com
Educational Outreach	http://www.radio-astronomy.org/contact/Educational-Outreach	
Grant Committee	Tom Crowley	grants@radio-astronomy.org
Membership Chair	http://www.radio-astronomy.org/contact/Membership-Chair	
Technical Queries (David Westman)	http://www.radio-astronomy.org/contact/Technical-Queries	
Webmaster	Ciprian (Chip) Sufitchi, N2YO	webmaster@radio-astronomy.org

Resources

Great Projects to Get Started in Radio Astronomy

Radio Observing Program

The Astronomical League (AL) is starting a radio astronomy observing program. If you observe one category, you get a Bronze certificate. Silver pin is two categories with one being personally built. Gold pin level is at least four categories. (Silver and Gold level require AL membership which many clubs have membership. For the bronze level, you need not be a member of AL.)

Categories include
1) SID
2) Sun (aka IBT)
3) Jupiter (aka Radio Jove)
4) Meteor back-scatter
5) Galactic radio sources

This program is a collaboration between NRAO and AL. Steve Boerner is the Lead Coordinator and a SARA member.

For more information:
Steve Boerner
2017 Lake Clay Drive
Chesterfield, MO 63017
Email: sboerner@charter.net
Phone: 636-537-2495
http://www.astroleague.org/programs/radio-astronomy-observing-program

Radio Jove

The Radio Jove Project monitors the storms of Jupiter, solar activity and the galactic background. The radio telescope can be purchased as a kit or you can order it assembled. They have a terrific user group you can join.
http://radiojove.gsfc.nasa.gov/

INSPIRE Program

The INSPIRE program uses build-it-yourself radio telescope kits to measure and record VLF emissions such as tweeks, whistlers, sferics, and chorus along with man-made emissions. This is a very portable unit that can be easily transported to remote sites for observations.
http://theinspireproject.org/default.asp?contentID=27

SARA/Stanford SuperSID

Stanford Solar Center and the Society of Amateur Radio Astronomers have teamed up to produce and distribute the SuperSID (Sudden Ionospheric Disturbance) monitor. The monitor utilizes a simple pre-amp to magnify the VLF radio signals which are then fed into a high definition sound card. This design allows the user to monitor and record multiple frequencies simultaneously. The unit uses a compact 1-meter loop antenna that can be used indoors or outside. This is an ideal project for the radio astronomer that has limited space. To request a unit, send an e-mail to supersid@radio-astronomy.org

Radio Astronomy Online Resources

A New Radio Telescope for Mexico - ORION 2021 01 20. Dr. Stan Kurtz https://www.youtube.com/watch?v=Q9aBWr1aBVc	National Radio Astronomy Observatory http://www.nrao.edu
AJ4CO Observation of Jovian decametric emission http://www.radiojove.org/SUG/Observation%20Reports/AJ4CO/	NRAO Essential Radio Astronomy Course http://www.cv.nrao.edu/course/astr534/ERA.shtml
British Astronomical Association – Radio Astronomy Group http://www.britastro.org/baa/	Pulsar Sounds: Audio recordings made by professional observatories http://www.typnet.net/AJ4CO/Pulsar_Sounds/
CALLISTO Receiver & e-CALLISTO http://www.reeve.com/Solar/e-CALLISTO/e-callisto.htm CALLISTO data archive: www.e-callisto.org	Radio Astronomy calculators http://www.typnet.net/AJ4CO/Calculators/Calculators.htm
Deep Space Exploration Society http://DSES.science	Radio Astronomy Supplies http://www.radioastronomysupplies.com
Deep Space Object Astrophotography Part 1 -- ORION 2021 02 17. George Sradnov https://www.youtube.com/watch?v=Pm_Rs17KIyQ	Radio Jove Spectrograph Users Group http://www.radiojove.org/SUG/
European Radio Astronomy Club http://www.eracnet.org	Radio Sky Publishing http://radiosky.com
Exotic Ions and Molecules in Interstellar Space -- ORION 2020 10 21. Dr. Bob Compton https://www.youtube.com/watch?v=r6cKhp23SUo&t=5s	RF Associates Richard Flagg, rf@hawaii.rr.com 1721-1 Young Street, Honolulu, HI 96826 RFSpace, Inc. http://www.rfspace.com
Forum and Discussion Group http://groups.google.com/group/sara-list	SARA Facebook page https://www.facebook.com/pages/Society-of-Amateur-Radio-Astronomers/128085007262843
GNU Radio http://www.gnu.org/licenses/gpl.html	SARA Twitter feed https://twitter.com/RadioAstronomy1
Graphs, plots, equations, miscellaneous cheat sheets http://www.typnet.net/AJ4CO/index.htm	SARA Web Site http://radio-astronomy.org
Inspire Project http://theinspireproject.org	SETI League http://www.setileague.org

Introduction to Amateur Radio Astronomy (presentation) http://www.typnet.net/AJ4CO/Publications/Intro%20to%20Amateur%20Radio%20Astronomy,%20Typinski%20(AAC,%202016)%20v2.pdf	Shirleys Bay Radio Astronomy Consortium marcus@propulsionpolymers.com
NASA Radio JOVE Project http://radiojove.gsfc.nasa.gov Archive: http://radiojove.org/archive.html	Simple Aurora Monitor Magnetometer http://www.reeve.com/SAMDescription.htm
National Radio Astronomy Observa¬tory http://www.nrao.edu	Stanford Solar Center http://solar-center.stanford.edu/SID/
NRAO Essential Radio Astronomy Course http://www.cv.nrao.edu/course/astr534/ERA.shtml	The Arecibo Radio Telescope; It's History, Collapse, and Future - ORION 2020.12.16. Dr. Stan Kurtz, Dr. David Fields https://www.youtube.com/watch?v=rBZlPOLNX9E
Pulsar Sounds: Audio recordings made by professional observatories http://www.typnet.net/AJ4CO/Pulsar_Sounds/	The Radio JOVE Project & NASA Citizen Science – ORION 2020.6.17. Dr. Chuck Higgins https://www.youtube.com/watch?v=s6eWAxJywp8&t=5s
Radio Astronomy calculators http://www.typnet.net/AJ4CO/Calculators/Calculators.htm	UK Radio Astronomy Association http://www.ukraa.com/

For Sale, Trade and Wanted

At the SARA online store: radio-astronomy.org/store.

SARA Polo Shirts

New SARA shirts have arrived.

We now have a good selection of X, XX, and XXX shirts available in all colors including white!

Shirts are $20 at the conference and $25 shipped.

Contact the treasurer at treas@radio-astronomy.org for availability and shipping.

Scope in a Box $295

radio-astronomy.org/store.

Kit of parts and software to build a working Radio Telescope to detect Hydrogen Line emissions. Available to USA addresses only at this time.

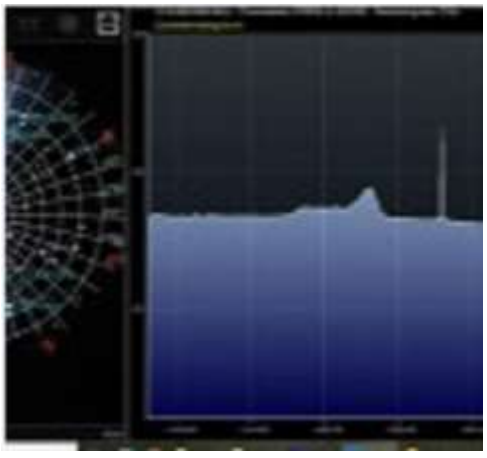

SuperSID Complete Kit ($112-$160 depending on options)
radio-astronomy.org/store.

SARA Publication, Journals and Conference Proceedings (various prices)
radio-astronomy.org/store.

SARA Journal USB Drive ($15-$35 depending on shipping option)
radio-astronomy.org/store.

The USB drive covers the society journal "Radio Astronomy" from the founding of the organization in 1981 thru 2020. Articles cover a wide range of topics including: cosmic radiation, pulsars, quasars, meteor detection, solar observing, Jupiter, Radio Jove, gamma ray bursts, the Itty Bitty Telescope (IBT), dark matter, black holes, the Jansky antenna, methanol masers, mapping at 408 MHz and more. This CD contains all of the above and more with over 4800 pages of articles on radio astronomy. Also included is a copy of Grote Reber's handwritten, 34 page document "Carriage and Mirror Detail" of his historic antenna now on display at the National Radio Astronomy Observatory (NRAO) in Green bank, WV. You also get an electronic copy of the 109 page "Basics of Radio Astronomy" from JPL Goldstone-Apple Valley Radio Telescope. Also included is the NRAO 40-foot radio telescope "Operators Manual", which by the way, you get to operate if you attend the Eastern SARA conference in July.

SARA Advertisements

There is no charge to place an ad in Radio Astronomy; but you must be a current SARA member. Ads must be pertinent to radio astronomy and are subject to the editor's approval and alteration for brevity. Please send your "For Sale," "Trade," or "Wanted" ads to edit@radio-astronomy.org. Please include email and/or telephone contact information. Please keep your ad text to a reasonable length. Ads run for one bimonthly issue unless you request otherwise.

Typinski Radio Astronomy, Inc., info@typinski.com
Antenna systems and feed line components for HF radio astronomy

Jeff Kruth, WA3ZKR, kmec@aol.com
RF components from HF to MMW, various types including mixers, RF switches, amplifiers, oscillators, coaxial components, waveguide components, etc. I have a very large collection of stuff and the facilities to test and provide data. Please email with your needs and I will see if I have something for you. Have fun!

Stuart and Lorraine Rumley, sales@valontechnology.com
The Valon Technology 2100 Downconverter, when combined with our 5009 frequency synthesizer module, provides a high-performance, compact receiver downconverter system. Applications include hydrogen line studies at 1420MHz and radio astronomy in the protected 30MHz segment of the 21 cm band. For more information visit http://www.valontechnology.com/2100downconverter.html or send an email.

Radio2Space, filippo.bradaschia@primalucelab.com
SPIDER radio telescopes and turn-key-systems designed specifically for education.
https://www.radio2space.com
We developed our SPIDER radio telescopes as turn-key-system just to avoid the problem you perfectly highlighted in your website: "Purchasing a radio telescope isn't like buying an optical telescope. They are harder to find, and usually require assembly and software troubleshooting. In some cases, a radio telescope must be built from components." Our SPIDER radio telescopes are not designed for amateurs that prefer to build a radio telescope but to schools, universities, museums, and other science institutes that needs for a complete and ready-to-use system, just like the optical telescopes they can normally buy!

Radio Astronomy Supplies
http://www.radioastronomysupplies.com
jeff@radioastronomysupplies.com
Research and Educational Radio Telescopes and all associated equipment since 1994

Membership Information

Annual SARA dues Individual $20, Classroom $20, Student $5 (US funds) anywhere in the world. Membership includes a subscription to Radio Astronomy, the bimonthly Journal of The Society of Amateur Radio Astronomers, delivered electronically (via a secure web link, emailed to you as each new issue is posted). We regret that printing and postage costs prevent SARA from providing hardcopy subscriptions to our Journal.

We would appreciate the following information included with your check or money order, made payable to SARA:

Name: .....

Email Address : .....
(required for electronic Journal delivery)

Ham call sign: ..... (if applicable)

Address: .....

City: .....

State: .....

Zip: .....

Country: .....

Phone: .....

Please include a note of your interests. Send your application for membership, along with your remittance, to our Treasurer.

For further information, see our website at:
http://radio-astronomy.org/membership

How to get started?

SARA has a made a kit of software and parts to detect the Hydrogen line signal from space. This is an excellent method to get started in radio astronomy. It teaches the principles of antenna design, signal detection, and signal processing. Read more about this and other projects on our web site.

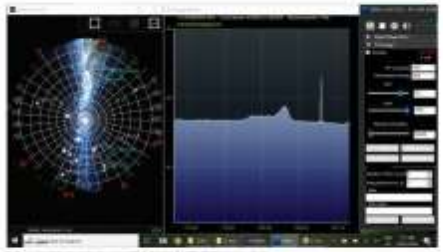

Society of Amateur Radio Astronomers, Inc.
Founded 1981

Membership supported, nonprofit [501(c) (3)]
Educational and Radio Astronomy Organization

Knowledge through Common Research, Education and Mentoring

SARA members have been privileged to use this forty foot diameter drift-scan hydrogen line radio telescope every year at their annual meeting in Green Bank.

http://radio-astronomy.org

Why Radio Astronomy?

Because about sixty five percent of our current knowledge of the universe has stemmed from radio astronomy alone. The discovery of quasars, pulsars, black holes, the 3K background from the "Big Bang" and the discovery of biochemical hydrogen/carbon molecules are all the result of professional radio astronomy.

The Society of Amateur Radio Astronomers

SARA was founded in 1981, with the purpose of educating those interested in pursuing amateur radio astronomy.

The society is open to all, wishing to participate with others, worldwide.

SARA members have many interests, some are as follows:

SARA Areas of Study and Research:

- Solar Radio Astronomy
- Galactic Radio Astronomy
- Meteor Detection
- Jupiter
- SETI
- Gamma Ray/High Energy Pulse
- Detection
- Antennas
- Design of Hardware / Software

The members of the society offer a friendly mentor atmosphere. All questions and inquiries are answered in a constructive manner. No question is silly!

SARA offers its members an electronic bi-monthly journal entitled Radio Astronomy. Within the journal, members report on their research and observations. In addition, members receive updates on the professional radio astronomy community and, society news.

Once a year SARA meets for a three-day conference at the Green Bank Observatory in Green Bank West Va.

There is also a spring conference held at various cities in the Western USA. Previous meeting have been at the VLA in Socorro, NM and at Stanford University.

How do I get started?

Just as a long journey begins with the first step, the project you elect must start with a clear idea of your objectives. Do you wish to study the sun? Jupiter? Make meteor counts? Do you wish to engage in imaging radio astronomy? What you decide will not only determine the type of equipment you will need, but also the local radio spectrum.

How do amateurs do radio astronomy?

Radio astronomy by amateurs is conducted using antennas of various shapes and sizes, from smaller parabolic dishes to simple wire antennas. These antennas are connected to receivers and most of these receivers are software defined radios these days. Data from the receivers are collected by computers, and the received signals will be displayed as charts, graphs or maybe even sky maps. As diverse as the observed objects, so is are the instruments and tools used. SARA members will always be supportive to find good solutions for what one wishes to observe.

Is amateur radio astronomy instrumentation expensive?

Technical information freely circulated in our monthly journal helps amateurs to obtain good low noise equipment from off the shelf assemblies, or to build their own units. The actual cash investment in radio astronomy equipment need not exceed that of any other hobby.

What are amateurs actually looking for in the received data?

The aim of the radio amateur is to find something new and unusual. Just as an amateur optical observer hopes to notice a supernova or a new comet, so does an amateur radio observer hope to notice a new radio source, or one whose radiation has changed appreciably.

The Reber Telescope at NRAO. Constructed by Grote Reber in 1937 in his back yard in Wheaton, Illinois

SARA Members discussing the IBT (Itty Bitty Telescope)